BANGALORE - ISIBANG – 2012 November 29

Future perspectives of SAR Polarimetry with applications to multi-parameter fully polarimetric POLSAR Remote Sensing & Geophysical Stress-change monitoring:
Implementation to agriculture, forestry & aqua-culture plus natural disaster assessment & monitoring within the *equatorial/sub-equatorial belts* by advancing implementation of equatorially orbiting POLSAR single and tandem satellite sensors (90 minutes)

Wolfgang-Martin Boerner

UIC-ECE Communications, Sensing & Navigation Laboratory
900 W. Taylor St., SEL (607) W-4210, M/C 154, CHICAGO IL/USA-60607-7018
T&F: +[1] (312) 996-5480, Email: boerner@ece.uic.edu

OUTLINE

1. Recent most pertinent POLinSAR Workshops

- 1. POLinSAR 2003 January 14 - 16: No space-borne SAR, participants: 80
  http://earth.esa.int/workshops/polinsar2003

- 2. POLinSAR 2005 January 17 - 21: No space-borne SAR, participants: 120
  http://earth.esa.int/workshops/polinsar2005

- 3. POLinSAR 2007 January 22 - 26 : ALOS-PALSAR, participants: 160+
  http://earth.esa.int/workshops/polinsar2007

- 4. POLinSAR 2009 January 26 - 30: 3 space-borne SAR, participants: 180+
  http://earth.esa.int/workshops/polinsar2009

- 5. POLinSAR 2011 January 24 - 28: 3 space-borne SAR, participants: 150+62
  http://earth.esa.int/workshops/polinsar2009

2. Advent of 3 Fully Polarimetric Space-borne SAR Sensors

- ALOS-PALSAR L-Band: January 2006
- RADARSAT-2 C-Band: December 2007
- TerraSAR-X X-Band: June 2007 **& TanDEM-X June 2010**

SUMMARY & PREVIEW of POLinSAR 2009 & 2011

POLinSAR 2011: 3 Fully Polarimetric SAR & 1 Tandem Sensors, ~ 200 + participants http://earth.esa.int/workshops/polinsar2011

- Summary: **further advancement of POLinSAR with all single & tandem fully polarimetric satellite POL-SAR sensors**

  - New Findings: POLinSAR old & young expert community is growing

  - What was accomplished: Excellent presentations especially by junior experts & advances made on several basic and applied POLinSAR R&D projects

  - What is still required: **More test-site multi-sensor data acquisitions**

  - Future perspectives: **Advance multi-band high-resolution wide-swath repeat-pass fully polarimetric spatial & temporal DIFF-POLinSAR environmental remote sensing & geo-physical stress-change monitoring**


YLD
WMB
MR
POLinSAR-2009 Participants: Wednesday, 2009 January 28

Apollo 11: 1969 July 16 – 24: Neil Armstrong, Michael Collins, Edwin Aldrin, Jr.

Apollo 17: 1972 Dec. 7 – 19: Eugene Cernan, Ronald Evans, Harrison Schmitt

Pacific and Indian Oceans

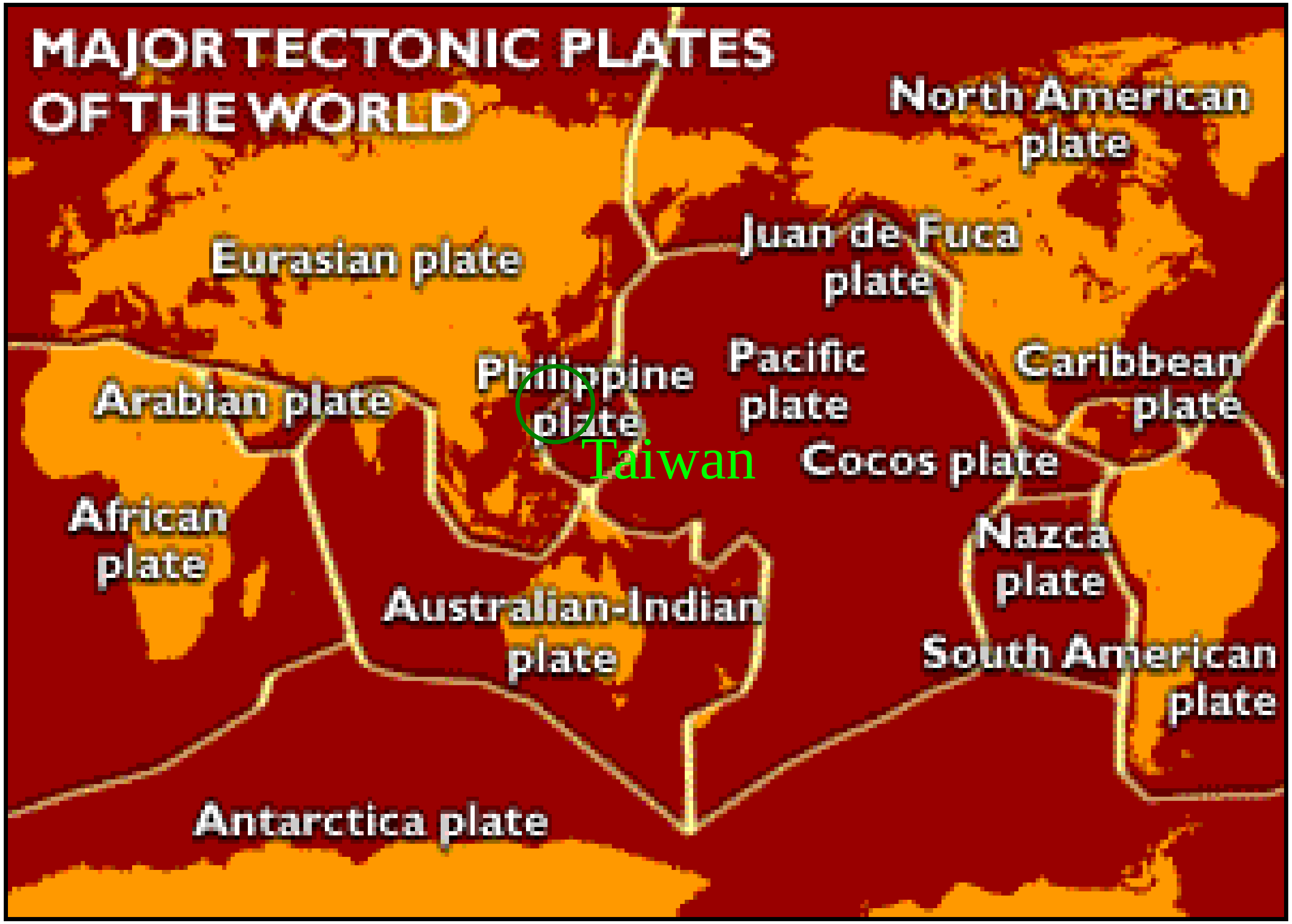

From BBC news site

The terrestrial tectonology: Alfred Wegener's tectonic plate theory and the two major seismic belts

The theory of plate tectonics was pioneered by Alfred Wegener in the early 20th C. He was originally drawn to the idea when he tried to explain the ancient climates.

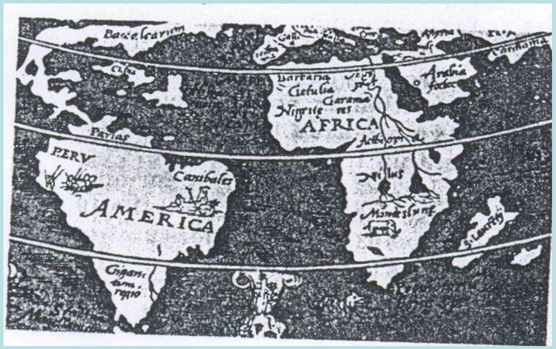

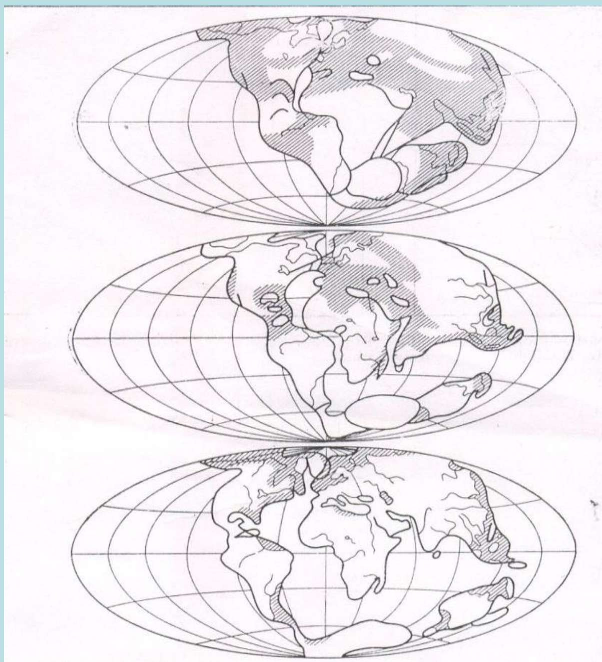

- Francis Bacon, who introduced inductive method in science in 1620 used the term “exporrecti” meaning expansion to describe the complementary outlines of Africa and South America depicted in the very first authentic map of the world.
- Since then many observers have attempted to explain the conspicuous matching characteristics of the two widely apart continents amongst them the work of German meteorologist Alfred Wegener (1912) attracted much attention.
- This however, had to face acrimonious criticisms specially from the renowned British geophysicist Sir Harold Jeffreys. The criticisms were not without reasons principally because of rigid nature of mantle and imperfect matching of the continents.

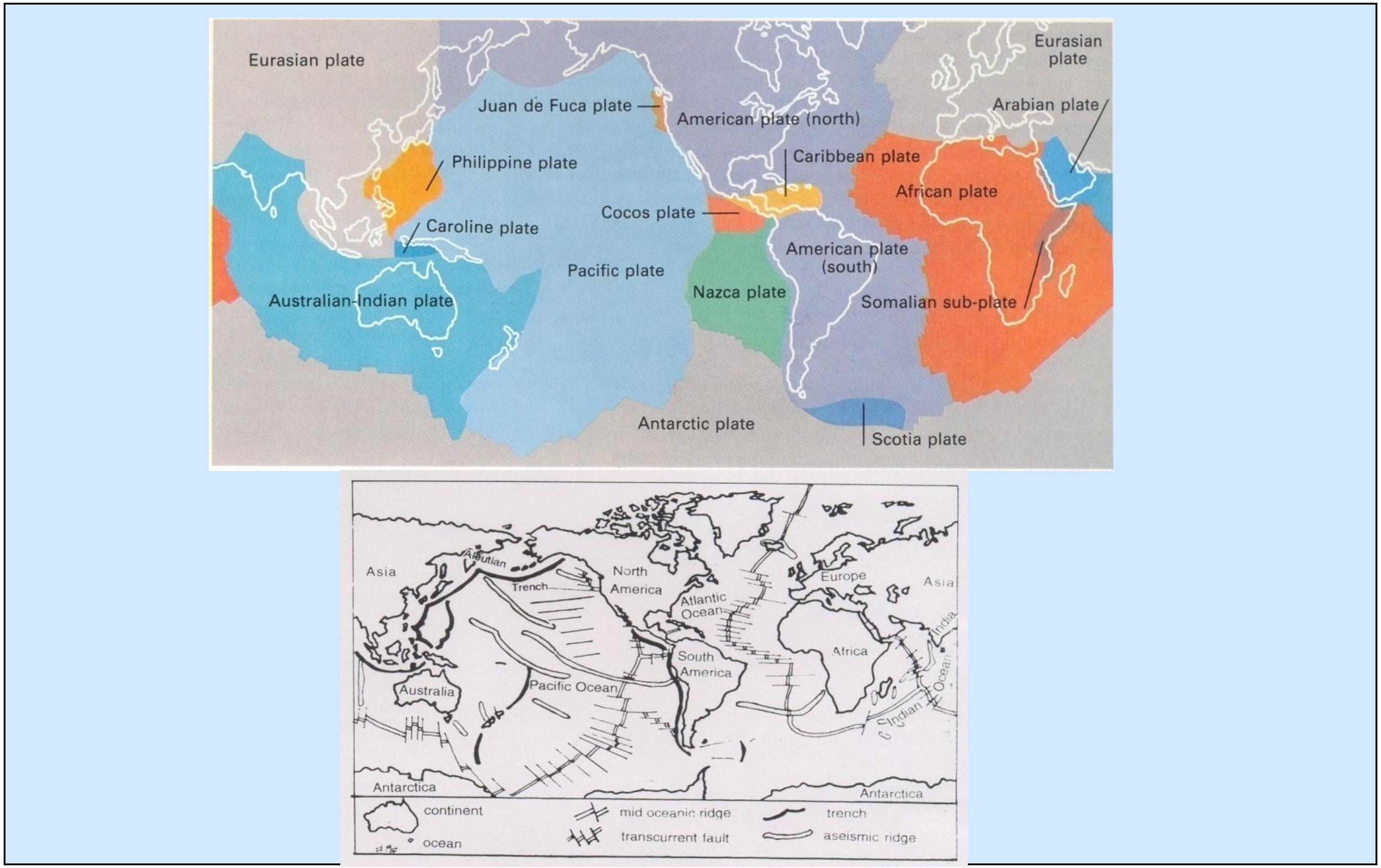

PLATE TECTONICS

The terrestrial tectonology: Alfred Wegener’s tectonic plate theory and the two major seismic belts

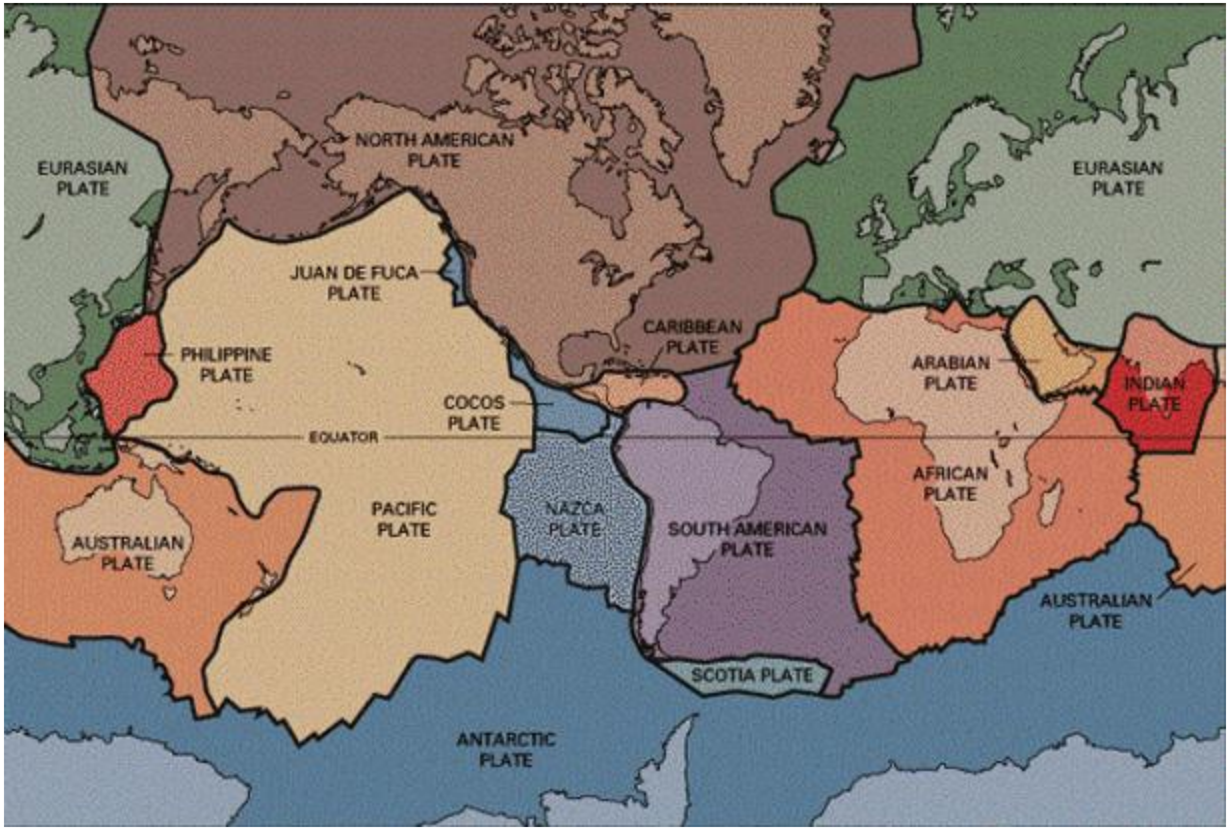

Major Plates of the World

The terrestrial tectonology: Alfred Wegener’s tectonic plate theory and the two major seismic belts

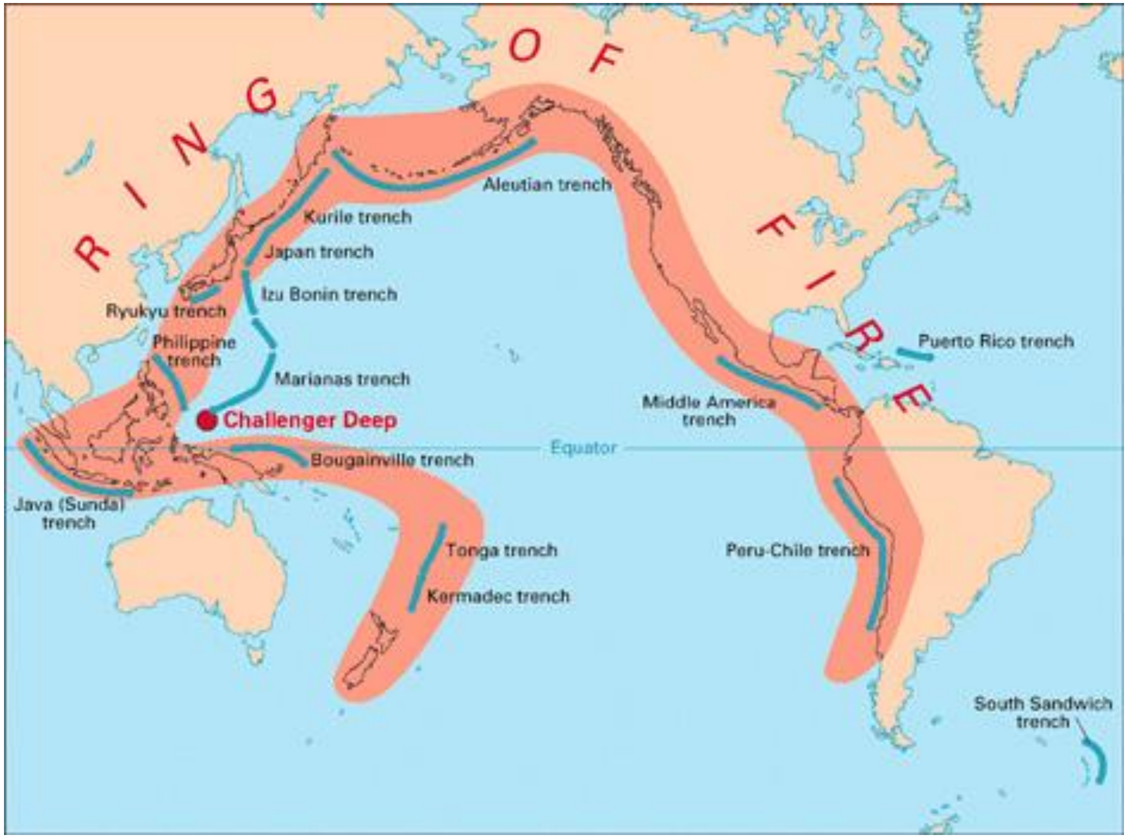

Belt 2, Circum-Pacific belt

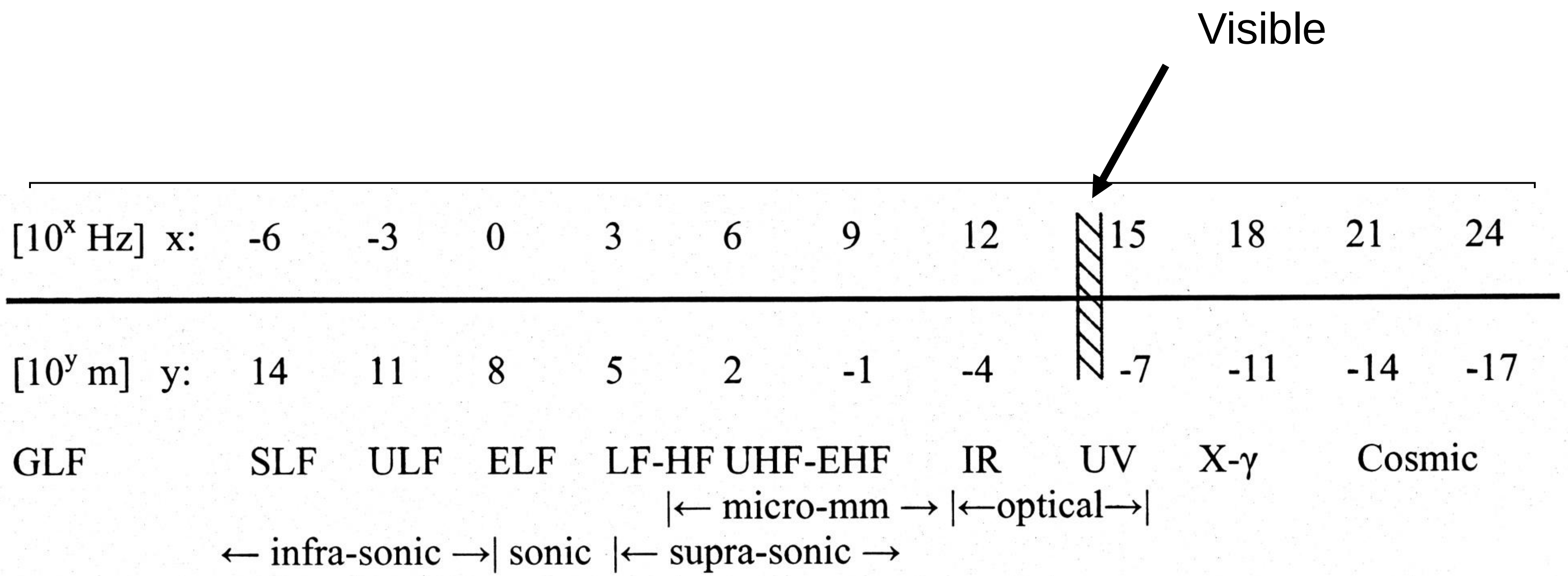

Electromagnetic Spectrum

Multi-Altitude Near-Range and Remote Sensing in Wide-Area Environmental Surveillance for Real Time Monitoring of the Earth's Biosphere

for an ecological investigation of the Earth through observation and identification of harmful anthropogenic influences due to the interaction of:

- **Oceans ⟷ Atmosphere/Stratosphere/Mesosphere**

  Biosphere (Water)

  $$81 \ll \varepsilon(f) \gg 1$$

  Hydrosphere

- **for an early warning system of natural and man-made environmental catastrophes and to take quick actions to buffer the impact to the catastrophe under the increasing pressures of a relentlessly un-abating population explosion:**

  Severe weather ⟷ Typhoons
  Earthquakes ⟷ Volcanic Eruptions

  ☆ **Global Weather Changes**

  Degeneration into steppe ⟷ Retreating Glaciers
  Pollution of Ground Water ⟷ Pollution of Air

  ☆ **Destruction of the Biosphere**

Hydrologic cycle with volcanologic & seismic activity

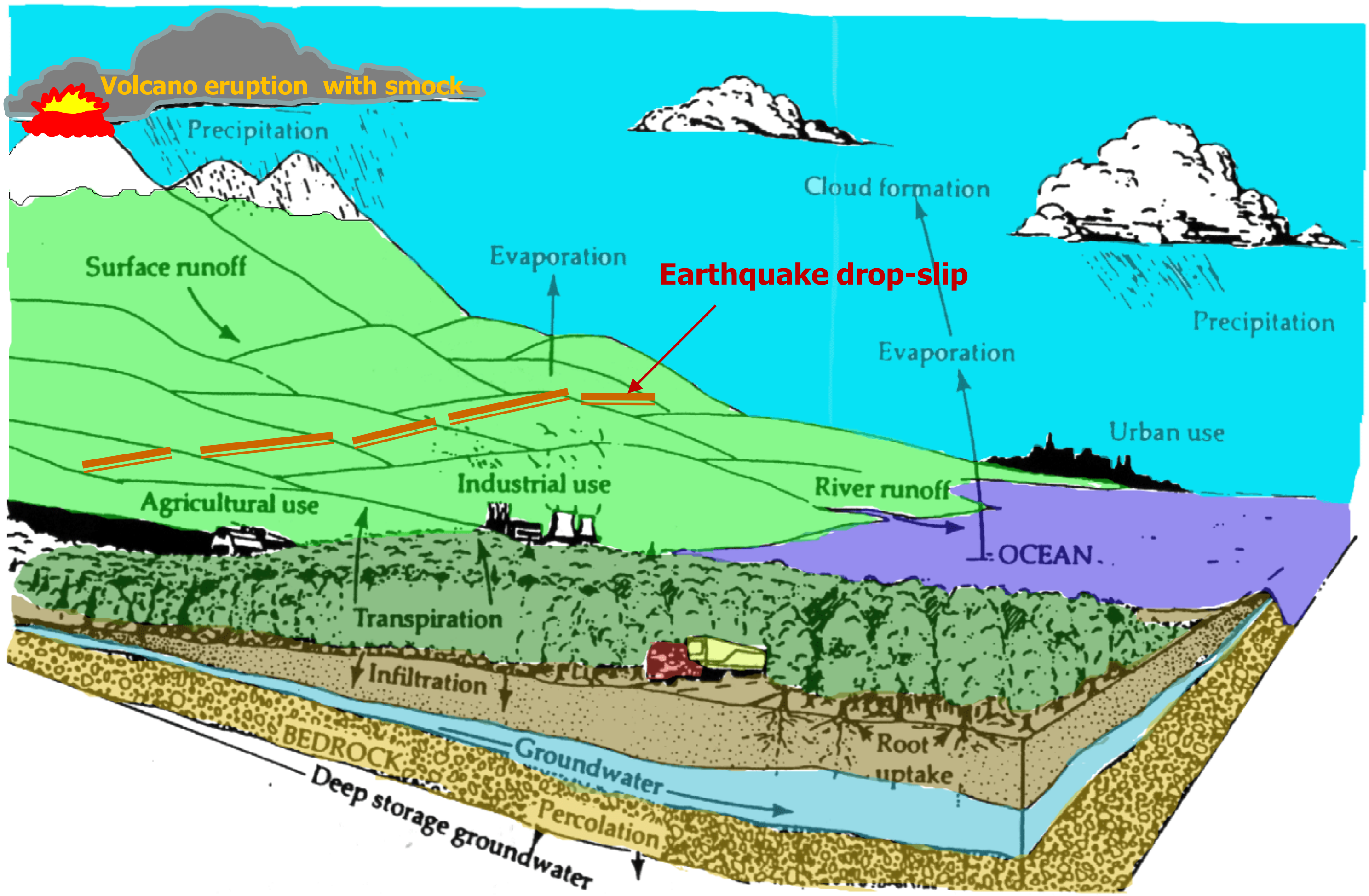

Signatures of Earth Surface Vegetation Cover

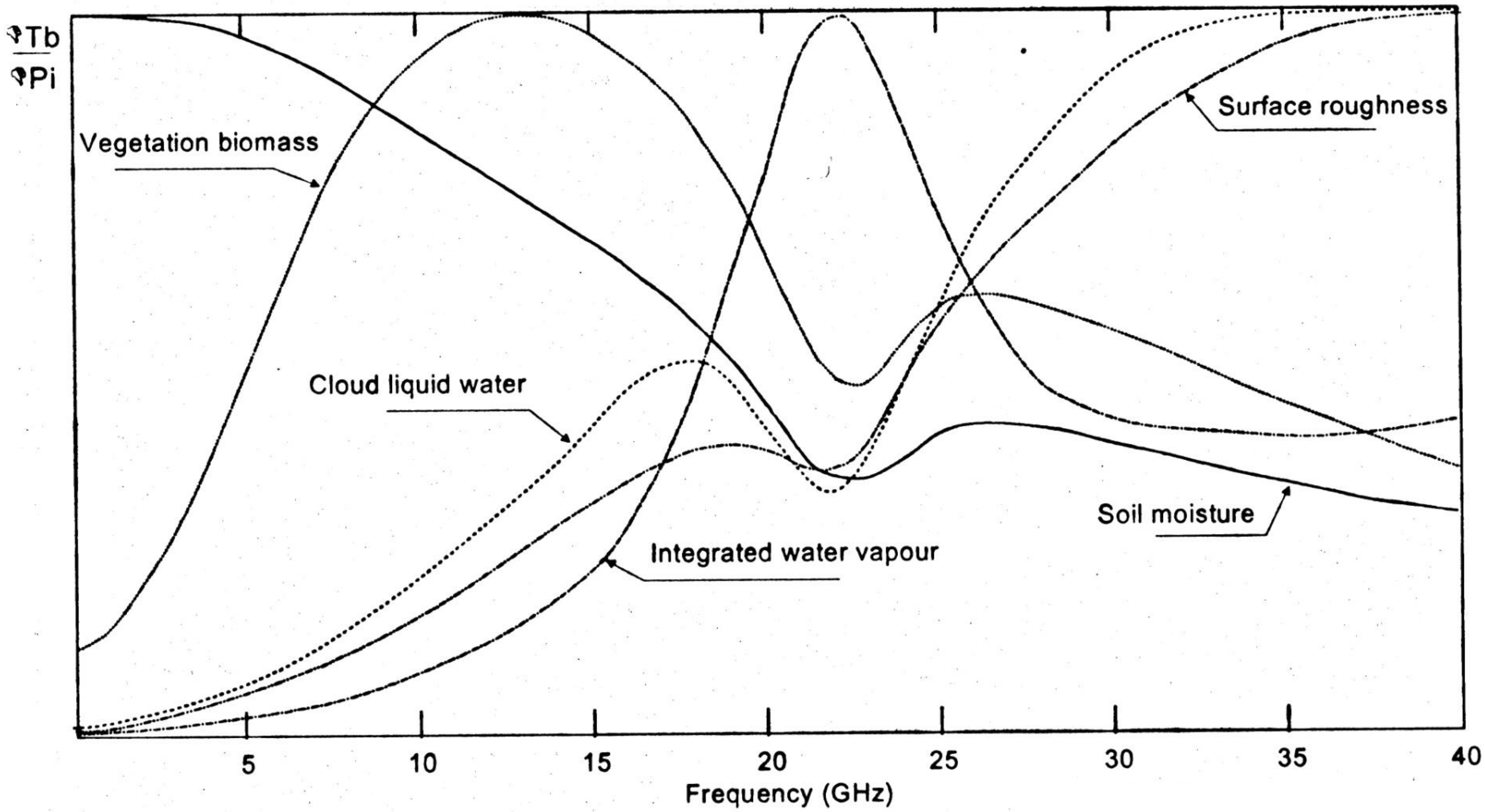

Sensitivity of brightness temperature to geophysical ocean-surface parameters

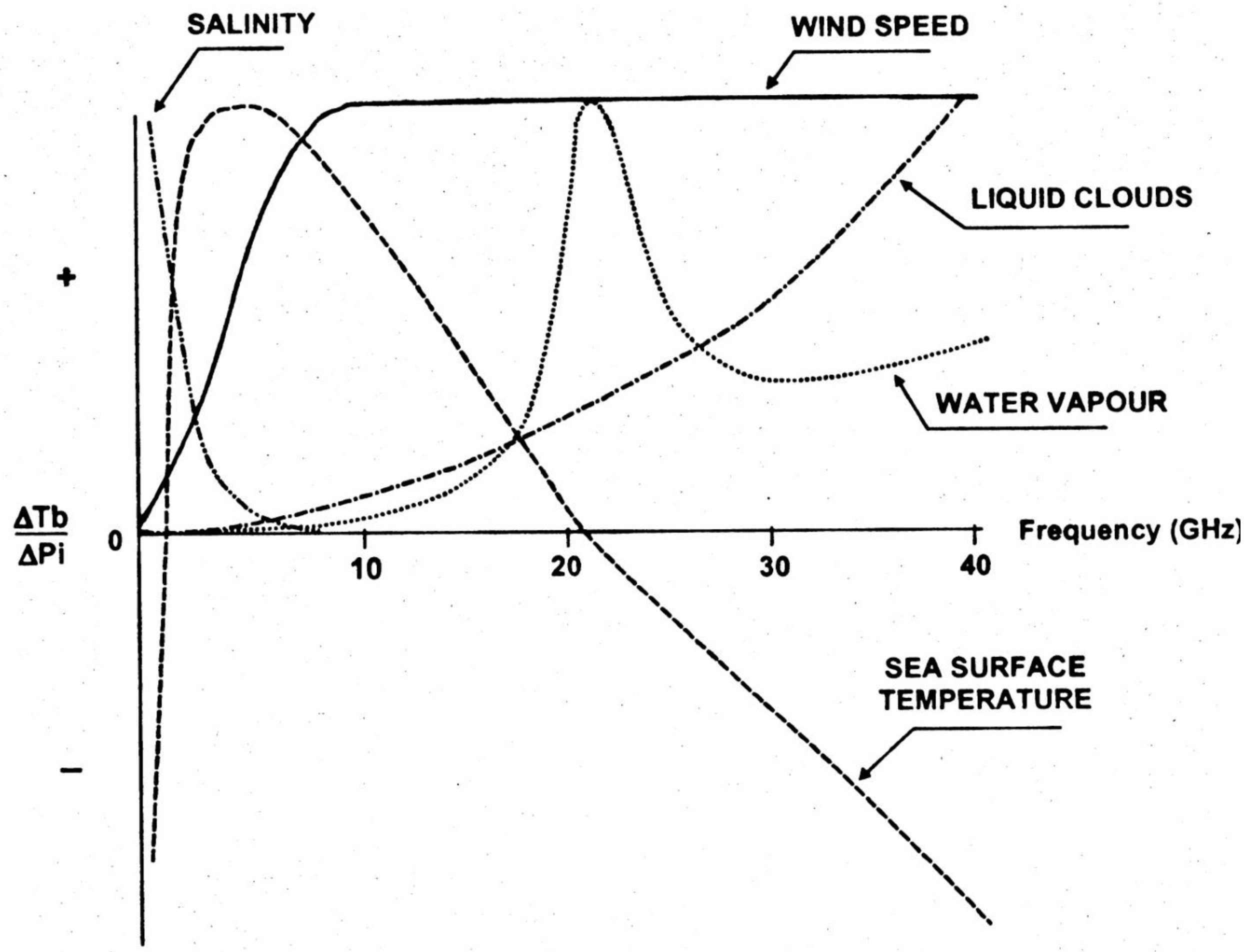

Transmission Spectrum of Atmosphere

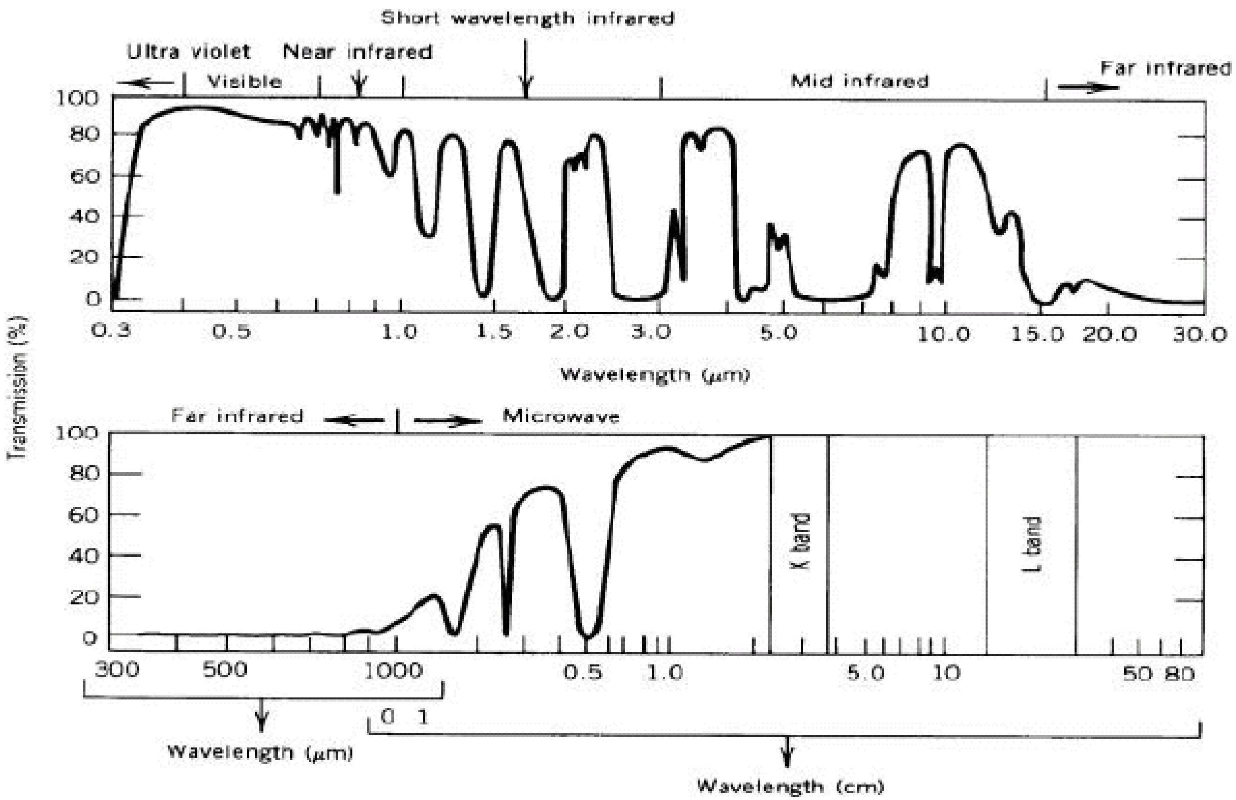

Transmission spectrum of the atmosphere / Attenuation

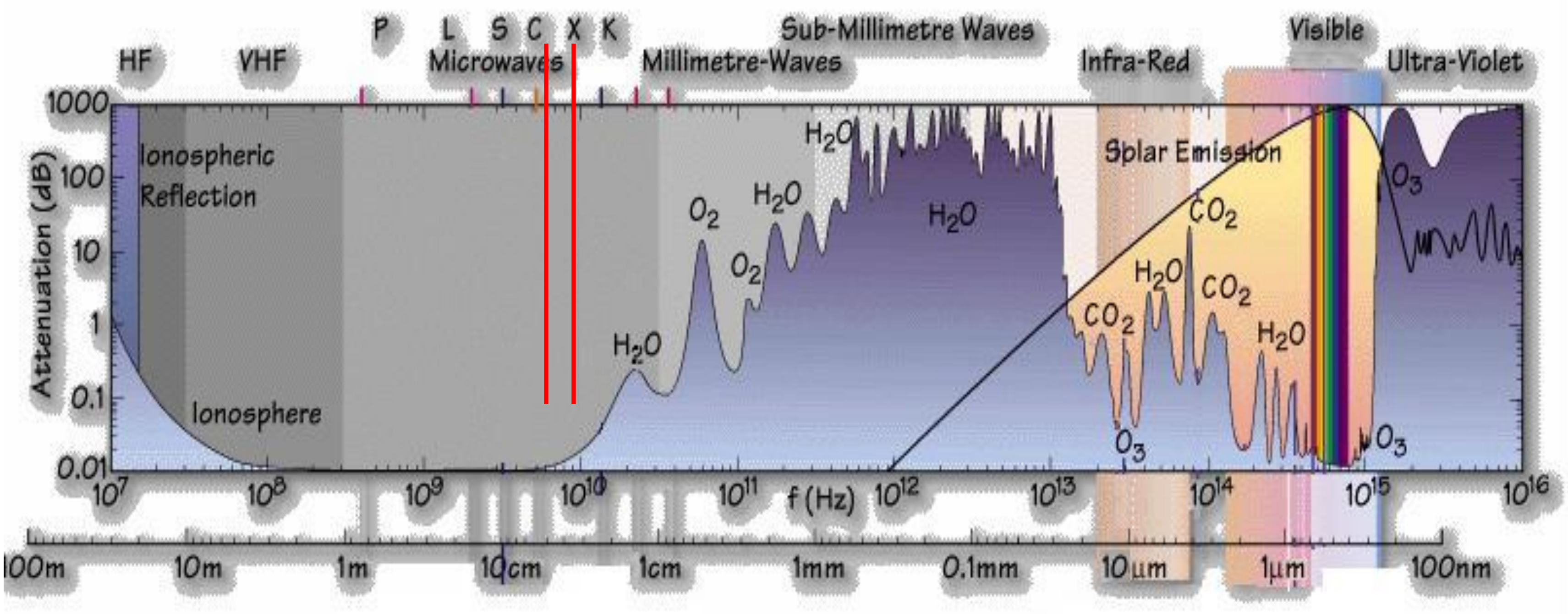

Gaseous attenuation negligible
→ focus on precipitation

→

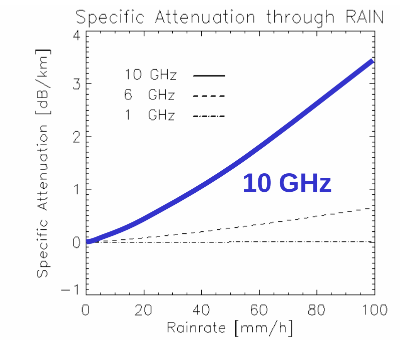

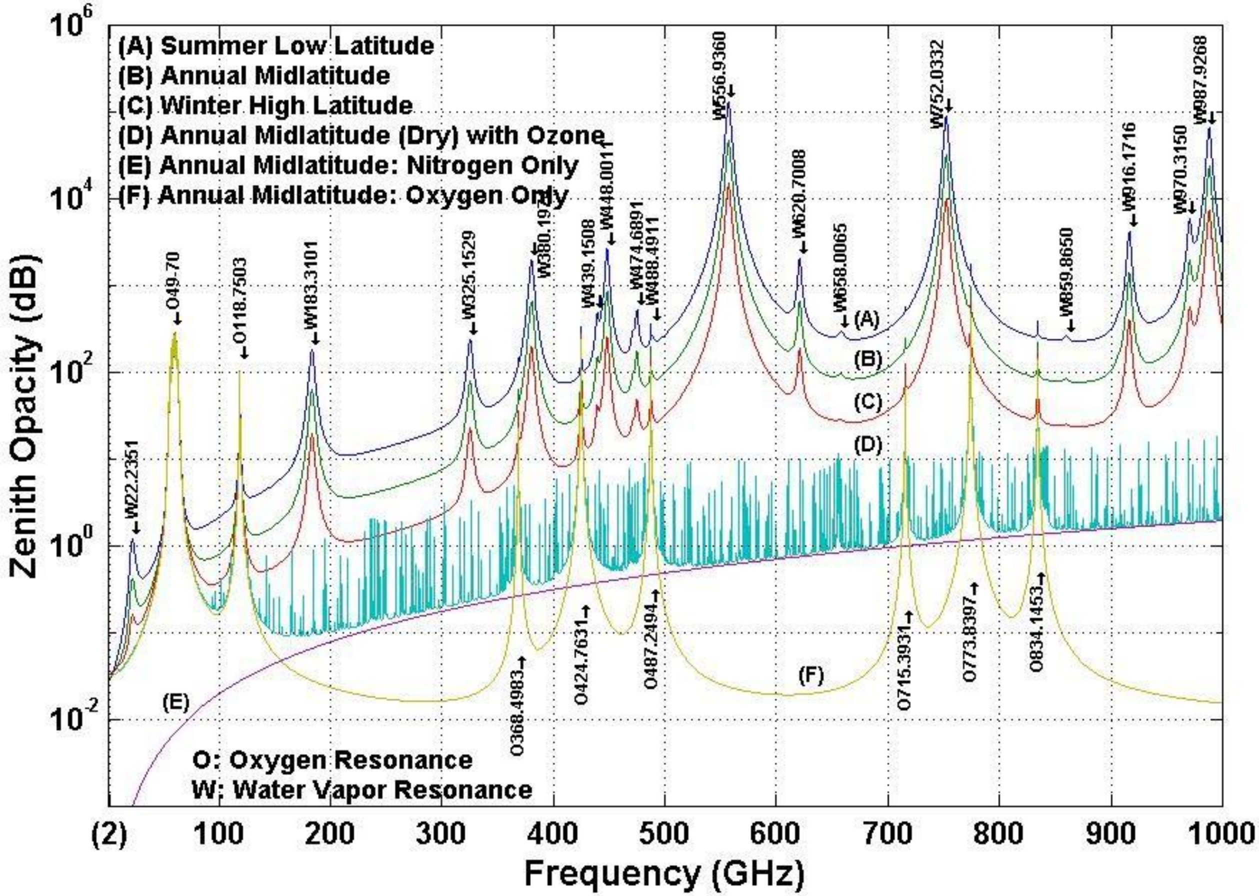

MinimeterWave Resonance Spectrum of Atmosphere

Most affected regions

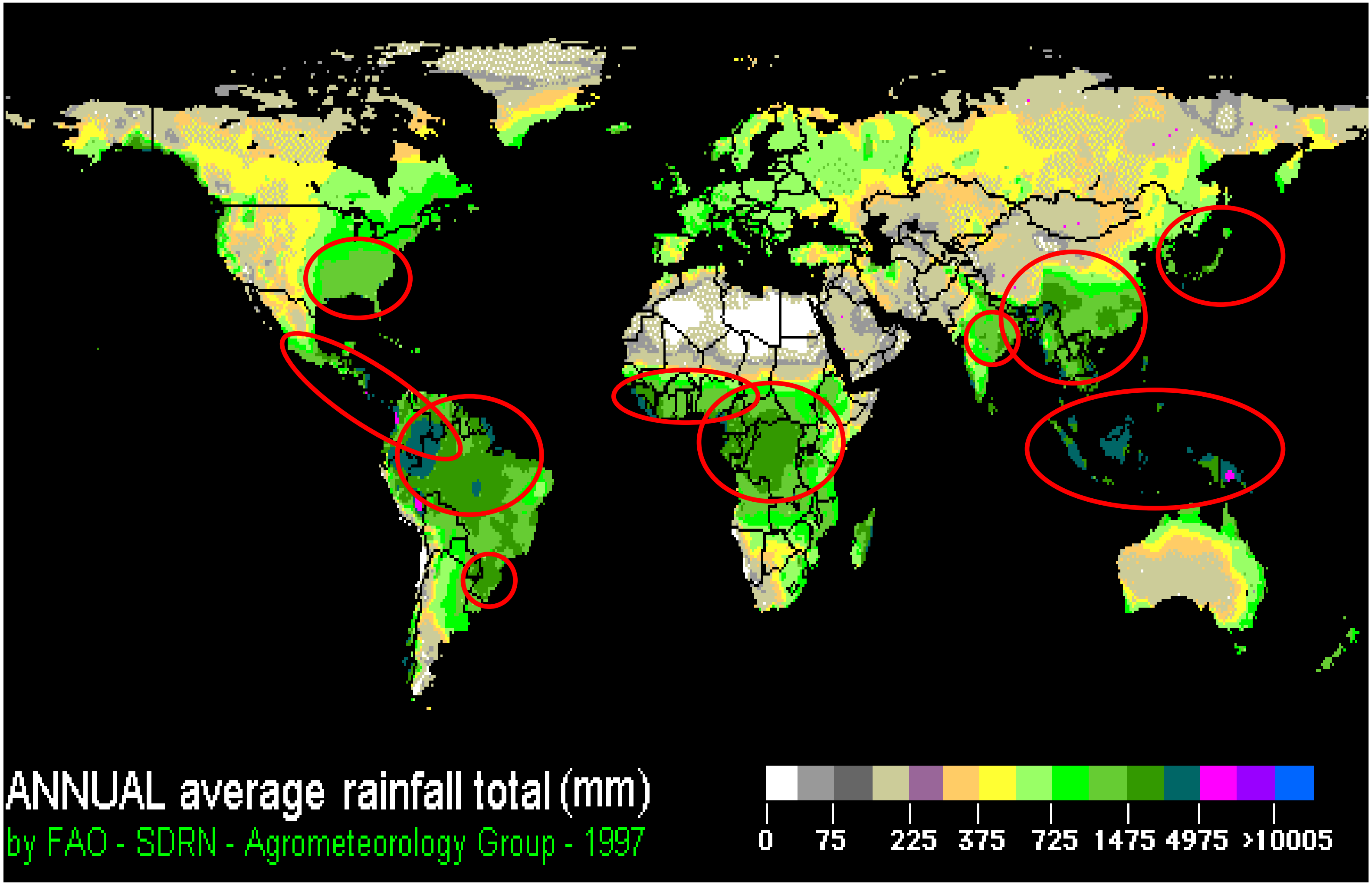

POLARIMETRIC AIRBORNE SAR SENSORS

AES1
AeroSensing (D)
GulfStream Commander
X-Band (HH), P-Band (Quad)

AIRSAR
NASA / JPL (USA)
DC8
P, L, C-Band (Quad)

DOSAR
EADS / Dornier GmbH (D)
DO 228 (1989), C160 (1998), G222 (2000)
S, C, X-Band (Quad), Ka-Band (VV)

RENE
UVSQ / CETP (F)
Écureuil AS350
S, X-Band (Quad)

ESAR
DLR (D)
DO 228
P, L, S-Band (Quad)
C, X-Band (Sngl)

EMISAR
DCRS (DK)
G3 Aircraft
L, C-Band (Quad)

MEMPHIS / AER II-PAMIR
FGAN (D)
Transal C160
Ka, W-Band (Quad) / X-Band (Quad)

STORM
UVSQ / CETP (F)
Merlin IV
C-Band (Quad)

PHARUS
TNO - FEL (NL)
CESSNA – Citation II
C-Band (Quad)

PISAR
NASDA / CRL (J)
GulfStream
L, X-Band (Quad)

RAMSES
ONERA (F)
Transal C160
P, L, S, C, X, Ku, Ka, W-Band (Quad)

SAR580
CCRS (CA)
Convair CV-580
C, X-Band (Quad)

+ CASSAR (China), MIT/Lincoln Lab (USA), P3-SAR (NADC / ERIM -USA), Military Systems …

PacRim2 Mission Statistics

- 46 flight days over a 3-month period, 21st July to 23rd Oct.
- 15 bases in 9 countries
- 648 flight lines collected at 201 sites in 18 countries & territories
- 54,623 km of flight-line data

Provided by
Prof. Tony Milne
PacRim-1&2 Coordinator

Landcover mapping, crop inventory and agricultural practices (PacRim2 2000)

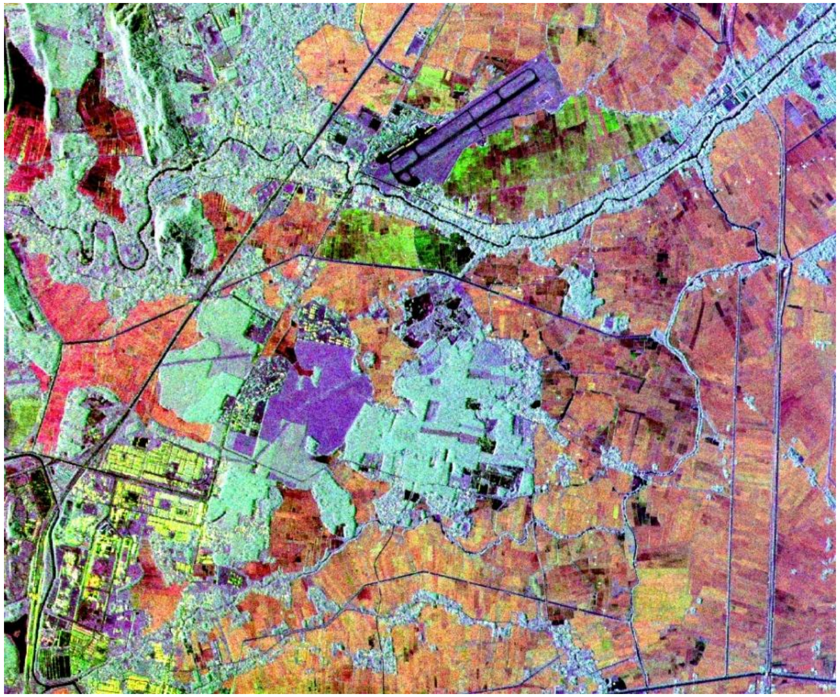

Kedah, Malaysia – radar's sensitivity to vegetation types and density permits the mapping of rice paddy-fields, rubber and palm-oil plantations.

Coastal Pannay, Philippines - broad alluvial plain supporting rural agriculture and fish pens

Prof. Tony Milne
PacRim-1&2 Coordinator

E-SAR and F-SAR

- The E-SAR and F-SAR are operated onboard DLR’s DO228-212 D-CFFU by the Microwaves and Radar Institute in cooperation with DLR’s Flight Facilities based in Oberpfaffenhofen

  The F-SAR is currently in development and is planned to fully replace the E-SAR until middle of 2011

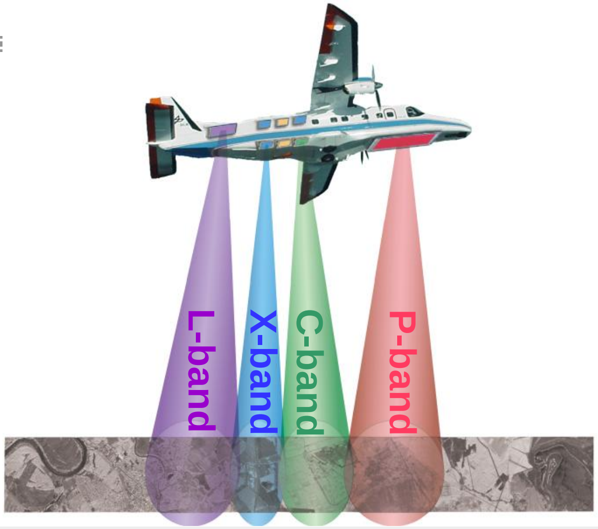

New features:
- significantly enhanced resolution and image quality
- simultaneous data recording in up to four frequency bands
- modular design for easy reconfiguration
- single-pass polarimetric interferometry in X- and S-band
- fully polarimetric capability in all frequencies

E-SAR technical characteristics

	X	C	L	P
RF [GHz]	9.6	5.3	1.3	0.35
BW [MHz]	50-100 (selectable)			
PRF [kHz]	up to 2			
Rg res. [m]	1.5	1.5	2.0	3.0
Az res. [m]	0.2	0.3	0.4	1.5
Pol/InSAR	-/+	-/-	+/o	+/o
Rg cov [km]	3-5			
Sampling	6-8 Bit complex; 100MHz; max number of samples 4 K per range line; 1 recording channel.			

F-SAR technical characteristics

	X	C	S	L	P
RF [GHz]	9.6	5.3	3.2	1.3	0.35
BW [MHz]	800	400	300	150	100
PRF [kHz]	up to 12				
Rg res. [m]	0.3	0.6	0.75	1.5	2.25
Az res. [m]	0.2	0.3	0.35	0.4	1.5
Pol/InSAR	+/+	+/o	+/+	+/o	+/o
Rg cov [km]	12.5 (at max.bandwith)				
Sampling	8 Bit real; 1000MHz; max number of samples 64 K per range line; 4 recording channels.				

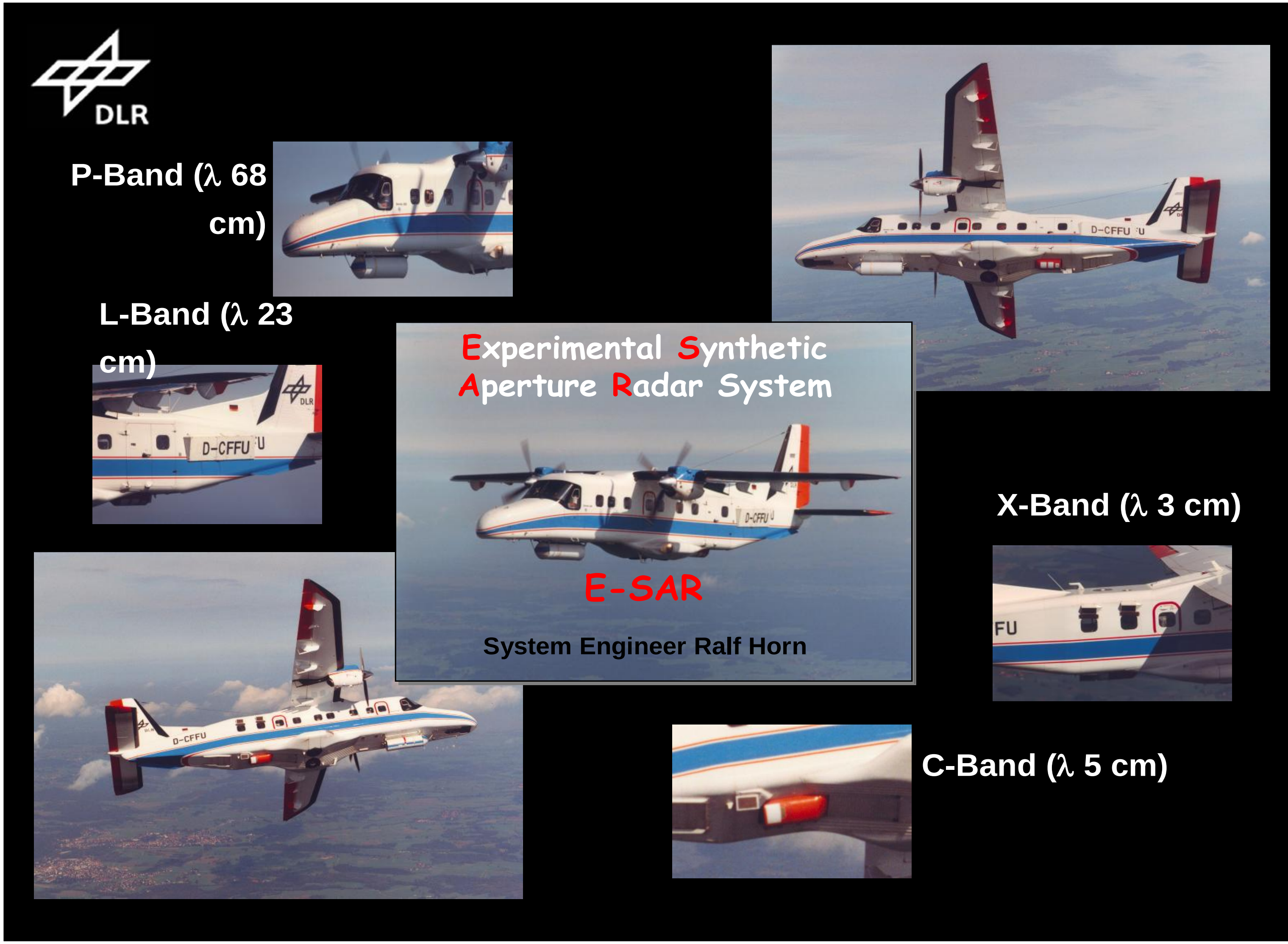
DLR
P-Band (λ 68 cm)
L-Band (λ 23 cm)
Experimental Synthetic Aperture Radar System
E-SAR
System Engineer Ralf Horn
X-Band (λ 3 cm)
C-Band (λ 5 cm)

DLR-HR's new SAR sensor

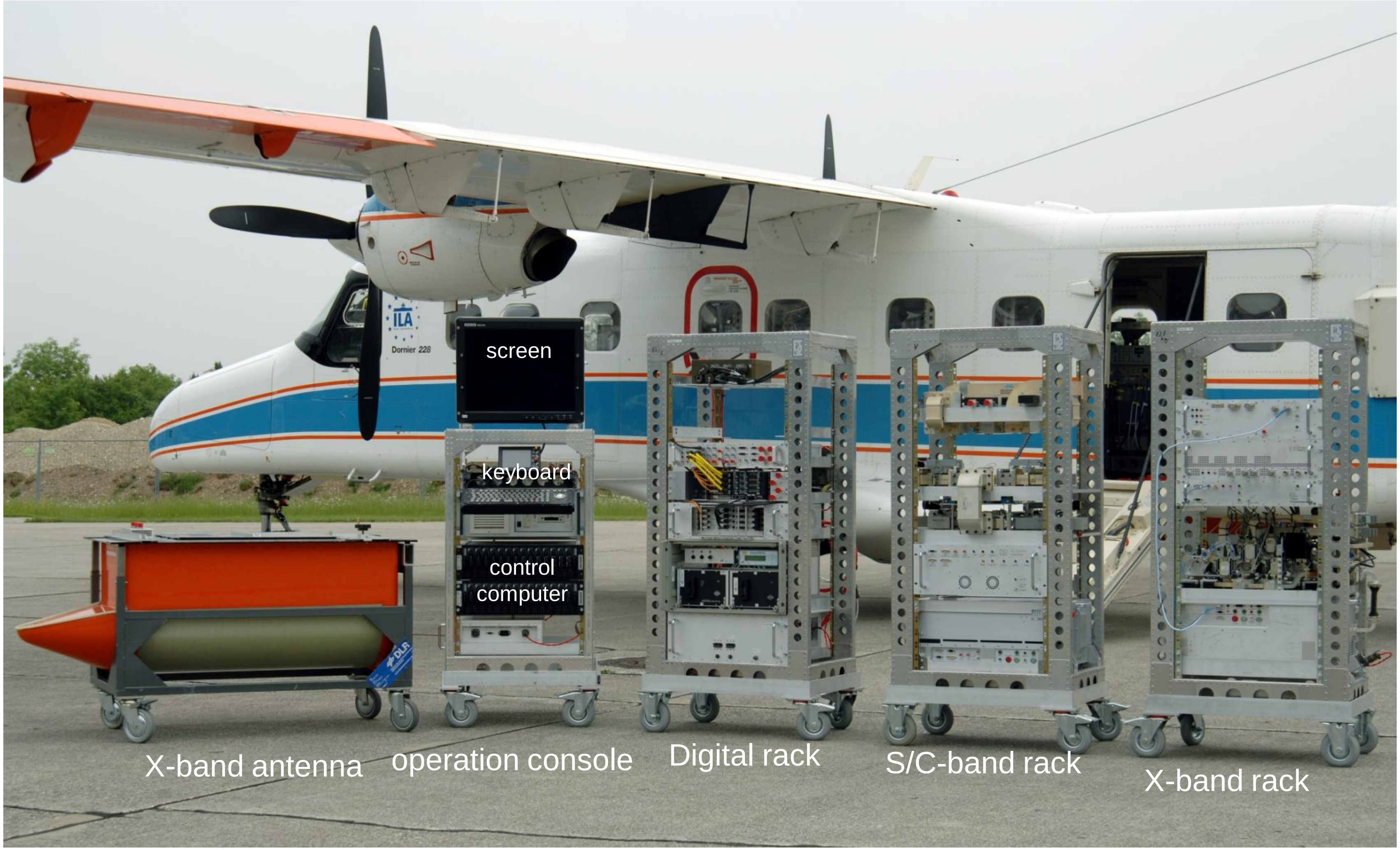

F-SAR X-Band Quad-Pol

DLR
F-SAR
S-band
Quad-Pol

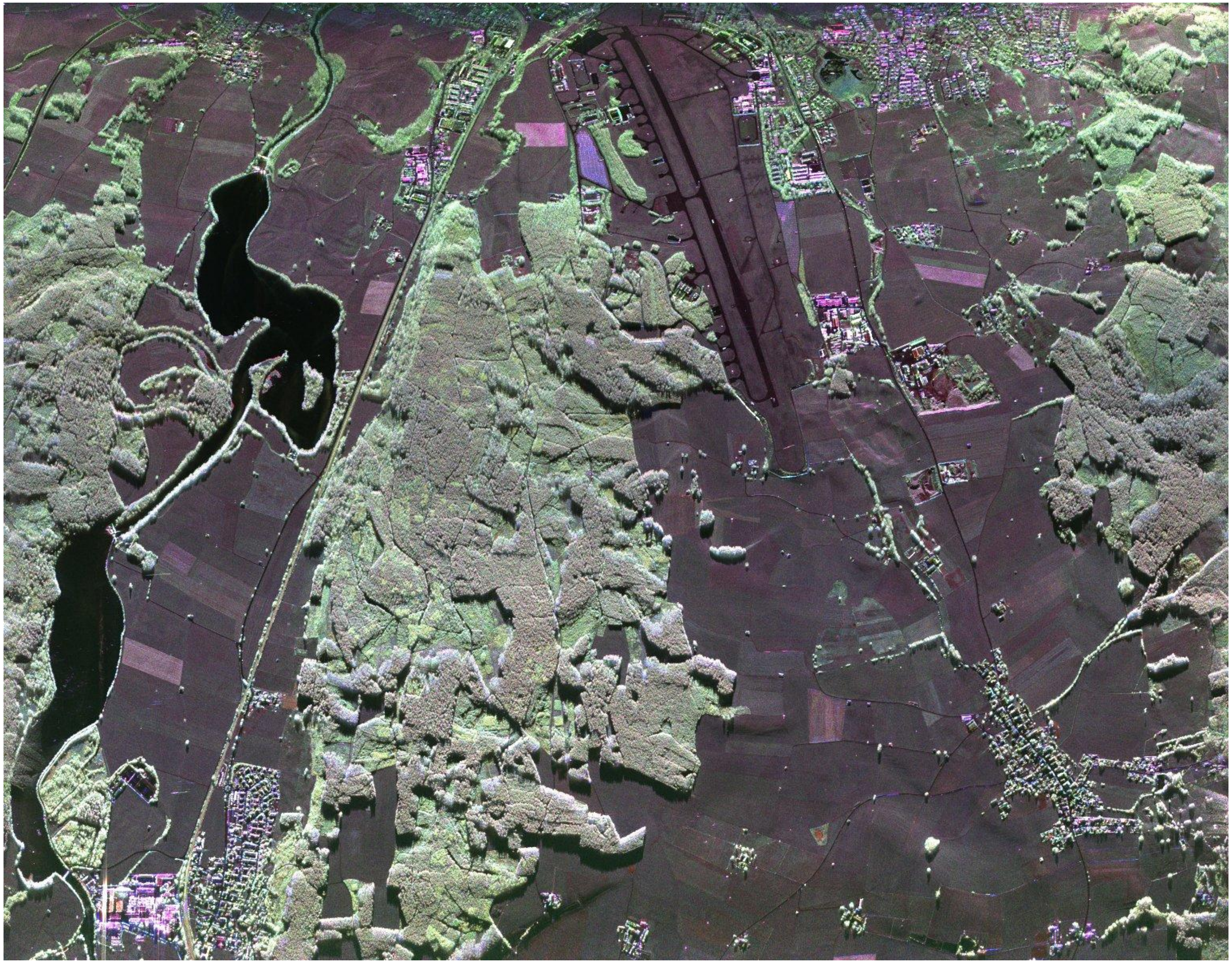

DLR
F-SAR
S-band
Quad-Pol

Zoom

Measurement of car velocities with F-SAR X-band (ATI mode)

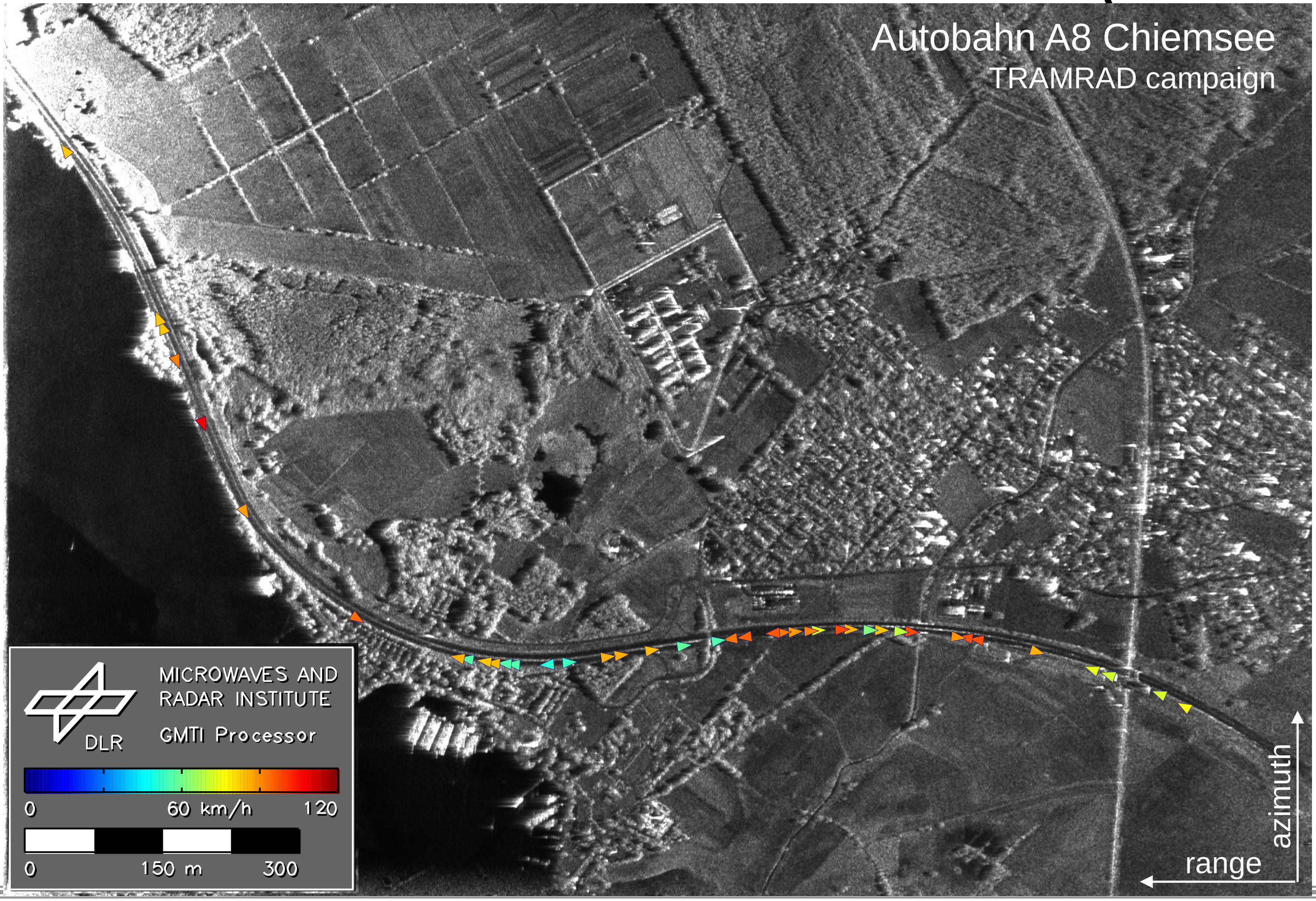

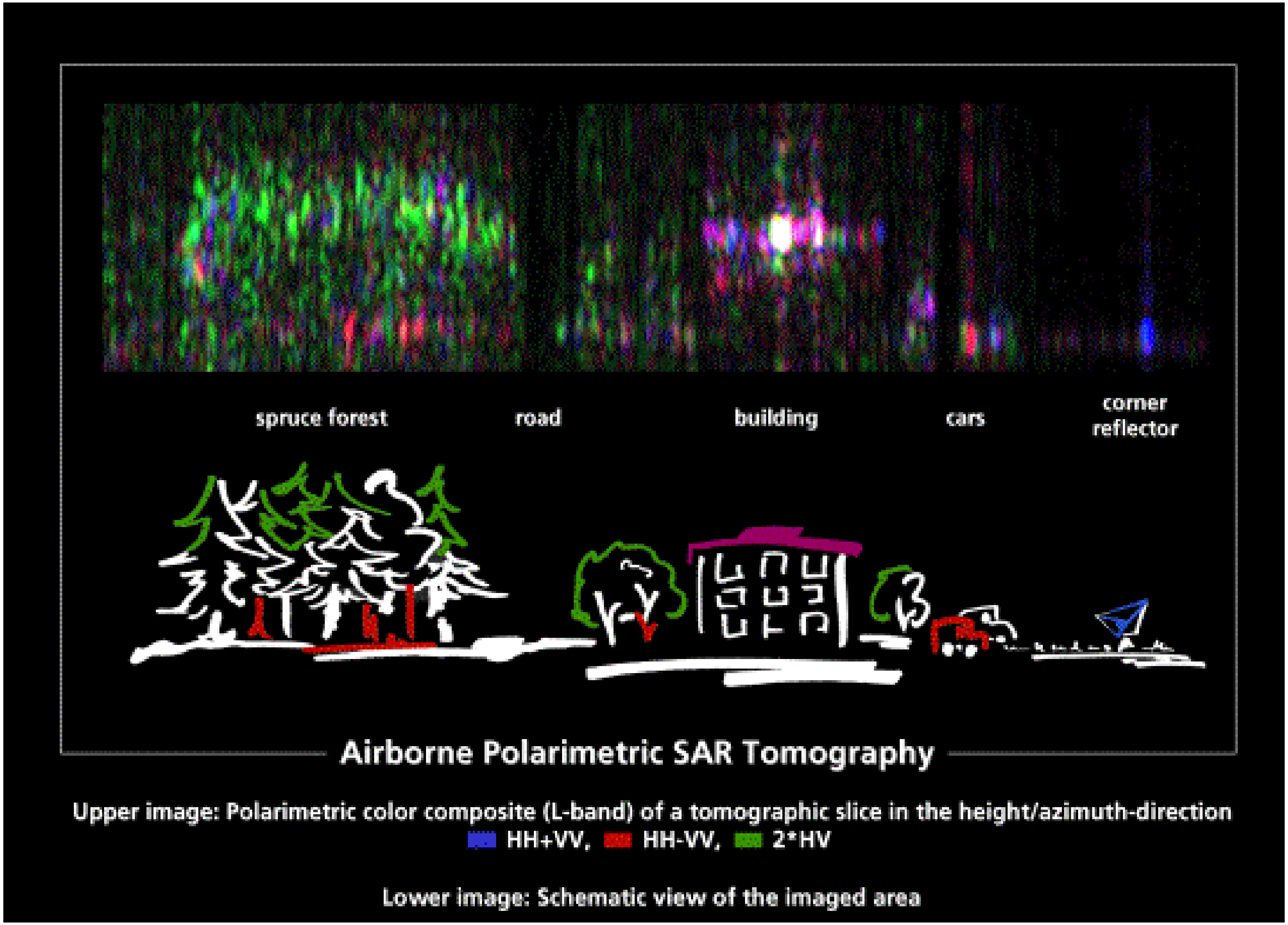
spruce forest
road
building
cars
corner reflector
Airborne Polarimetric SAR Tomography
Upper image: Polarimetric color composite (L-band) of a tomographic slice in the height/azimuth-direction
HH+VV, HH-VV, 2*HV
Lower image: Schematic view of the imaged area

Random-Volume-over-Ground Model Inversion Results

ESAR / Test Site: Kuettighoffen, Switzerland

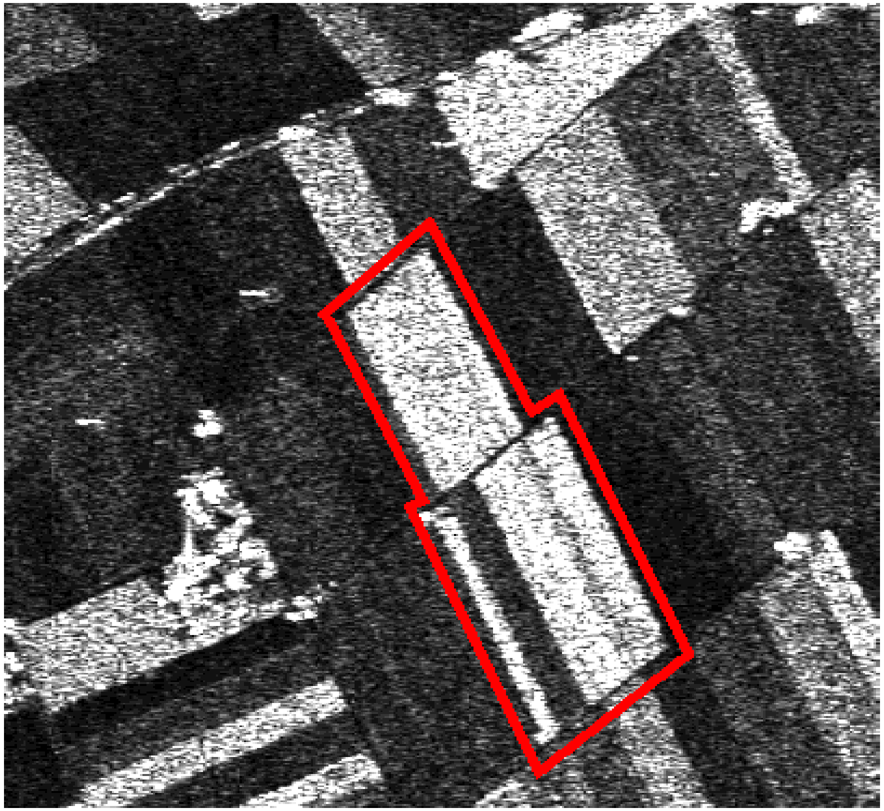

SAR Image L-band

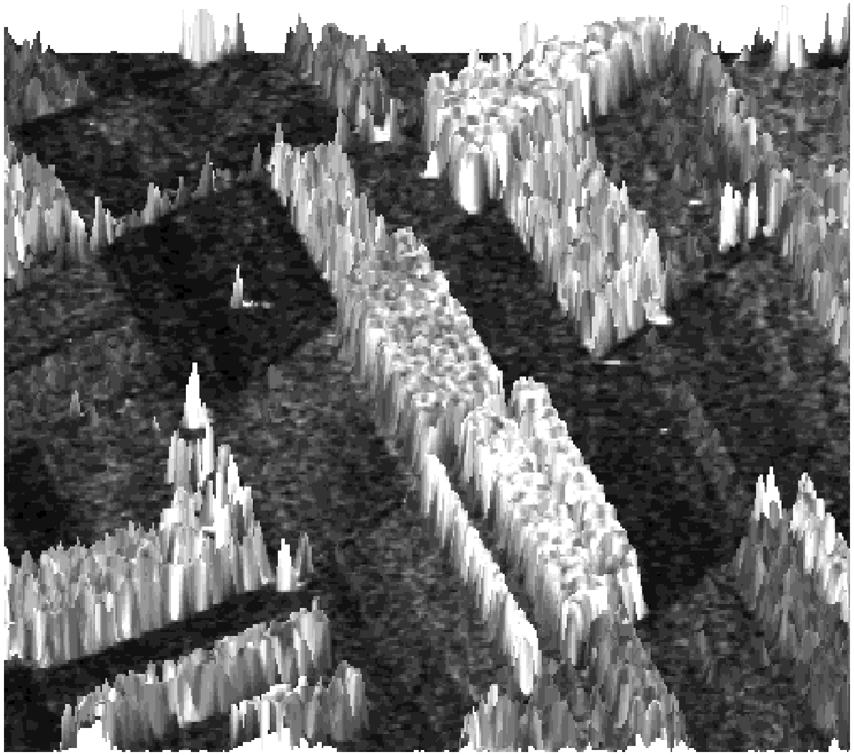

Corn Height Map

Polarimetric SAR Tomography

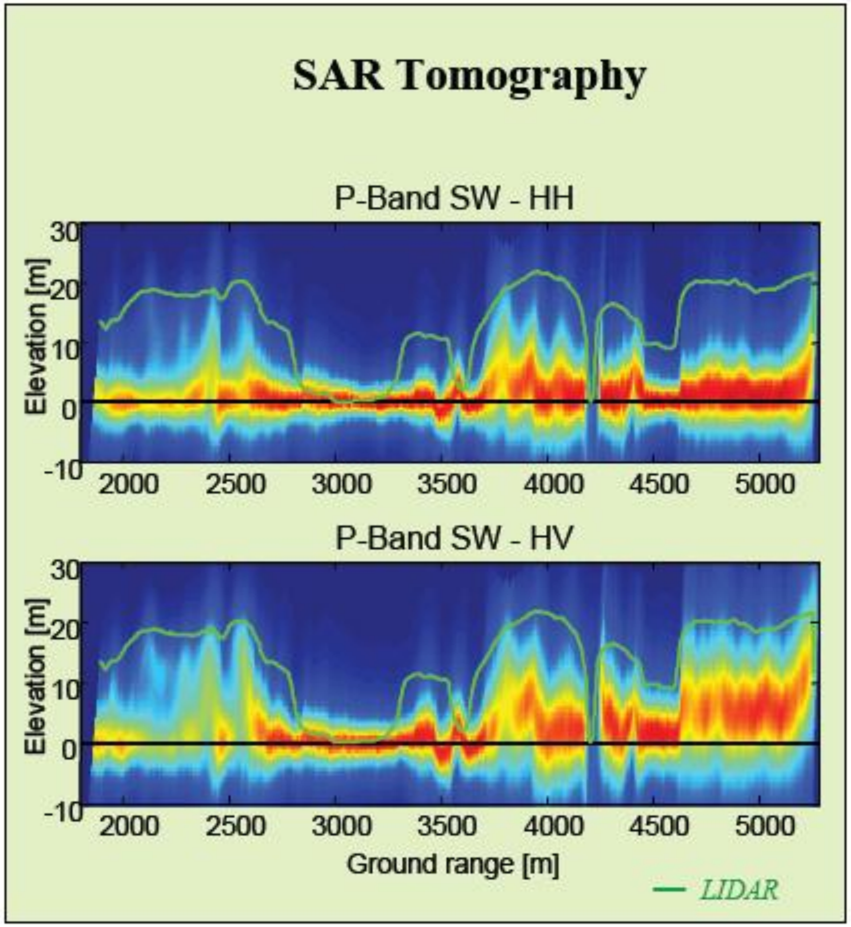

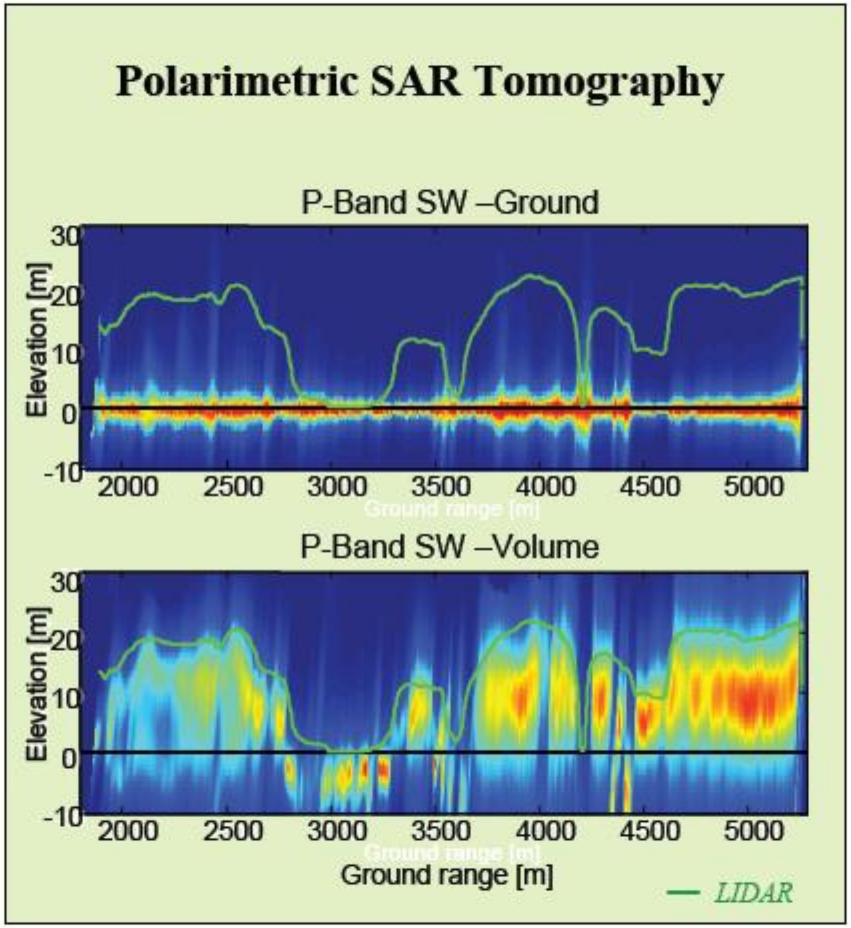

Goal: Separation Of the backscattered power profiles associated with ground and volume scattering

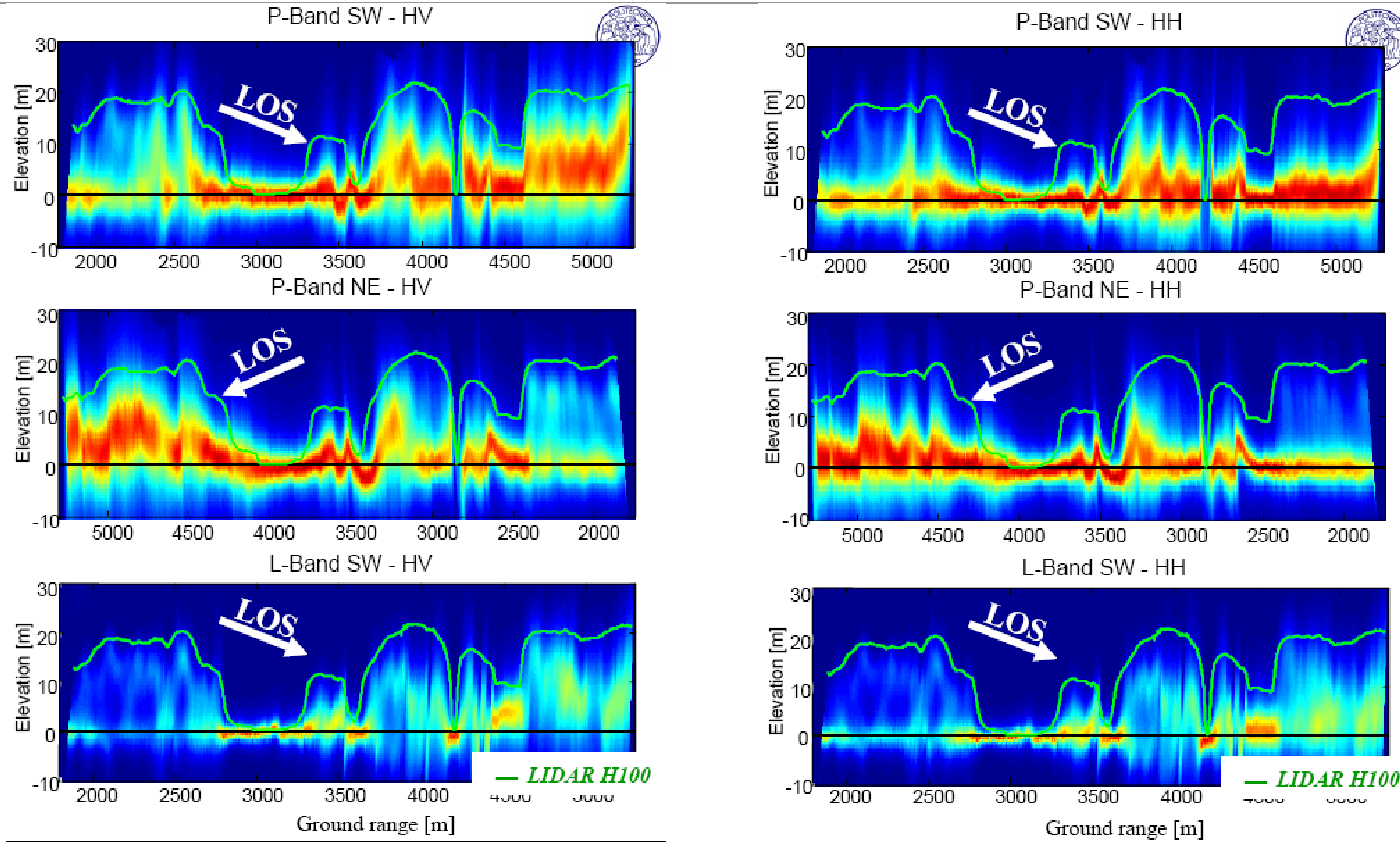
P-Band SW - HV
P-Band SW - HH
P-Band NE - HV
P-Band NE - HH
L-Band SW - HV
L-Band SW - HH
LOS
Elevation [m]
Ground range [m]
— LIDAR H100

PI-SAR=TU-CNEAS-Sato-lab-Koike-Takafumi-1=030317

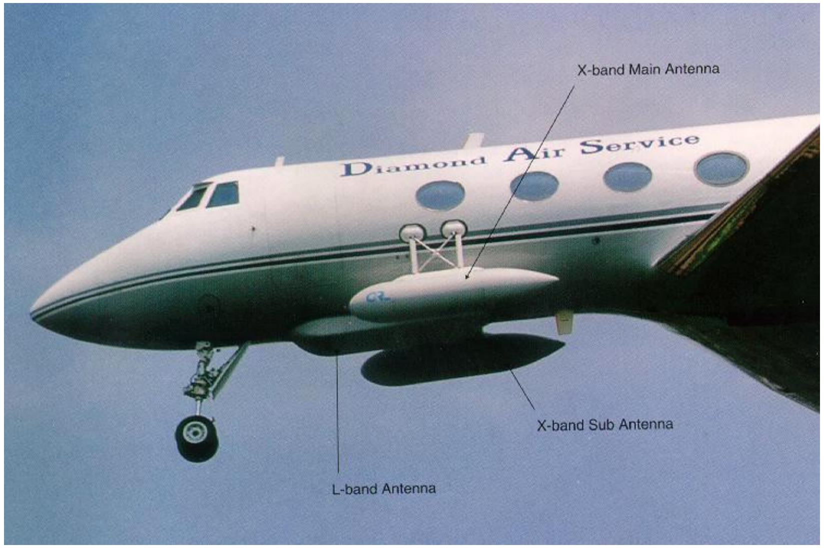

X-band Main Antenna

X-band Sub Antenna

PI-SAR

PI-SAR=TU-CNEAS-Sato-lab-Koike-Takafumi-2=030317

N

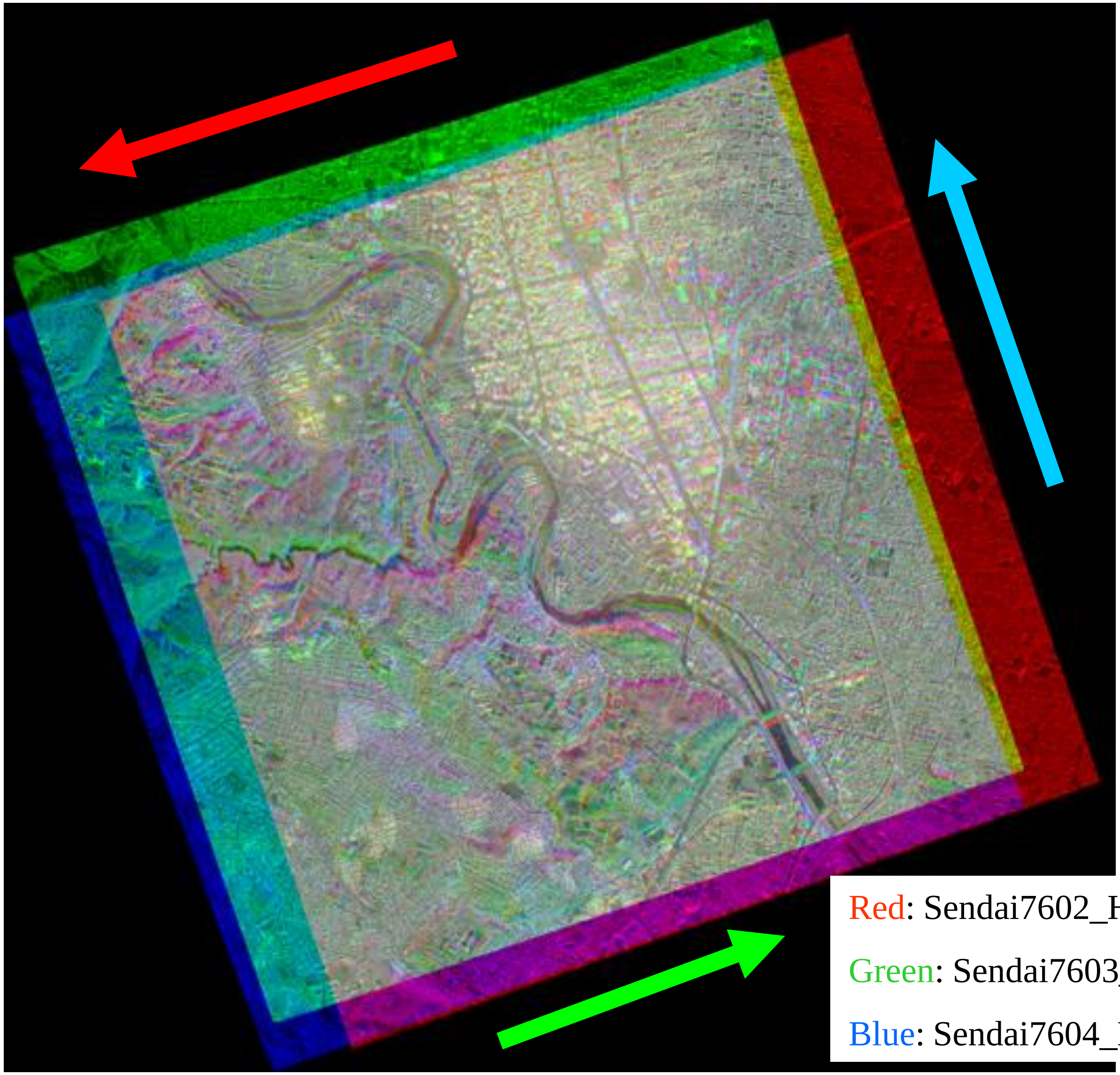

Red: Sendai7602_HH polarization

Green: Sendai7603_HH polarization

Blue: Sendai7604_HH polarization

Square path data

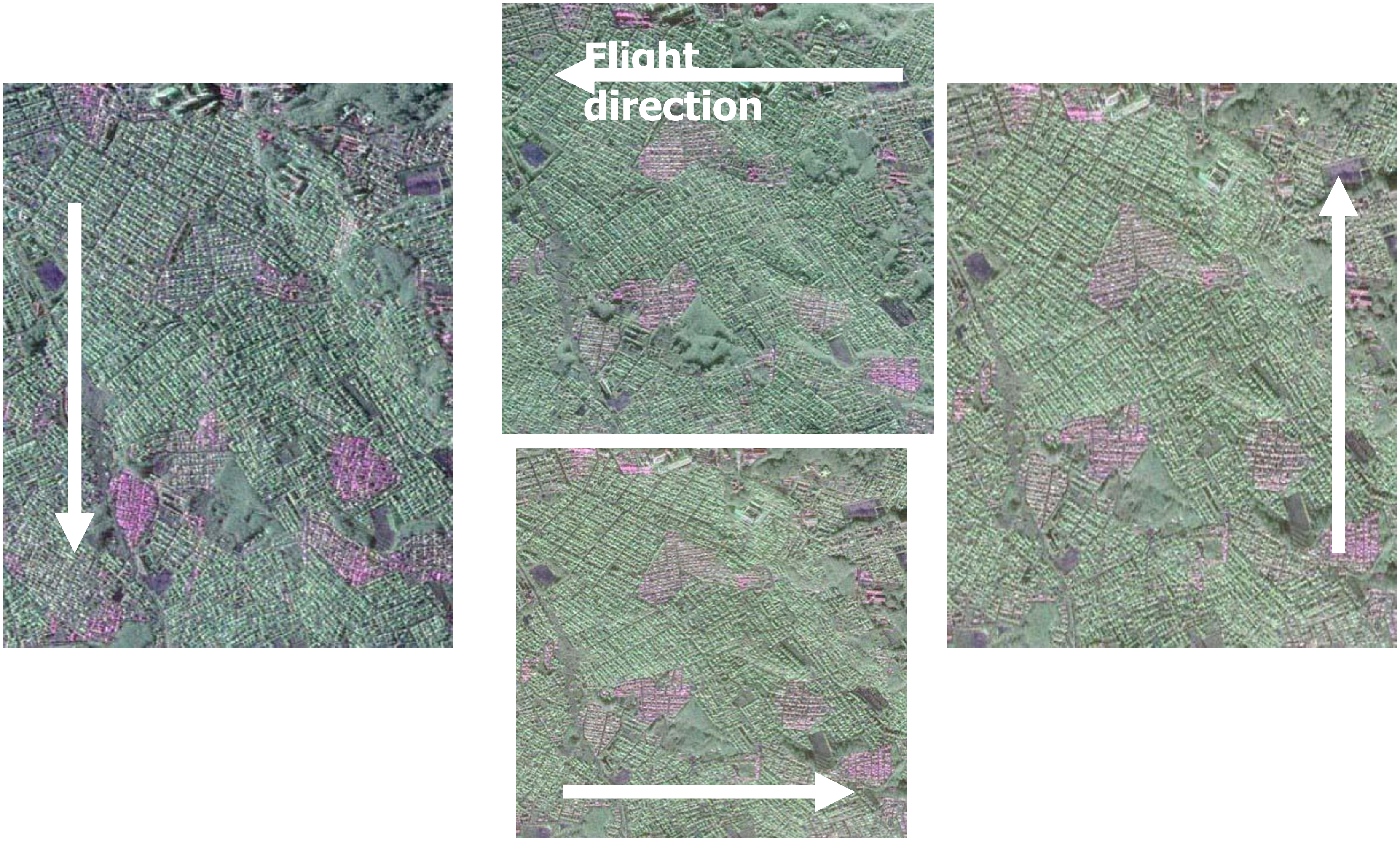

SIR-C/X-SAR-1994-Oct-11 C&L-Band POL-IN-SAR Optimization

By Kostas Papathanassiou, Dissertation DLR, 1994

Polarimetric Interferometry

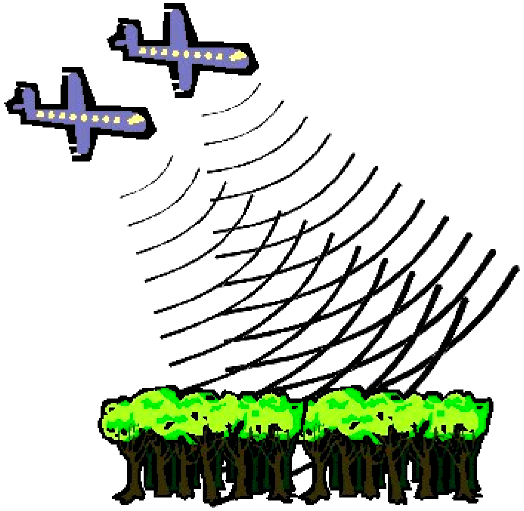

Image 1: Scattering Matrix: $[S_1] = \begin{bmatrix} S^1_{HH} & S^1_{HV} \\ S^1_{VH} & S^1_{VV} \end{bmatrix}$

Scattering Vector: $\vec{k}_1 = \frac{1}{\sqrt{2}} [S^1_{HH} + S^1_{VV} \quad S^1_{HH} - S^1_{VV} \quad 2S^1_{HV}]^T$

Image 2: Scattering Matrix: $[S_2] = \begin{bmatrix} S^2_{HH} & S^2_{HV} \\ S^2_{VH} & S^2_{VV} \end{bmatrix}$

Scattering Vector: $\vec{k}_2 = \frac{1}{\sqrt{2}} [S^2_{HH} + S^2_{VV} \quad S^2_{HH} - S^2_{VV} \quad 2S^2_{HV}]^T$

Image formation: $i_1 = \vec{w}_1^+ \cdot \vec{k}_1$ and $i_2 = \vec{w}_2^+ \cdot \vec{k}_2$ where $\vec{w}_i$ are complex unitary vectors

Interferogram formation: $i_1 \; i_2^* = (\vec{w}_1^+ \cdot \vec{k}_1)(\vec{w}_2^+ \cdot \vec{k}_2)^+ = \vec{w}_1 (\vec{k}_1 \cdot \vec{k}_2^+) \vec{w}_2^+ = \vec{w}_1 [\Omega] \vec{w}_2^+$

Interferometric Coherence: (complex)

$$\tilde{\gamma}(\vec{w}_1, \vec{w}_2) = \frac{< i_1 \, i_2^* >}{\sqrt{< i_1 \, i_1^* > < i_2 \, i_2^* >}} = \frac{< \vec{w}_1 [\Omega] \vec{w}_2^+ >}{\sqrt{< (\vec{w}_1 [\Omega] \vec{w}_1^+) > < (\vec{w}_2 [\Omega] \vec{w}_2^+) >}}$$

SIR-C/X-SAR-1994-Oct-11 C&L-Band POL-IN-SAR Optimization

By Kostas Papathanassiou, Dissertation DLR, 1994

Pol-SAR Pauli Images: SIR-C / Test Site: Selenge-River, Kudara/Buryatia,Russia

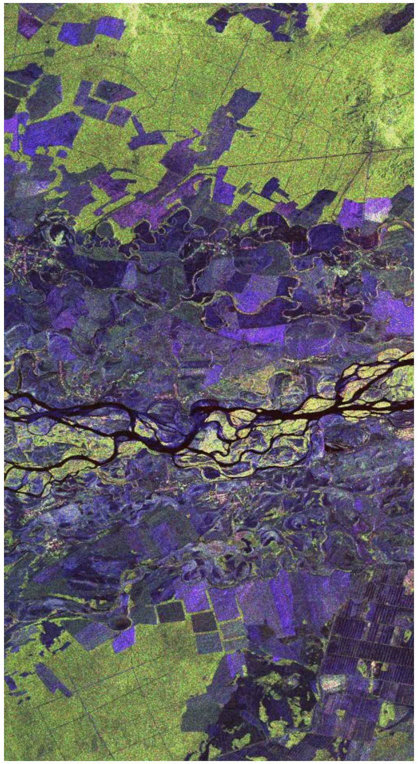

< Selenge River >

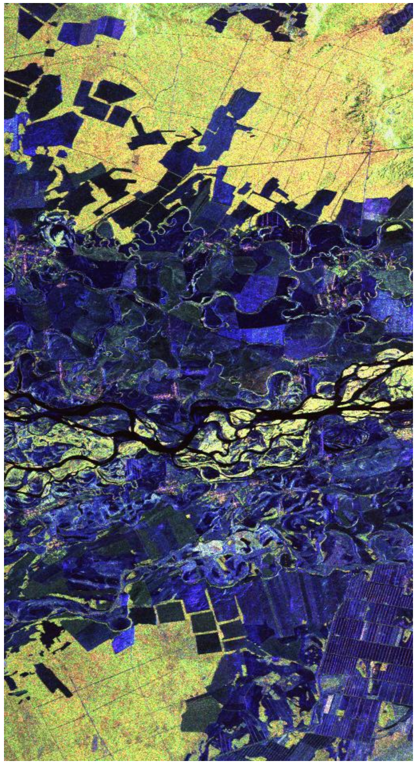

RGB-Coding:

HH-VV

2HV

HH+VV

C-band

L-band

SIR-C/X-SAR-1994-Oct-11 C&L-Band POL-IN-SAR Optimization

By Kostas Papathanassiou, Dissertation DLR, 1994

Interferometric Coherence Images

L-band

SIR-C / Test Site: Kudara, Russia

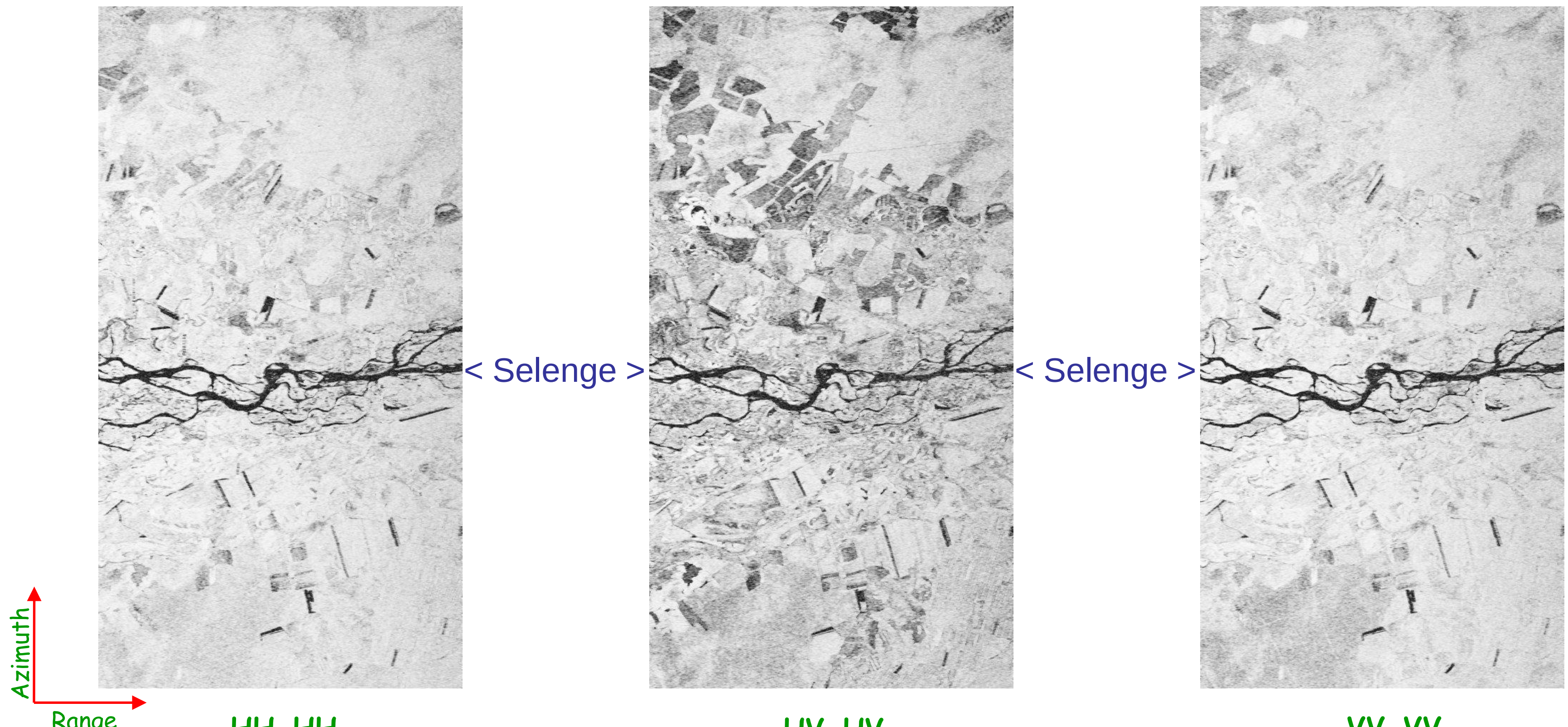

HH-HH **HV-HV** **VV-VV**

SIR-C/X-SAR-1994-Oct-11 C&L-Band POL-IN-SAR Optimization

By Kostas Papathanassiou, Dissertation DLR, 1994

Interferometric Coherence Images

L-band

SIR-C / Test Site: Kudara,Russia

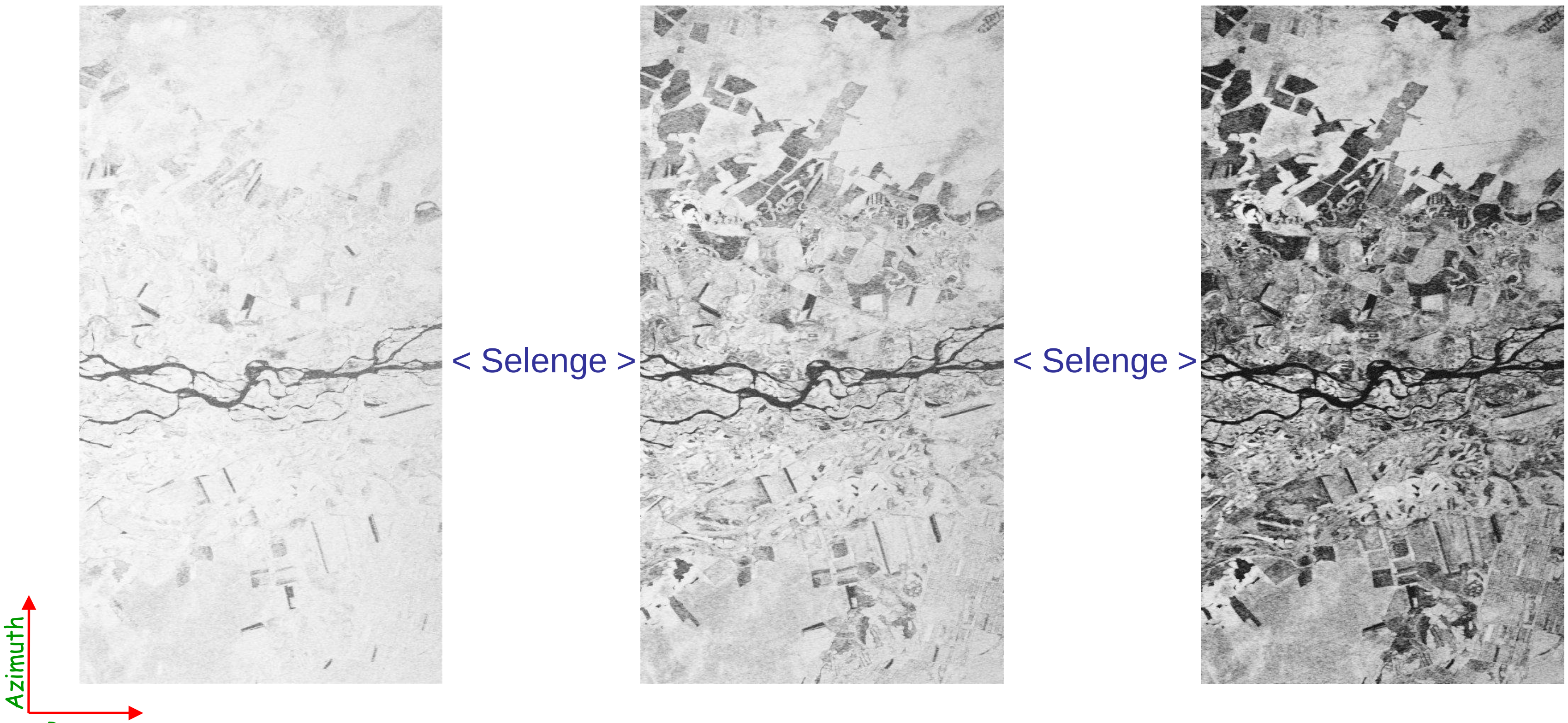

Opt 1 **Opt 2** **Opt 3**

SIR-C/X-SAR-1994-Oct-11 C&L-Band POL-IN-SAR Optimization

By Kostas Papathanassiou, Dissertation DLR, 1994

Random Volume+Ground Scattering Model

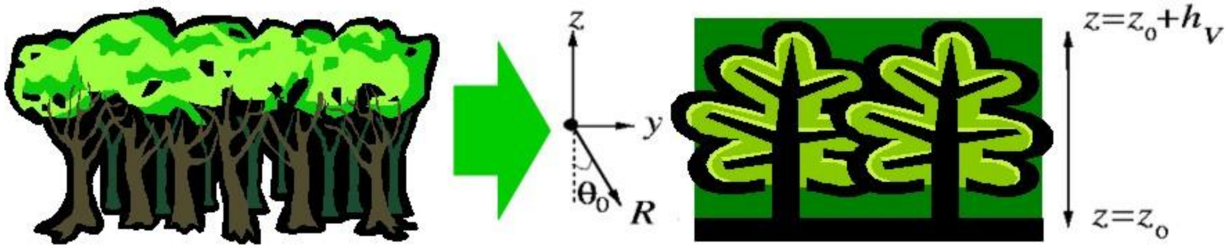

$$\boxed{\tilde{\gamma}(\vec{w}) = \exp(i\varphi_0)\,\frac{\tilde{\gamma}_V + m(\vec{w})}{1 + m(\vec{w})}}$$

Volume Coherence: $\tilde{\gamma}_V = \frac{I}{I_0}$

$$\begin{cases} I = \int_0^{h_V} \exp(i\kappa_z z')\exp\left(\frac{2\ \sigma\ z'}{\cos\theta_0}\right)dz' \\ I_0 = \int_0^{h_V} \exp\left(\frac{2\ \sigma\ z'}{\cos\theta_0}\right)dz' \end{cases}$$

G/V Ratio: $m(\vec{w}) = \frac{m_G(\vec{w})}{m_V(\vec{w})I_0}$ Vertical Wavenumber: $\kappa_z = \frac{\kappa\Delta\theta}{\sin(\theta_0)}$

4 Parameters:

- Volume height h_V
- Extinction σ
- Topography φ_0
- G/V Ratio $m(\vec{w})$

SIR-C/X-SAR-1994-Oct-11 C&L-Band POL-IN-SAR Optimization

By Kostas Papathanassiou, Dissertation DLR, 1994

Phase Difference between Scattering Mechanisms

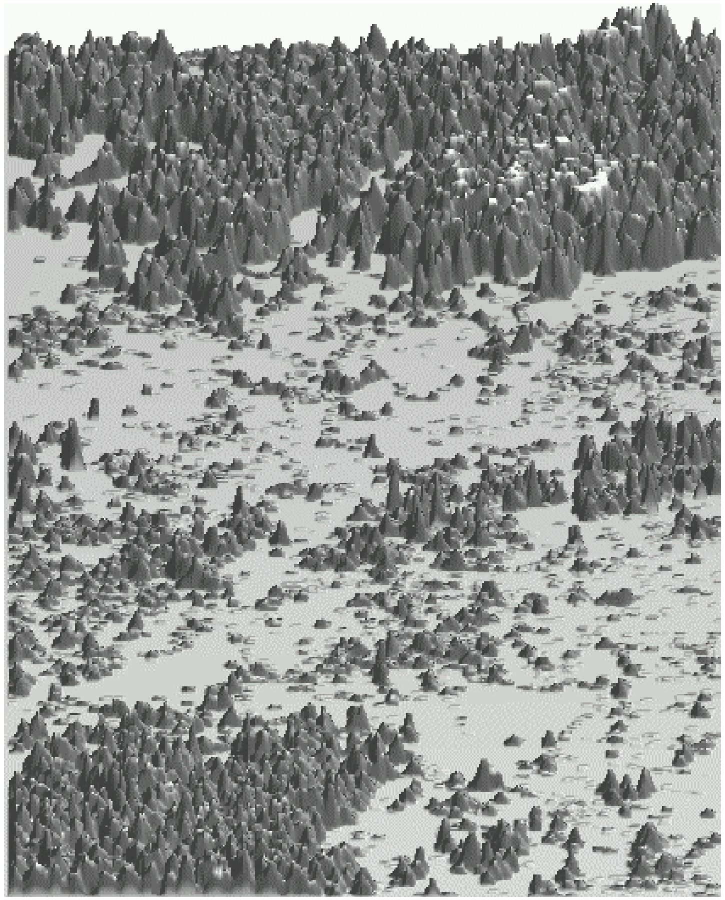

SIR-C : L-band

Test Site: Kudara, Russia

L-band

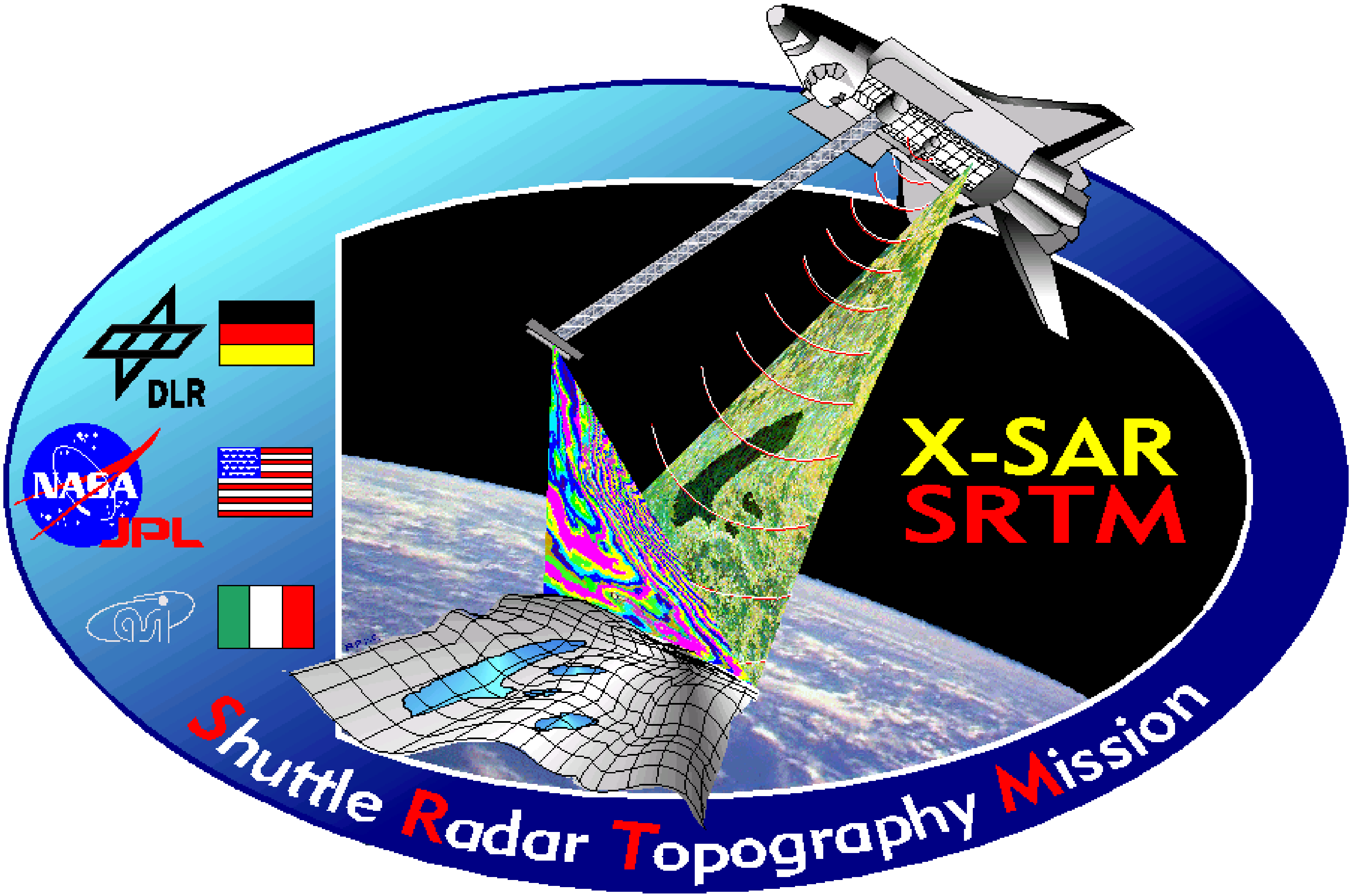
DLR
NASA
JPL
X-SAR
SRTM
Shuttle Radar Topography Mission

SRTM/X-SAR Image of Volcano Koma-ga-Take, Hokkaido

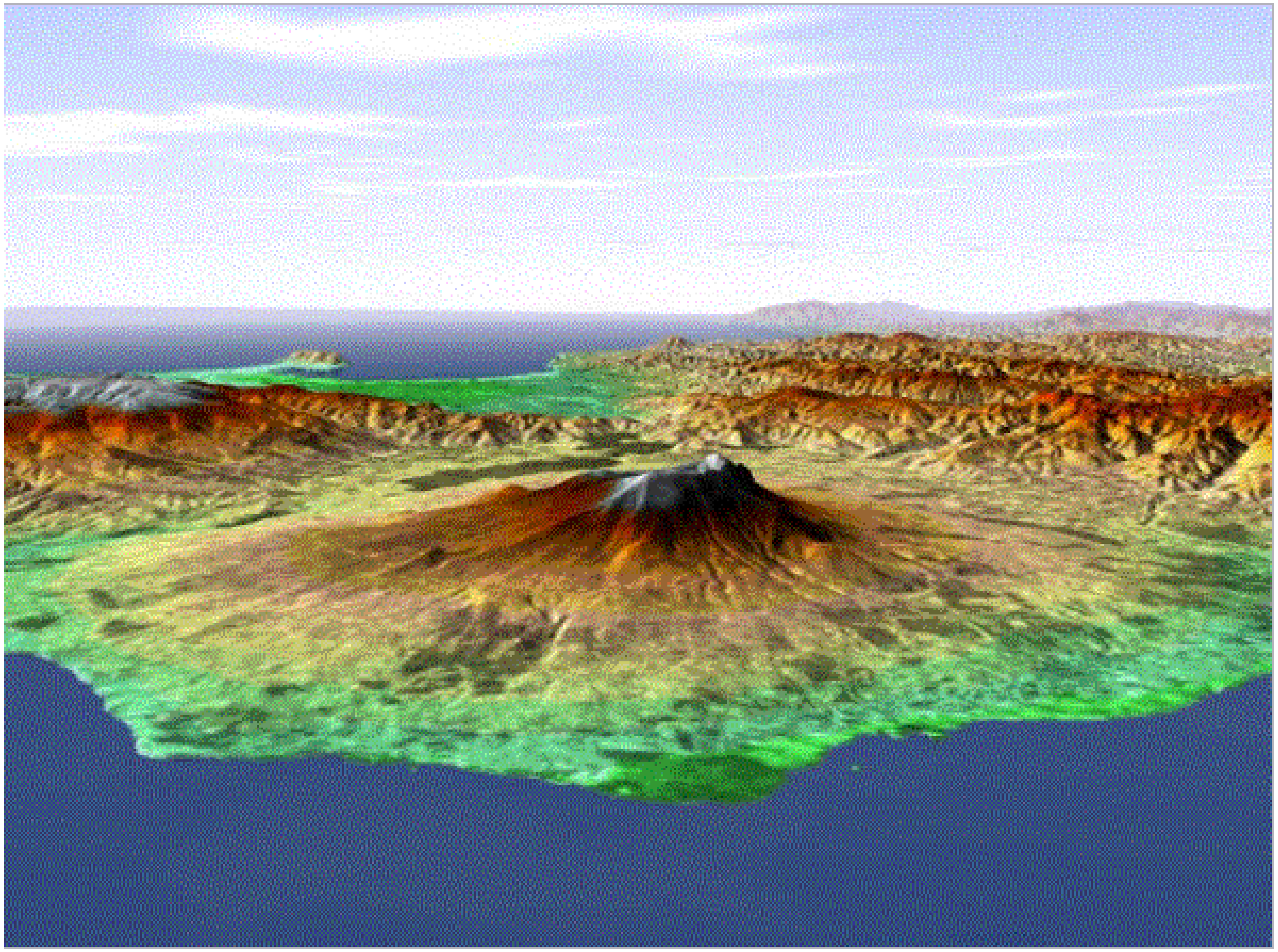

Brief introduction of DIFF-RP-IN-SAR

6D DIFFERENTIAL SAR INTERFEROMETRY
HOW DOES IT WORK?

- Three-pass "repeat track" interferometry uses two baselines $(B_1,\alpha_1);\ (B_2,\alpha_2)$ to acquire interferograms at different times.
- Despite exaggeration in picture on the right, the incidence angles and absolute ranges are nearly the same.
- Now suppose that the surface deformed slightly between the second and third acquisitions in such a way that the range changed by an amount $\Delta\rho$
- In the repeat-track implementation of interferometry, the signal travels each path twice, since the transmitter and receiver are in the same place. Therefore, the interferometric phase is

$$\Delta\phi = \frac{2\pi}{\lambda} 2\times\text{range} = \frac{4\pi}{\lambda}\text{range}$$

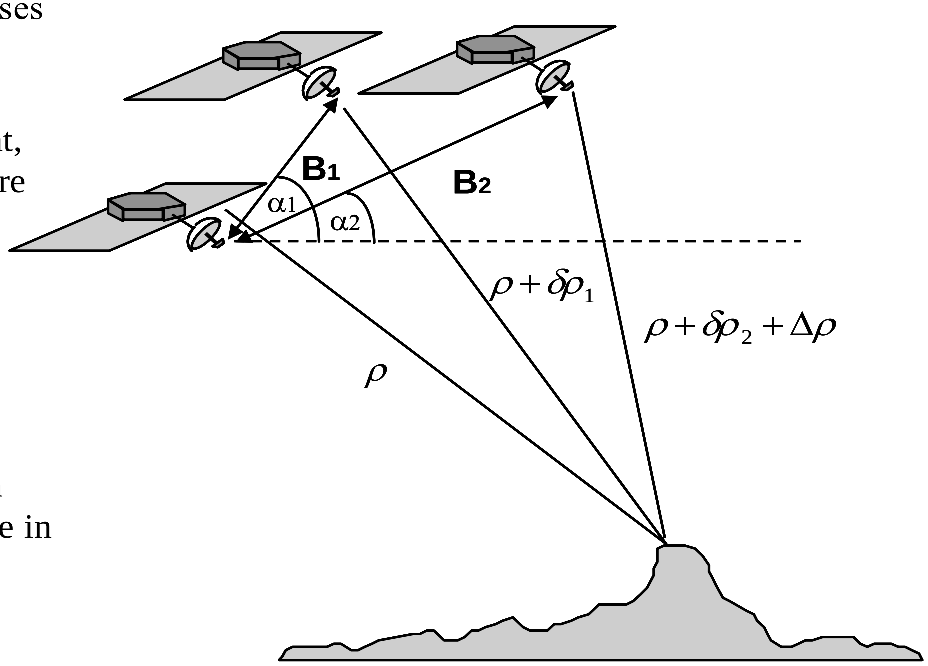

Brief introduction of DIFF-RP-IN-SAR

DIFFERENTIAL SAR INTERFEROMETRY
Example: 1995 North Sakhalin Earthquake (M 7.6)

Radar Differential Interferogram

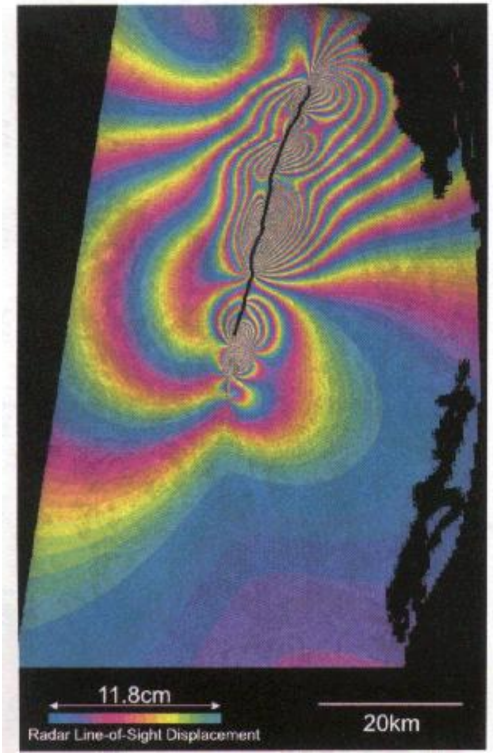

Deformation Model Predictions

Reference: Tobita, et al., Earth Planets Space, 50, 1998

POLARIMETRIC SPACEBORNE SAR SENSORS

RADARSAT 2
CSA / MDA (CA)
2004
C-Band (Quad)

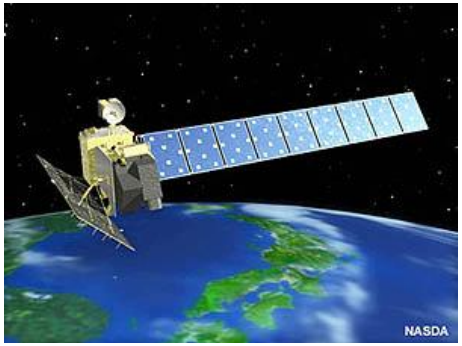

ALOS / PALSAR
NASDA / JAROS (J)
2003
L-Band
HH,VV, (HH,HV), (VV,VH)

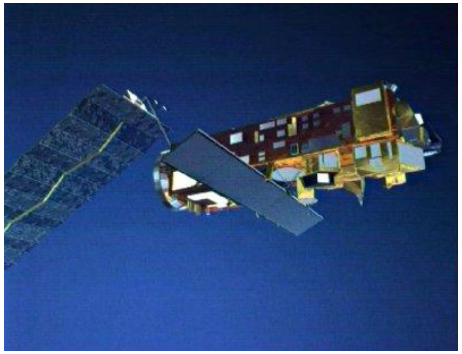

ENVISAT / ASAR
ESA (EU)
2002
C-Band (Sngl / Twin)
HH, VV, (HH,VV), (HH,HV), (HV,VV)

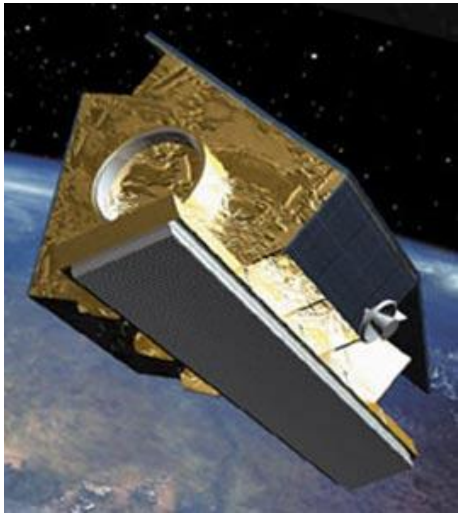

TERRASAR
BMBF / DLR / ASTRIUM
2005
X-Band (Twin)
(HH,VV), (HH,HV), (HV,VV)
L-Band (Quad)

Table 1. Comparison of High-Level Parameters			
Parameter	**PALSAR**	**RADARSAT-2**	**TerraSAR-X**
Orbit: LEO, circular	Sun-synchronous	Sun-synchronous	Sun-synchronous
Repeat Period (*days*)	46	24	11
Equatorial Crossing time (*hrs*)	22:30 (ascending)	18:00 (ascending)	18.00 (ascending)
Inclination (*degrees*)	98.16	98.6	97.44
Equatorial Altitude (*km*)	692	798	515
Wavelength (*Band*)	23 cm (*L*)	5.6 cm (*C*)	3 cm (*X*)
Fully polarimetric mode	Yes	Yes	Yes

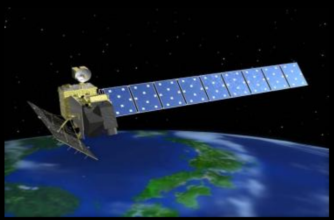

ALOS / PALSAR
Japanese Space Agency (JAXA)
L-Band (quad), 2006

RadarSAT-II
Canadian Space Agency (CSA)
C-Band (quad), 2007

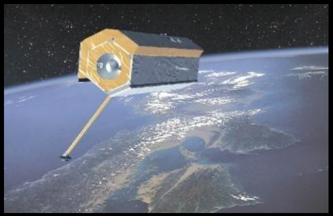

TerraSAR-X
German Aerospace Center (DLR) / Astrium
X-Band (quad), 2007

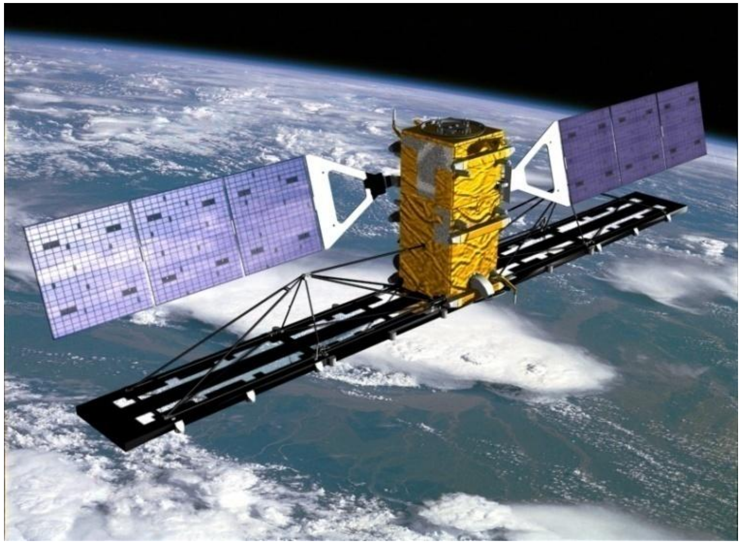

The RADARSAT-2 satellite bus is based on the PRIMA architecture developed by Alenia Spazio of Italy. The bus features a primary rectangular structure with the body-mounted SAR antenna on the Earth-facing panel, and two solar panel arrays mounted on single-degree-of-freedom axels. The antenna and solar arrays are parallel to each other, a consequence of the dawn-dusk sun-synchronous orbit. The X-Band down link presents no interference hazard with the C-band SAR. Dawn-dusk operations permit a relatively large 28-minute data acquisition time per orbit.

Table 1. Selected RADARSAT-2 Modes

Mode	Resolution (m)	Swath (km)	Looks	Polarization
Standard, stripmap	25	100	4	HH or VV
Fine	8	50	8	HH or VV
ScanSAR Wide	100	500	8	HH or VV
Dual polarization	(as above)	(as above)	(as above)	(HH, HV), (VV, VH)
Quad-pol (standard)	25 x 8	25	4	Full polarization
Quad-pol (fine)	8	25	1	Full polarization

RADARSAT-2

Orbit Parameters

ORBIT CHARACTERISTICS	
Altitude (average)	798 km
Inclination	98.6 degrees
Period	100.7 minutes
Ascending node	18 hrs (± 15 min)
Sun-synchronous	14 orbits per day
Repeat cycle	24 days

COVERAGE ACCESS USING 500 KM SWATH WIDTH	
North of 70°	Daily
North of 48°	Every 1-2 days
Equator	Every 2-3 days

RADARSAT-2 will operate in an orbit identical as RADARSAT-1 except for an offset in time

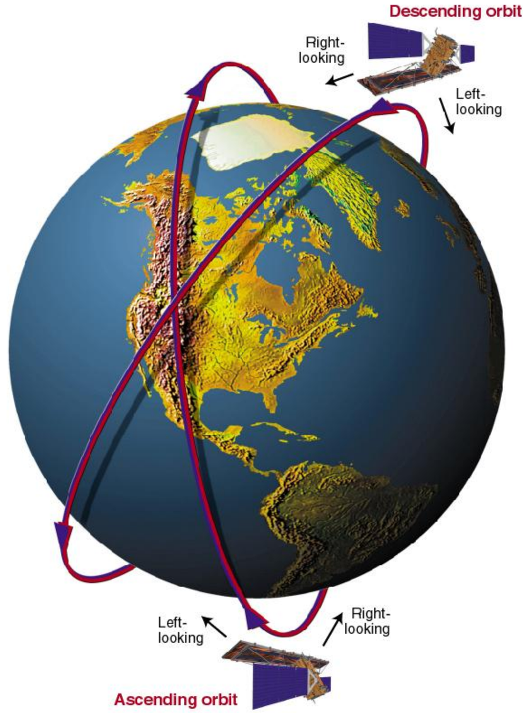

RADARSAT-2 Imaging Modes

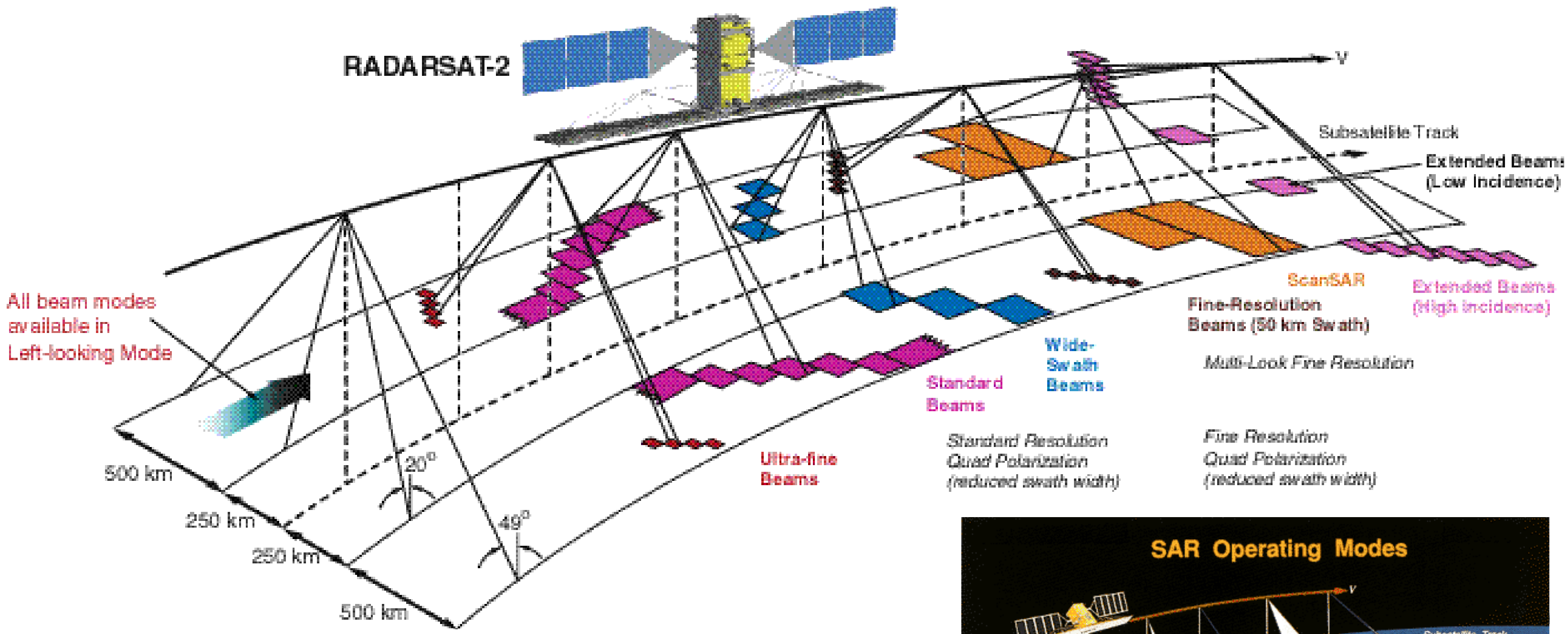

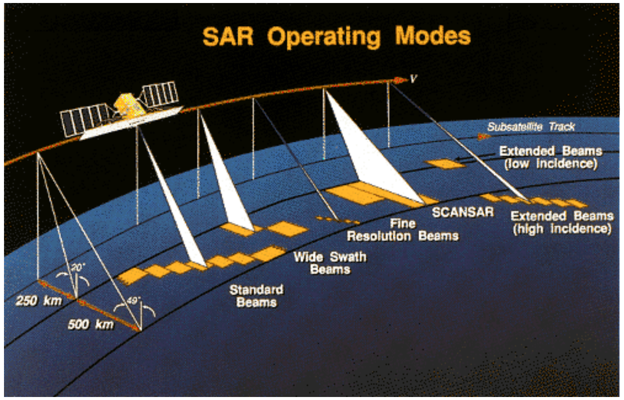

Space-borne RADARSAT2 PolSAR Sensors

San Francisco Bay – July 2008

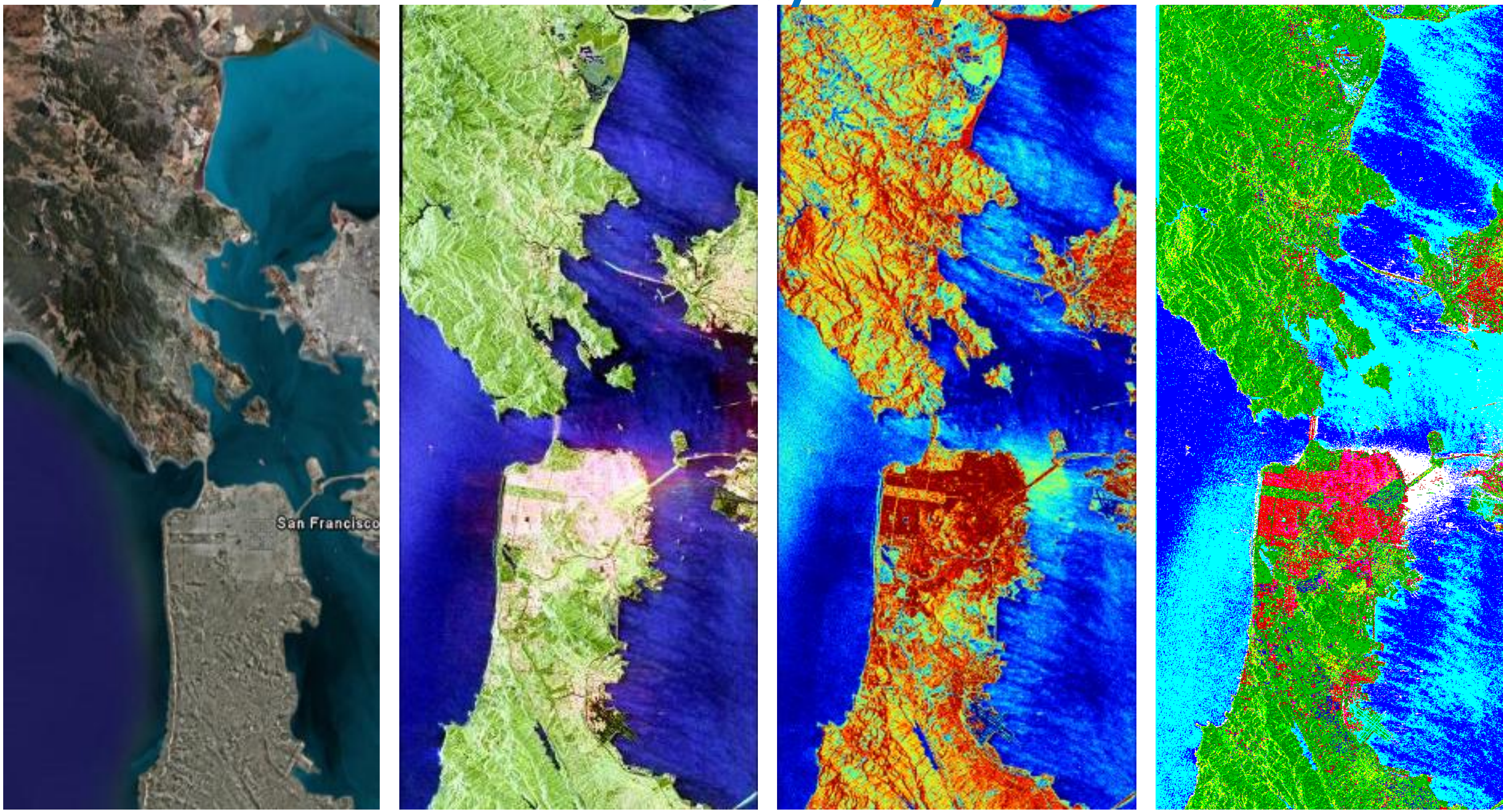

Space-borne RADARSAT-2 PolSAR Sensors

Flevoland – July 2008

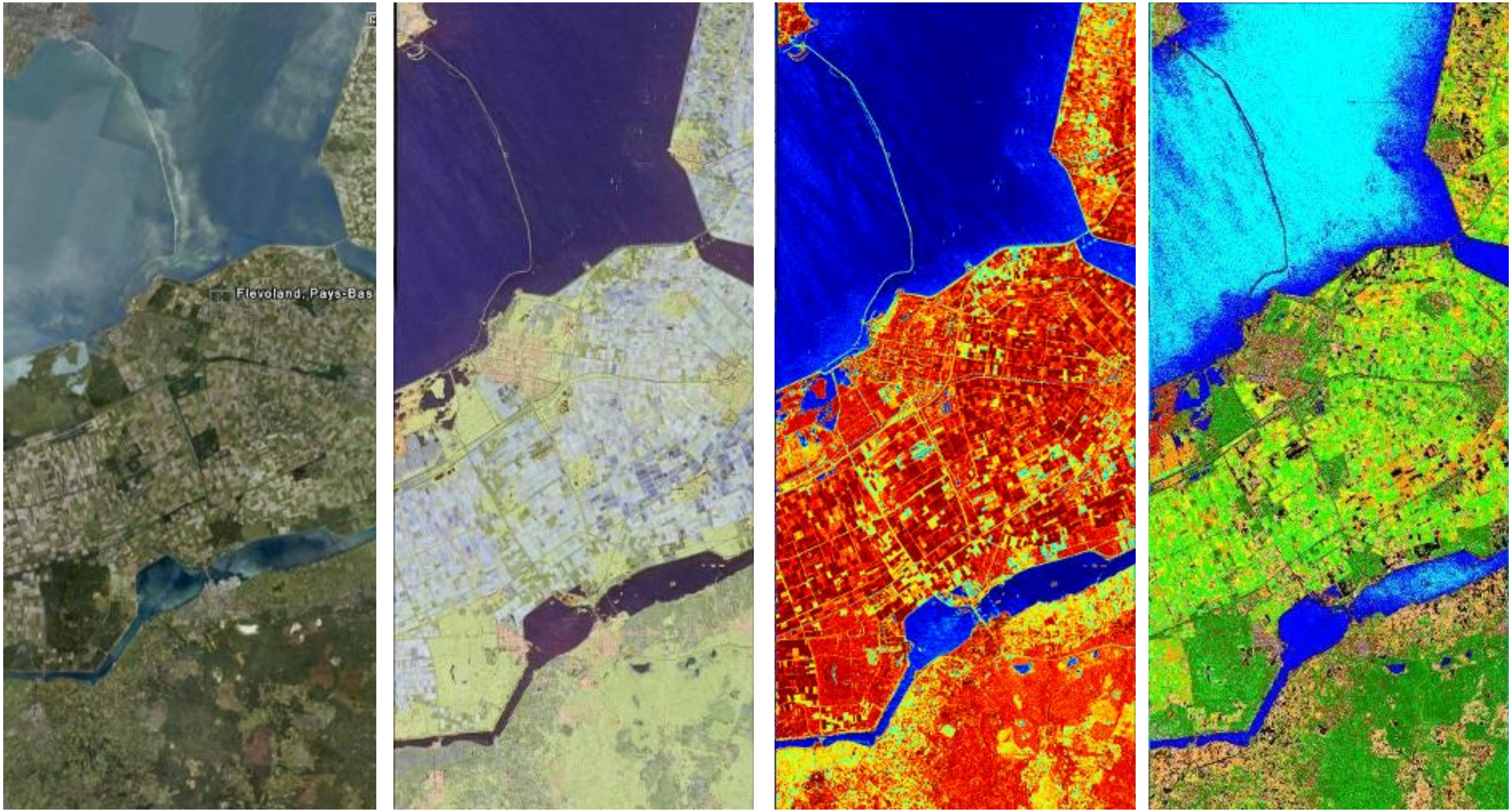

The TerraSAR-X satellite bus claims heritage from the successful Champ and Grace Missions. The spacecraft bus features a primary structure with a hexagonal cross section. The active phased array SAR antenna is attached on the Earth-facing panel in the figure. The solar array is body-mounted, a satisfactory scheme for the sun-synchronous orbit plan. The X-Band down link antenna is mounted on a 3.3 m long deployable boom in order to prevent interference with the X-Band SAR instrument. This concept enables simultaneous data acquisition and data down link.

Table 1. Selected Mode Parameters

Mode (selected)	Resolution (m)	Swath (km)	Looks	Polarization
Standard, stripmap	3	30	1	HH or VV
High-resolution Spotlight	1	10	1	HH or VV
ScanSAR	16	100	1	HH or VV
Quad-pol (experimental)	3	15	1	Full polarization

Dual Receive Antenna Mode (DRA Mode)

Transmit

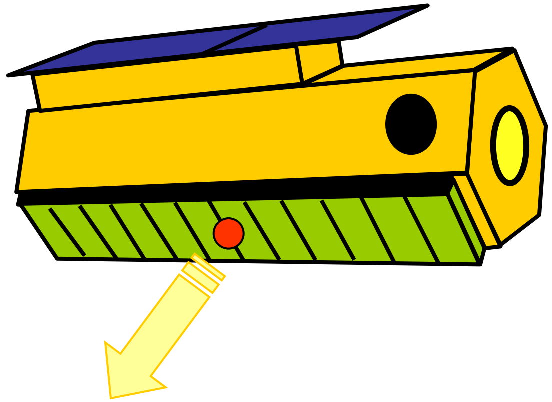

Receive

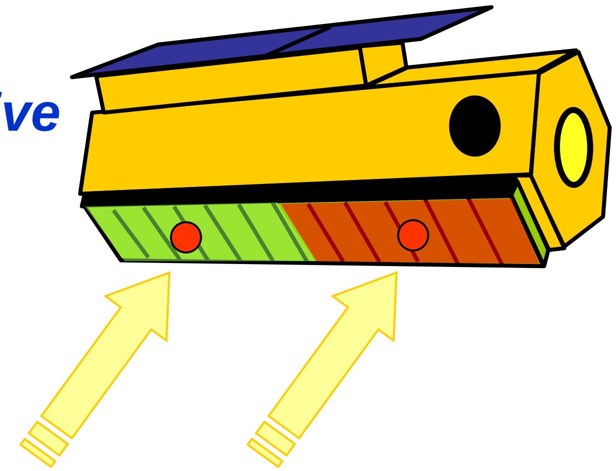

Principle

- **For <u>transmit</u> the full antenna is used**
- **For <u>receive</u> the antenna is ‚electrically' divided into two sections in azimuth direction ➔ two independent receive channels are available**

New Experimental Modes

- **Along-Track Interferometry (ATI)**

  (Moving Target Indication, Widespread Traffic Control, Ocean Current Measurement)

- **Quad polarization**

  (Sea/Ice, Snow Cover, Urban Environment)

Quadpol switching scheme

TX:	V	H	V	H	…
RX_1:	V	V	V	V	…
RX_2:	H	H	H	H	…
CH_1:	VV	HV	VV	HV	…
CH_2:	VH	HH	VH	HH	…

Polarization Modes

Single Polarization
- 1 polarization channel, {HH, VV}
- stripmap, spotlight, ScanSAR

Dual Polarization
- 2 polarization channels, {HH/VV, HH/HV, VV/VH}
- stripmap, spotlight
- coherent pol. phase
- smaller elevation beam

Twin Polarization
- 2 polarization channels, {HH/VV, HH/HV, VV/HV}
- Stripmap, incoherent pol-phase, full el beam

Quad Polarization
- All 4 pol. channels
- Stripmap
- coherent pol. Phase
- smaller elevation beam
- Experimental product

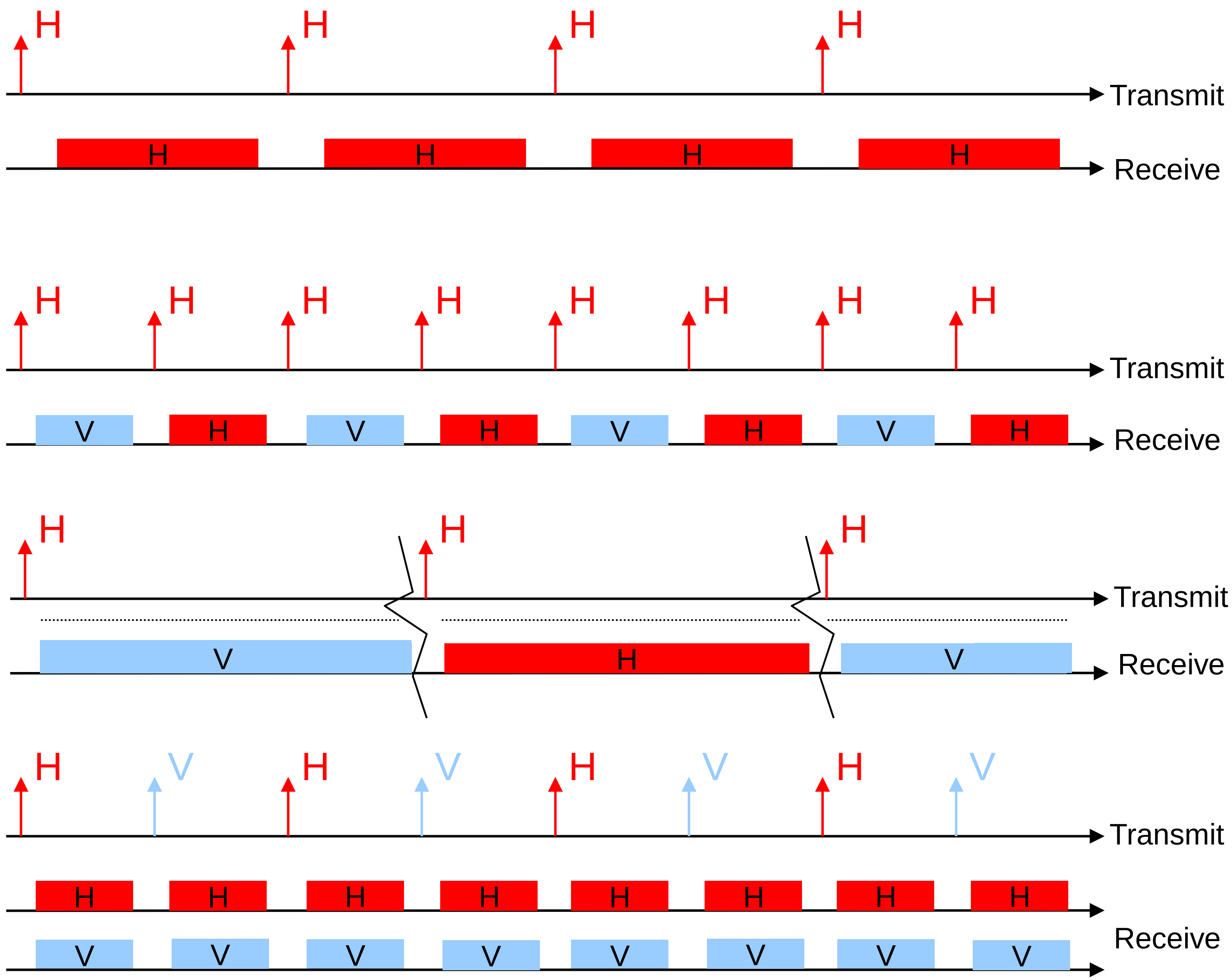

First TerraSAR-X Quadpol Image!

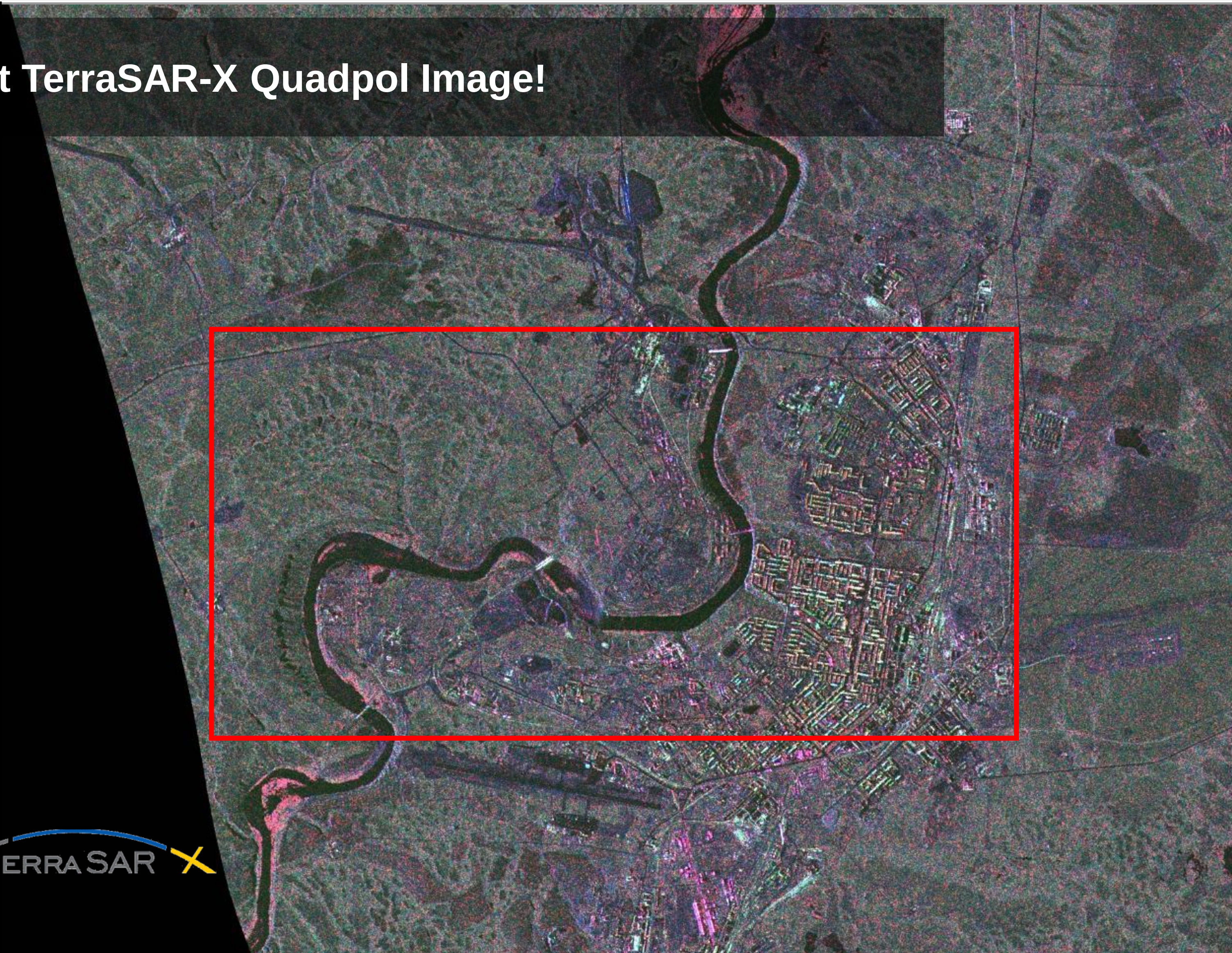

Workuta, Russia
Stripmap
June 23, 2008
red: HH-VV
green: (HV+VH)/2
blue: HH+VV

DLR

TerraSAR X

Polarimetric Analysis (dual pol HHVV vs quad pol)

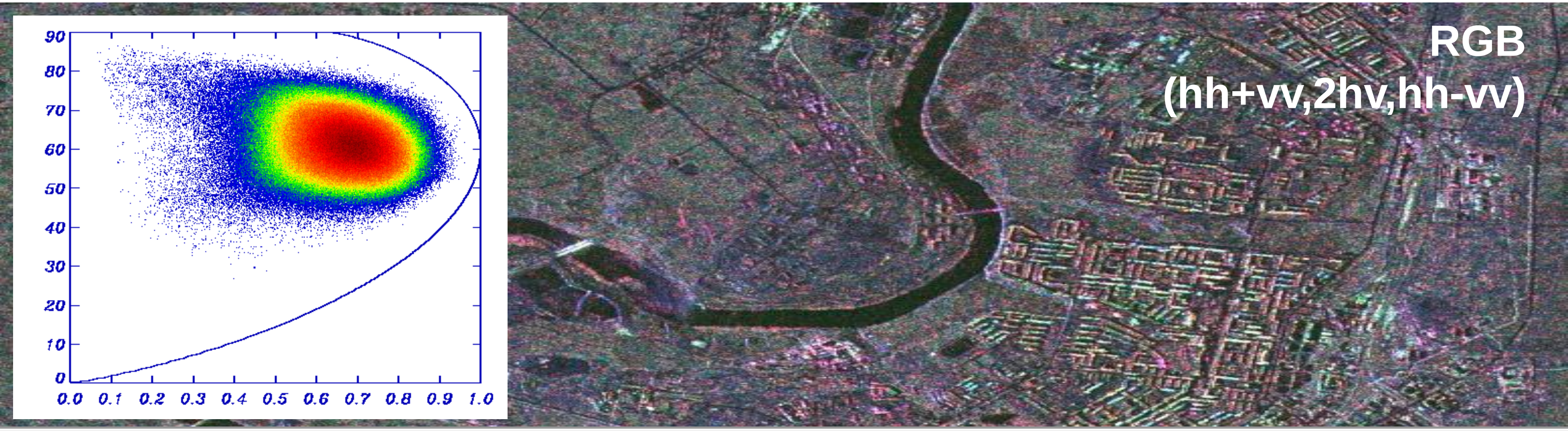

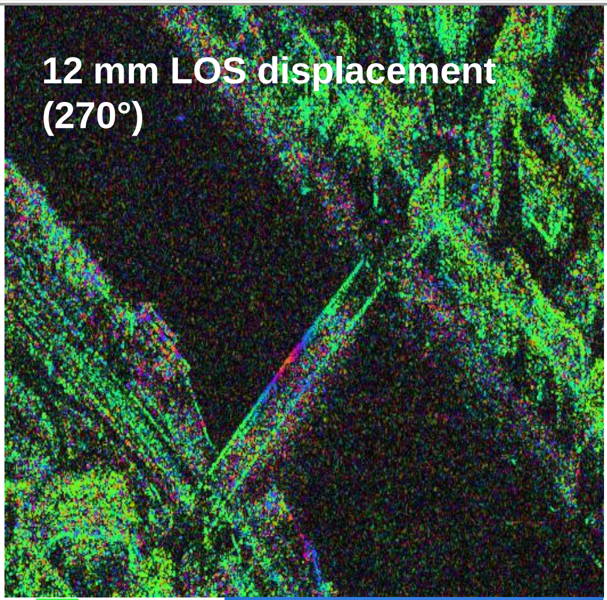
12 mm LOS displacement
(270°)


360°
0°


325 m

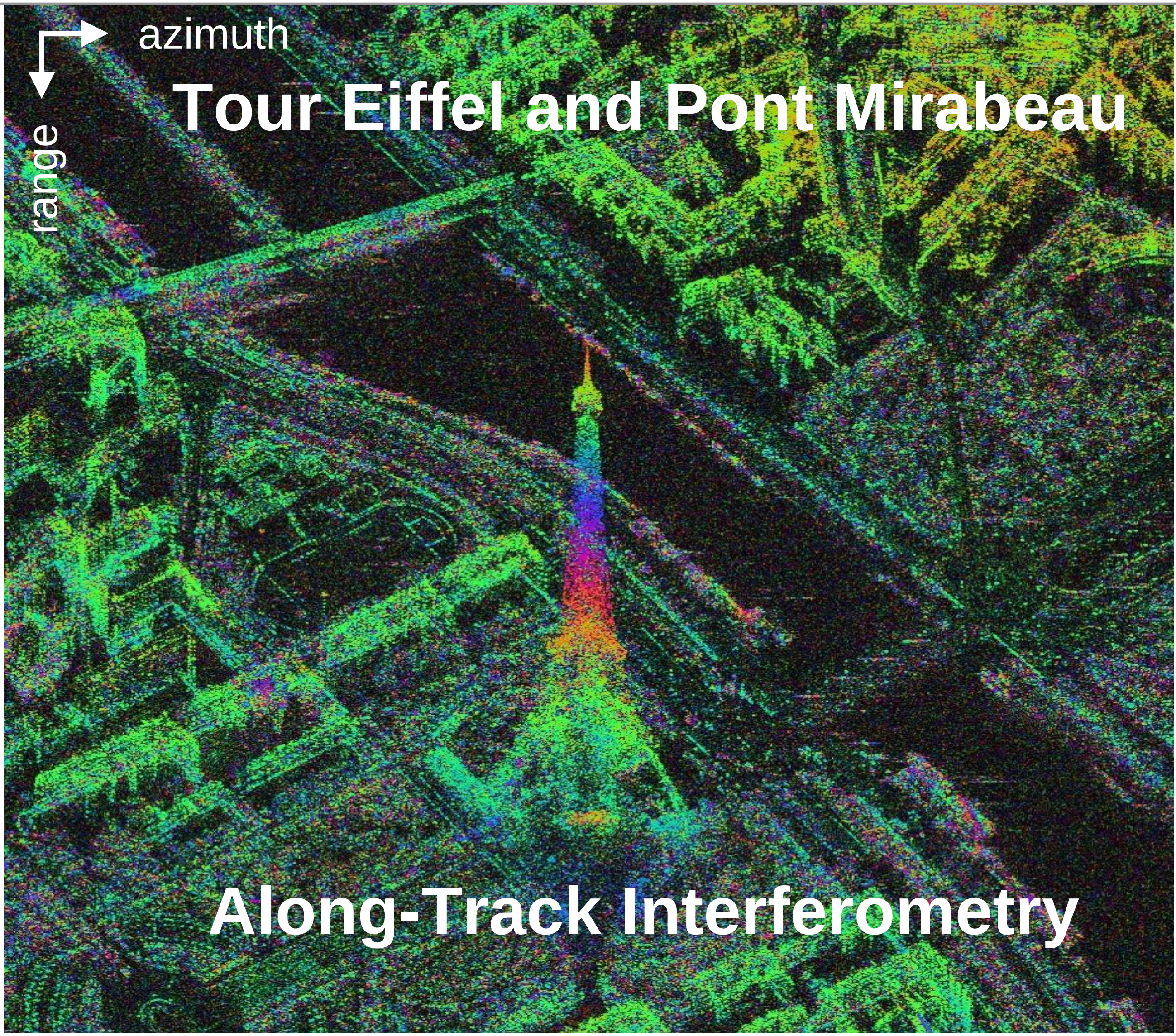
azimuth
range
Tour Eiffel and Pont Mirabeau
Along-Track Interferometry

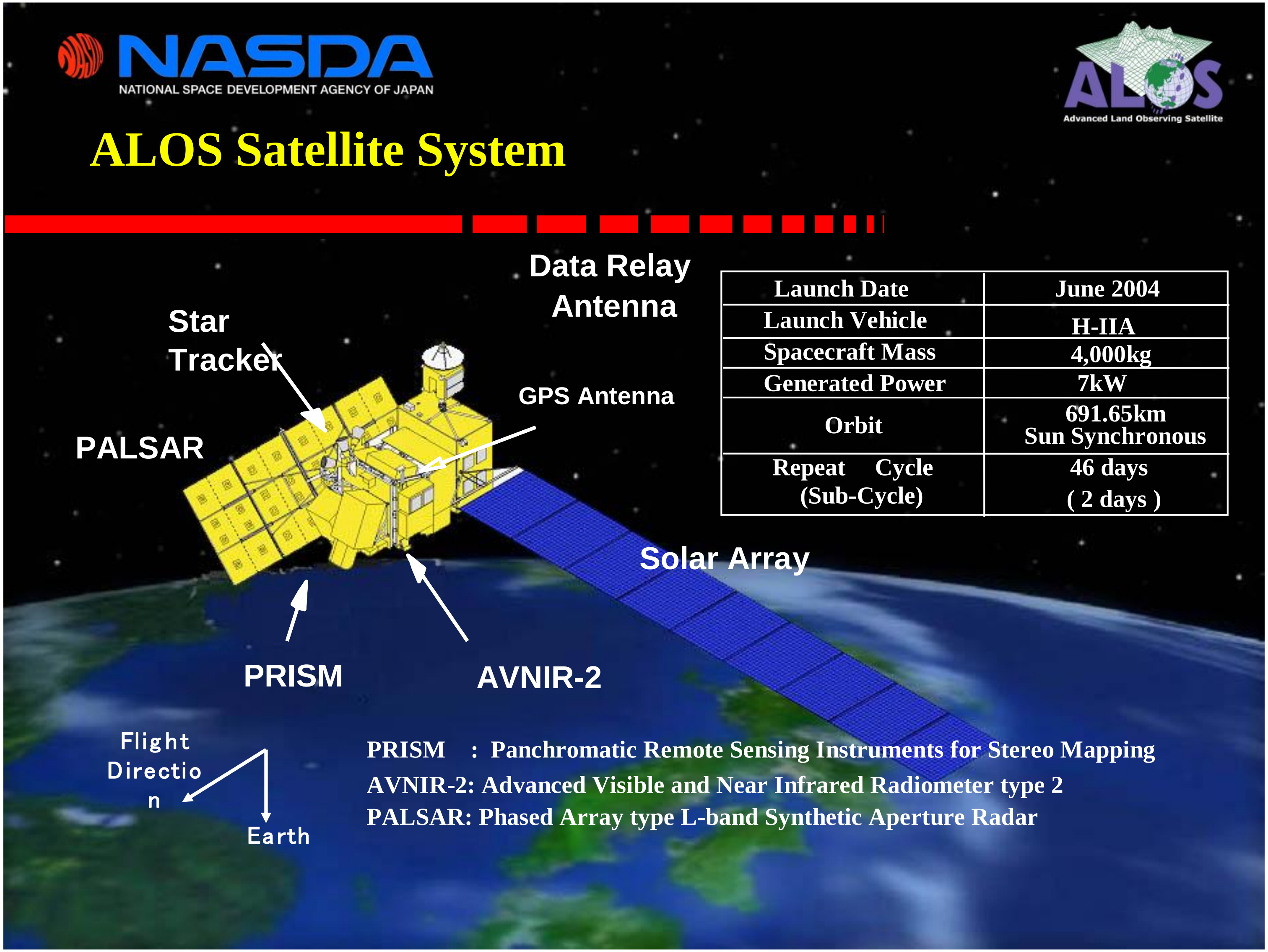

Launch Date	June 2004
Launch Vehicle	H-IIA
Spacecraft Mass	4,000kg
Generated Power	7kW
Orbit	691.65km Sun Synchronous
Repeat Cycle (Sub-Cycle)	46 days (2 days)

PRISM : Panchromatic Remote Sensing Instruments for Stereo Mapping
AVNIR-2: Advanced Visible and Near Infrared Radiometer type 2
PALSAR: Phased Array type L-band Synthetic Aperture Radar

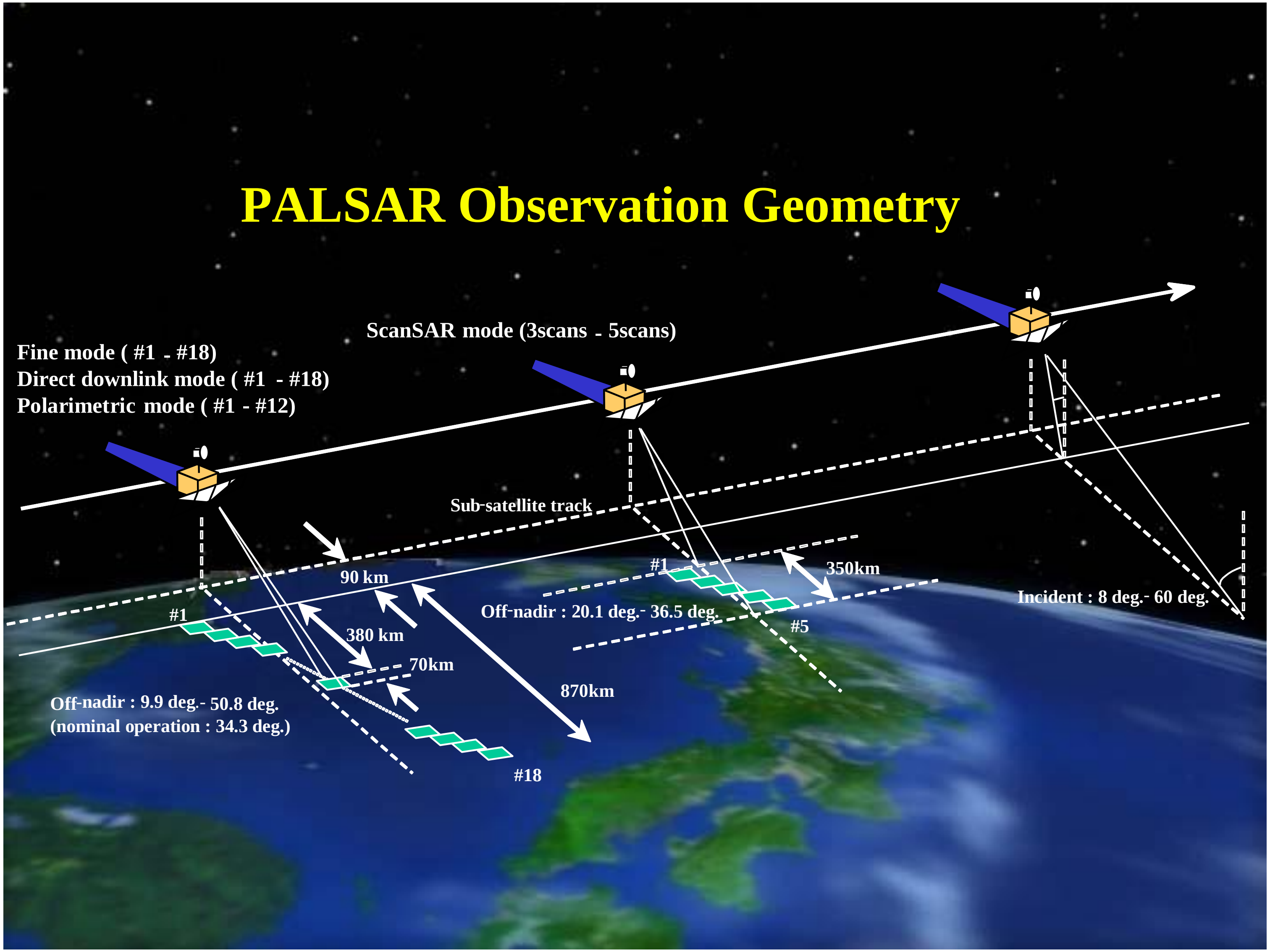
PALSAR Observation Geometry
ScanSAR mode (3scans - 5scans)
Fine mode (#1 - #18)
Direct downlink mode (#1 - #18)
Polarimetric mode (#1 - #12)
Sub-satellite track
90 km
#1
350km
Off-nadir : 20.1 deg.- 36.5 deg.
Incident : 8 deg.- 60 deg.
#1
380 km
#5
70km
870km
Off-nadir : 9.9 deg.- 50.8 deg.
(nominal operation : 34.3 deg.)
#18

ALOS is one of the largest Earth observing satellites ever developed, at 3850 kg. It is in a near-exact 45-day repeat sun-synchronous orbit, 690 km altitude above the equator. The active phased array SAR antenna is obliquely Earth-facing, aligned with the spacecraft velocity vector. The solar array is arranged at right angles to the orbit plane, consistent with the near-mid-day orbit phasing. The X-band down-link must be shared with optical instruments, which constrains SAR operation times.

Table 1. Selected PALSAR Mode Parameters

Mode (selected)	Resolution (m)	Swath (km)	Looks	Polarization
Standard, stripmap	20 x 10	70	2	HH or VV
Fine	10	70	1	HH or VV
ScanSAR (5-beam)	~ 100	350	8	HH or VV
Dual polarization	(as above)	(as above)	(as above)	(HH, HV), (VV, VH)
Quad-pol	30 x 10	30	2	Full polarization

ALOS-PALSAR In Orbit Demonstration Study

Exploration / Validation of the INDREX-II Campaign

Classification of Land Cover Types using PALSAR WB & Dual Pol

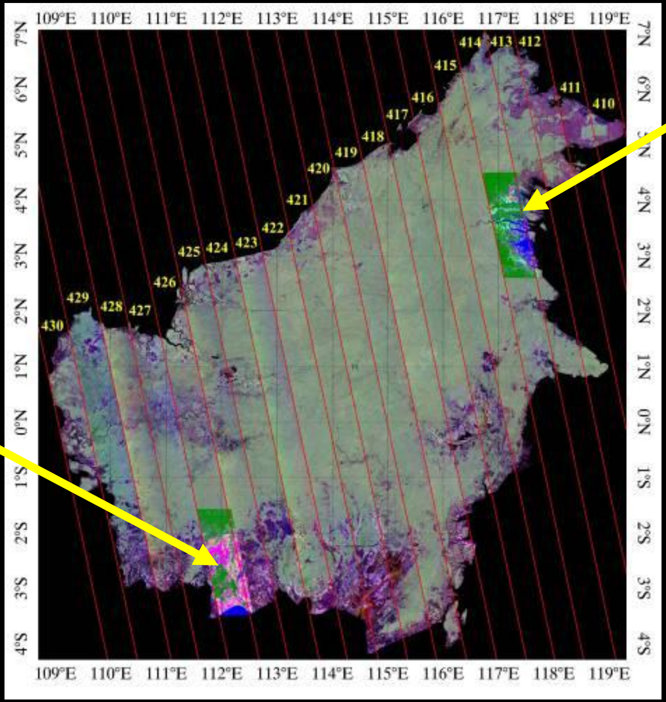

414: Mangrove area

426: Oil palm development area

Courtesy Prof. D. Hoekman – POLINSAR09

SarVision

WAGENINGEN UNIVERSITY ENVIRONMENTAL SCIENCES

esa

ALOS-PALSAR In Orbit Demonstration Study

Exploration / Validation of the INDREX-II Campaign

SarVision — Wageningen University Environmental Sciences

Classification of Land Cover Types using PALSAR WB & Dual Pol

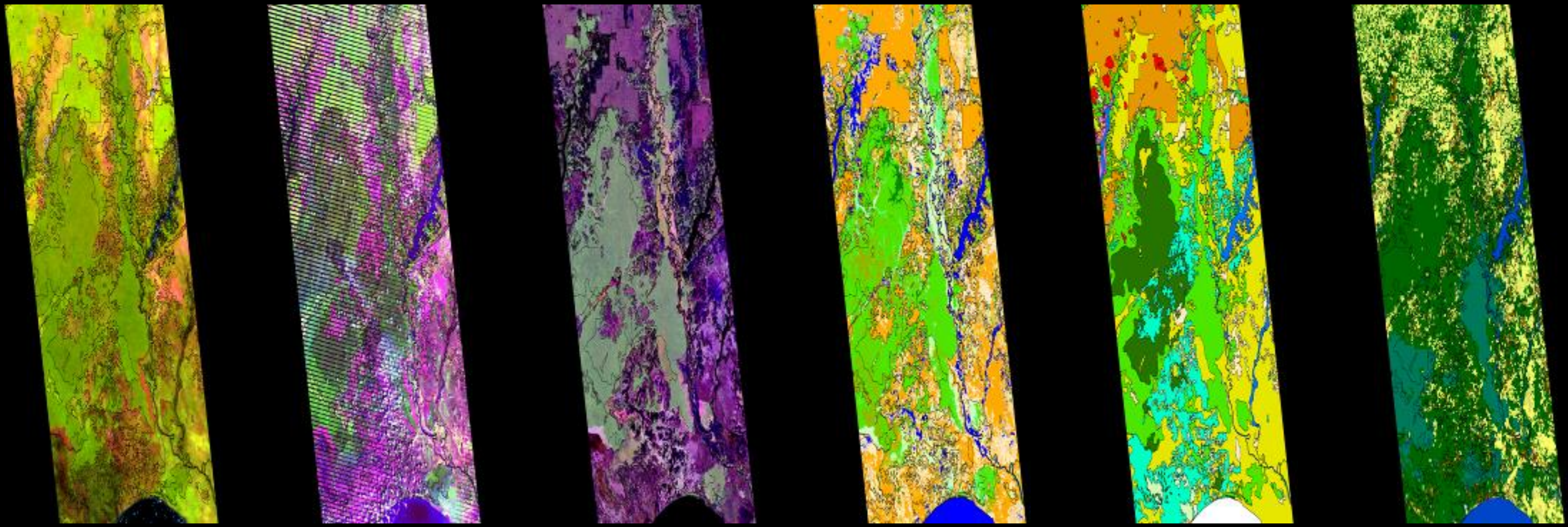

(a) (b) (c) (d) (e) (f)

(a) SarVision MODIS 2007 aggregate;
(b) Landsat 2008;
(c) PALSAR FBS-FBD 2007

(d) PALSAR 2007 classification;
(e) Ministry of Forestry 2005 classification based on Landsat;
(f) GlobCover 2005-2006 regional classification

Courtesy Prof. D. Hoekman – POLINSAR09

esa

ALOS-PALSAR In Orbit Demonstration Study

Exploration / Validation of the INDREX-II Campaign

SarVision WAGENINGEN UNIVERSITY ENVIRONMENTAL SCIENCES

Classification of Land Cover Types using PALSAR WB & Dual Pol

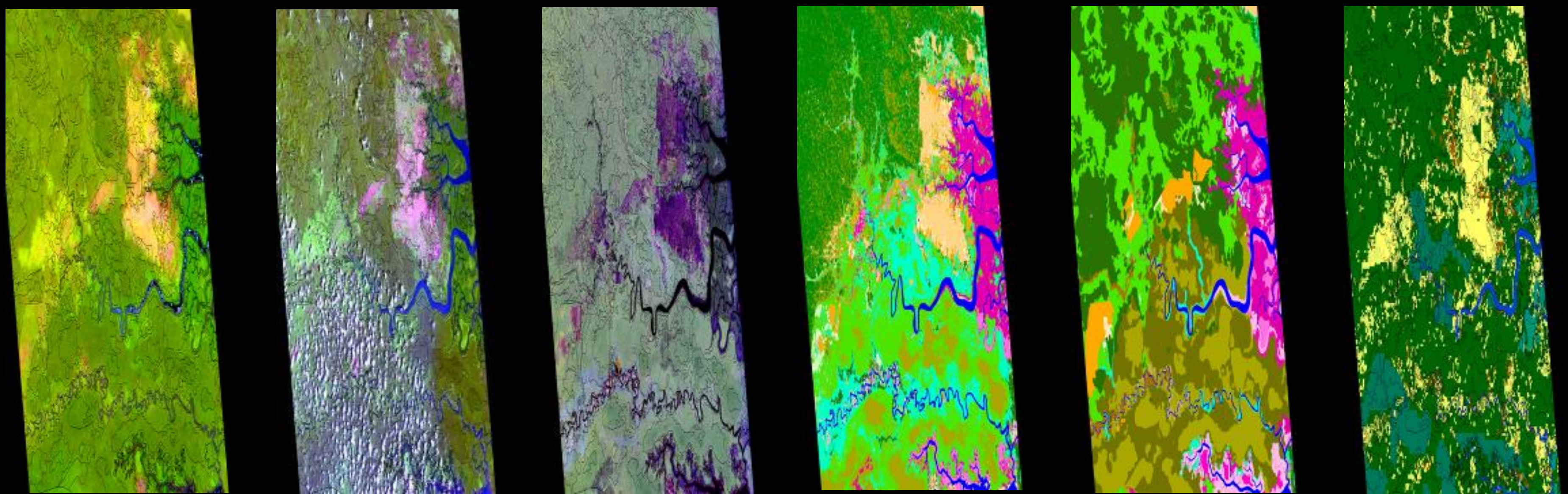

(a) (b) (c) (d) (e) (f)

(a) SarVision MODIS 2007 aggregate;
(b) Landsat 2007;
(c) PALSAR FBS-FBD 2007
(d) PALSAR 2007 classification;
(e) NRM 1997 classification based on Landsat;
(f) GlobCover 2005-2006 regional classification

esa

Courtesy Prof. D. Hoekman – POLINSAR09

ALOS-PALSAR Polarimteric Mode

Ascending

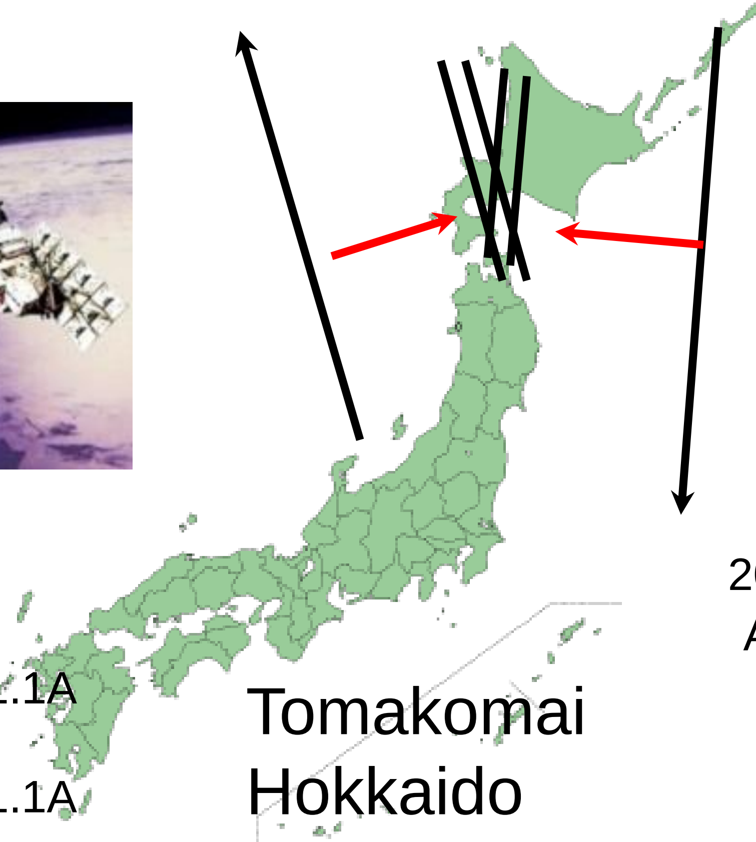

Descending

2006/8/17
ALPSRP029970850-1.1A
2006/10/2
ALPSRP036680850-1.1A

2007/10/10
ALPSRP091090850-1.1A

Tomakomai
Hokkaido

2006/8/19
ALPSRP030192750-1.1D

©JAXA, METI

Yoshio Yamaguchi

Niigata University

POLSAR image analysis

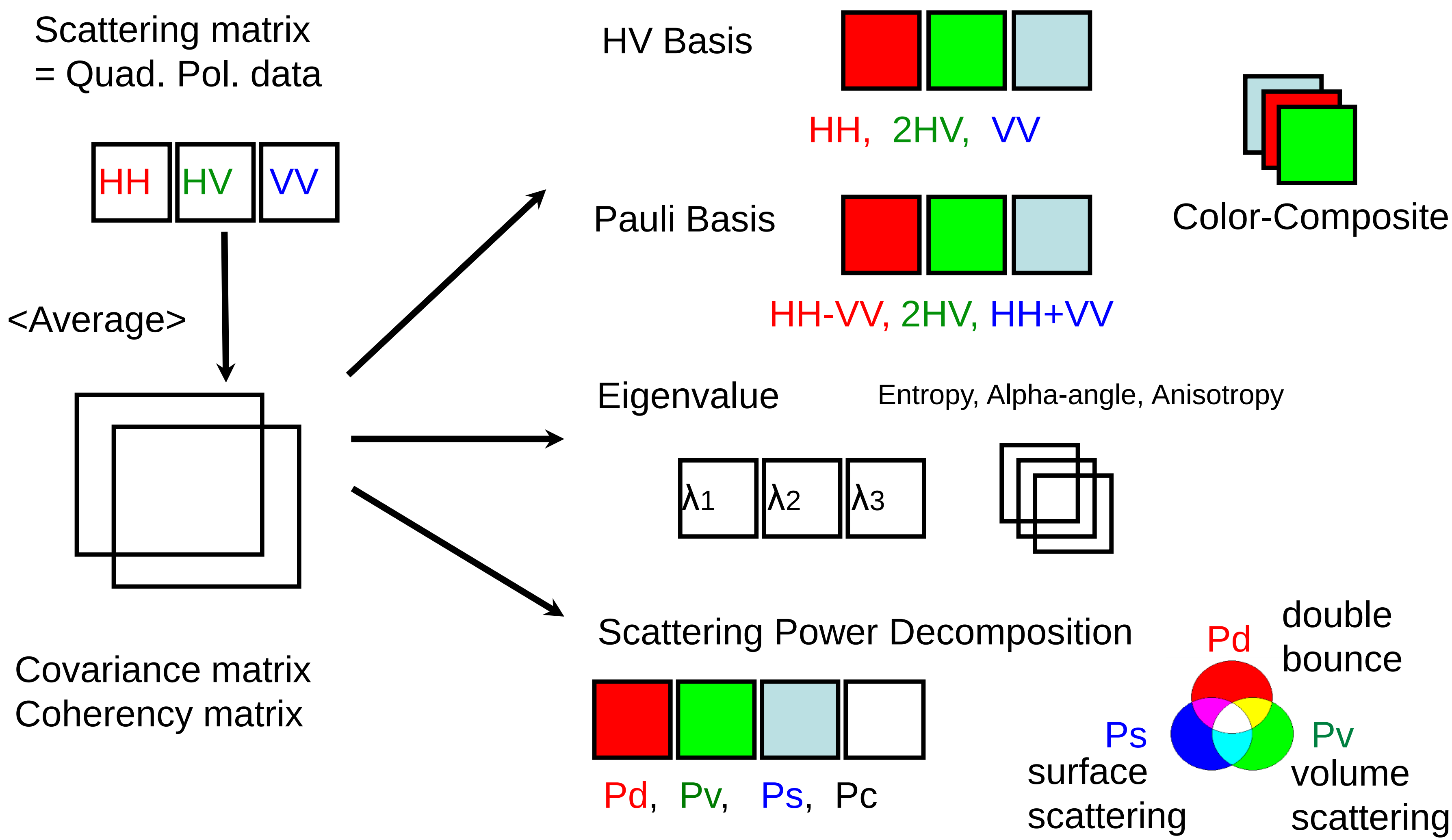

Surface scattering + Double bounce + Volume scattering + Helix scattering

expansion matrix

$$\begin{bmatrix} 1 & \beta^* & 0 \\ \beta & |\beta|^2 & 0 \\ 0 & 0 & 0 \end{bmatrix} \quad \begin{bmatrix} |\alpha|^2 & \alpha & 0 \\ \alpha^* & 1 & 0 \\ 0 & 0 & 0 \end{bmatrix} \quad \frac{1}{30}\begin{bmatrix} 15 & 5 & 0 \\ 5 & 7 & 0 \\ 0 & 0 & 8 \end{bmatrix}, \ \frac{1}{4}\begin{bmatrix} 2 & 0 & 0 \\ 0 & 1 & 0 \\ 0 & 0 & 1 \end{bmatrix}, \ \frac{1}{30}\begin{bmatrix} 15 & -5 & 0 \\ -5 & 7 & 0 \\ 0 & 0 & 8 \end{bmatrix} \quad \frac{1}{2}\begin{bmatrix} 0 & 0 & 0 \\ 0 & 1 & \pm j \\ 0 & \mp j & 1 \end{bmatrix}$$

Scattering Power

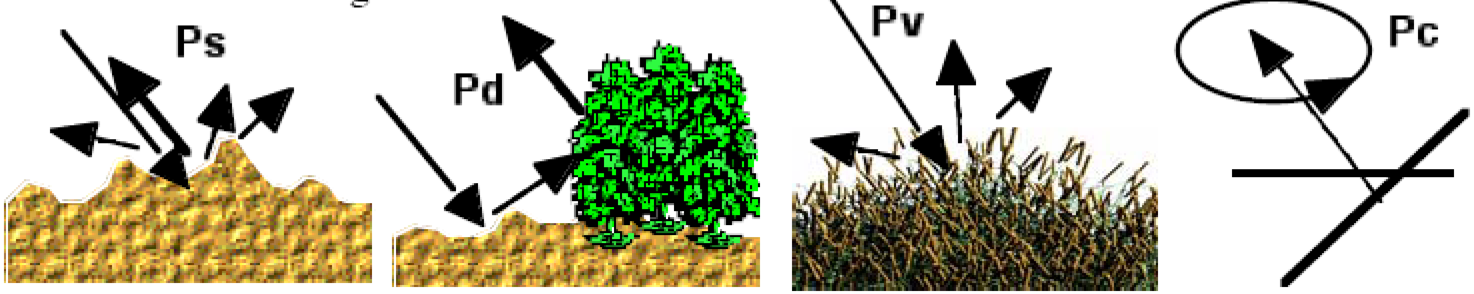

The four-component decomposition of scattering powers Ps, Pd, Pv, and Pc

Fugen-dake
Unzen

32.825N
130.364E

Google earth optical image

ALOS-PALSAR pol. image

ALPSRP072570650-1.1A

©JAXA, METI

2007/6/5

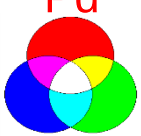

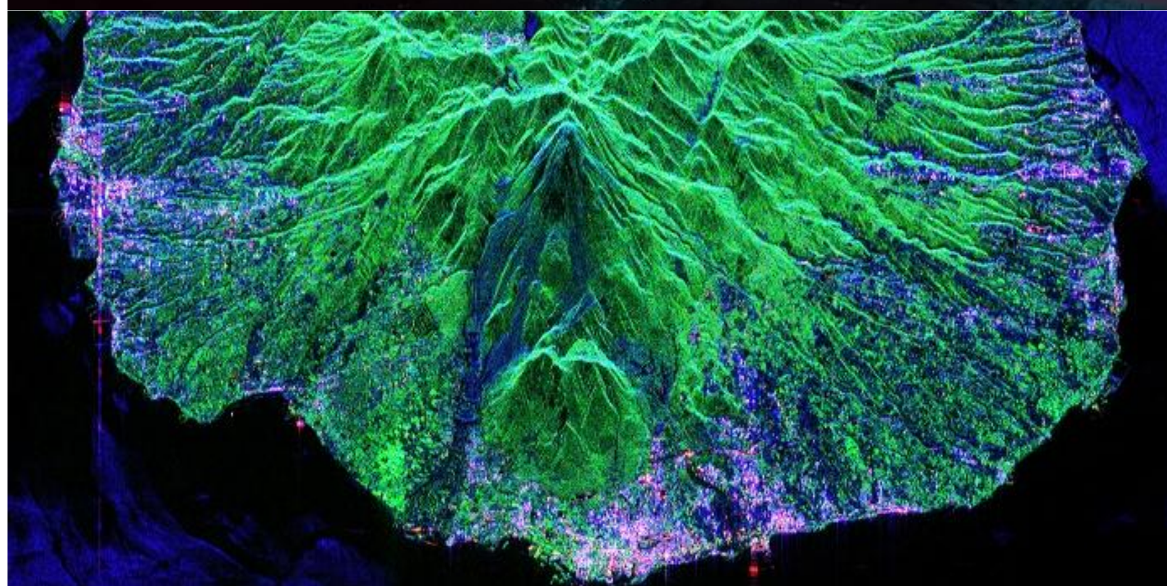

Niigata University

Scattering power decomposition

Pd

Ps  Pv

Niigata University

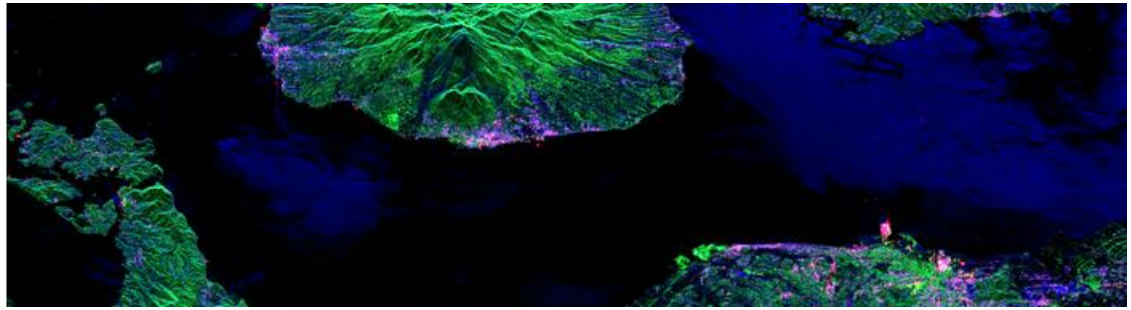

Pd, Pv, Ps

Pauli-basis

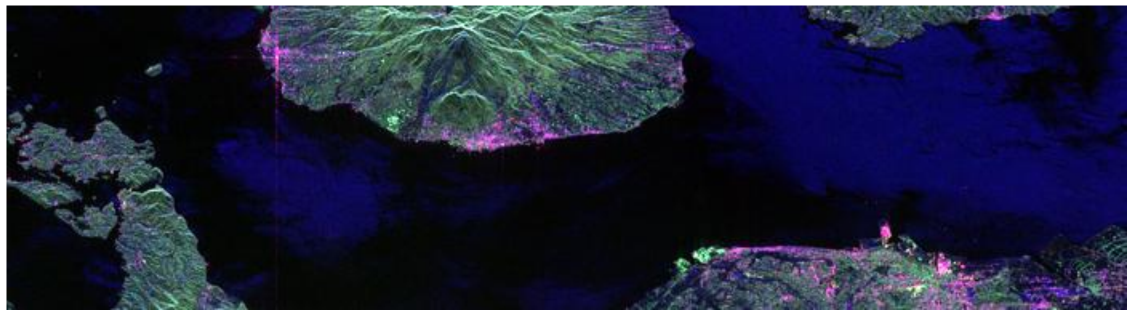

HH-VV, 2HV, HH+VV

HV-basis

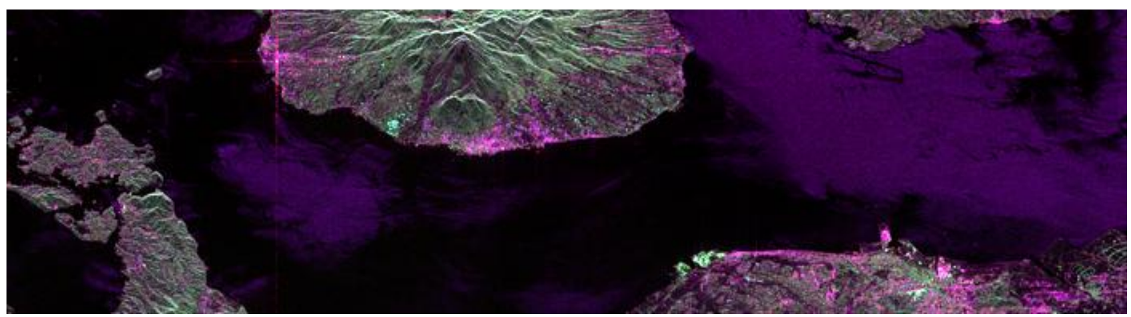

HH, 2HV, VV

Fugen-dake Unzen

32.825N
130.364E

2007/6/5 ALPSRP072570650-1.1A

©JAXA, METI

4-component scattering power decomposition algorithm using rotated coherency matrix

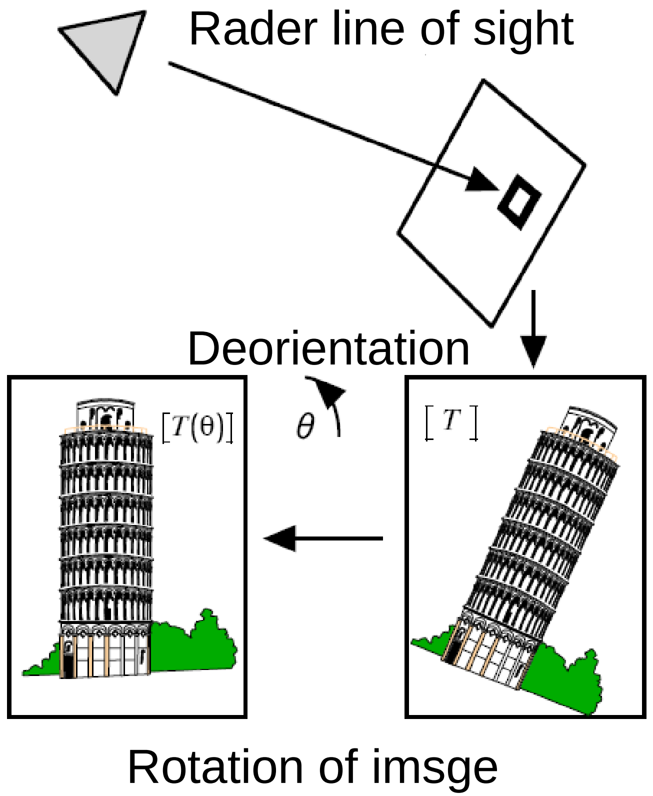

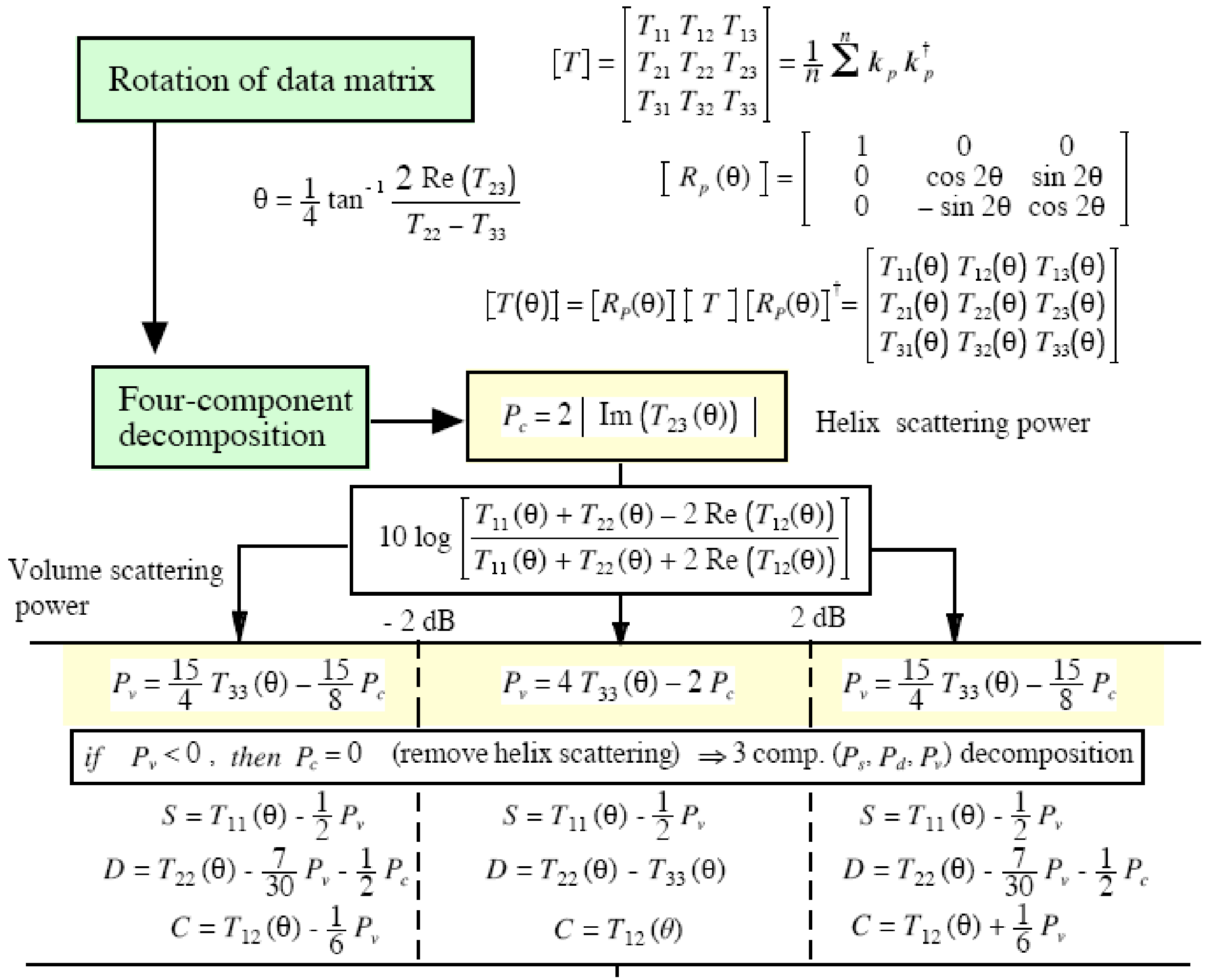

4-compornent scattering power decomposition algorithm using rotated coherency matrix

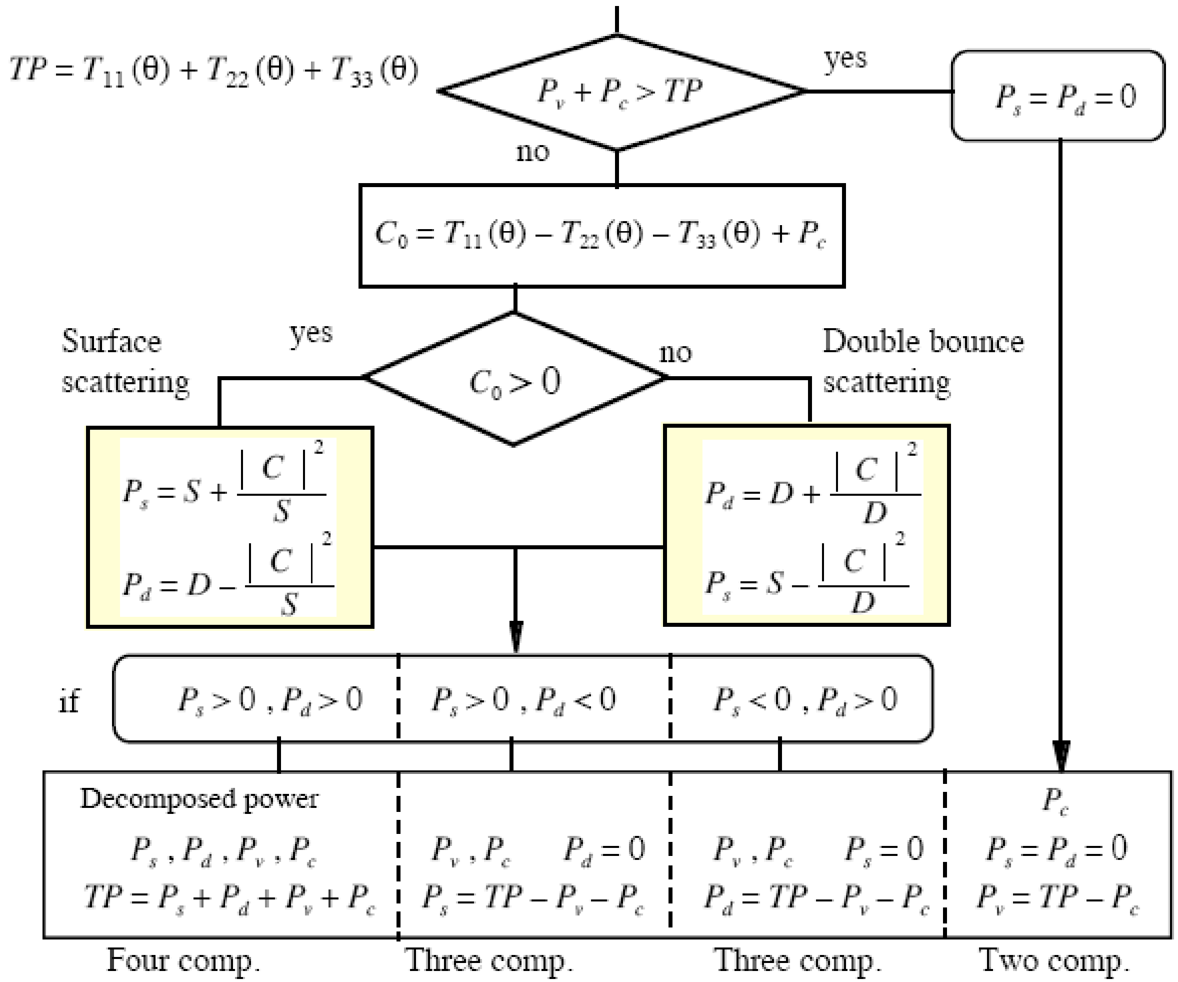

4-compornent scattering power decomposition algorithm using rotated coherency matrix

Four-component decomposition

New rotated decomposition

Scattering power decomposition by rotation of coherency matrix for Niigata City area in Niigata Prefecture of Japan

Kyoto City, Kyoto Prefecture, Japan

(a) Original decomposition

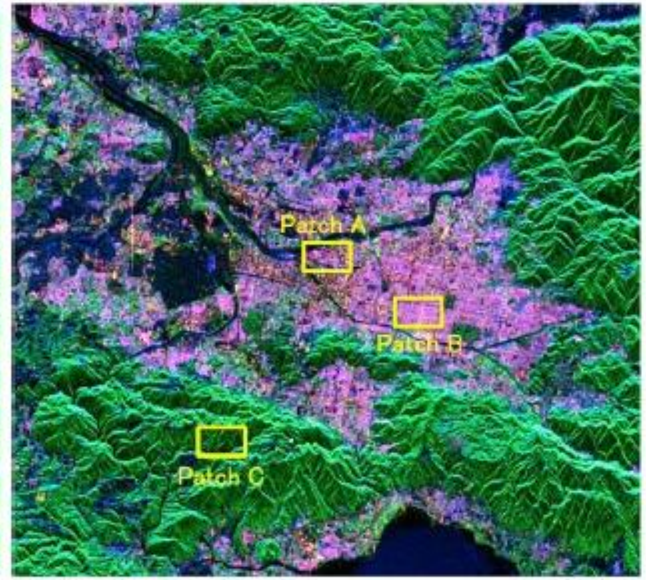

(b) Decomposition after T33 rotation

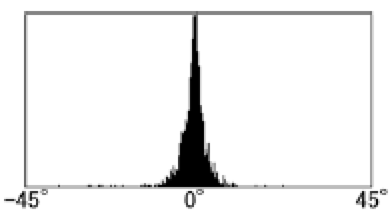

(c) Patch A: orthogonal urban

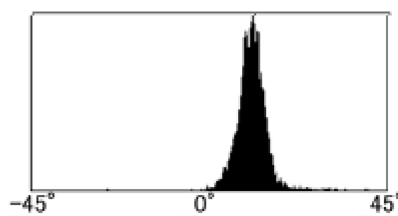

(d) Patch B: oriented urban

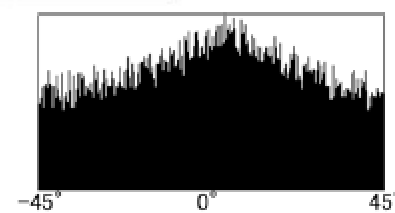

(e) Patch C: forest

Deorientation

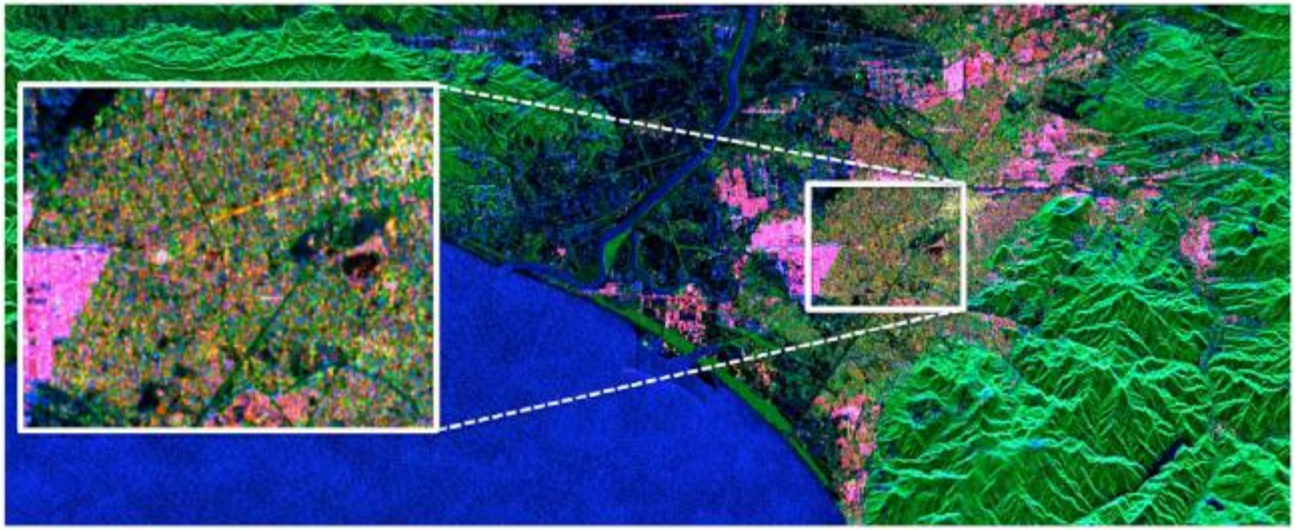

Decomposed color coded image of Sapporo, Japan

Monitoring of ongoing surface deformation along Cheleng-Pu fault

Taiwan

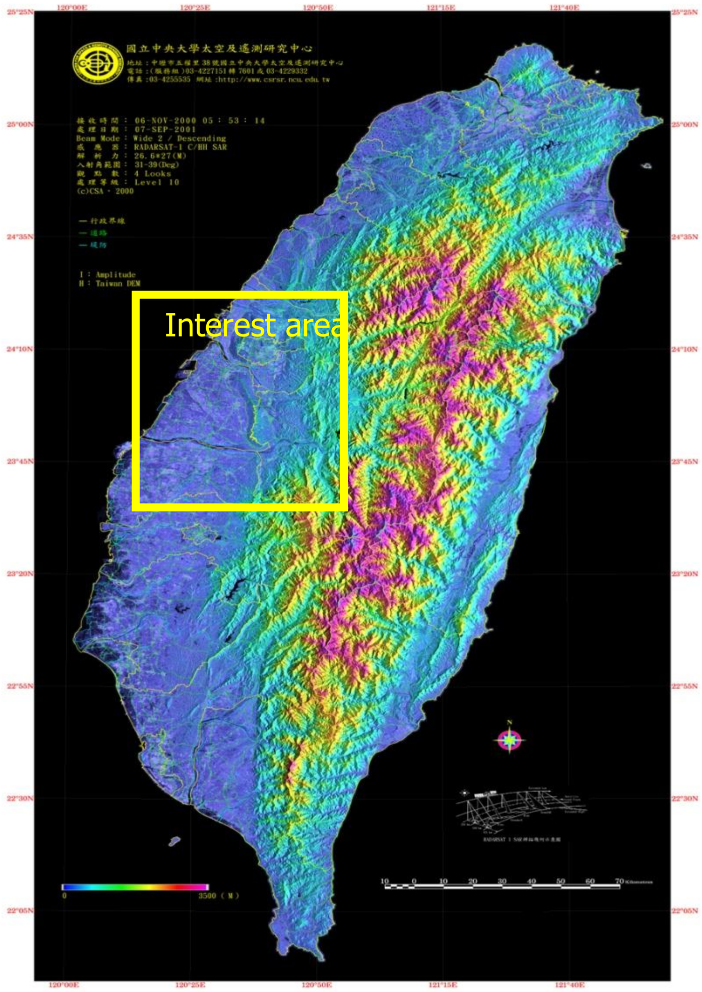

Data fusion of DEM and RADARSAT SAR images By CSRSR.

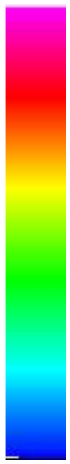

ELF/ULF Electromagnetic Spectrum

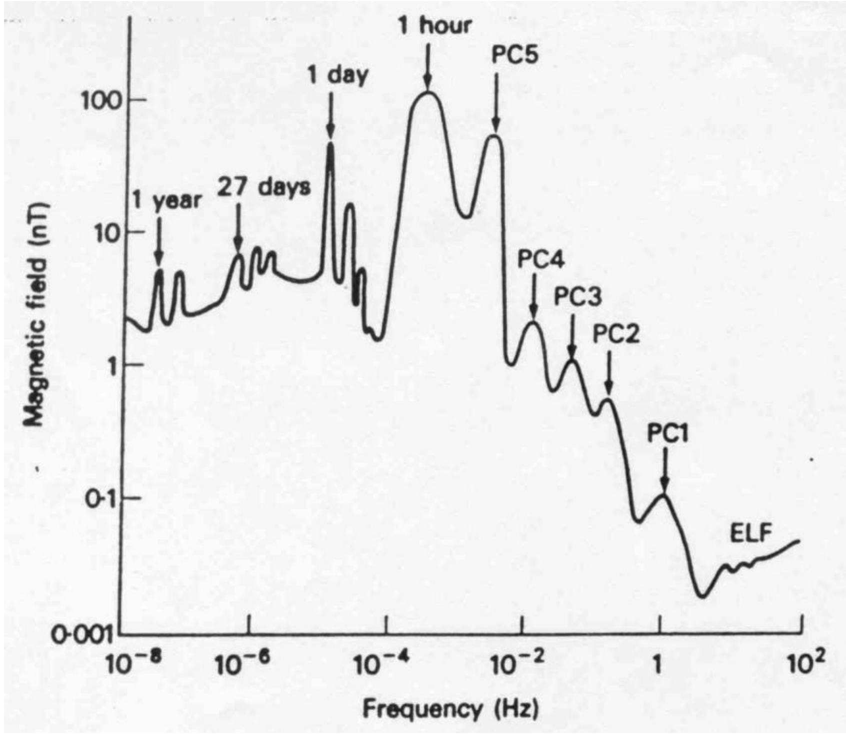

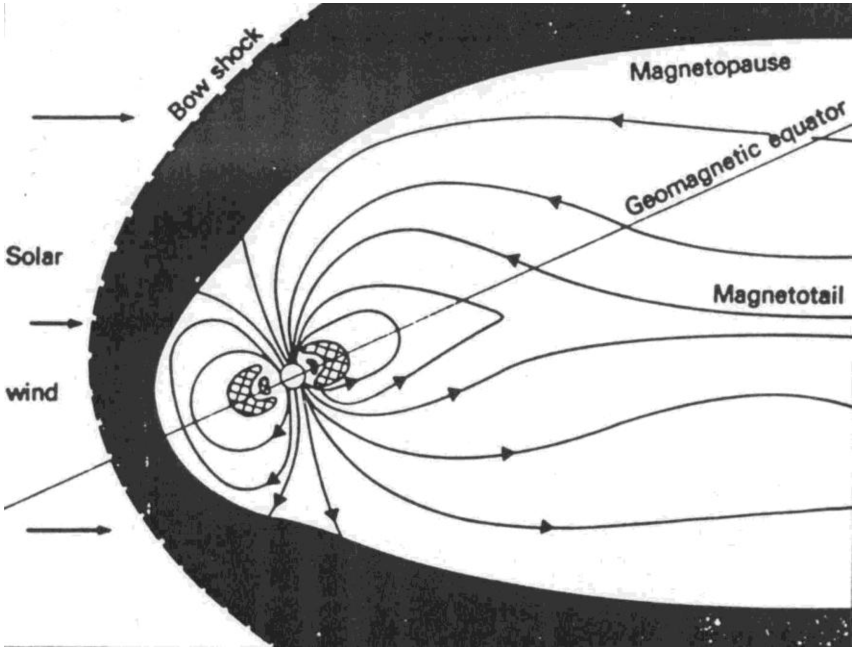

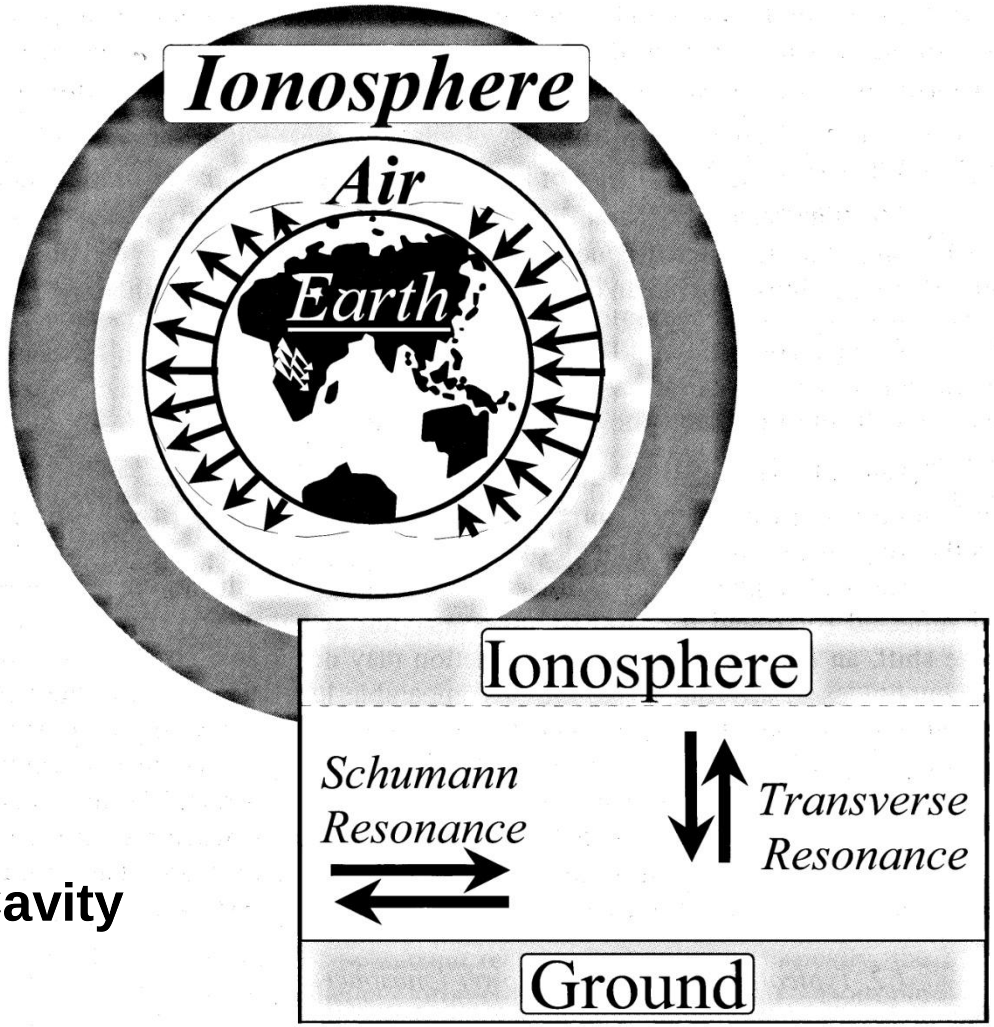

Earth-Ionosphere Cavity

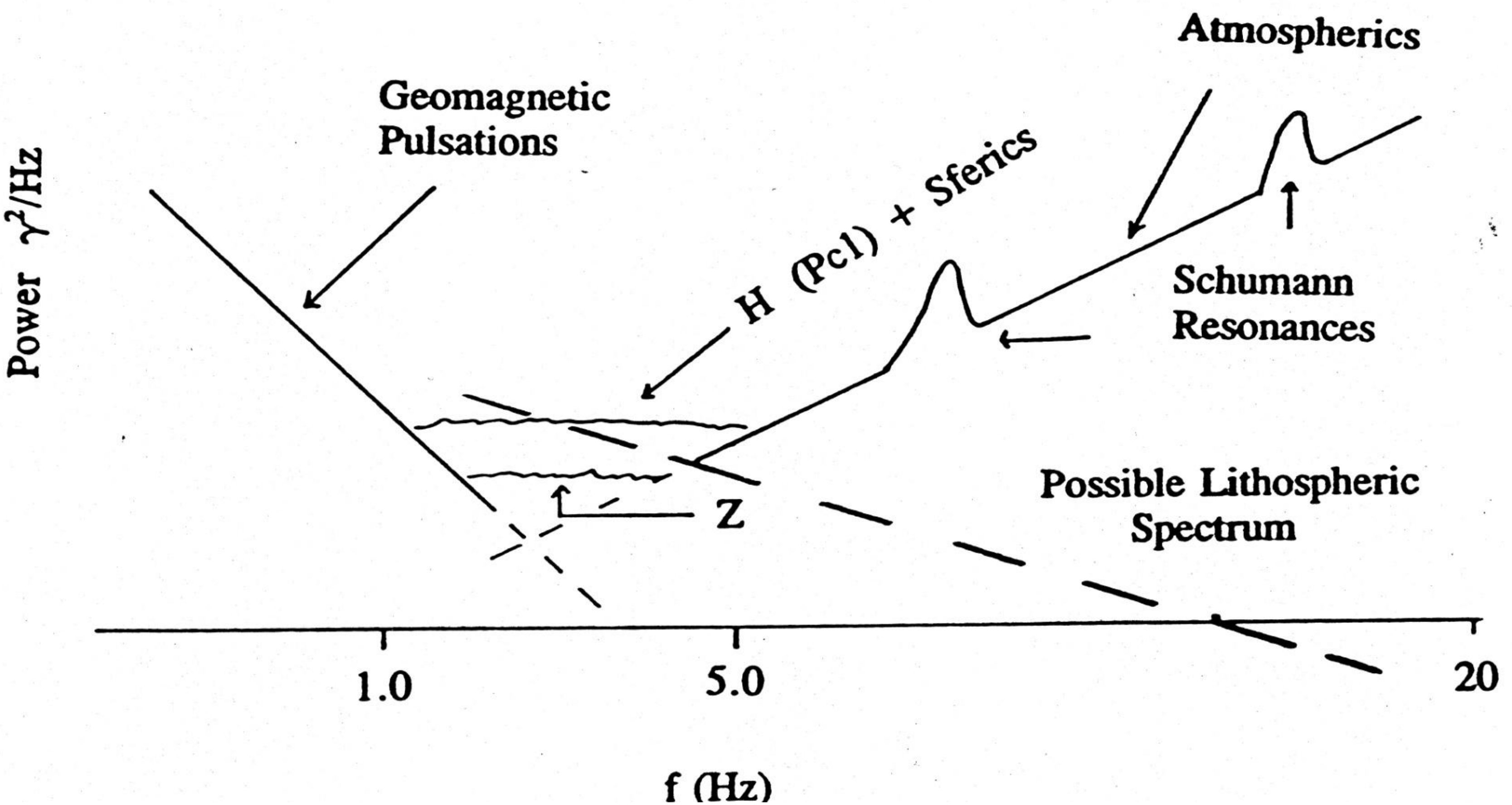

Tectonic Stress Electromagnetic Signatures

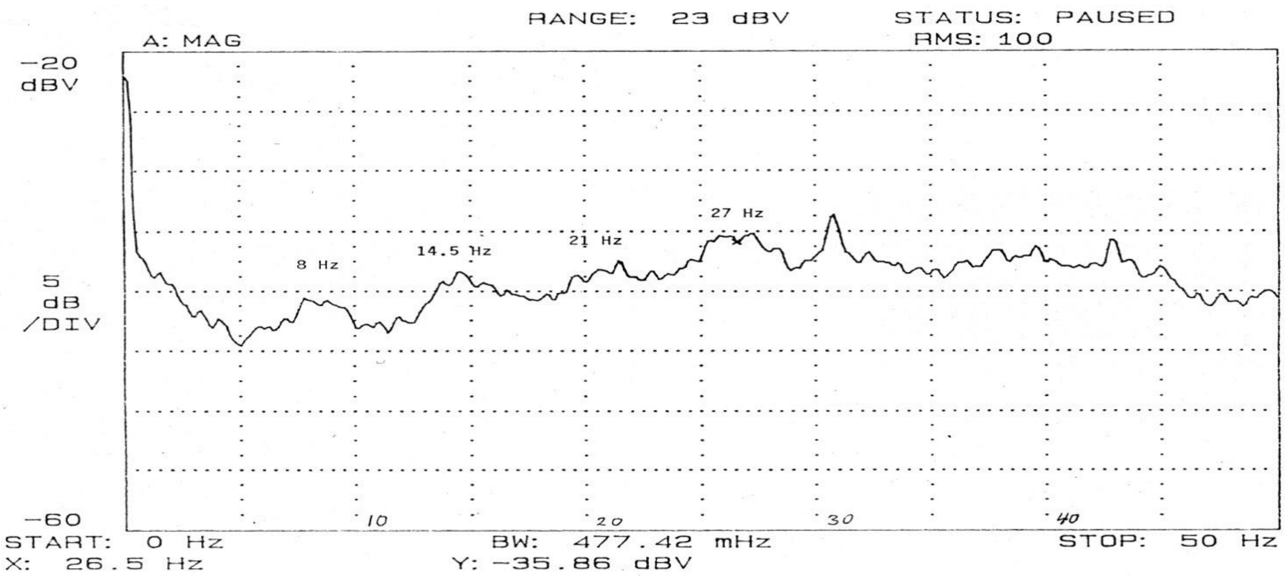

Schumann Spherics (Electric Storm) Signatures

Recent electromagnetic signatures associated with the Chi-Chi and Chia-Yi earthquakes of 1999.

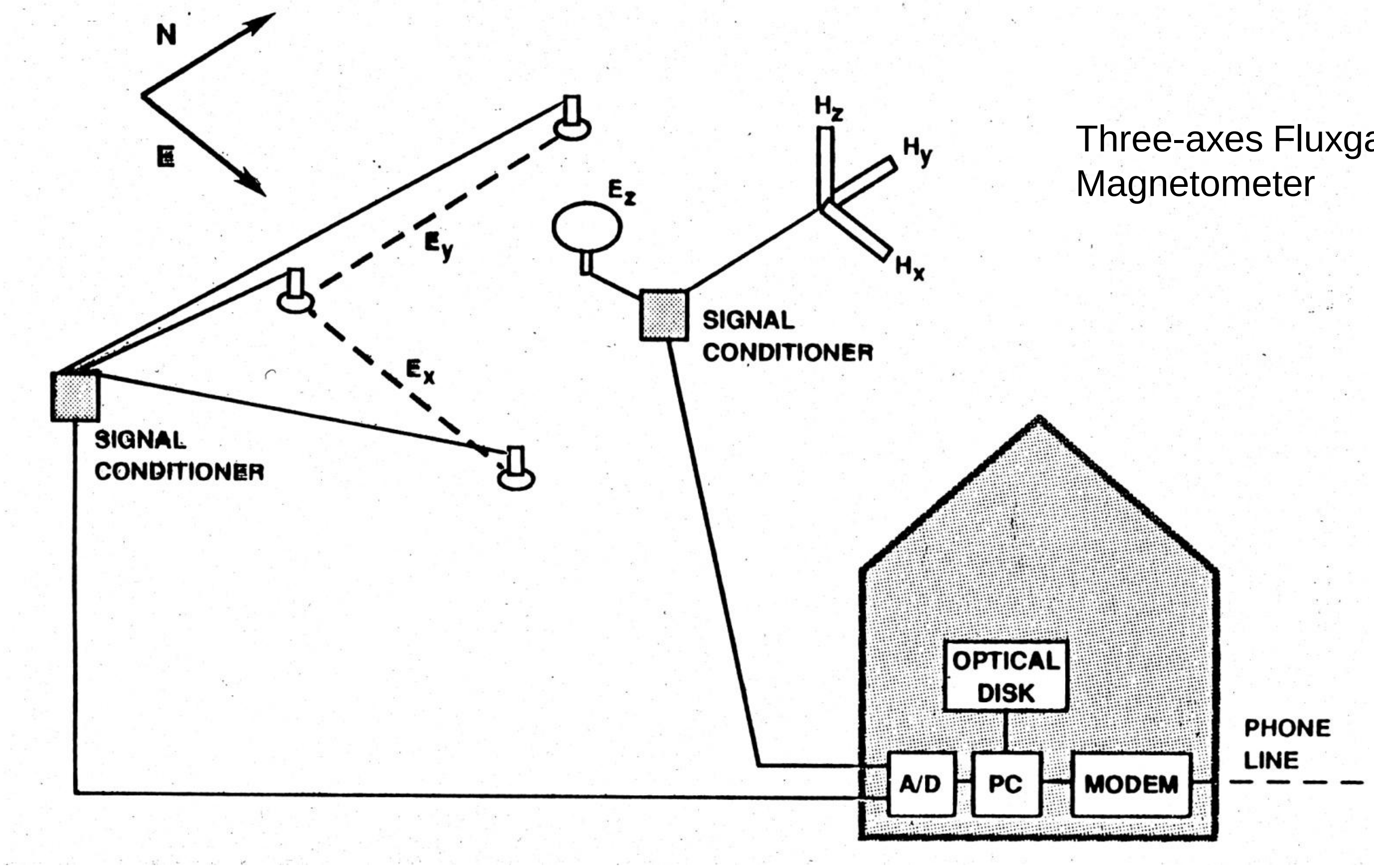

Three-axes Fluxgate Magnetometer

ULF Magnetometric & Electrometric Measurement Arrangement

Recent electromagnetic signatures associated with the Chi-Chi and Chia-Yi earthquakes of 1999.

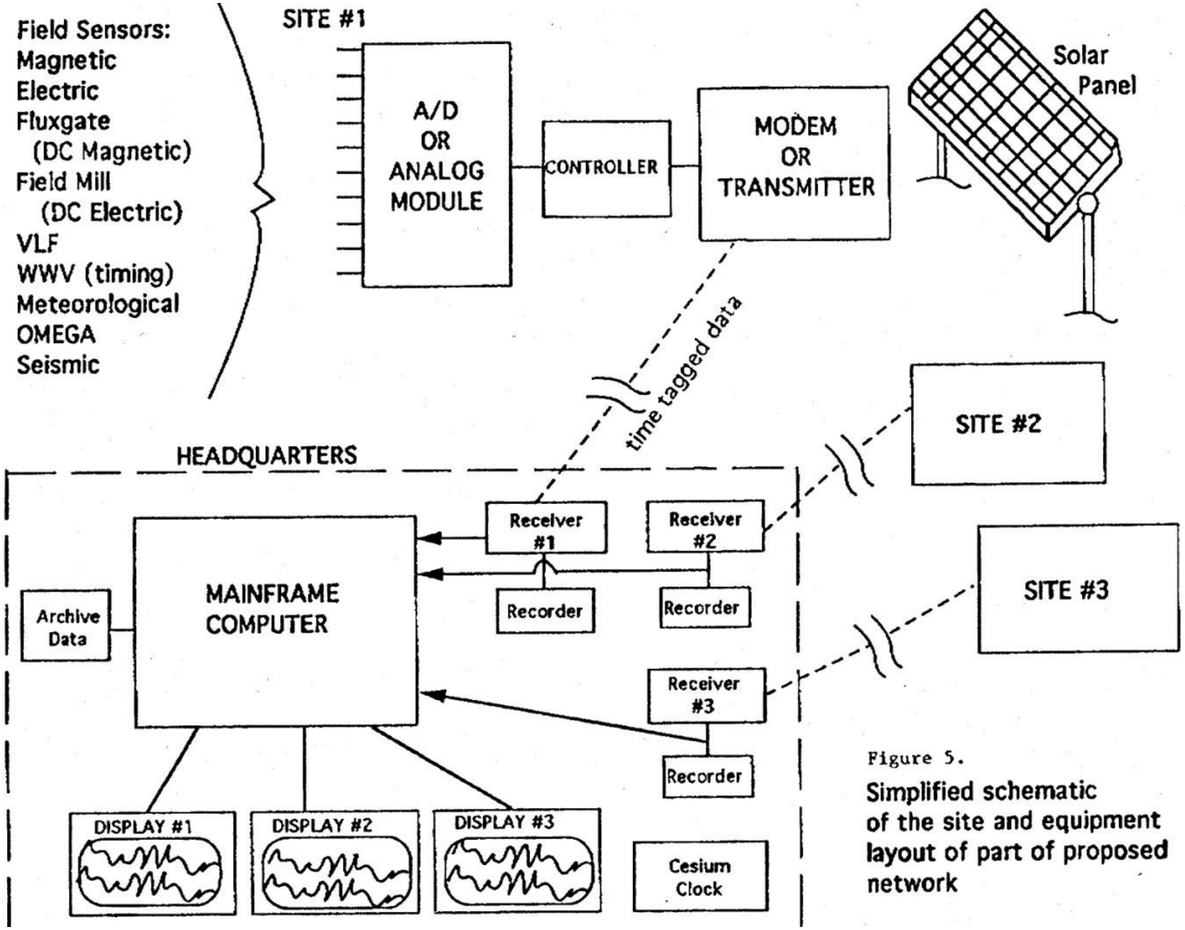

Figure 5.
Simplified schematic of the site and equipment layout of part of proposed network

Simplified Schematic of the Site and Equipment Layout

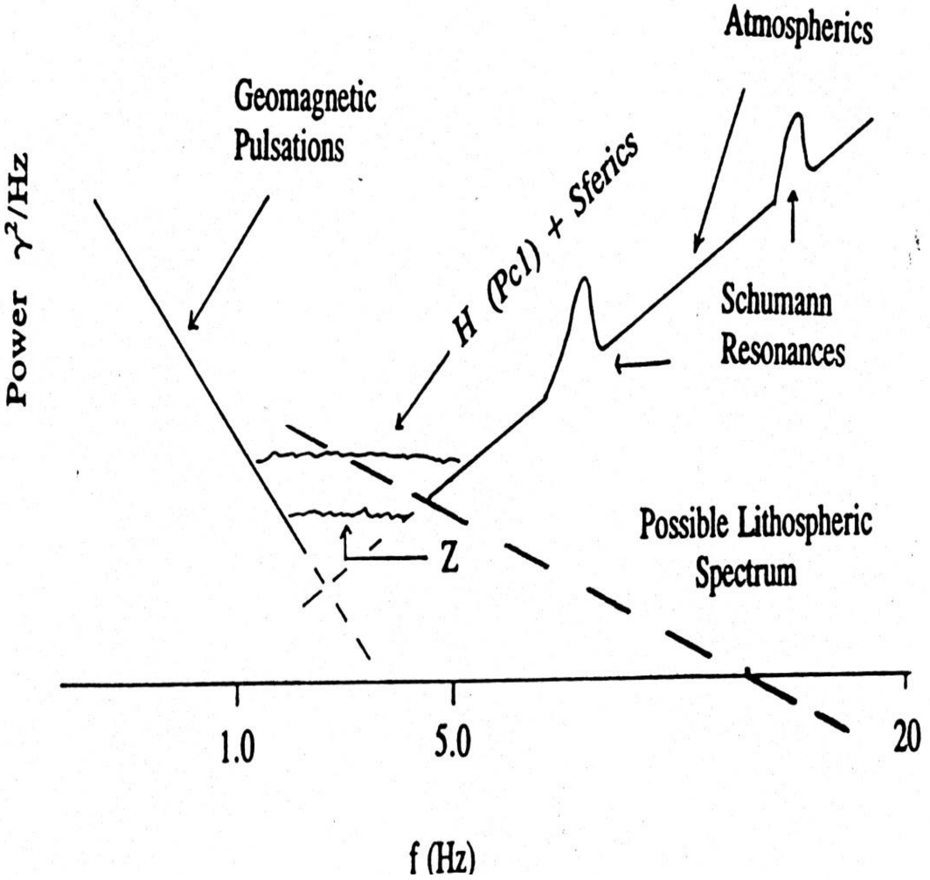

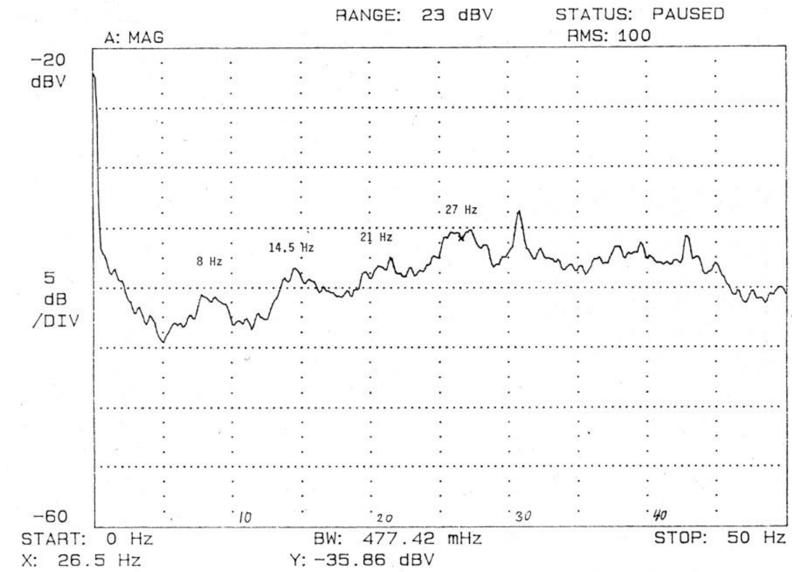

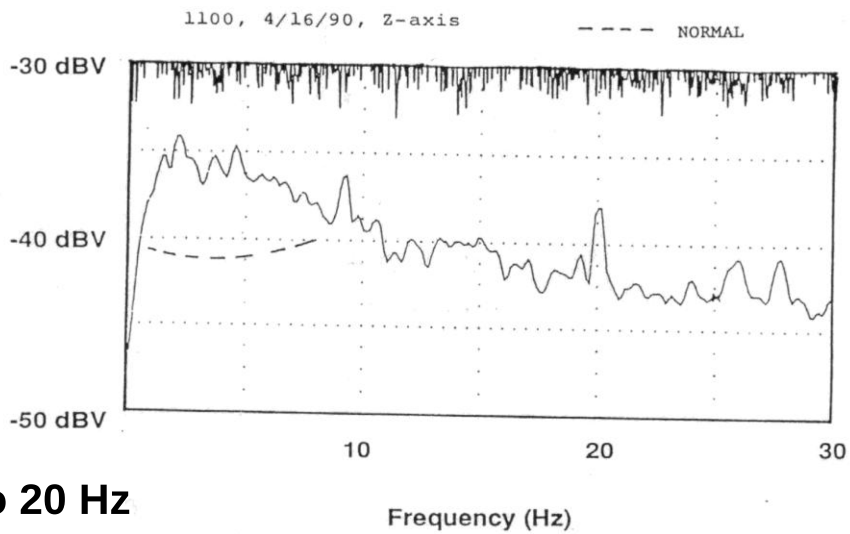

ULF Tectonic & Spherics Signatures at About .1 to 20 Hz

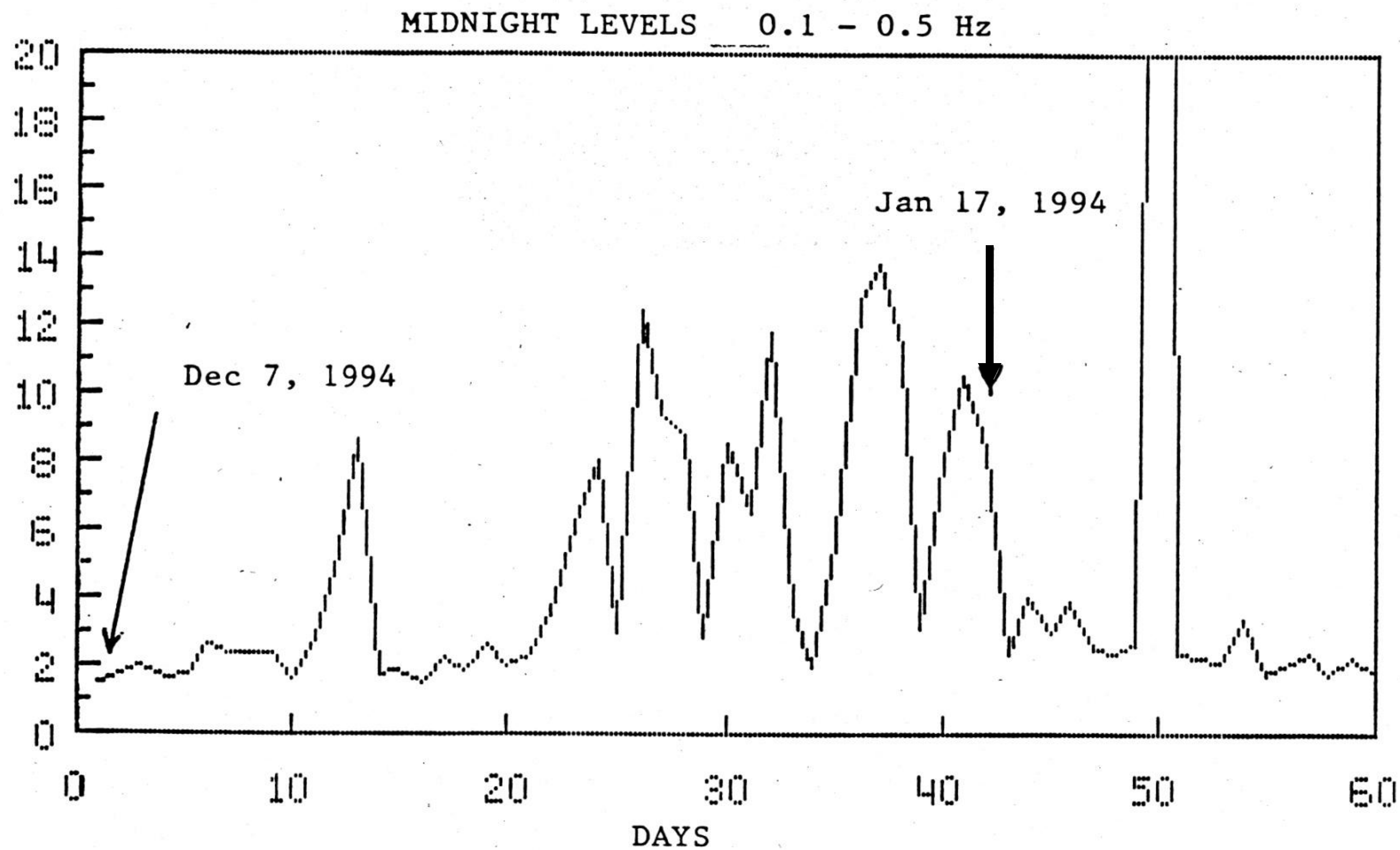

Averaged Tectonic Stress Signatures during Northridge Earthquake

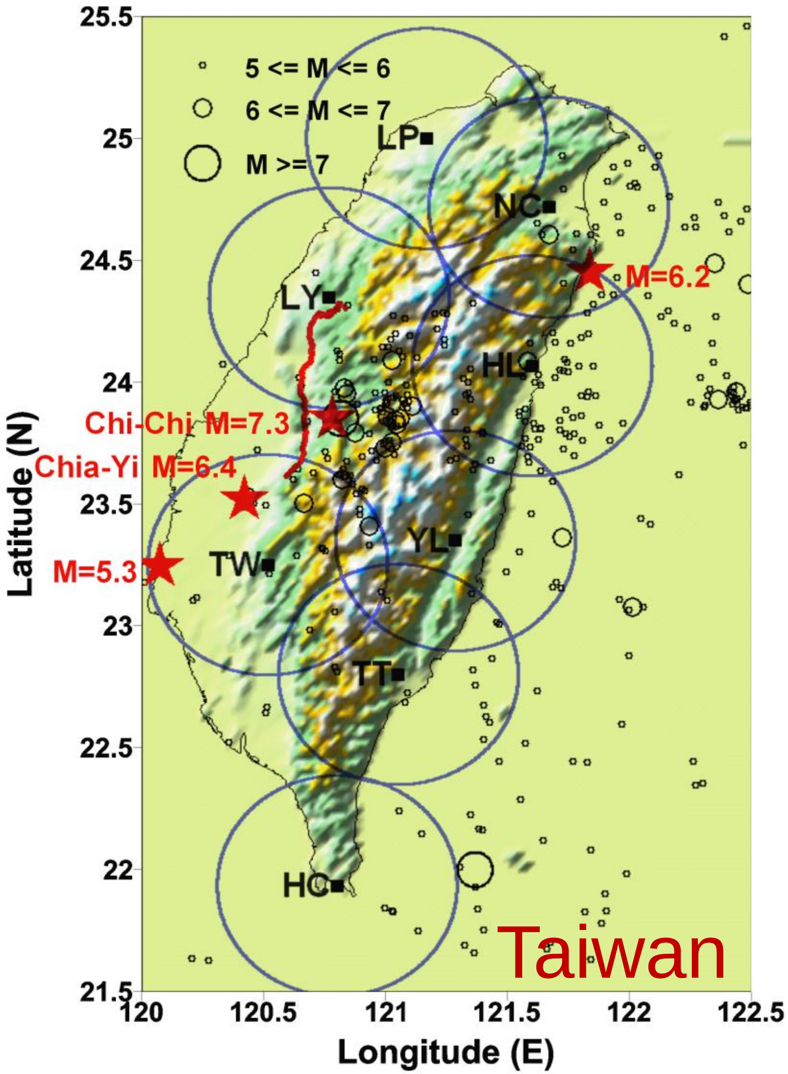

Earthquakes

- **Blue circle:**
  Radius 50 Km
- **Red line:**
  Chelungpu fault
- **Star mark: Three sample earthquakes**
- **Black circle: Earthquakes M >= 5.0**

Earthquakes occurred in six blue circles (except HC, LP) were compared with the anomaly

Recent electromagnetic signatures associated with the Chi-Chi and Chia-Yi earthquakes of 1999, May to December in Taiwan

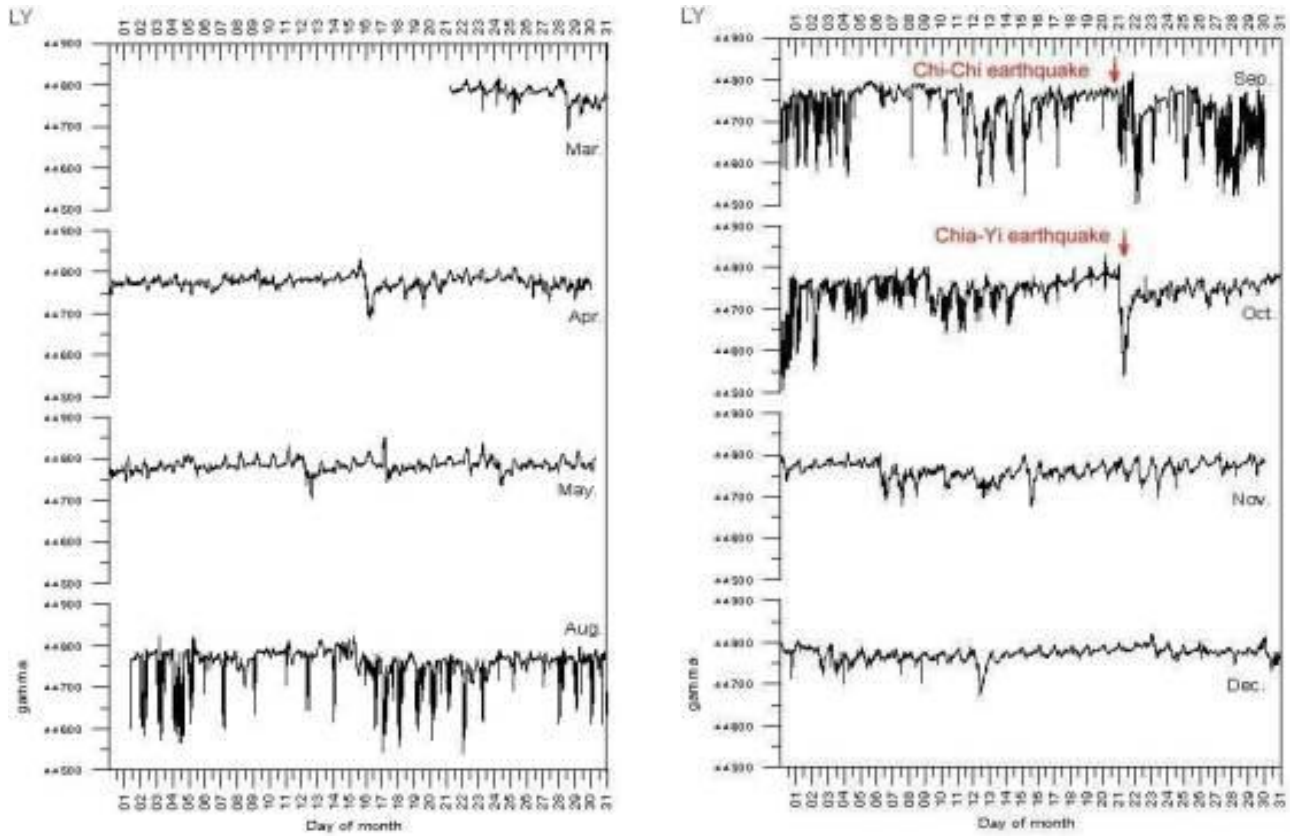

The raw data in LY station in March, April May, August, September, October, November and December, 1999.

Brief introduction of DIFF-RP-IN-SAR

6D DIFFERENTIAL SAR INTERFEROMETRY
HOW DOES IT WORK?

- Three-pass "repeat track" interferometry uses two baselines (B_1,α_1); (B_2,α_2) to acquire interferograms at different times.
- Despite exaggeration in picture on the right, the incidence angles and absolute ranges are nearly the same.
- Now suppose that the surface deformed slightly between the second and third acquisitions in such a way that the range changed by an amount $\Delta\rho$
- In the repeat-track implementation of interferometry, the signal travels each path twice, since the transmitter and receiver are in the same place. Therefore, the interferometric phase is

$$\Delta\phi = \frac{2\pi}{\lambda} 2 \times \text{range} = \frac{4\pi}{\lambda}\text{range}$$

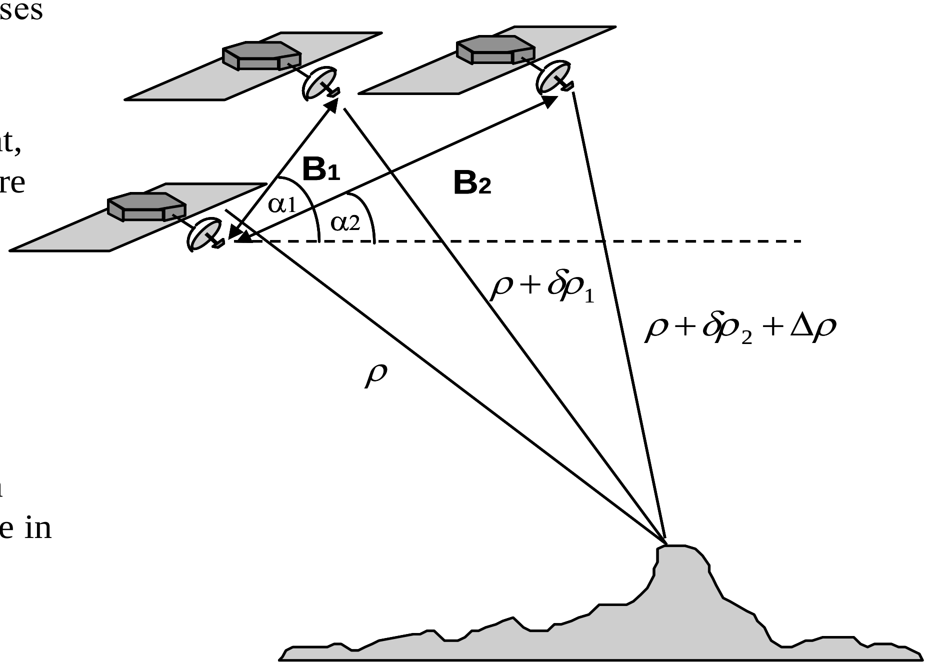

Monitoring of ongoing surface deformation along Cheleng-Pu fault

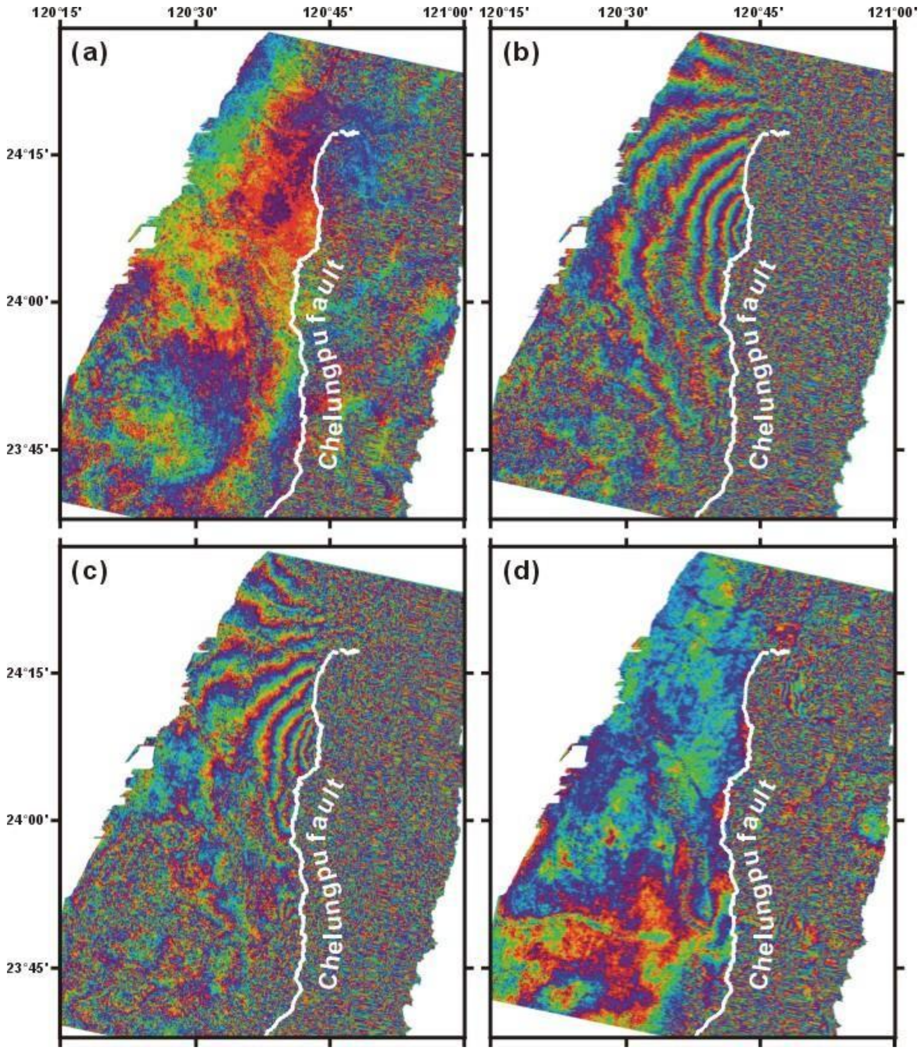

The destruction along the Cheleng-Pu fault caused by the Chi-Chi earthquake of 1999 September 21

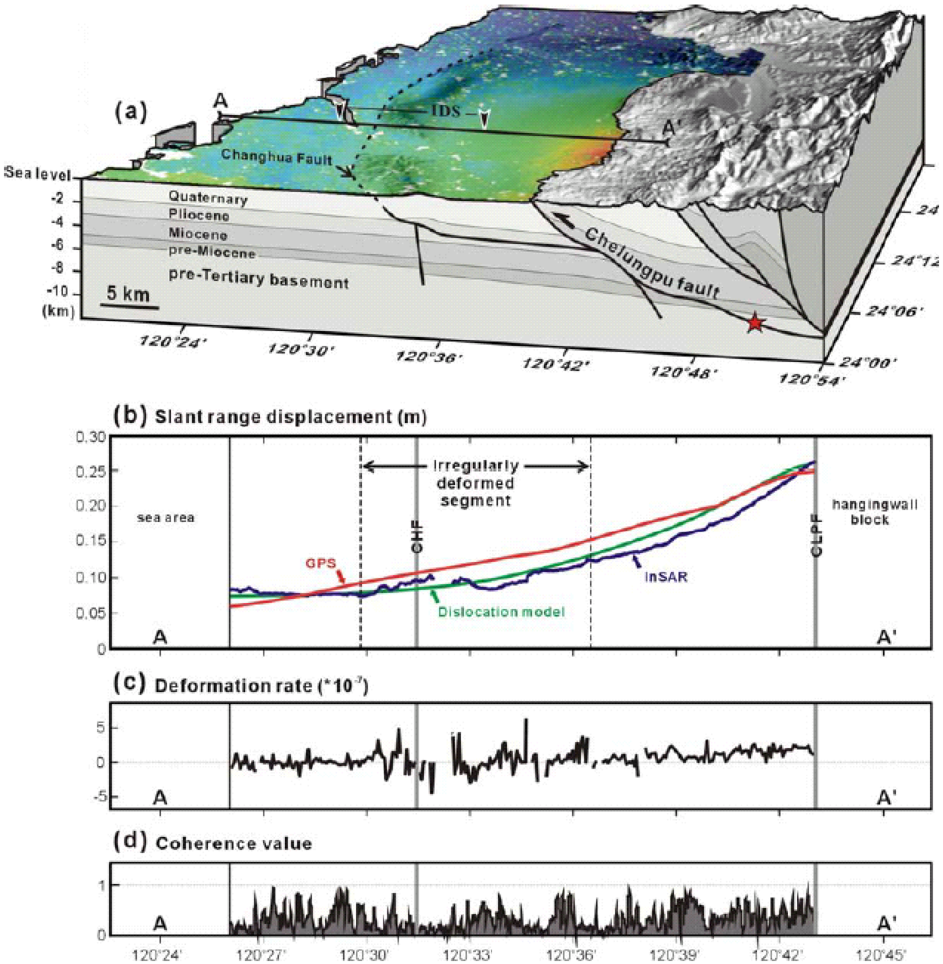

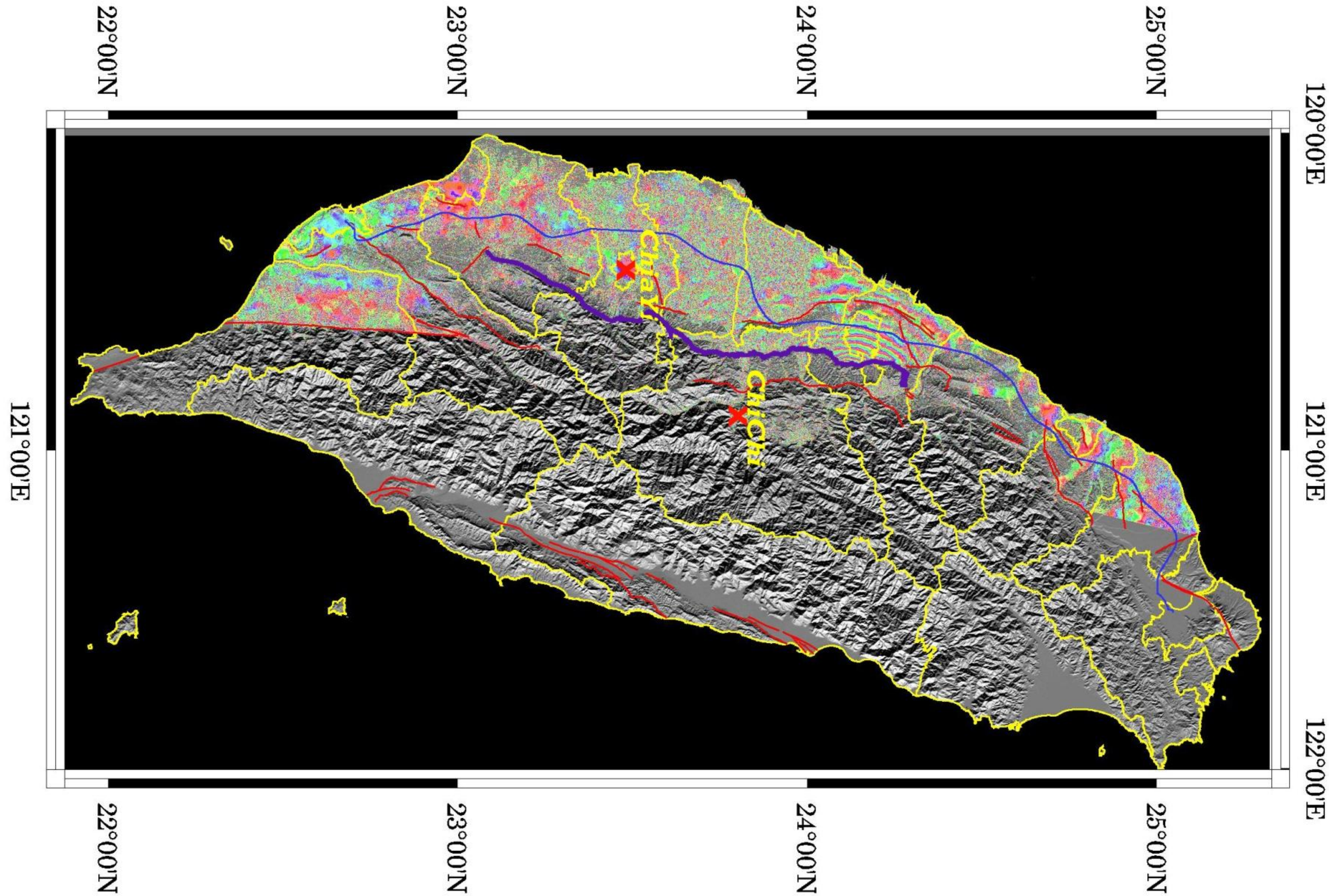
22°00'N
23°00'N
24°00'N
25°00'N
120°00'E
121°00'E
122°00'E
ChiChi

1022 EQs

2 earthquakes occurred on 10/22/1999 in Chiayi area

Combined surface deformation of the two eqs were observed by SAR Interferometry (B_n=232m)

Approx. 2 fringes can be observed from interferogram, representing 5~6cm slant range deformation

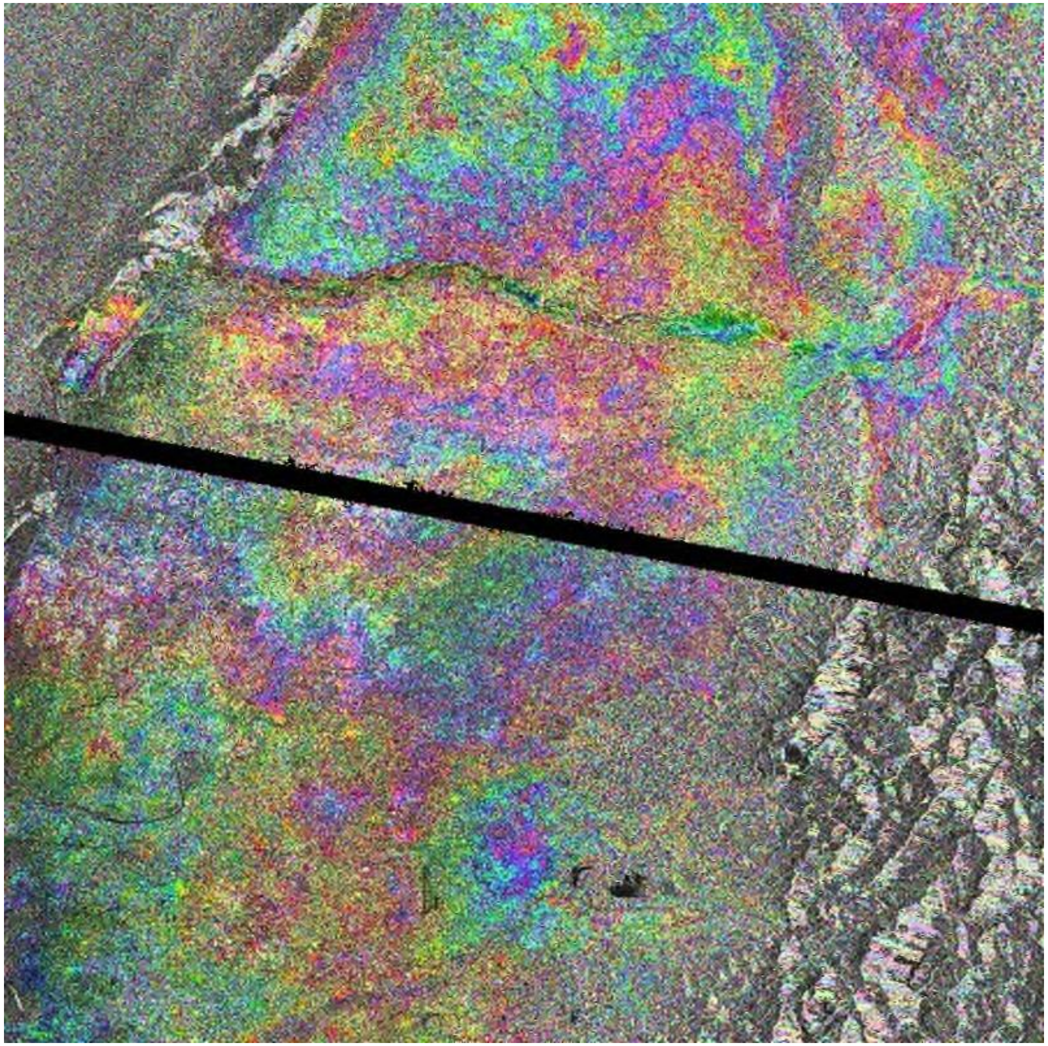

The destruction along the Cheleng-Pu fault caused by the Chi-Chi earthquake of 1999 September 21

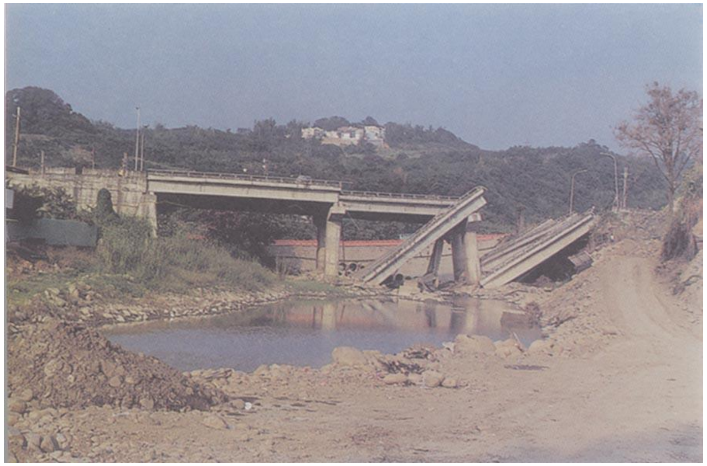


The destruction along the Cheleng-Pu fault caused by the Chi-Chi earthquake of 1999 September 21

ALOS is one of the largest Earth observing satellites ever developed, at 3850 kg. It is in a near-exact 45-day repeat sun-synchronous orbit, 690 km altitude above the equator. The active phased array SAR antenna is obliquely Earth-facing, aligned with the spacecraft velocity vector. The solar array is arranged at right angles to the orbit plane, consistent with the near-mid-day orbit phasing. The X-band down-link must be shared with optical instruments, which constrains SAR operation times.

Table 1. Selected PALSAR Mode Parameters

Mode (selected)	Resolution (m)	Swath (km)	Looks	Polarization
Standard, stripmap	20 x 10	70	2	HH or VV
Fine	10	70	1	HH or VV
ScanSAR (5-beam)	~ 100	350	8	HH or VV
Dual polarization	(as above)	(as above)	(as above)	(HH, HV), (VV, VH)
Quad-pol	30 x 10	30	2	Full polarization

3.4.5.6.7.8

Polarimetric mode

Incident angle :23.1°

Date:2009/05/01

Path:442

Frame:430(3),440(4)
450(5),460(6)
470(7),480(8)

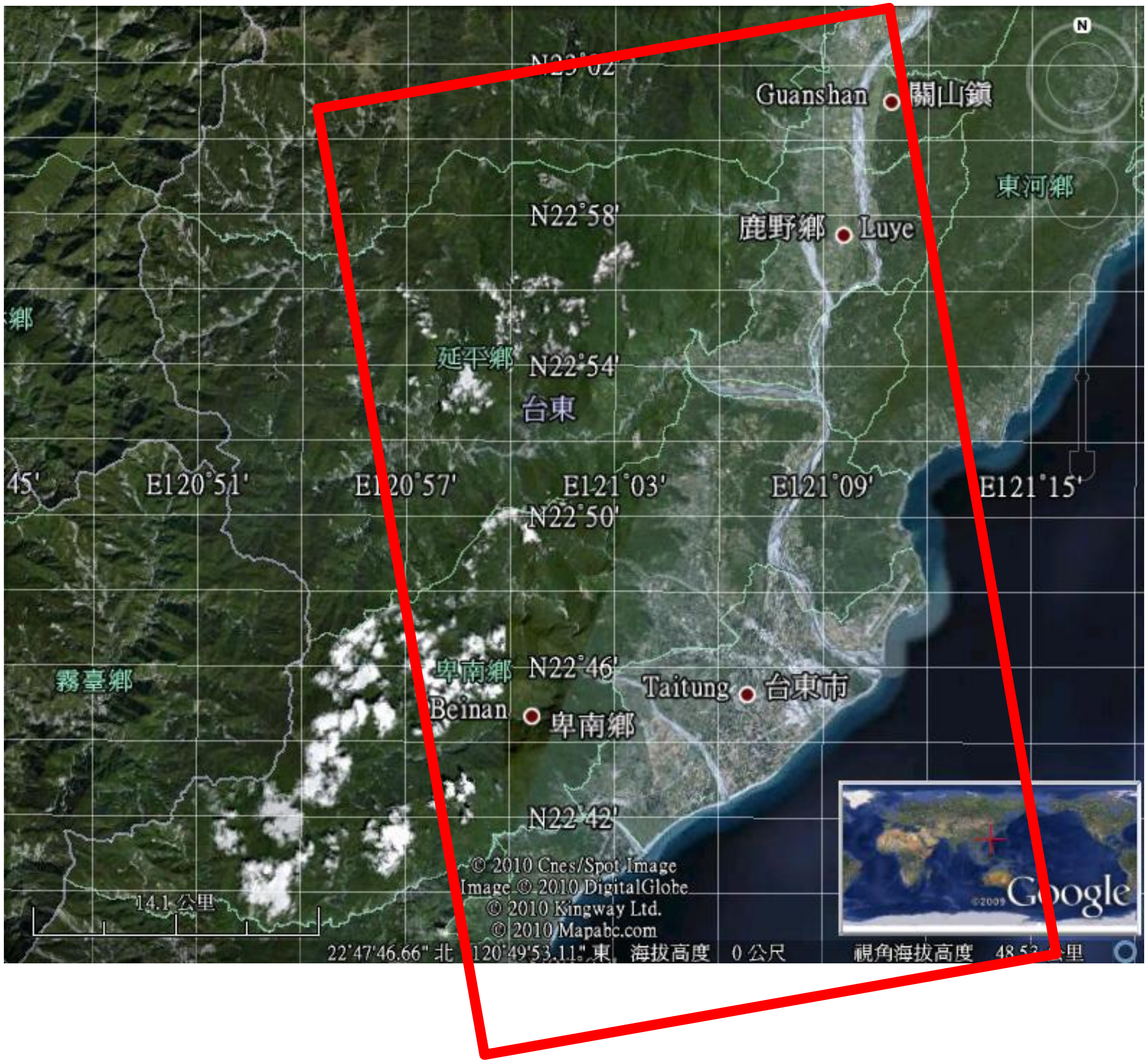
Guanshan
關山鎮
東河鄉
N22°58'
鹿野鄉
Luye
延平鄉
N22°54'
台東
E120°51'
E120°57'
E121°03'
E121°09'
E121°15'
N22°50'
霧臺鄉
卑南鄉
N22°46'
Beinan
卑南鄉
Taitung
台東市
N22°42'
© 2010 Cnes/Spot Image
Image © 2010 DigitalGlobe
© 2010 Kingway Ltd.
© 2010 Mapabc.com
14.1 公里
Google


Luye
N
Taitung
Pd
Pv

Taiwan

2009/5/1
22.710N
121.091E

PASL110090501
14242009070200
00

©METI, ERSDAC

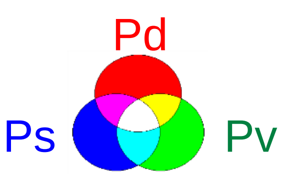

Niigata University

Google earth optical image

Scattering power decomposition (Pd, Ps, Pv)


Taitong

Scattering power decomposition

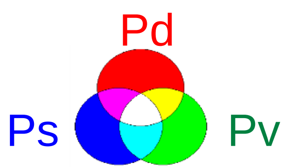

Niigata University

Pd, Pv, Ps

Pauli-basis

Taiwan

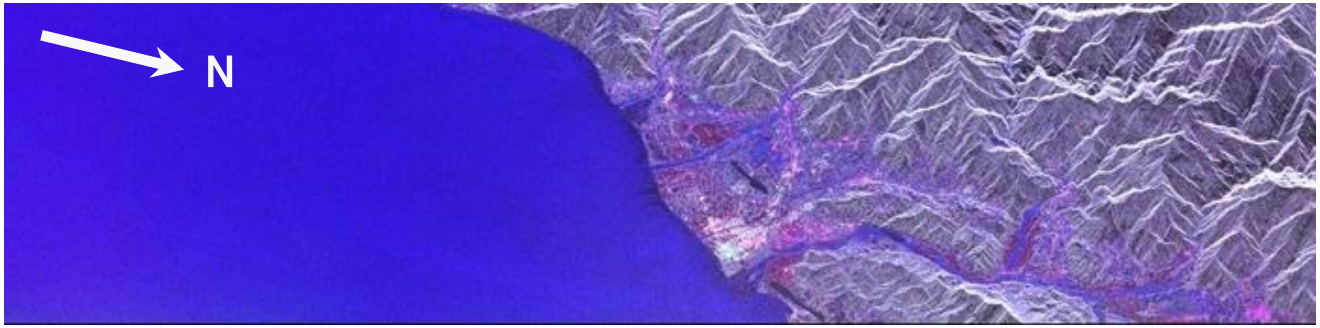

HH-VV, 2HV, HH+VV

HV-basis

2009/5/1
22.710N
121.091E

PASL11009050114242009070200

©METI, ERSDAC

HH, 2HV, VV

Scattering power decomposition

Pd

Ps 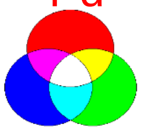 Pv

Niigata University

T33 Rotation

Pauli-basis

Taiwan

HV-basis

22.710N
121.091E

Pd, Pv, Ps

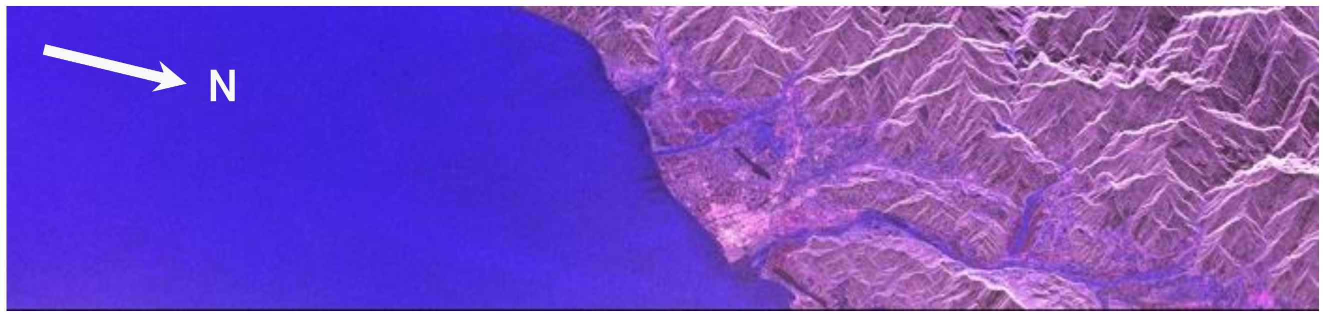

HH-VV, 2HV, HH+VV

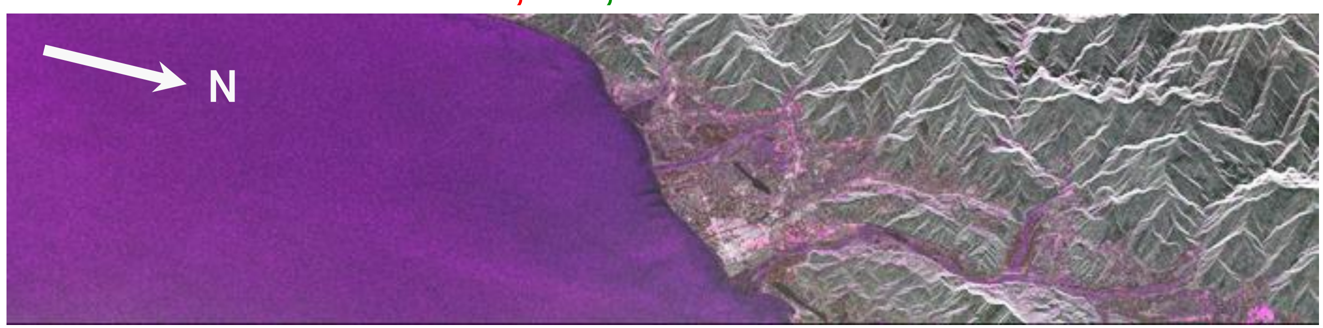

HH, 2HV, VV

2009/5/1

PASL110090501142420090702000

©METI, ERSDAC

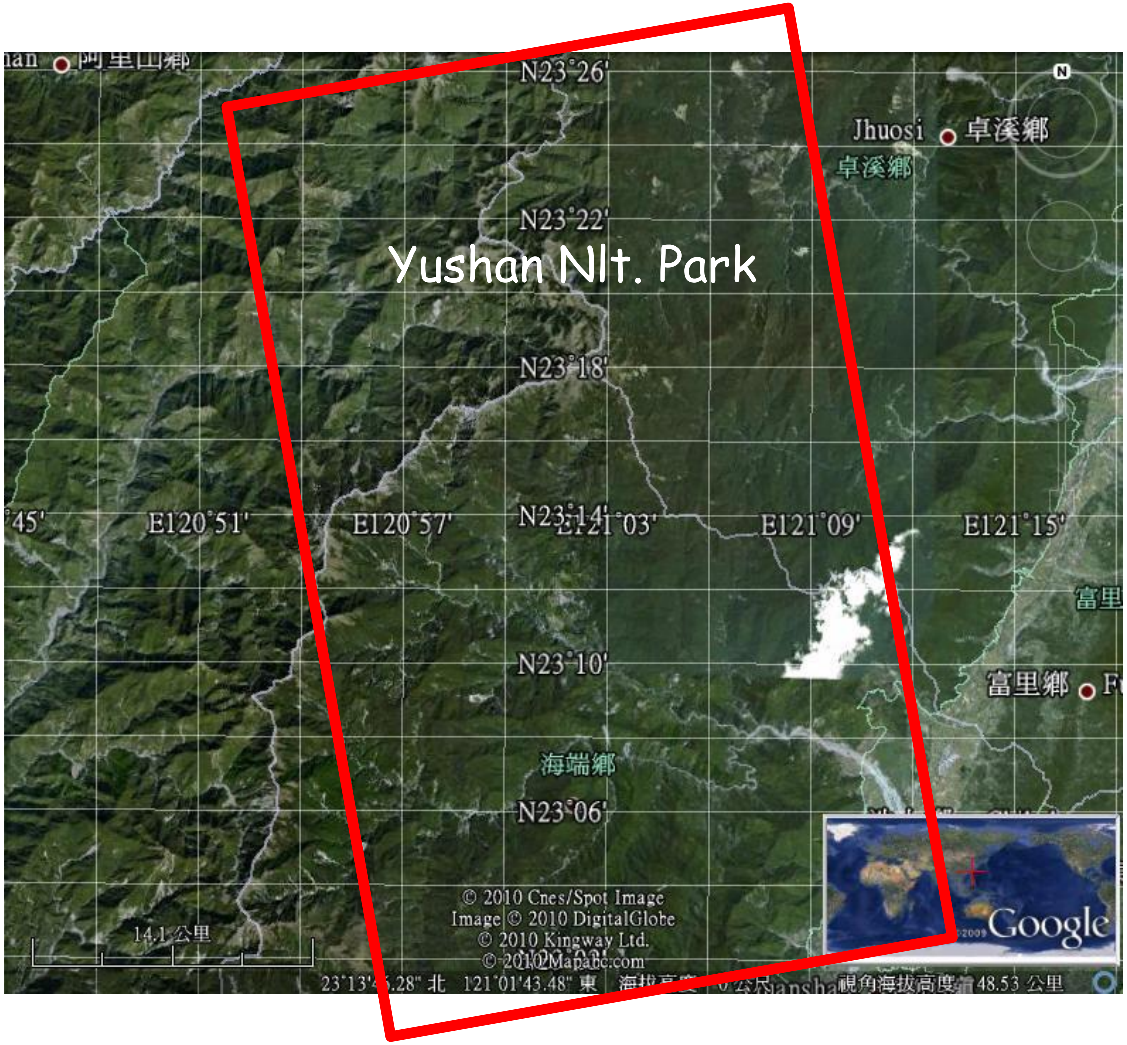
N23°26'
Jhuosi 卓溪鄉
N23°22'
Yushan Nlt. Park
N23°18'
E120°51'
E120°57'
E121°09'
E121°15'
N23°10'
富里鄉
海端鄉
N23°06'
© 2010 Cnes/Spot Image
Image © 2010 DigitalGlobe
© 2010 Kingway Ltd.
Google


N
Luye
Pd
Ps
Pv


Yushan Mountain
Minolta D7i
玉山 2003.07.31-08.03 Kevin Lin

Taiwan

2009/5/1
23.207N
120.983E

Google earth optical image

PASL110090501
14242009070200
01

©METI, ERSDAC

Scattering power decomposition (Pd, Ps, Pv)

Pd
Ps
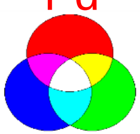
Pv

Niigata University

Scattering power decomposition

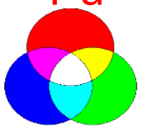

Niigata University

Pauli-basis

Taiwan

23.207N
120.983E

HV-basis

PASL1100905011424200907020001

©METI, ERSDAC

2009/5/1

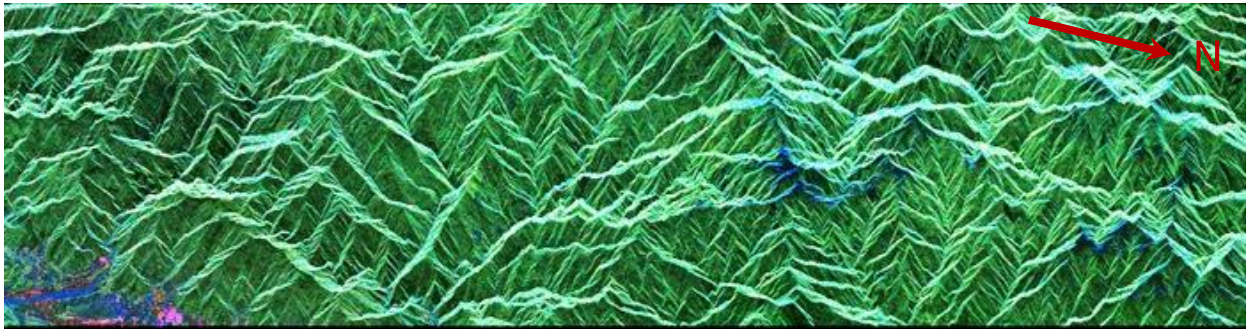

Pd, Pv, Ps

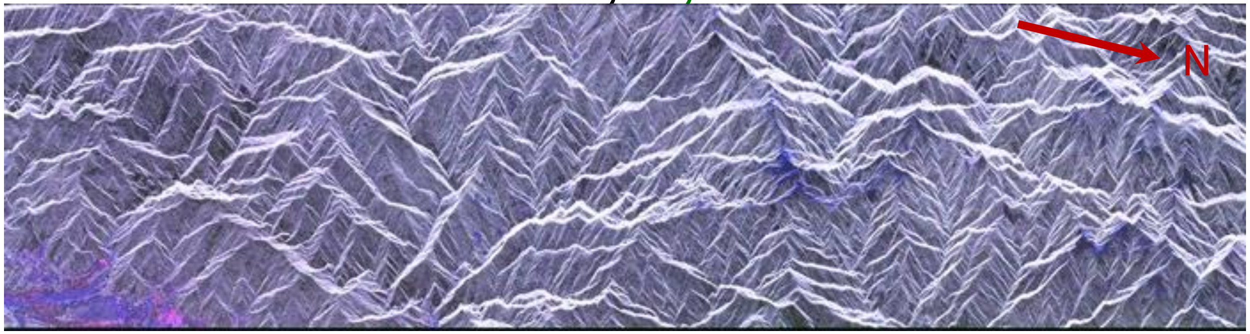

HH-VV, 2HV, HH+VV

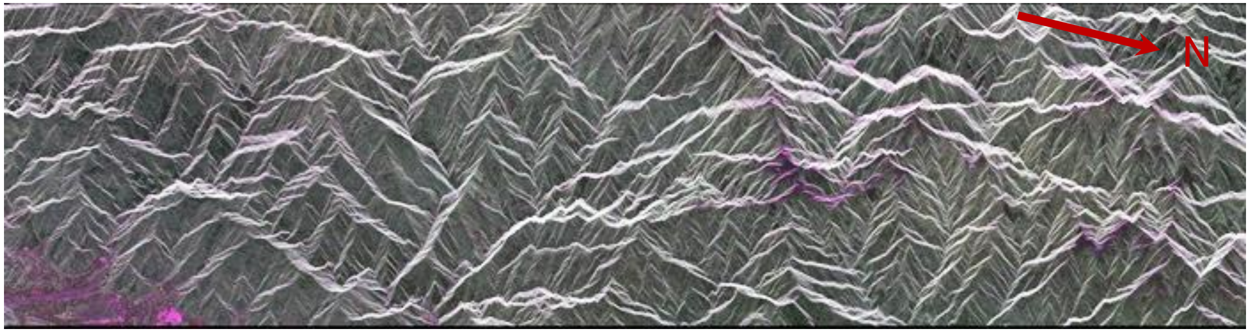

HH, 2HV, VV

Scattering power decomposition

Pd

Ps 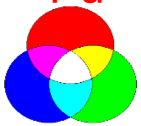 Pv

Niigata University

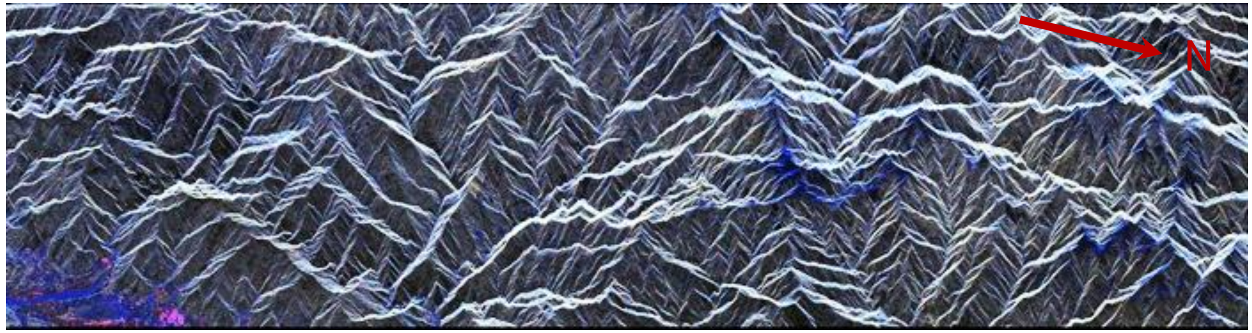

Pd, Pv, Ps

T33 Rotation

Pauli-basis

2009/5/1

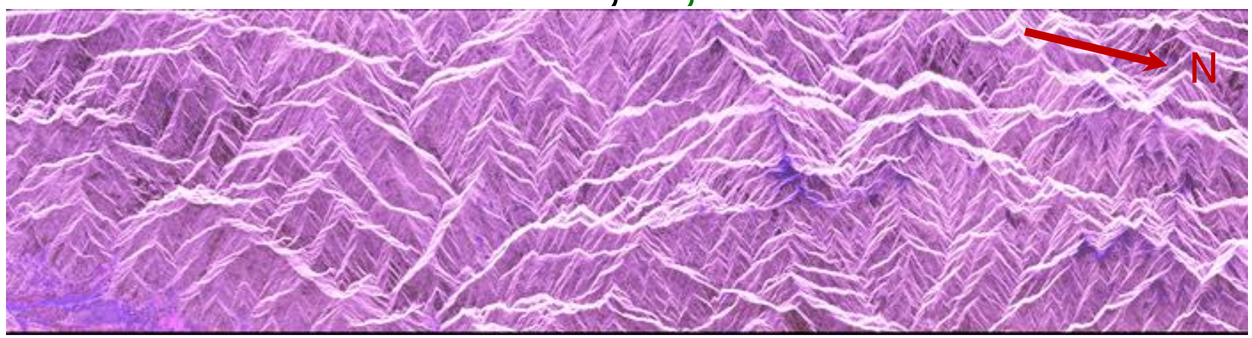

HH-VV, 2HV, HH+VV

HV-basis

Taiwan

23.207N
120.983E

PASL110090501142420090702 0001

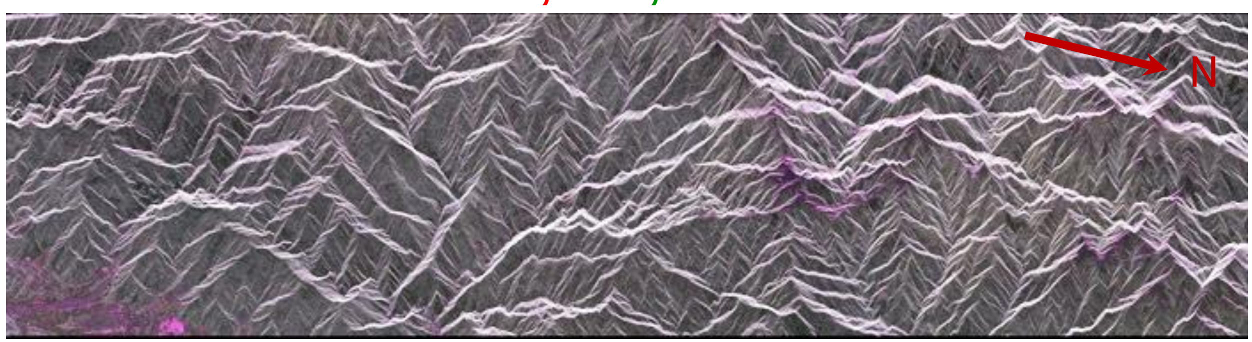

HH, 2HV, VV

©METI, ERSDAC

Taiwan

23.703N
120.875E

PASL110090501
14242009070200
02

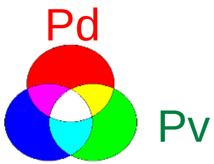

Niigata University

©METI, ERSDAC

2009/5/1

Google earth optical image

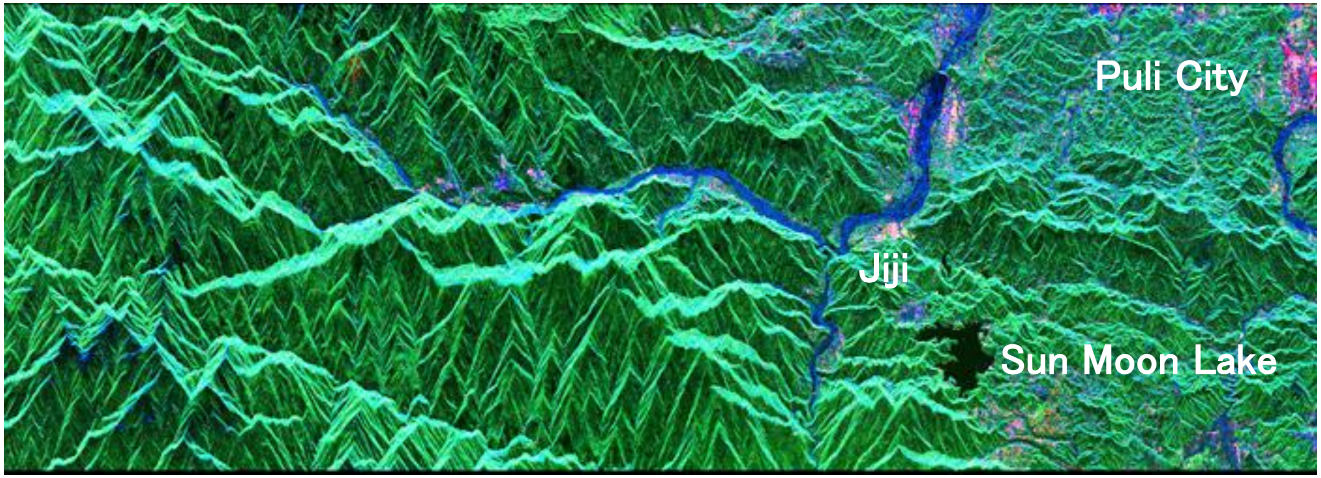

Scattering power decomposition (Pd, Ps, Pv)


Sun-Moon Lake

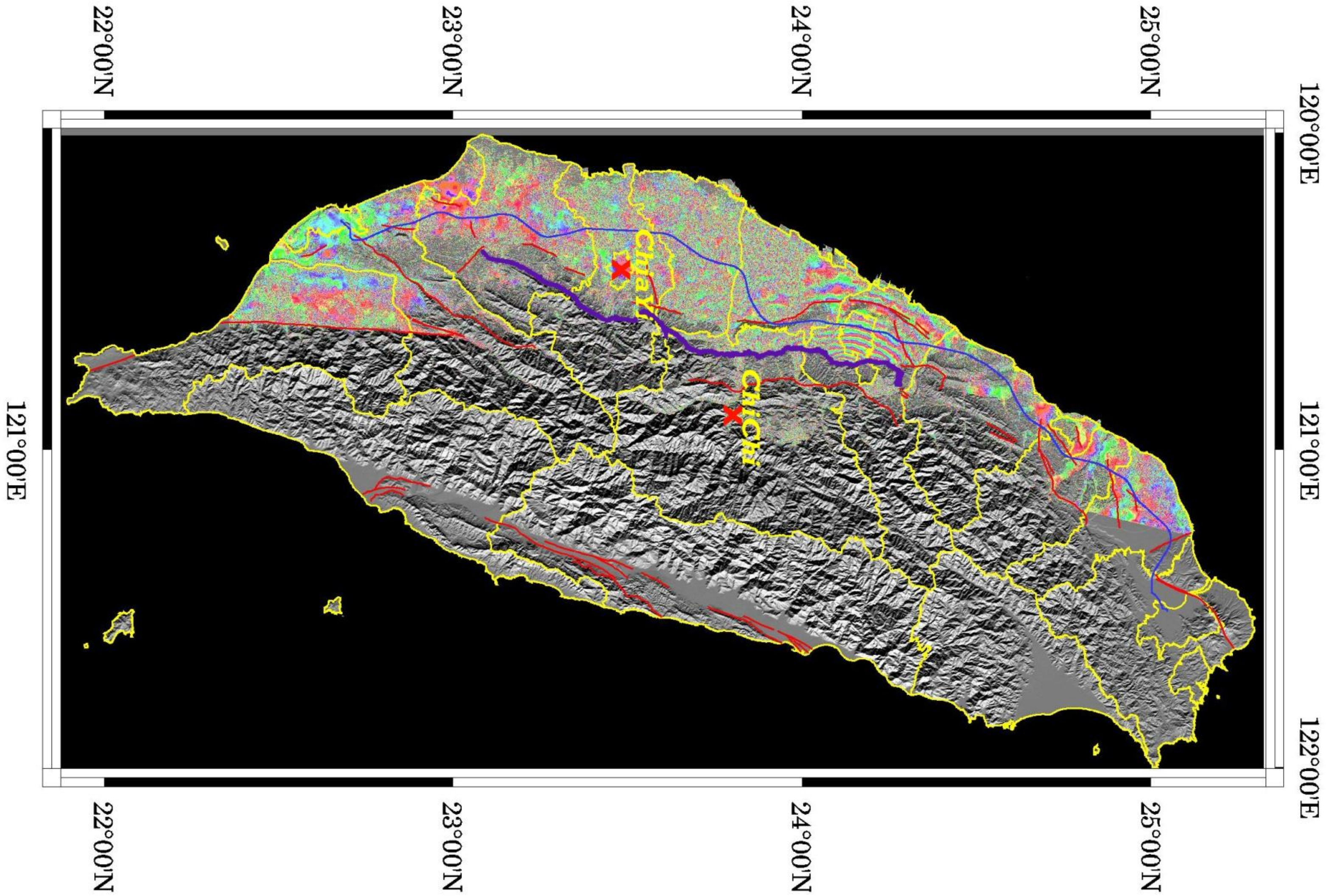
22°00'N
23°00'N
24°00'N
25°00'N
120°00'E
121°00'E
122°00'E
ChiaYi
ChiChi

Scattering power decomposition

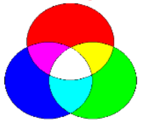

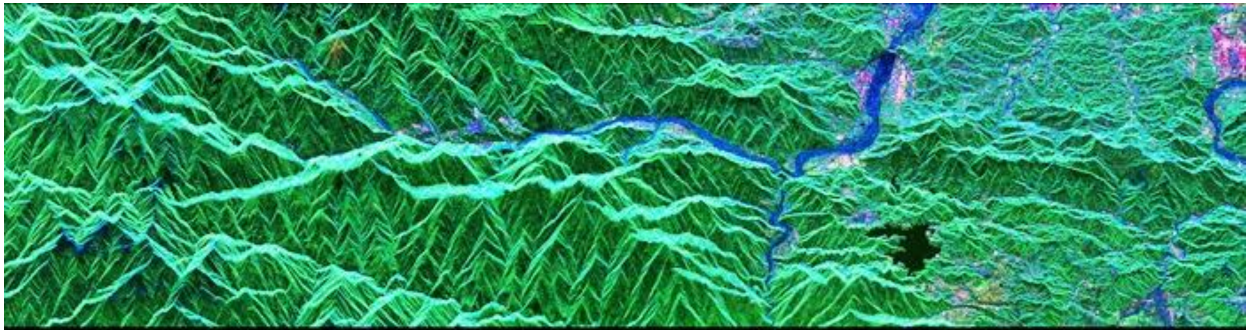

Pd, Pv, Ps

Niigata University

Pauli-basis

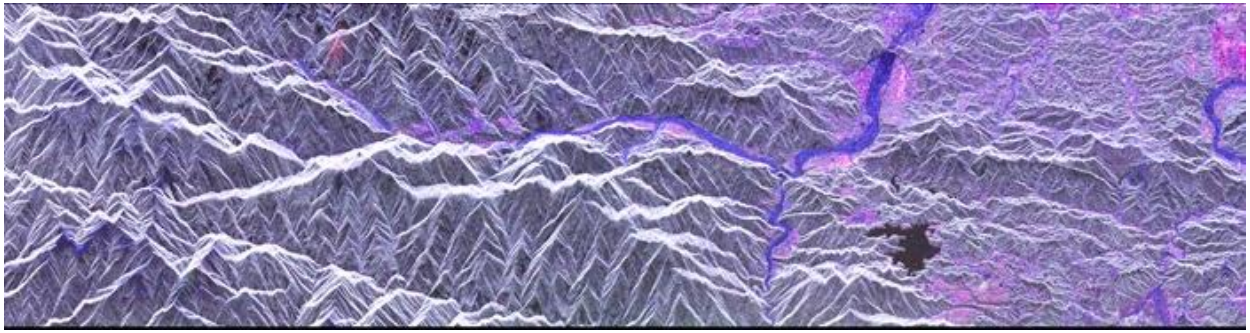

HH-VV, 2HV, HH+VV

Taiwan

23.703N
120.875E

HV-basis

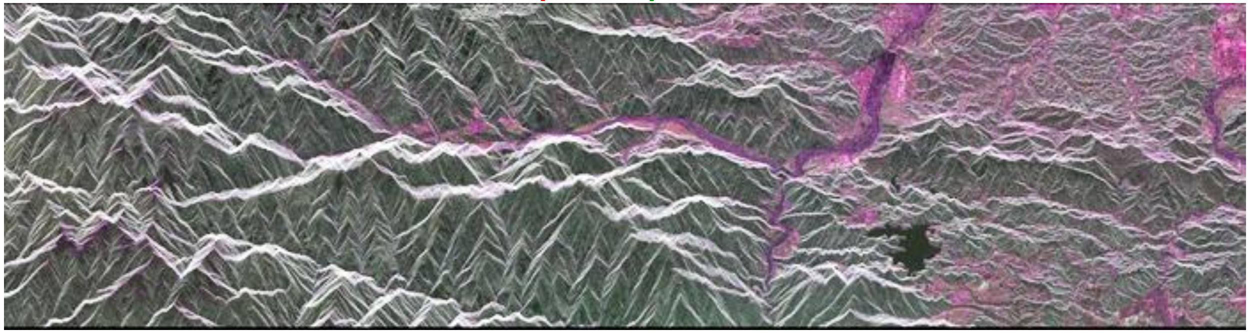

HH, 2HV, VV

2009/5/1

PASL1100905011424200907020002

©METI, ERSDAC

The destruction along the Cheleng-Pu fault caused by the Chi-Chi earthquake of 1999 September 21

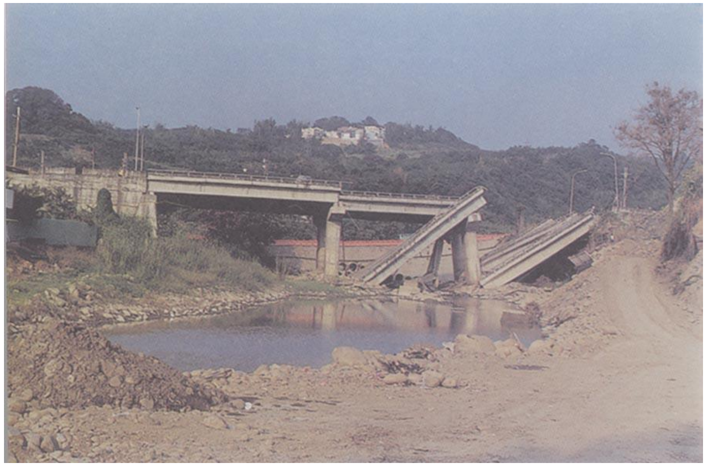


Scattering power decomposition

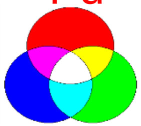

Niigata University

T33 Rotation

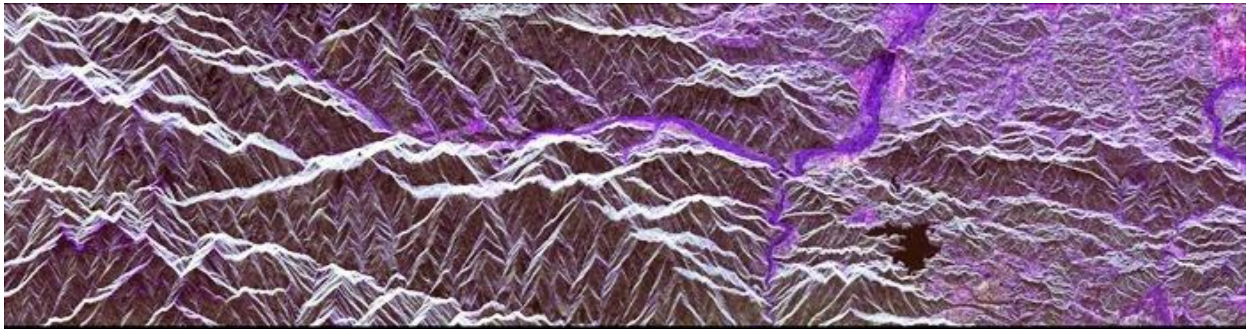

Pd, Pv, Ps

Pauli-basis

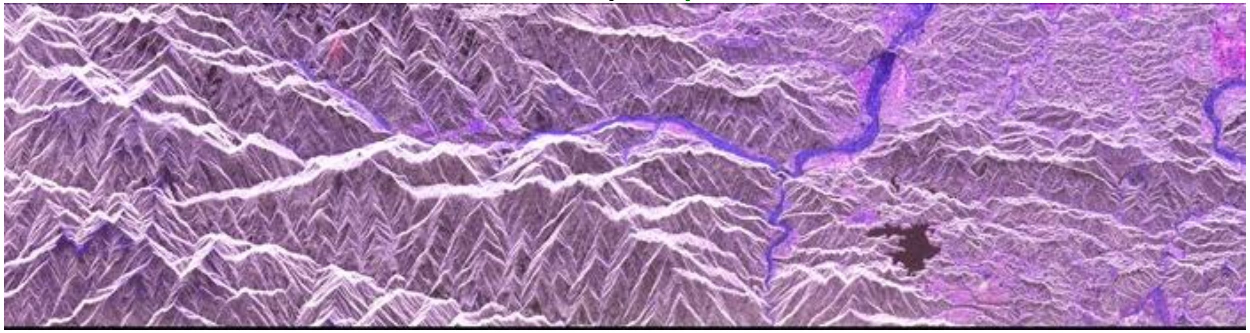

HH-VV, 2HV, HH+VV

HV-basis

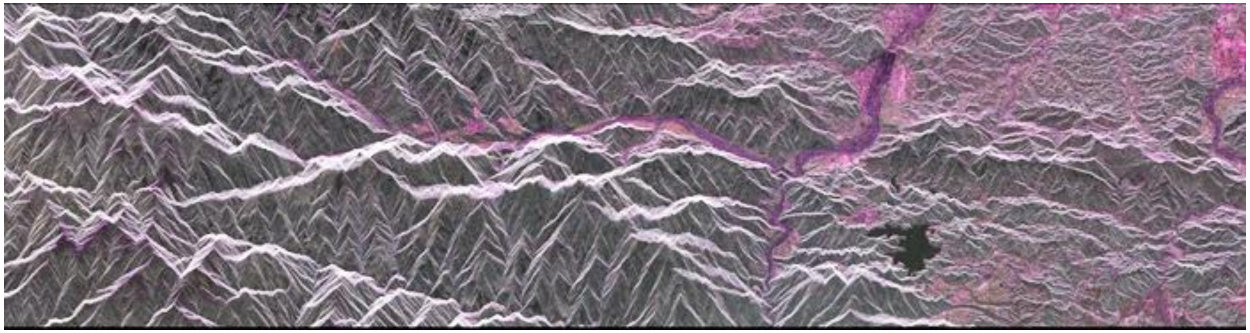

HH, 2HV, VV

Taiwan

23.703N
120.875E

2009/5/1

PASL1100905011424200907020002

©METI, ERSDAC

Taiwan

24.200N
120.766E
PASL110090501
14242009070200
03

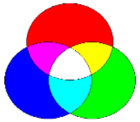

Niigata University

©METI, ERSDAC

2009/5/1

Google earth optical image

Scattering power decomposition (Pd, Ps, Pv)

Scattering power decomposition

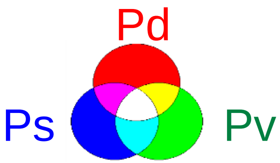

Niigata University

Pd, Pv, Ps

Pauli-basis

Taiwan
24.200N
120.983E

2009/5/1

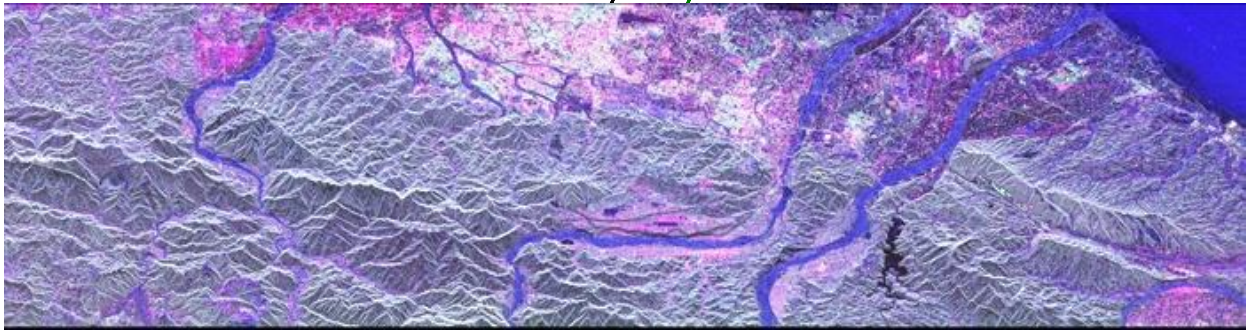

HH-VV, 2HV, HH+VV

HV-basis

PASL110090501142420090702003

©METI, ERSDAC

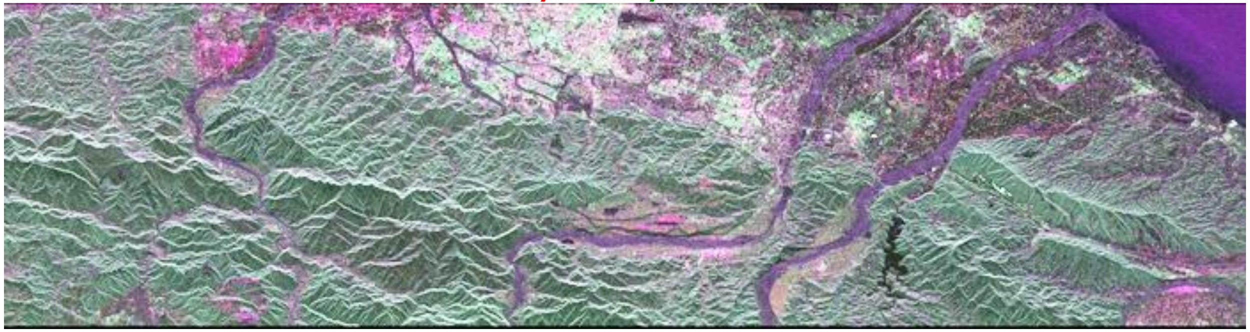

HH, 2HV, VV

Scattering power decomposition

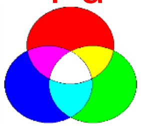

Niigata University

T33 Rotation

Taiwan
24.200N
120.983E

2009/5/1

PASL110090501142420090702003

©METI, ERSDAC

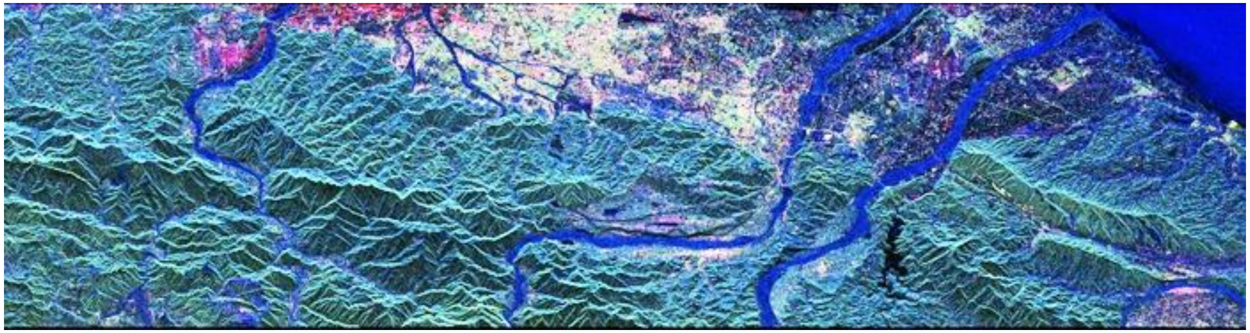

Pd, Pv, Ps

Pauli-basis

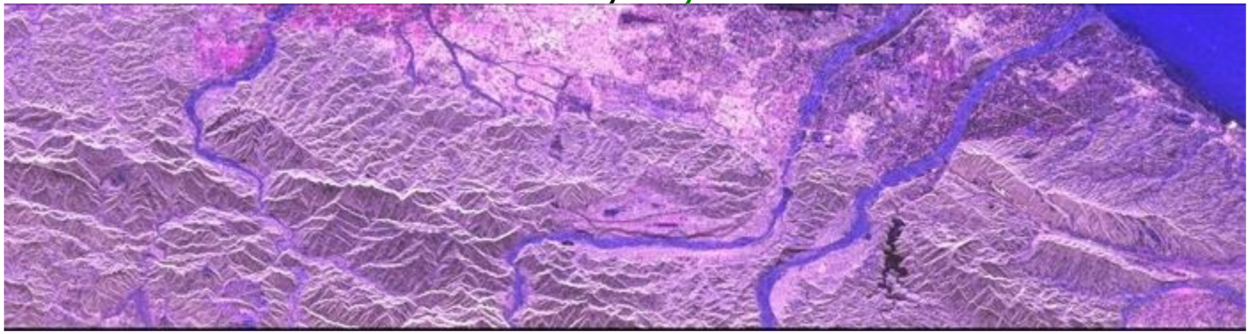

HH-VV, 2HV, HH+VV

HV-basis

HH, 2HV, VV

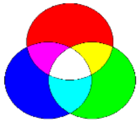

Niigata University

Taiwan

24.697N
120.656E

2009/5/1

PASL1100905011424200907020004

©METI, ERSDAC

Google earth optical image

Scattering power decomposition (Pd, Ps, Pv)

Scattering power decomposition

Pd

Ps 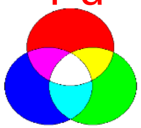 Pv

Niigata University

T33 Rotation

Taiwan
24.200N
120.766E
2009/5/1

PASL110090501142420090702004

©METI, ERSDAC

Pd, Pv, Ps

Pauli-basis

HH-VV, 2HV, HH+VV

HV-basis

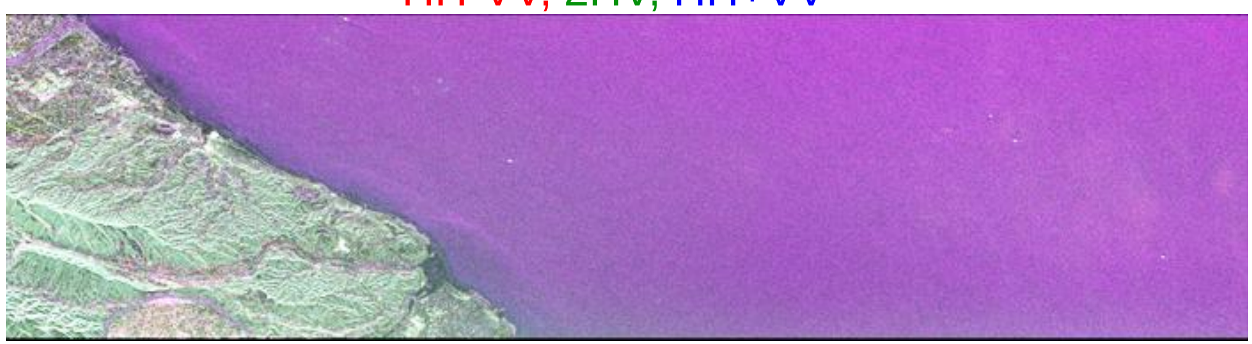

HH, 2HV, VV

ALOS-PALSAR Polarimteric Mode

2008 Sichuan earthquake, China

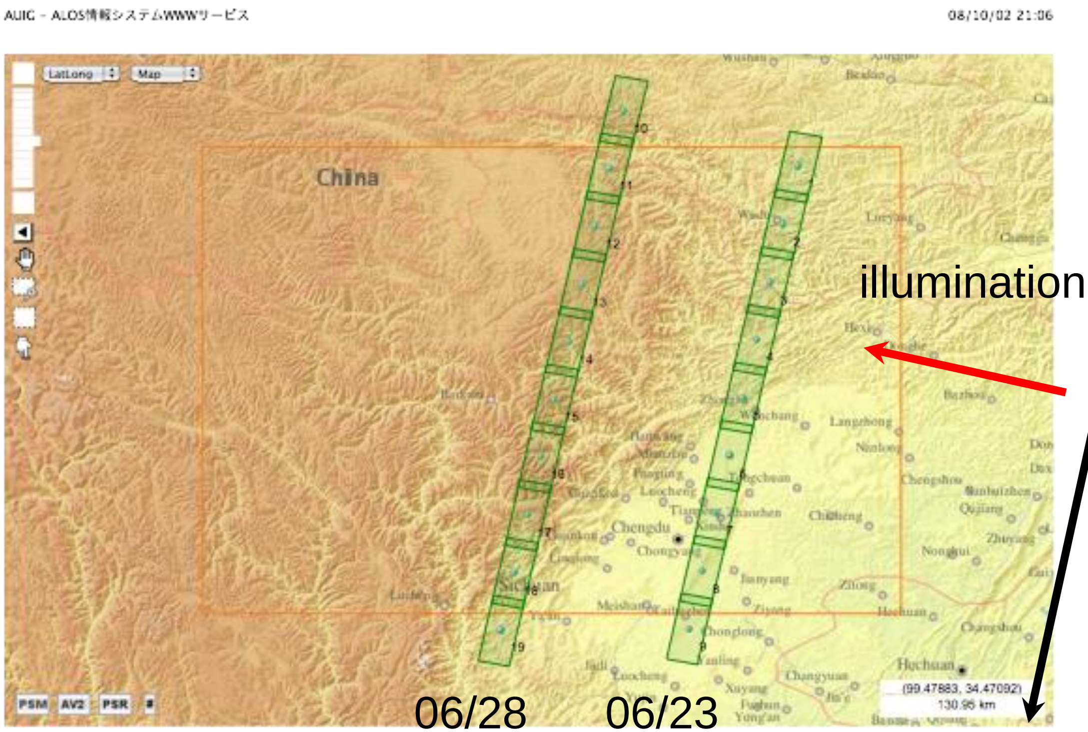

Descending

©JAXA, METI

Yoshio Yamaguchi

Niigata University

2008 Sichuan earthquake China

31.850N
104.644E

2008/6/23

ALPSRP128522970-P1.1__D

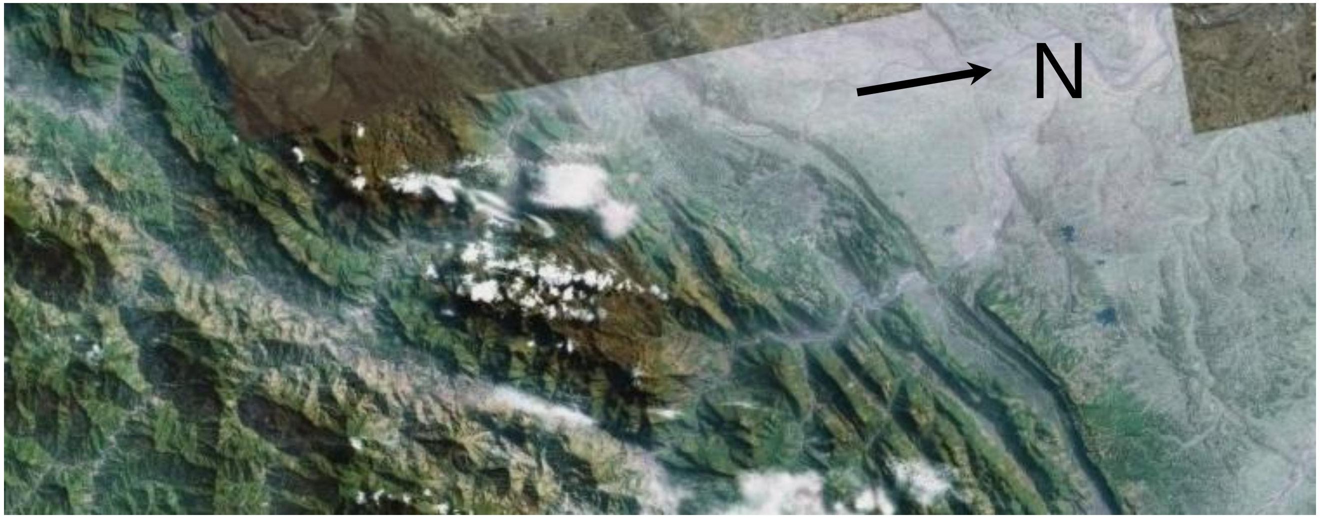

Google earth optical image

©JAXA, METI

Scattering power Decomposition

Pd

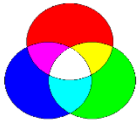

Ps Pv

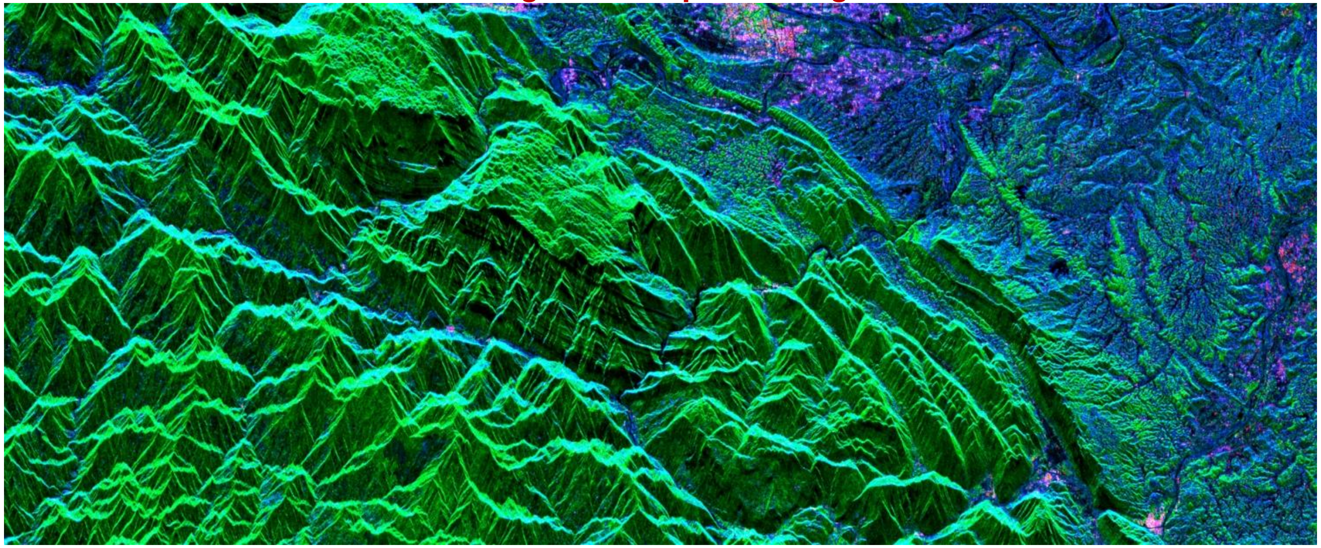

Decomposed image (Ps, Pd, Pv)

Scattering power decomposition

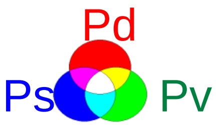

Niigata University

ALPSRP128522970-P1.1__D

2008/6/23

Pauli-basis

2008 Sichuan earthquake China

HV-basis

31.850N
104.644E

©JAXA, METI

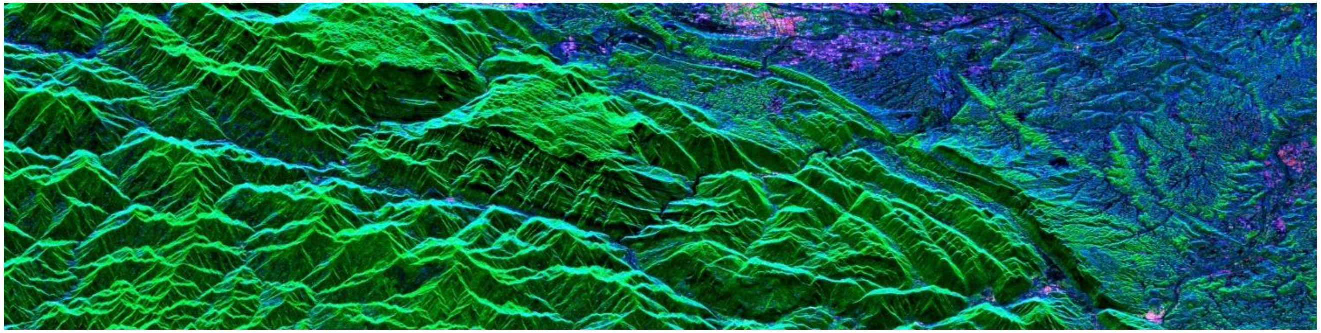

Pd, Pv, Ps (80 up)

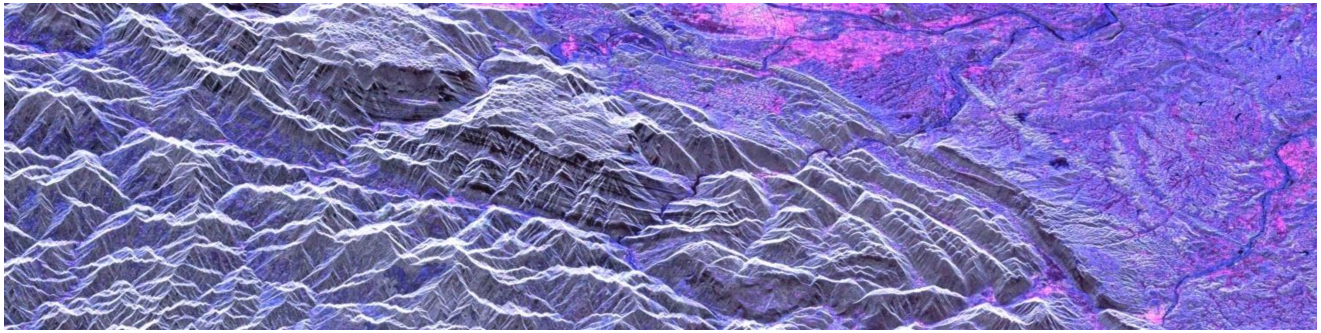

HH-VV, 2HV, HH+VV (0-50 up)

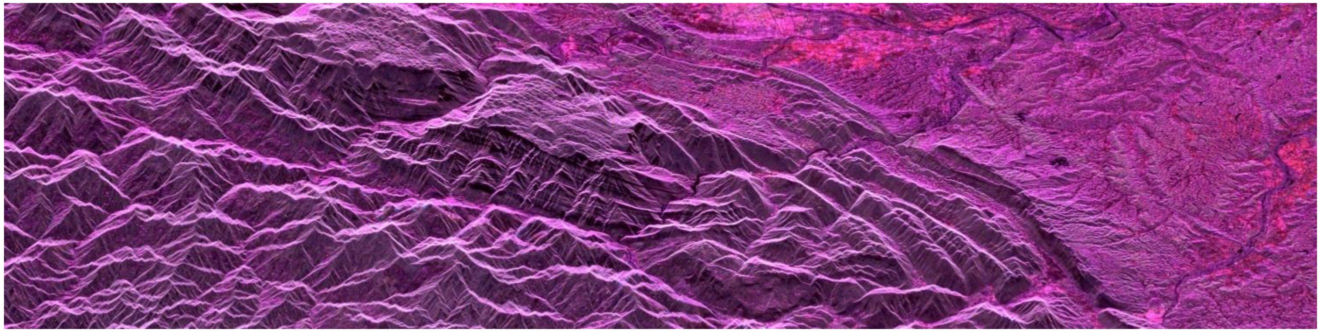

HH, 2HV, VV (50 up)

Scattering power decomposition

Niigata University

ALPSRP128522970-P1.1__D

2008/6/23

T33 Rotation

2008 Sichuan earthquake China

31.850N
104.644E

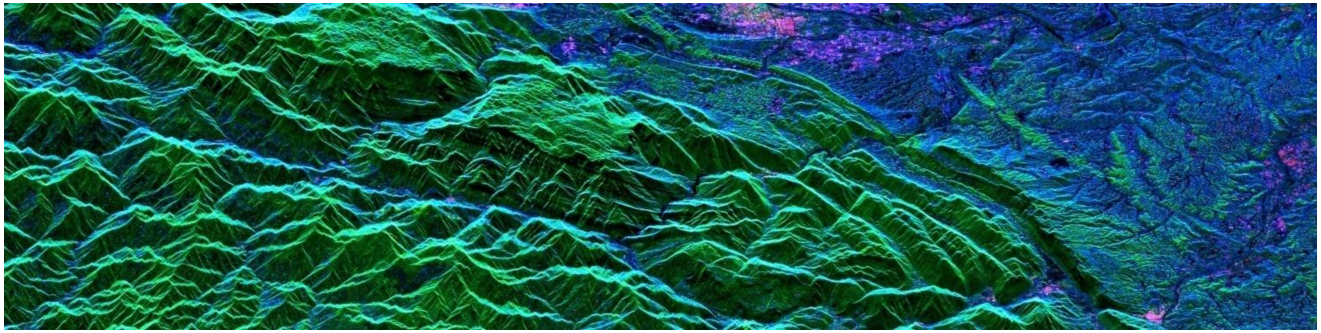

Pd, Pv, Ps (80 up)

Pauli-basis

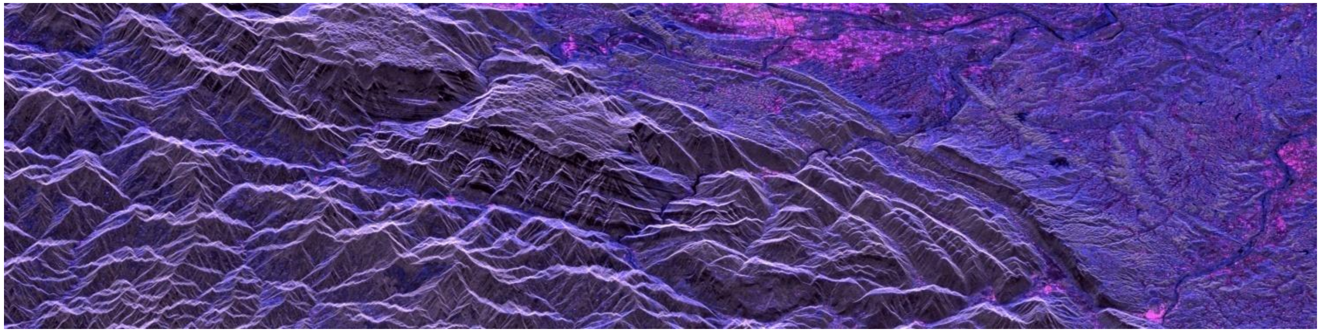

HH-VV, 2HV, HH+VV (80 up)

HV-basis

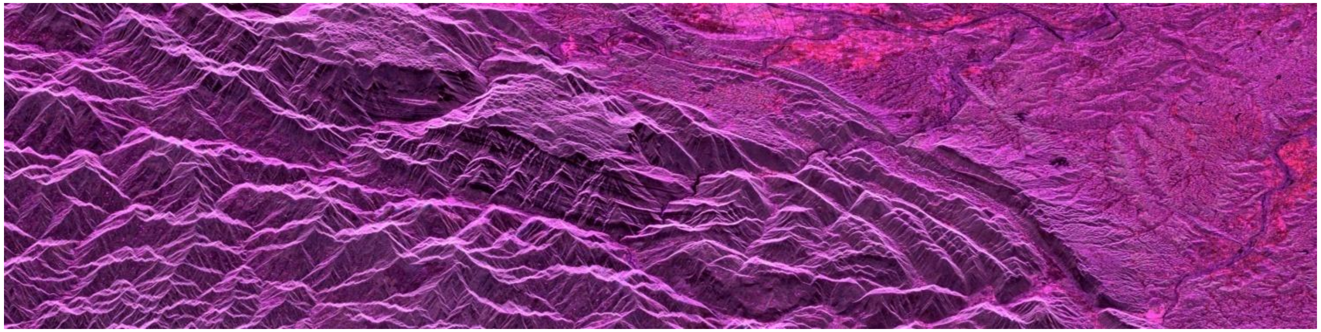

HH, 2HV, VV (50 up)

©JAXA, METI

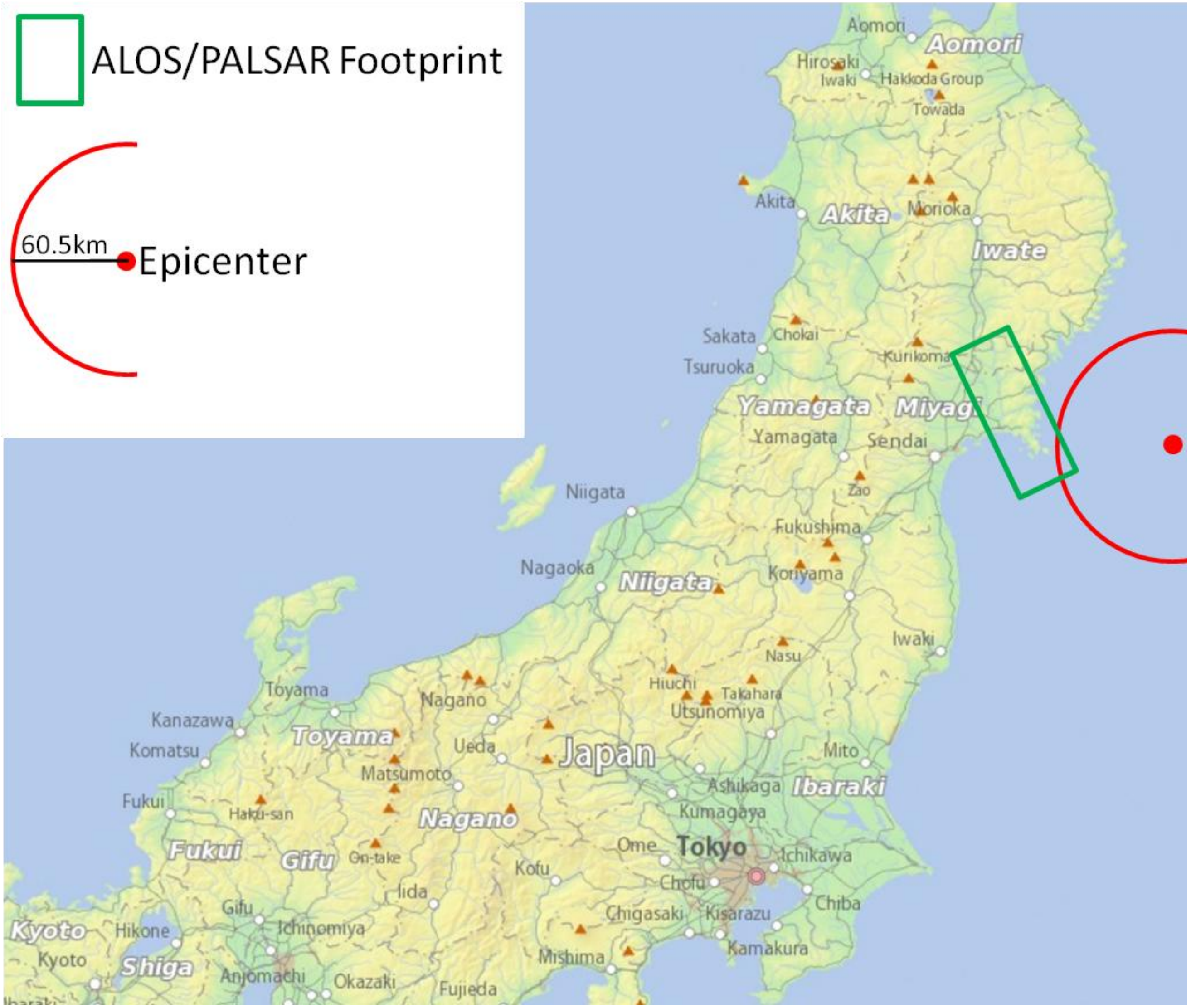

Off-Tohoku 9.0 Earthquake with Super-Tsunami

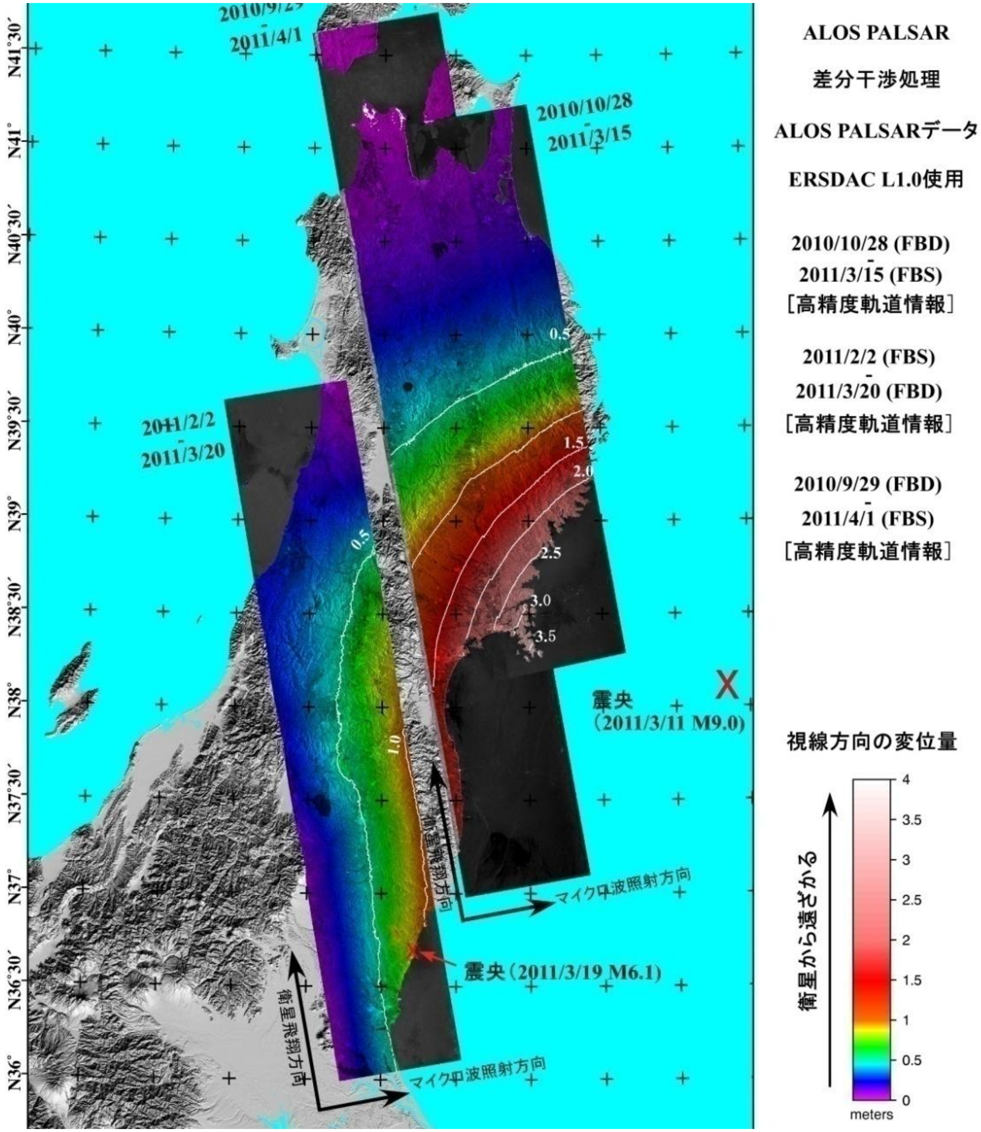
ALOS PALSAR
差分干渉処理
ALOS PALSARデータ
ERSDAC L1.0使用
2010/10/28 (FBD)
-
2011/3/15 (FBS)
[高精度軌道情報]
2011/2/2 (FBS)
-
2011/3/20 (FBD)
[高精度軌道情報]
2010/9/29 (FBD)
-
2011/4/1 (FBS)
[高精度軌道情報]
震央
(2011/3/11 M9.0)
震央(2011/3/19 M6.1)
視線方向の変位量
衛星から遠ざかる
meters
衛星飛翔方向
マイクロ波照射方向
2010/10/28
2011/3/15
2011/2/2
2011/3/20
2011/4/1

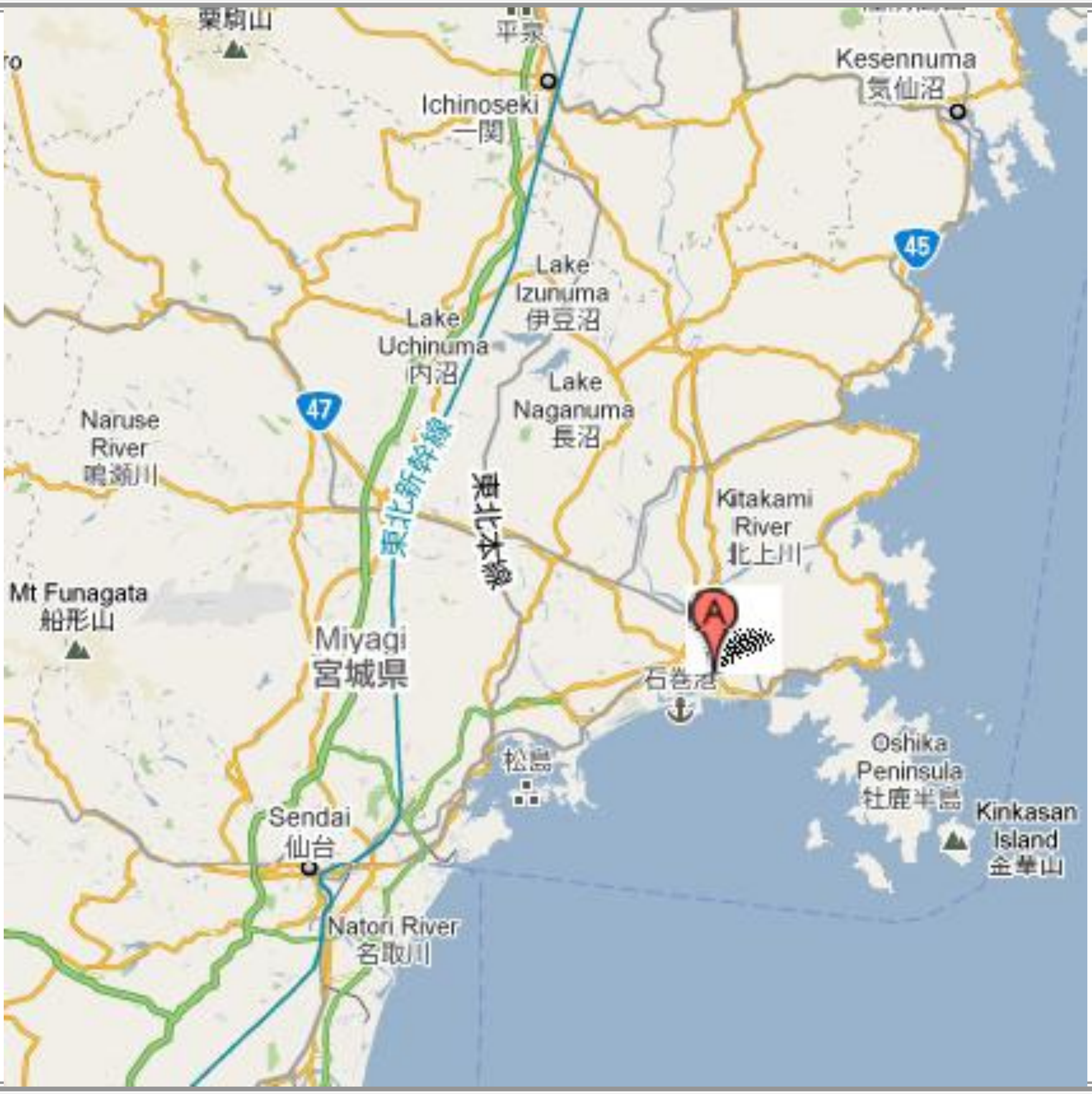

Ishinomaki harbor
38*25’N, 141*18’E

Destruction of City and Harbor of Ishinomaki by 110311 Tsu-nami (Harbor-Wave)


Before
Ishinomaki
Matsushima Air Field
After

Off-Tohoku M9 Seaquake & Tsunami 110311

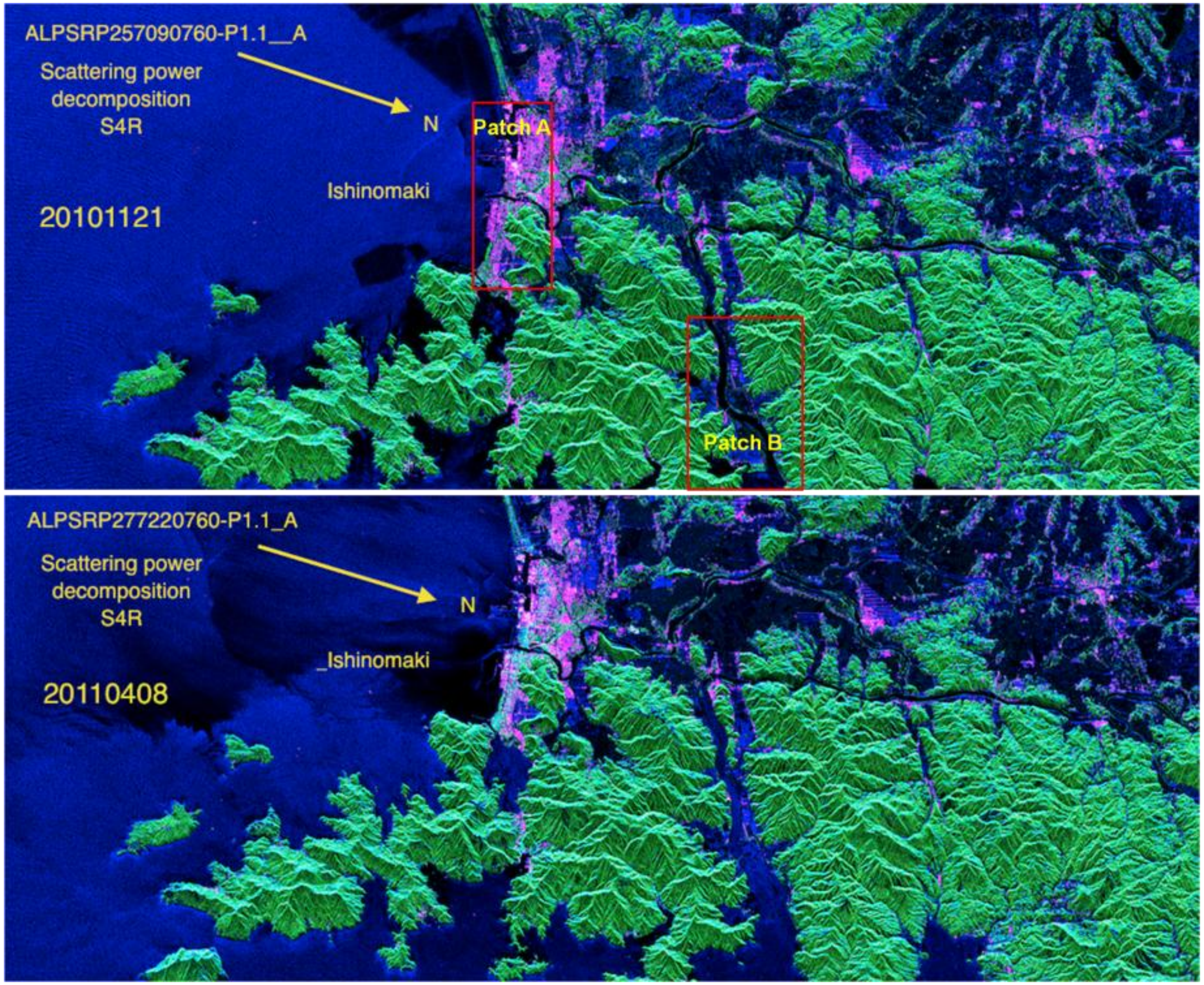

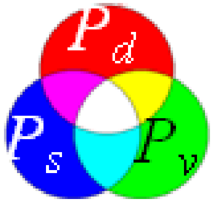

Off-Tohoku M9 Seaquake & Tsunami 110311

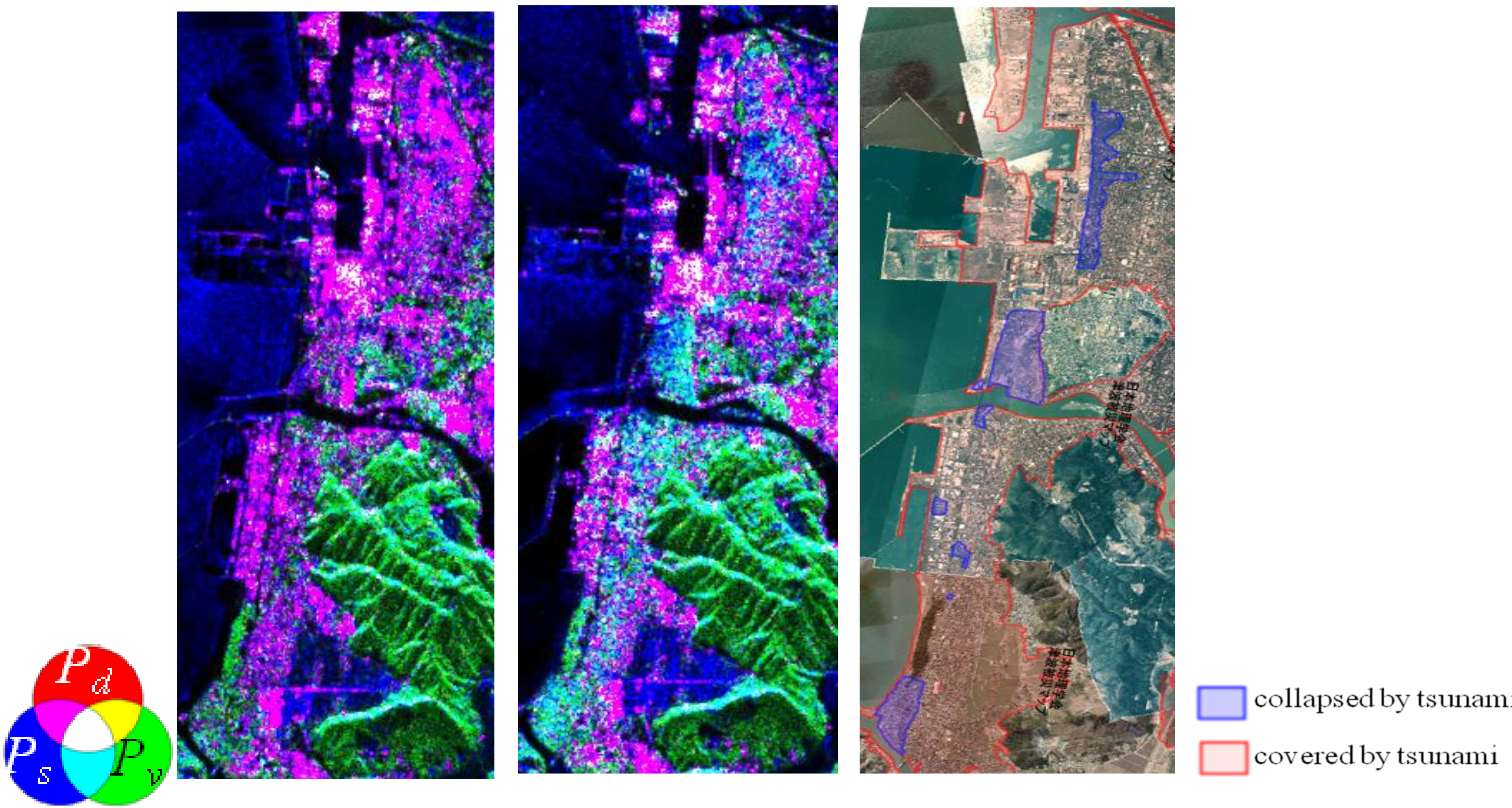

Off-Tohoku M9 Seaquake & Tsunami 110311

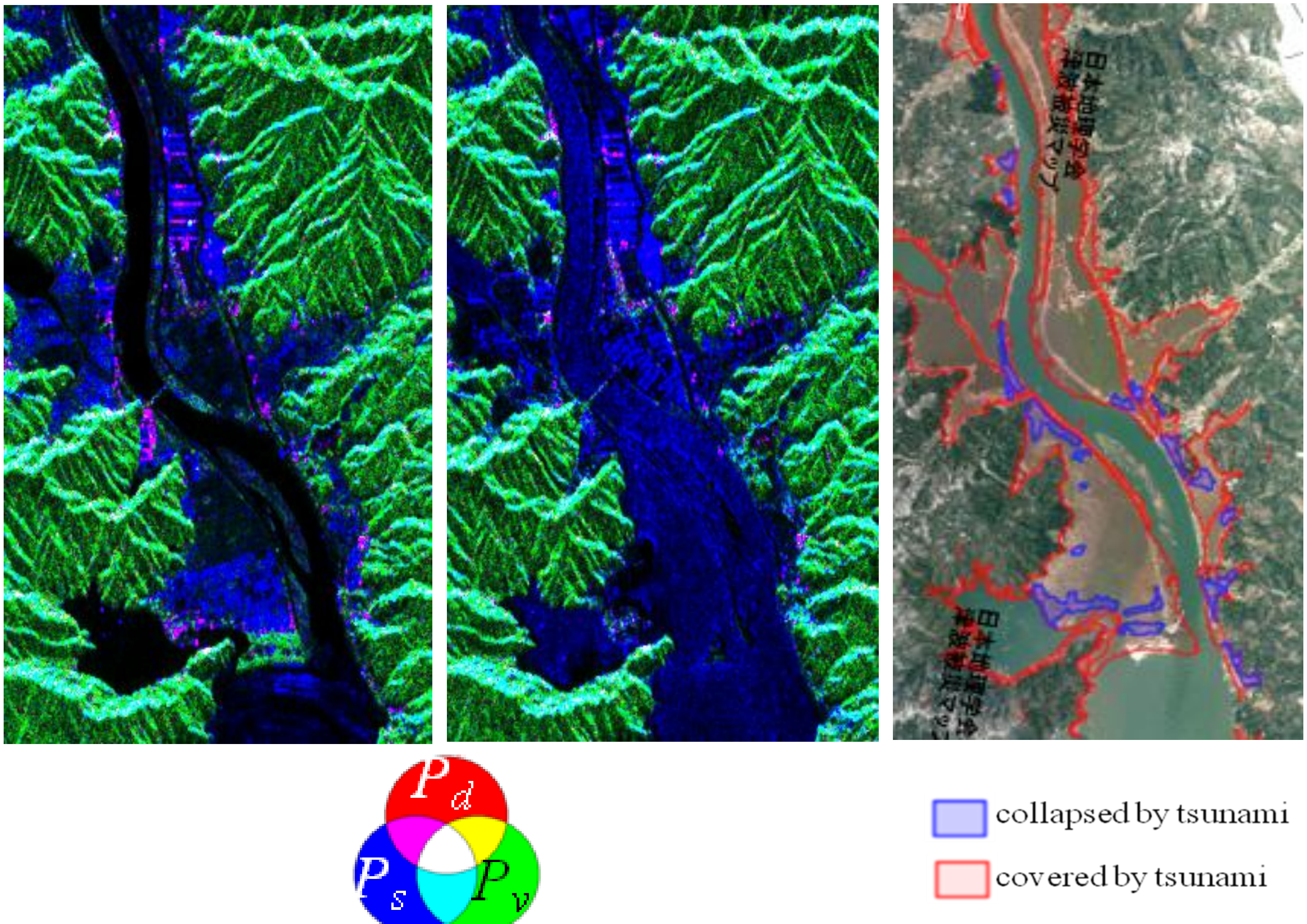

ALOS-2

2013~

ALOS-1

2006~2011

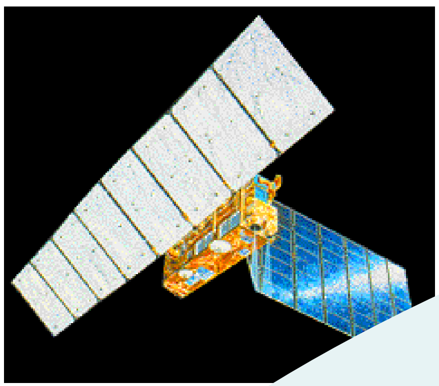

JERS-1

1992-1998

ALOS-PALSAR Polarimetric Mode

Philippines

Ascending

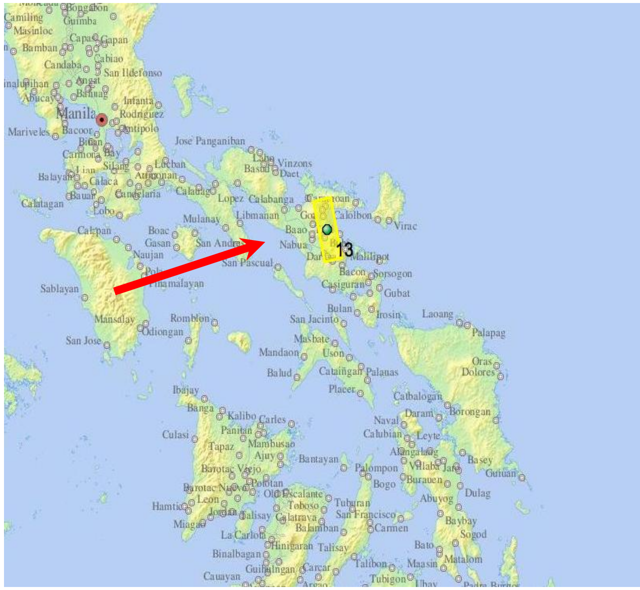

13.501N
123.551E

2009/5/30

Data no.
ALPSRP178330
260

© METI, JAXA

Yoshio Yamaguchi
Niigata University

Mt. Mayon – The pearl of the Orient

Philippines

Mt. Mayon

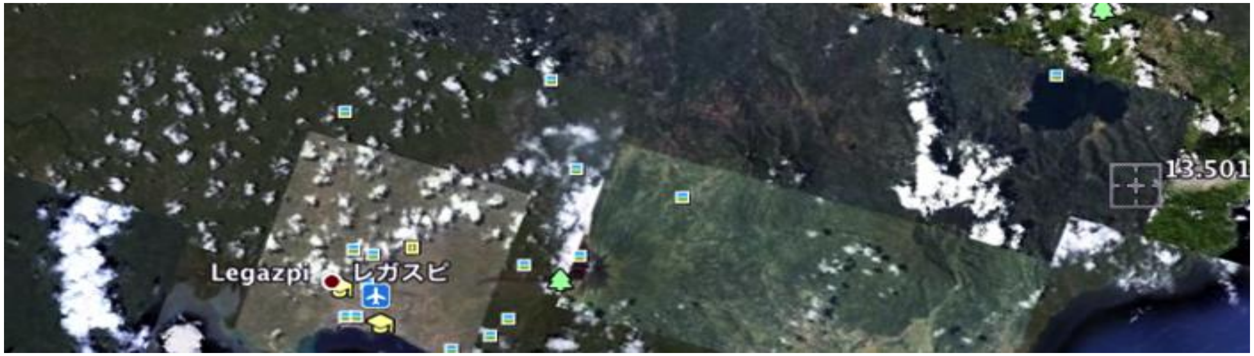

Google Earth optical image

N

13.501N
123.551E

2009/5/30

Data no.
ALPSRP178330260

©METI, JAXA

Scattering power Decomposition

Pd
Ps
Pv

Niigata University

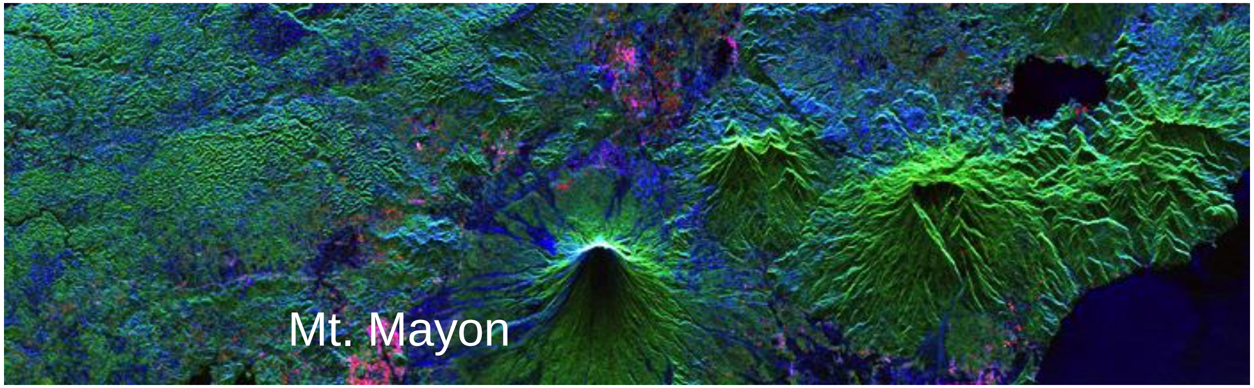

Decomposed image (Ps, Pd, Pv) with rotation 2*12 window

Philippines

13.498N
123.561E

2010/1/15

Data no.
ALPSRP211880260

©METI, JAXA

Scattering power Decomposition

Pd

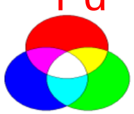

Ps Pv

Niigata University

Mt. Mayon

Google Earth optical image

N

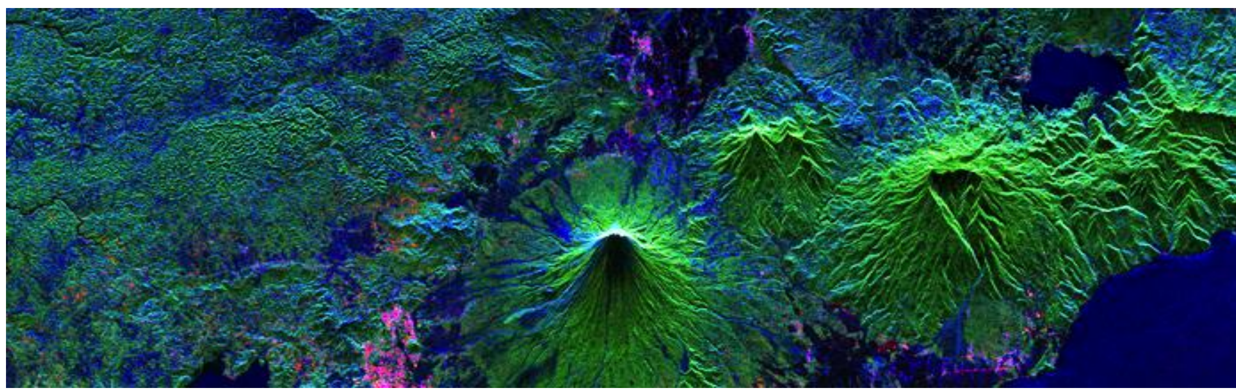

Decomposed image (Ps, Pd, Pv) with rotation 2*12 window

Philippines

Mt. Mayon

13.498N
123.568E

2010/4/17

N

Google Earth optical image

Data no.
ALPSRP225300260-P1.1__A

©METI, JAXA

Scattering power Decomposition

Pd

Ps 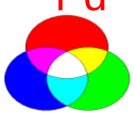 Pv

Niigata University

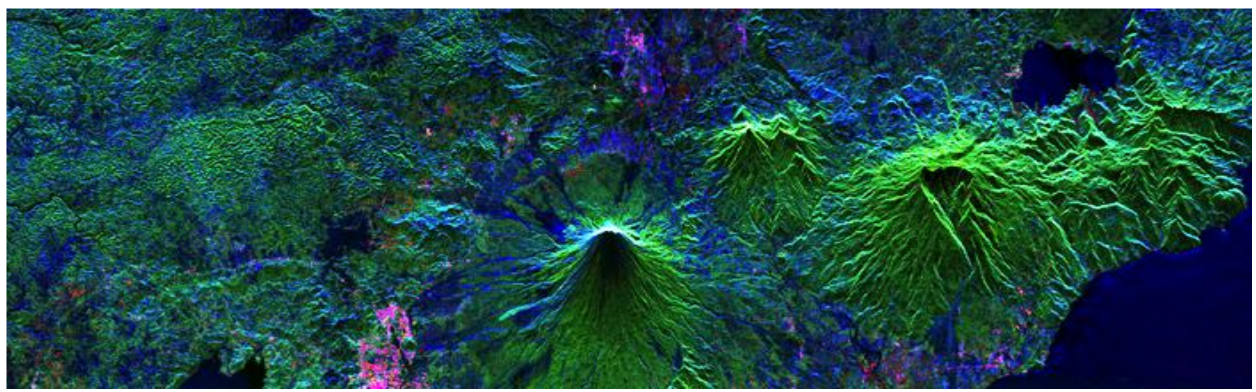

Decomposed image (Ps, Pd, Pv) with rotation 2*12 window

Philippines

Mt. Mayon

2009/5/30

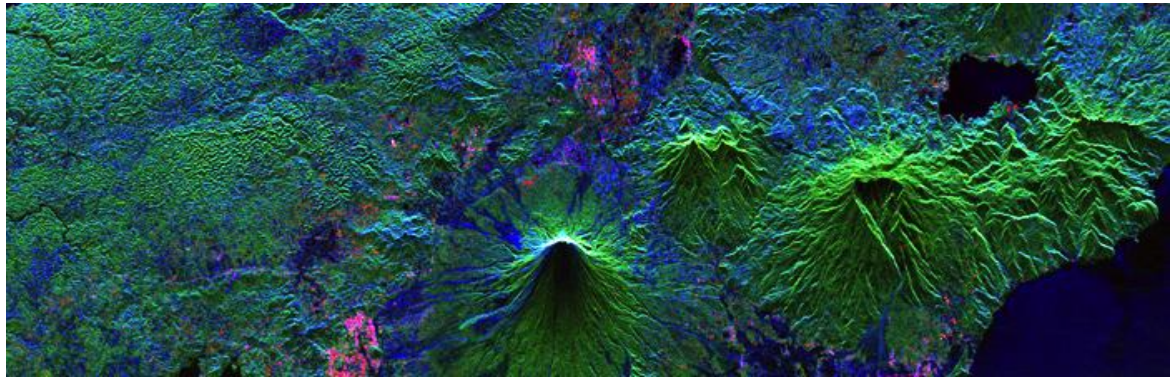

2010/1/15

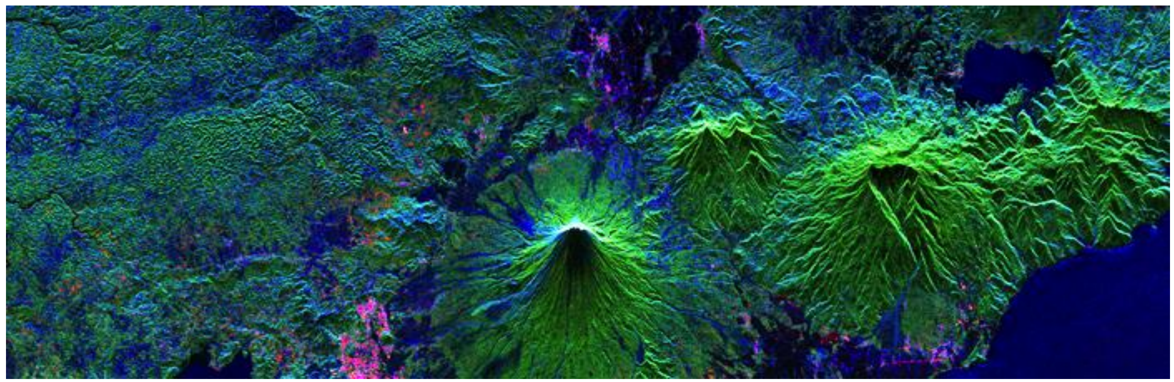

2010/4/17

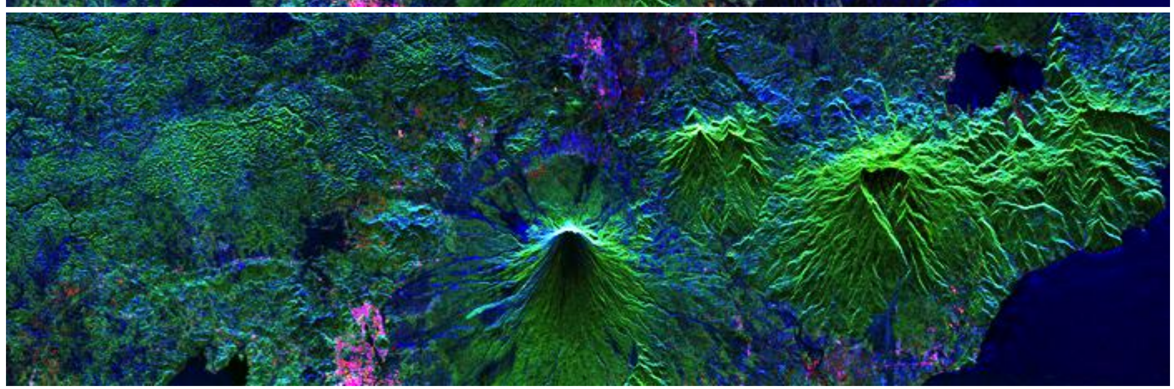

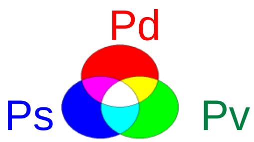

Niigata University

South-East Asia

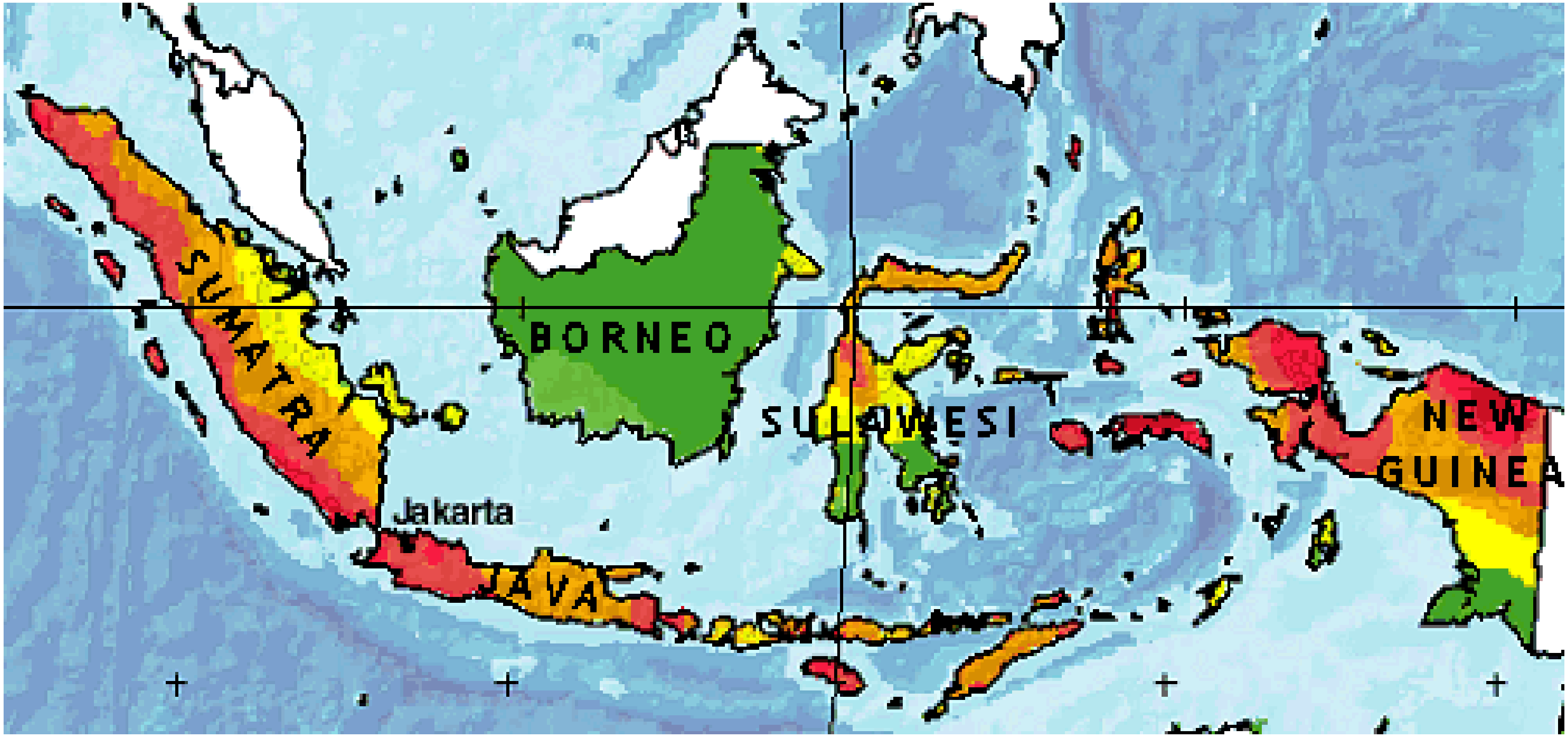

ALOS-PALSAR Polarimteric Mode

Ascending

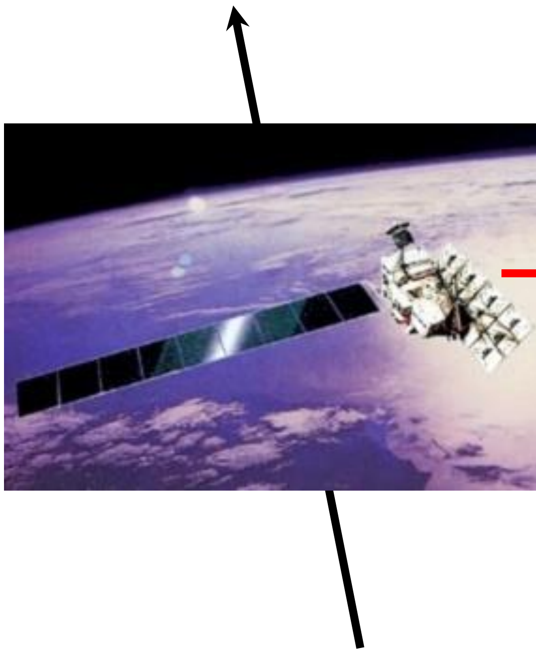

Indonesia

2007/3/10

Data no.
ALPSRP059887030
ALPSRP059887040

2009/3/15

Data no.
ALPSRP167247030
ALPSRP167247040

©JAXA, METI

Yoshio Yamaguchi

Niigata University

Indonesia

−7.942N
112.870E

2007/3/10

ALPSRP059887030-P1.1__A

©JAXA, METI

Scattering power Decomposition

Pd

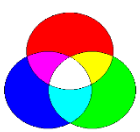

Ps Pv

Niigata University

Google earth optical image

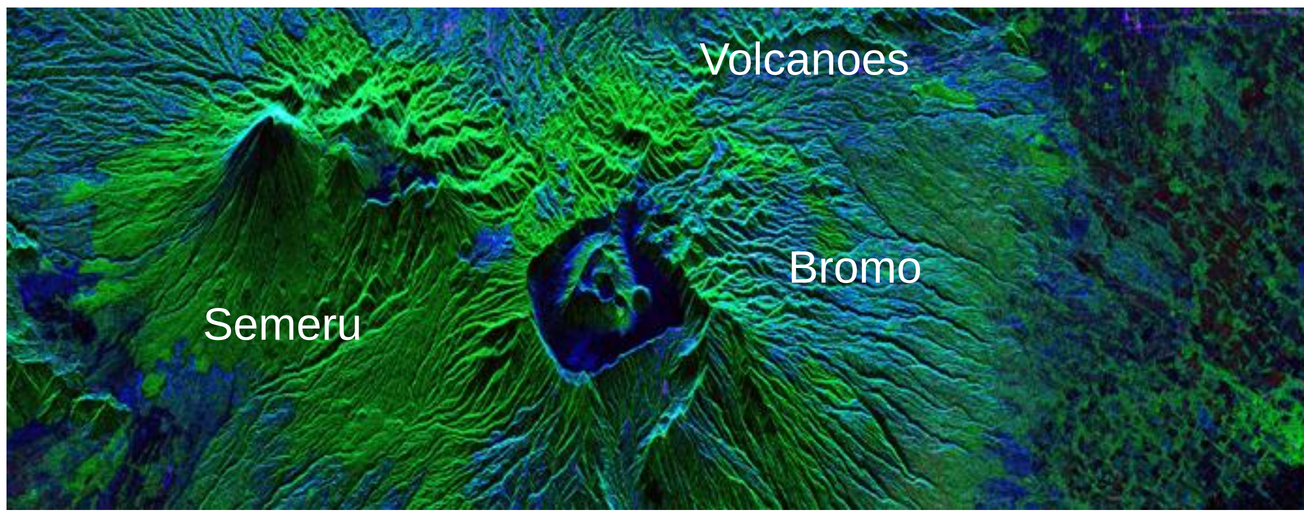

Decomposed image (Ps, Pd, Pv)

Mount Semeru puffs steam behind a cloud of sulphur gas from Mount Bromo in the Tengger caldera on Java.

Scattering power decomposition

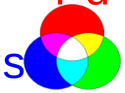

Niigata University

2007/3/10

Pauli-basis

−7.942N
112.870E

HV-basis
Indonesia

ALPSRP059887030-P1.1__A

©JAXA, METI

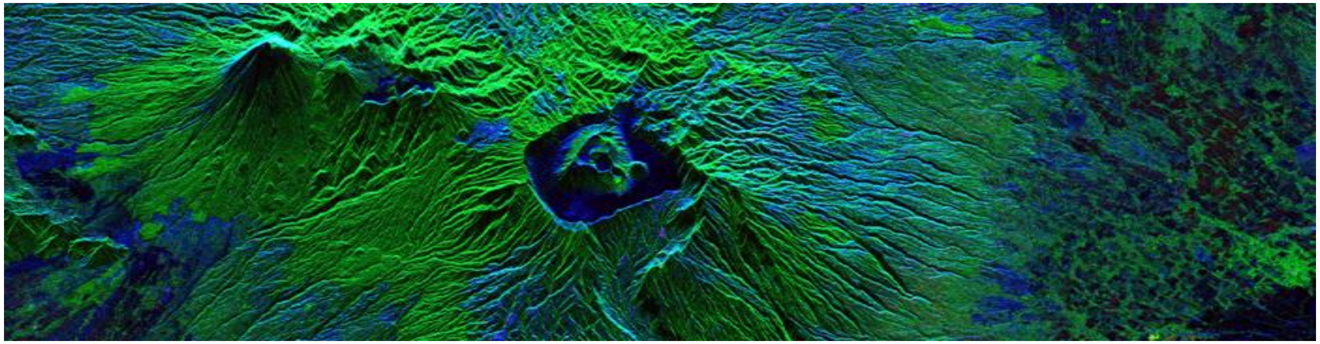

Pd, Pv, Ps (80 up)

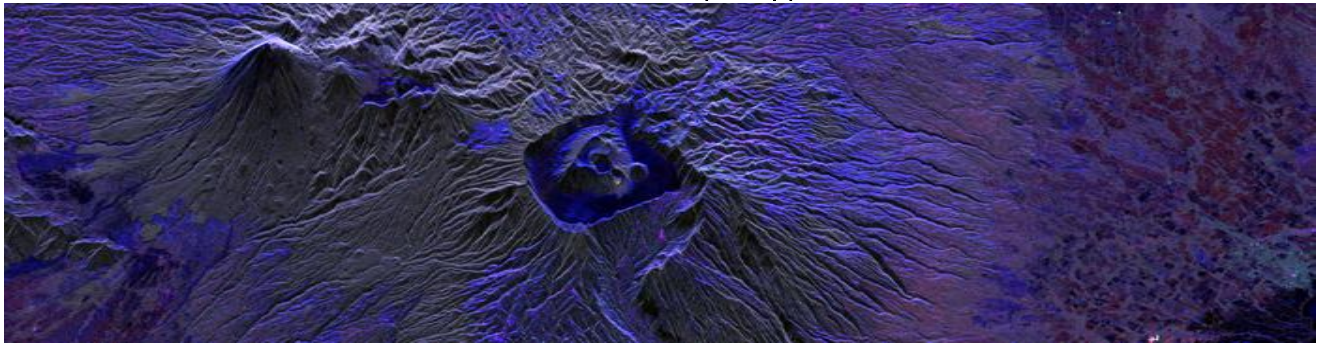

HH-VV, 2HV, HH+VV (0-50 up)

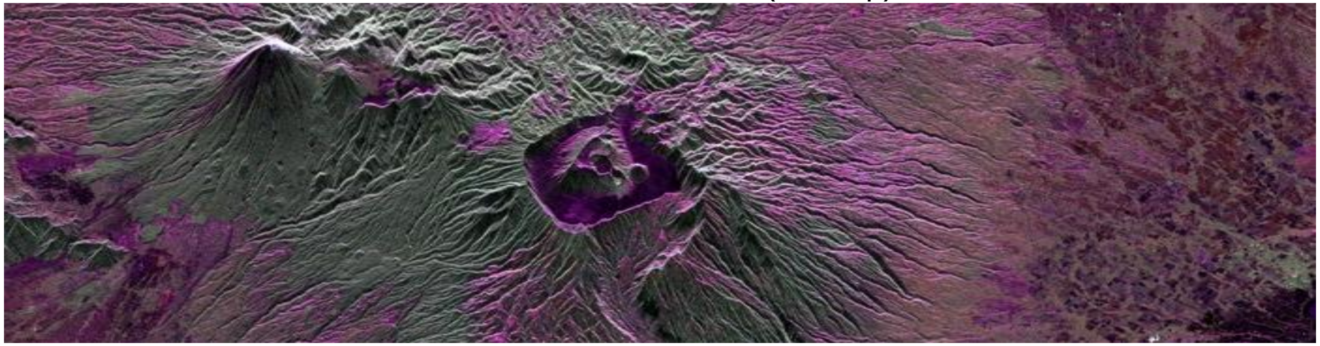

HH, 2HV, VV (50 up)

Scattering power decomposition

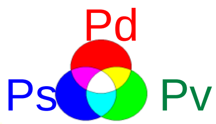

Niigata University

2007/3/10

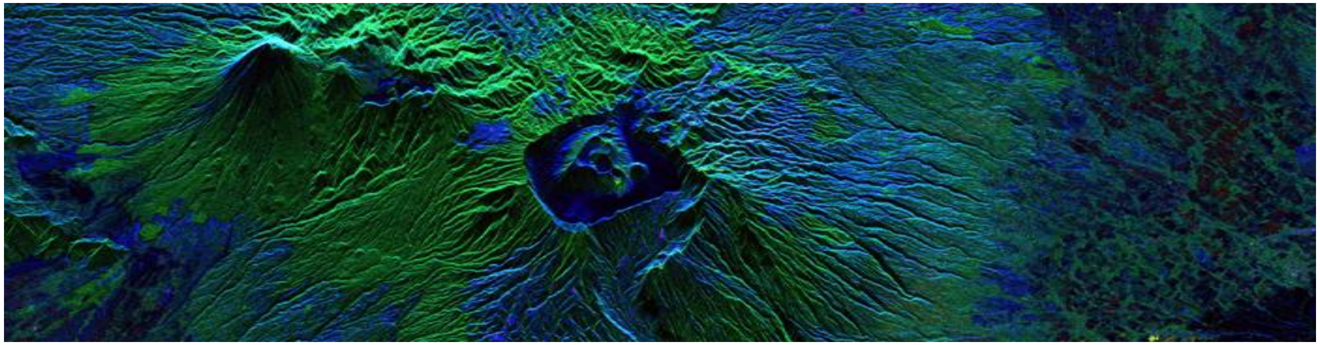

Pd, Pv, Ps (80 up)

T33 Rotation

Pauli-basis

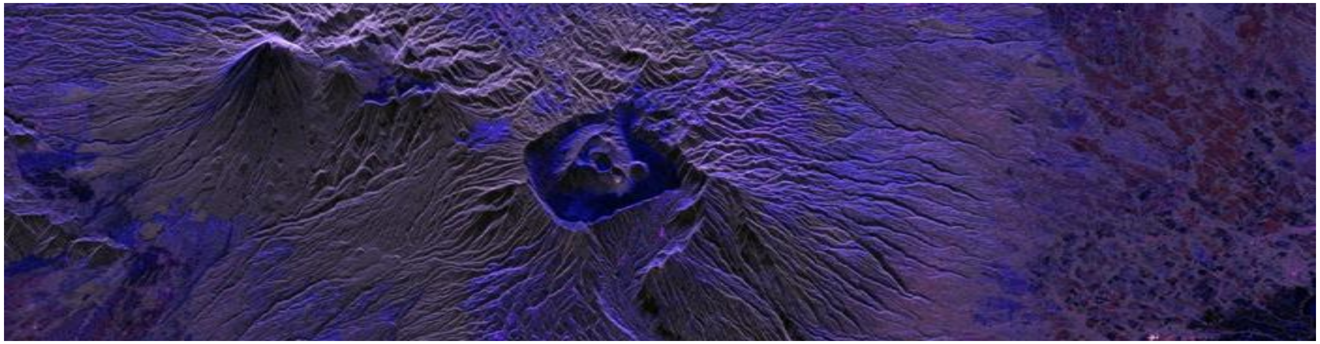

HH-VV, 2HV, HH+VV (80 up)

HV-basis

Indonesia
−7.942N
112.870E

ALPSRP059887030-P1.1__A

©JAXA, METI

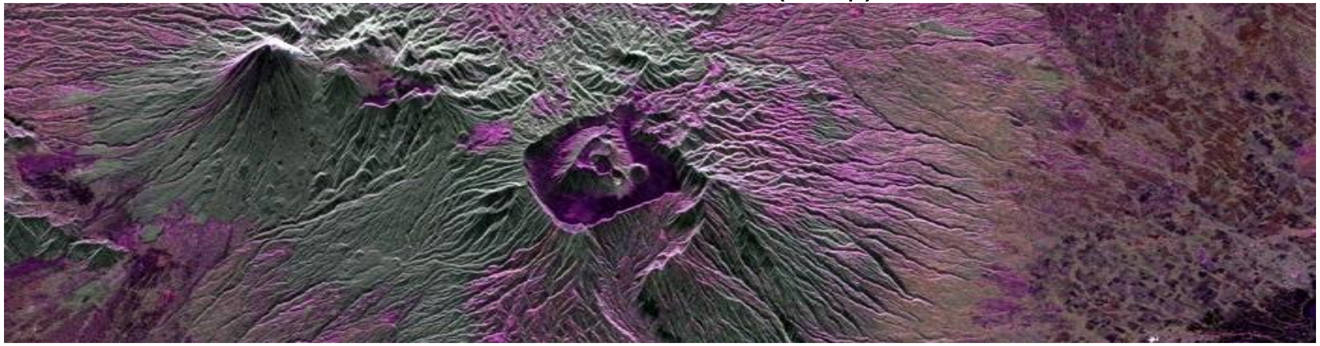

HH, 2HV, VV (50 up)

"Natural hazards are inevitable.
Natural disasters are not."

ALOS-PALSAR Polarimteric Mode: 2007 ~ 2010

Ascending

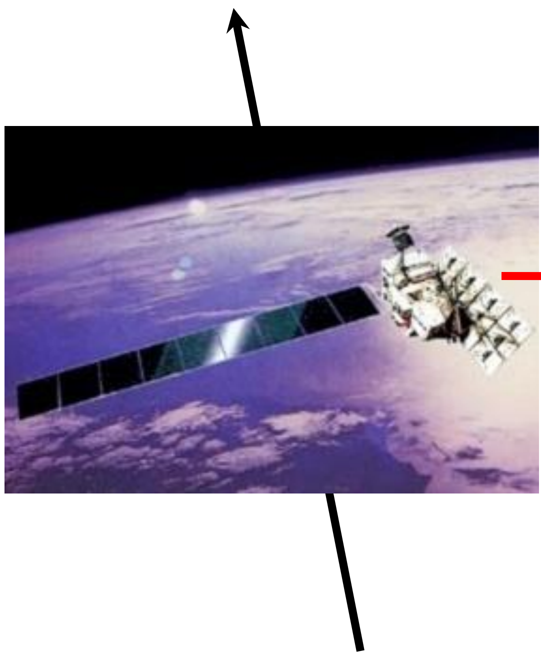

Indonesia

2007/3/10

Data no.
ALPSRP059887030
ALPSRP059887040

2009/3/15

Data no.
ALPSRP167247030
ALPSRP167247040

©JAXA, METI

Yoshio Yamaguchi

Niigata University

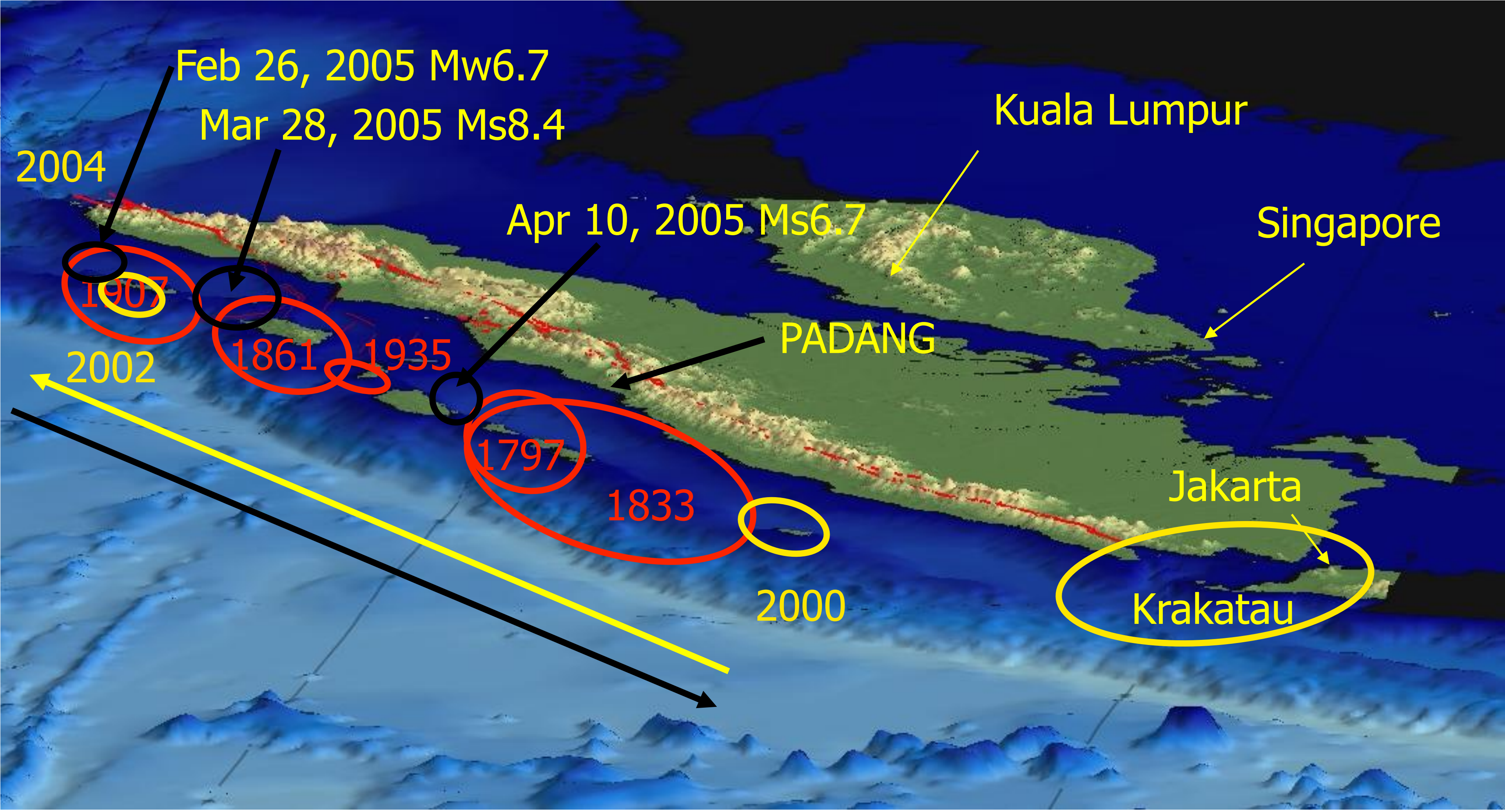

A flurry of ruptures have occurred since 2000

EARTH'S EXPANSION

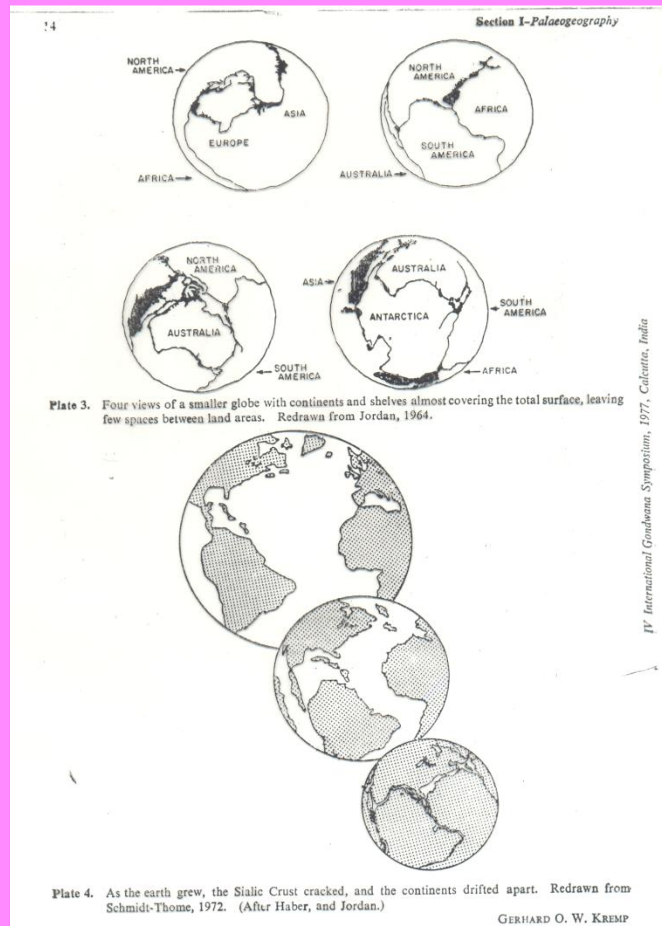

:4 Section I–*Palaeogeography*

Plate 3. Four views of a smaller globe with continents and shelves almost covering the total surface, leaving few spaces between land areas. Redrawn from Jordan, 1964.

IV International Gondwana Symposium, 1977, Calcutta, India

Plate 4. As the earth grew, the Sialic Crust cracked, and the continents drifted apart. Redrawn from Schmidt-Thome, 1972. (After Haber, and Jordan.)

GERHARD O. W. KREMP

EARTH'S EXPANSION

1932 HILGENBERG Model of Primondial Earth

• O. C. Hilgenberg of Germany in 1933 showed that if the radius in a model of earth could be reduced to two-third of its length, all the continental blocks could be adjusted in a perfectly snug-fit manner. The concept of earth's expansion was revived in the 1960s by S. W. Carey of Australia.

• It can be noted that in the primordial small earth there were no oceans although epicontinental seas or lakes were present. The ocean-forming water at that stage must have been associated with the mantle. Under such condition, namely, association of large quantum of water under pressure, the mantle rock must have been considerably fluid (Sen, 1983-2003).

• **This vital clue has been based on experimental studies conducted by Roy and Tuttle (1961) confirming depression of melting point of silicate rocks under hydrothermal and ultrahigh pressure condition.**

Internal structure of the expanded earth

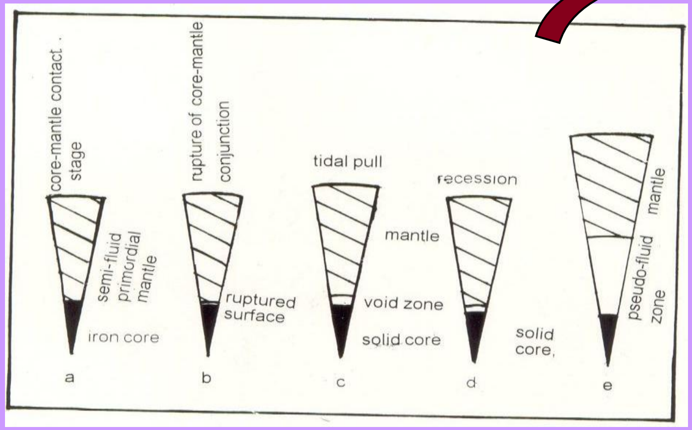

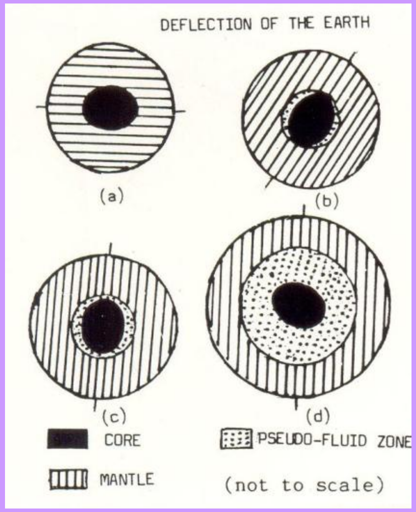

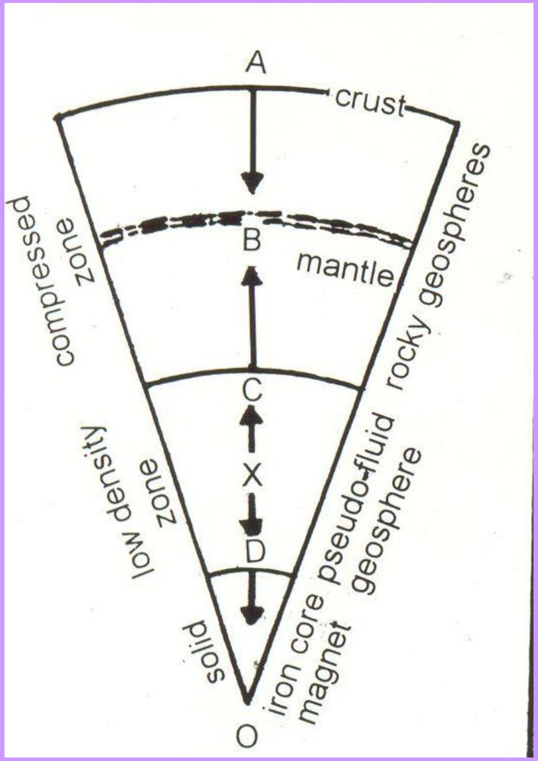

Fundamental Earth Parameters

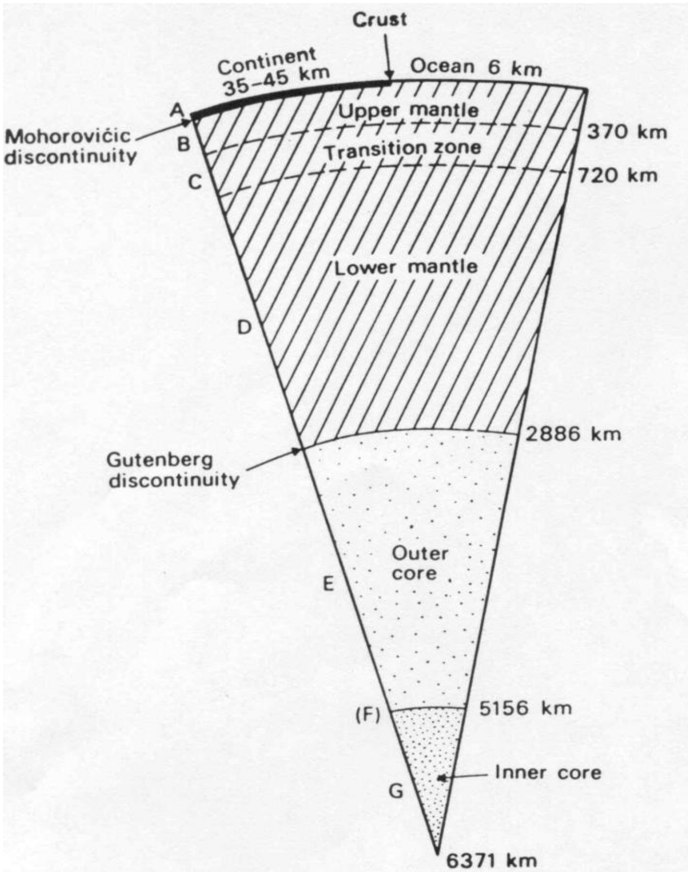

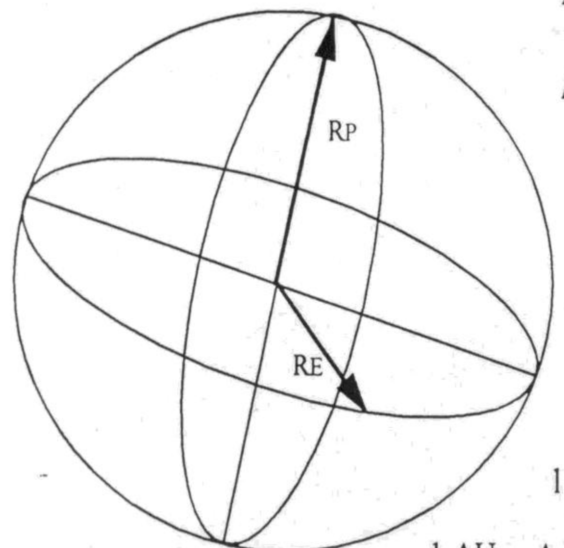

$R_{EQUATOR} \cong 6.378 \times 10^{6} m$

$R_{POLAR} \cong 6.356 \times 10^{6} m$

$L = 2\pi R \qquad L_E \cong 40,054 km$

$L_P = 39,918 km$

1 mi = 5280 ft = 1.609 km

1 AU ≡ Astronomial Unit = 1.496×10^{11} m

The layering within the planet earth and its equatorial and polar radius

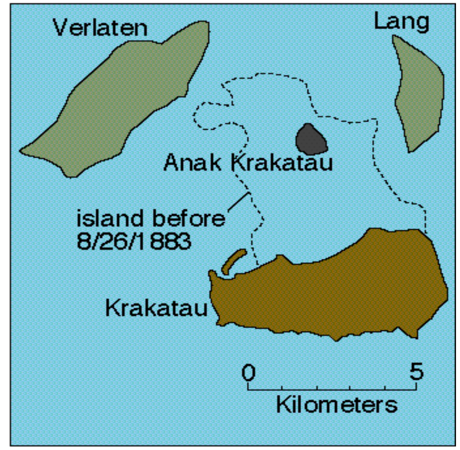

From Simkin and Fiske, 1983

Krakatau

8/26/1883

Next major eruption within 20 years

Indian Ocean Tsunamis: 1833 & 2004

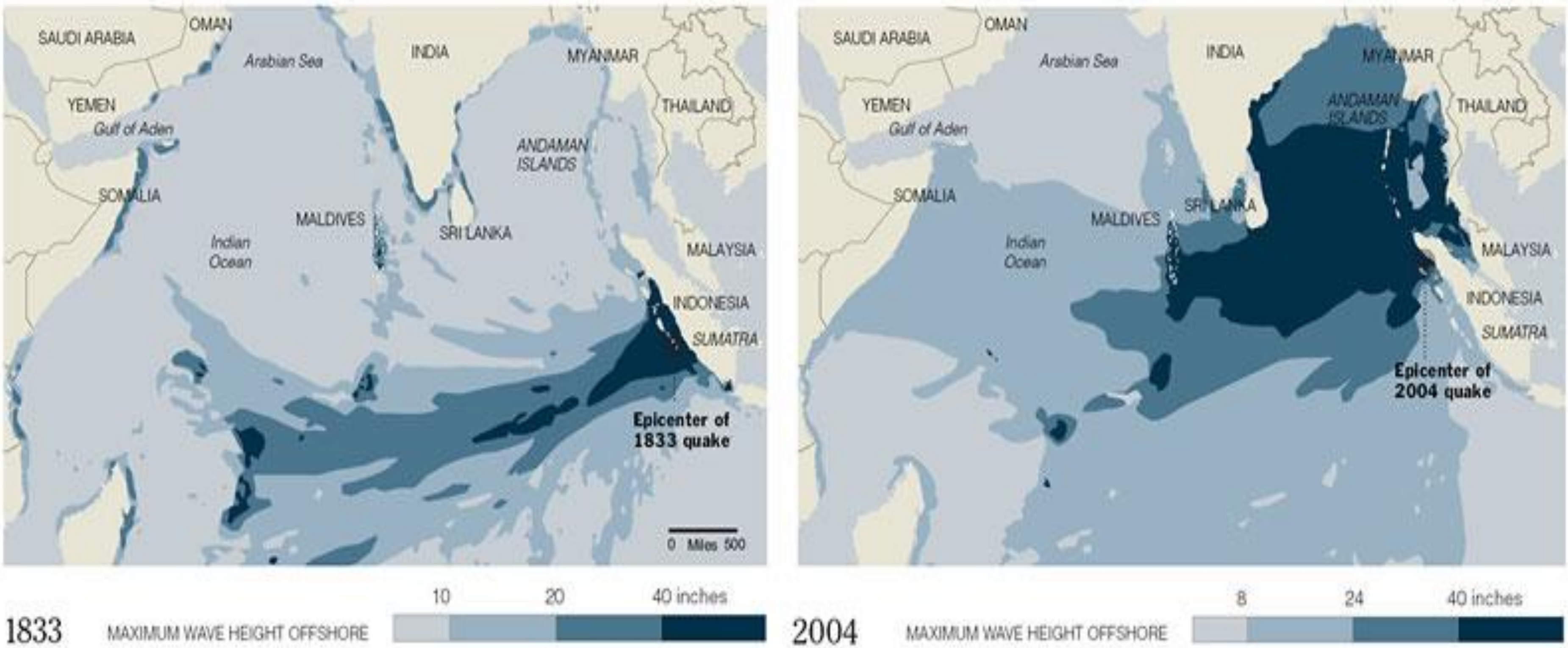

Hannah Fairfield/The New York Times, Science Section, January 4, 2005

Physical interpretation of rain cell signatures

- Partial backscattering at hydrometeors (precipitation volume)
- Attenuation of incident wave

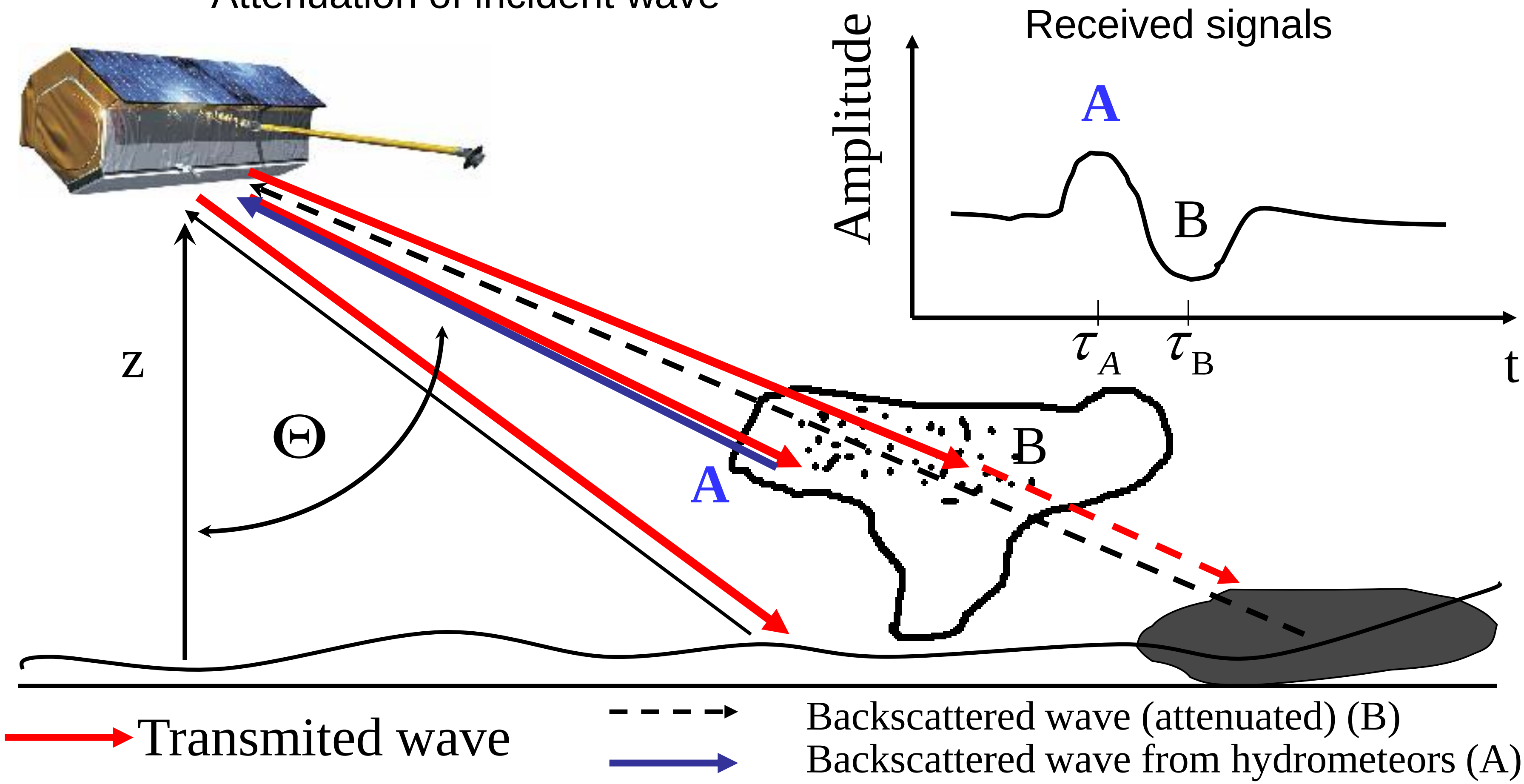

Slant range reflectivity profile („A-scope“) for the rain cell cut from a very recent TerraSAR-X measurement

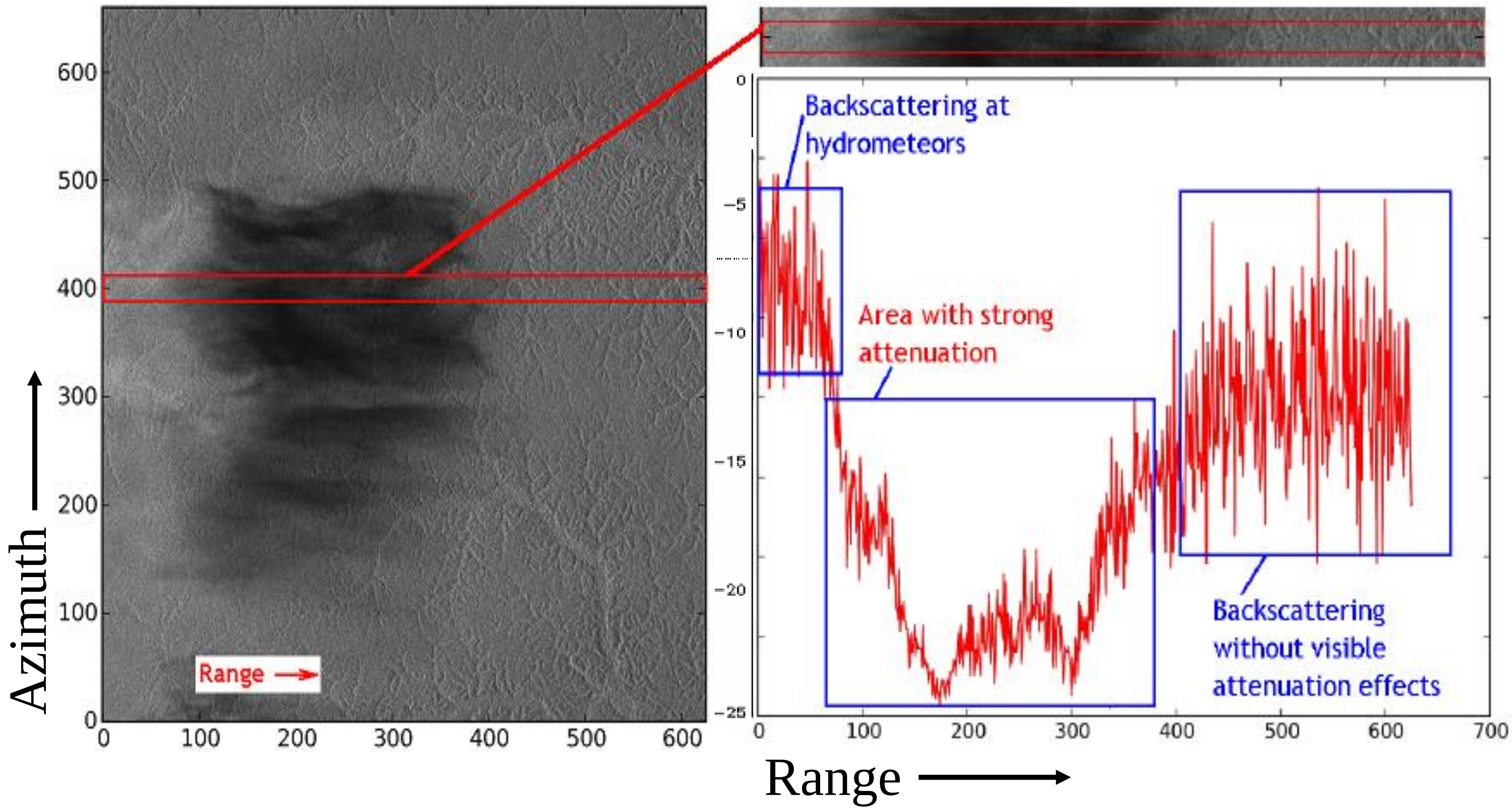

Recent examples of propagation effects recorded withTerraSAR-X

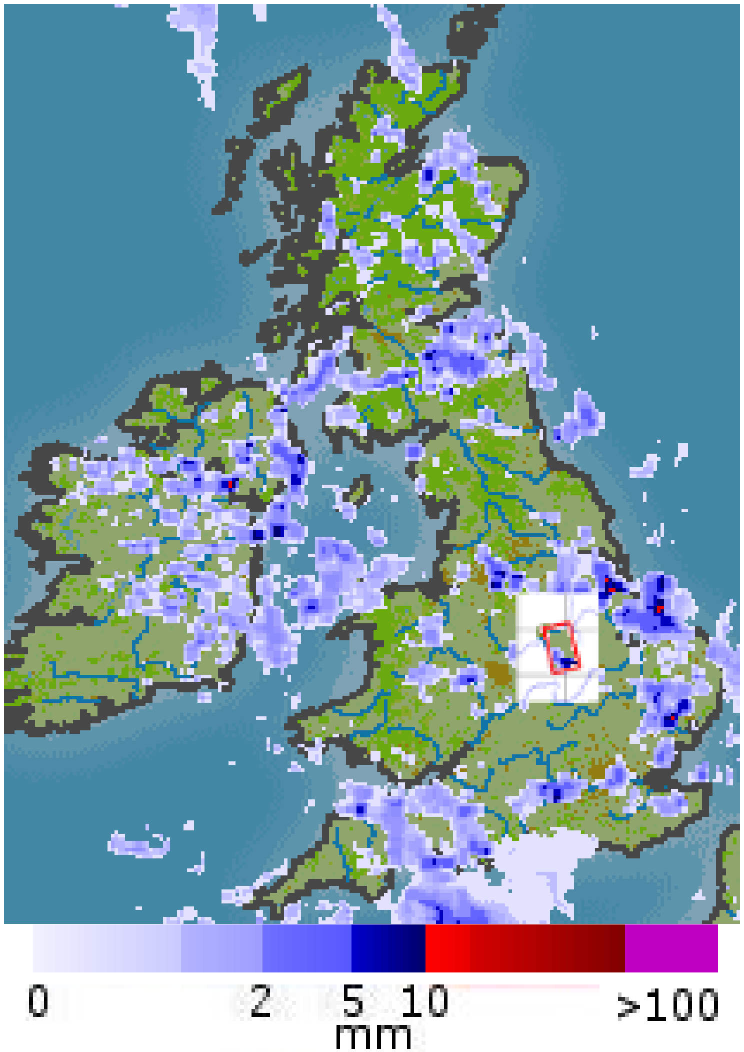

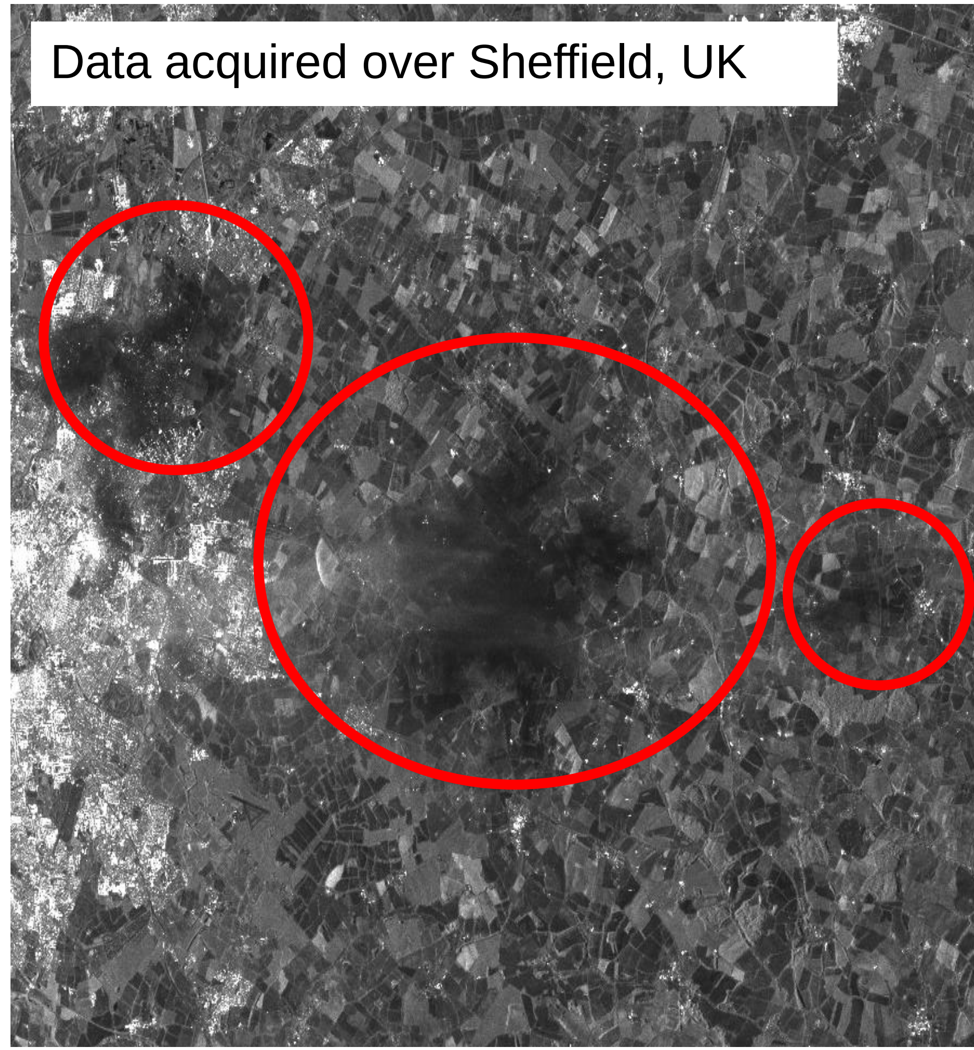

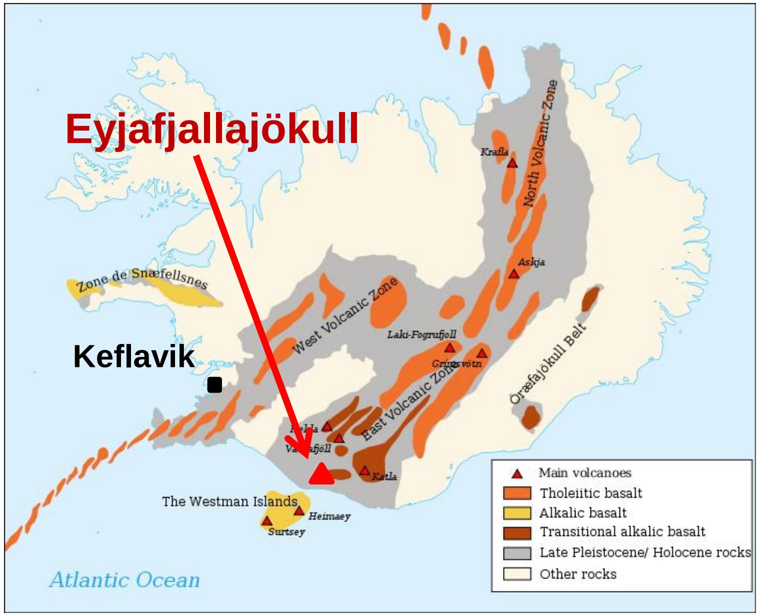

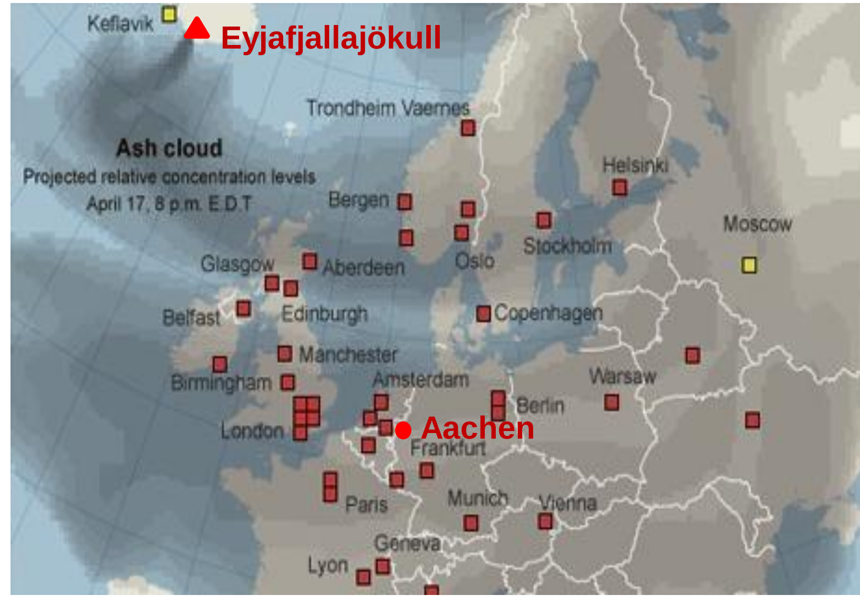

Iceland, Eyjafjallajökull Volcano

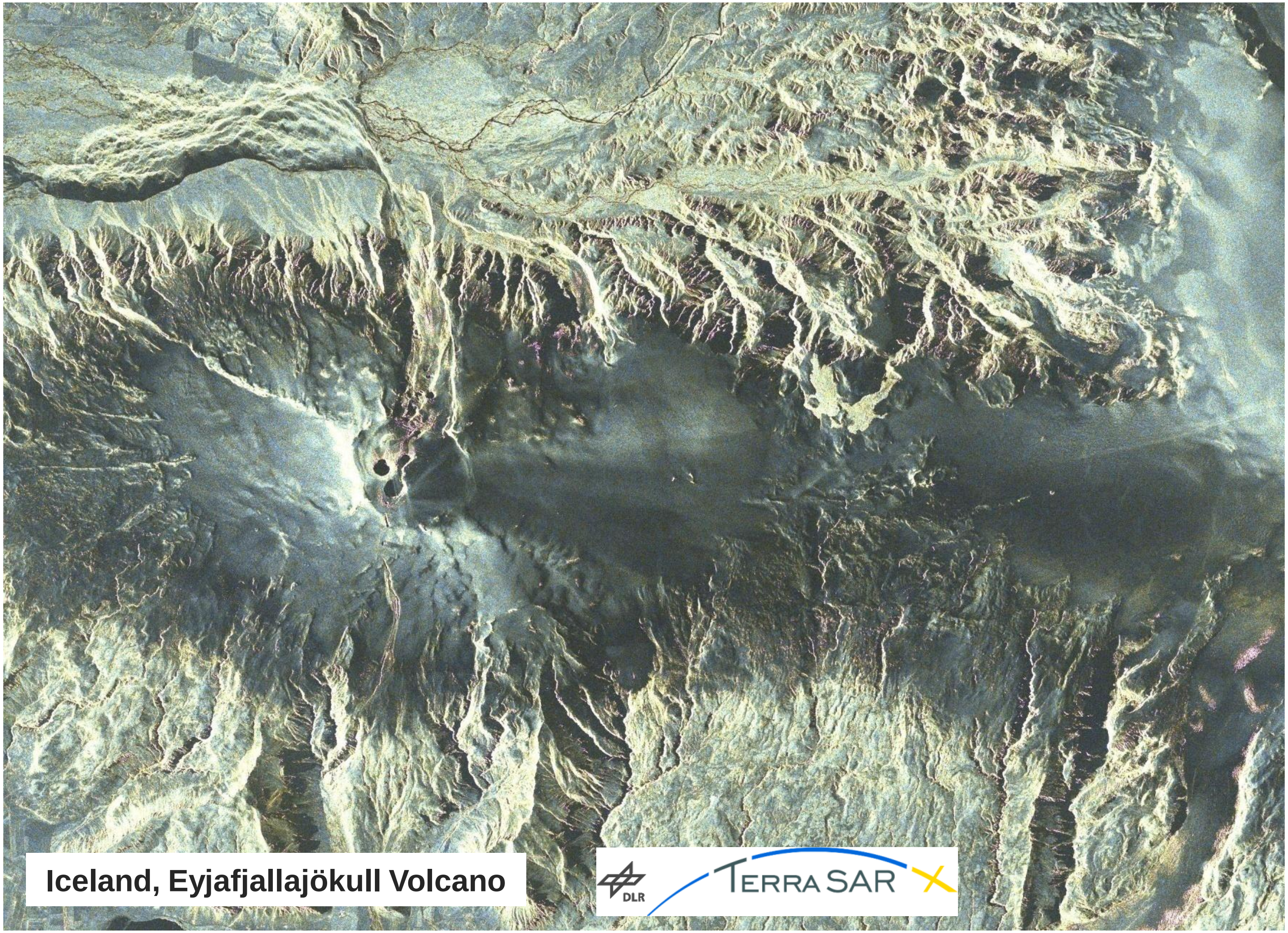
Iceland, Eyjafjallajökull Volcano
DLR
TERRASAR X

NASA-JPL UAVSAR on Global Hawk

Upcoming High-altitude PolSAR Sensors

UAVSAR

Gulf-Stream III

L (Quad - Pol)

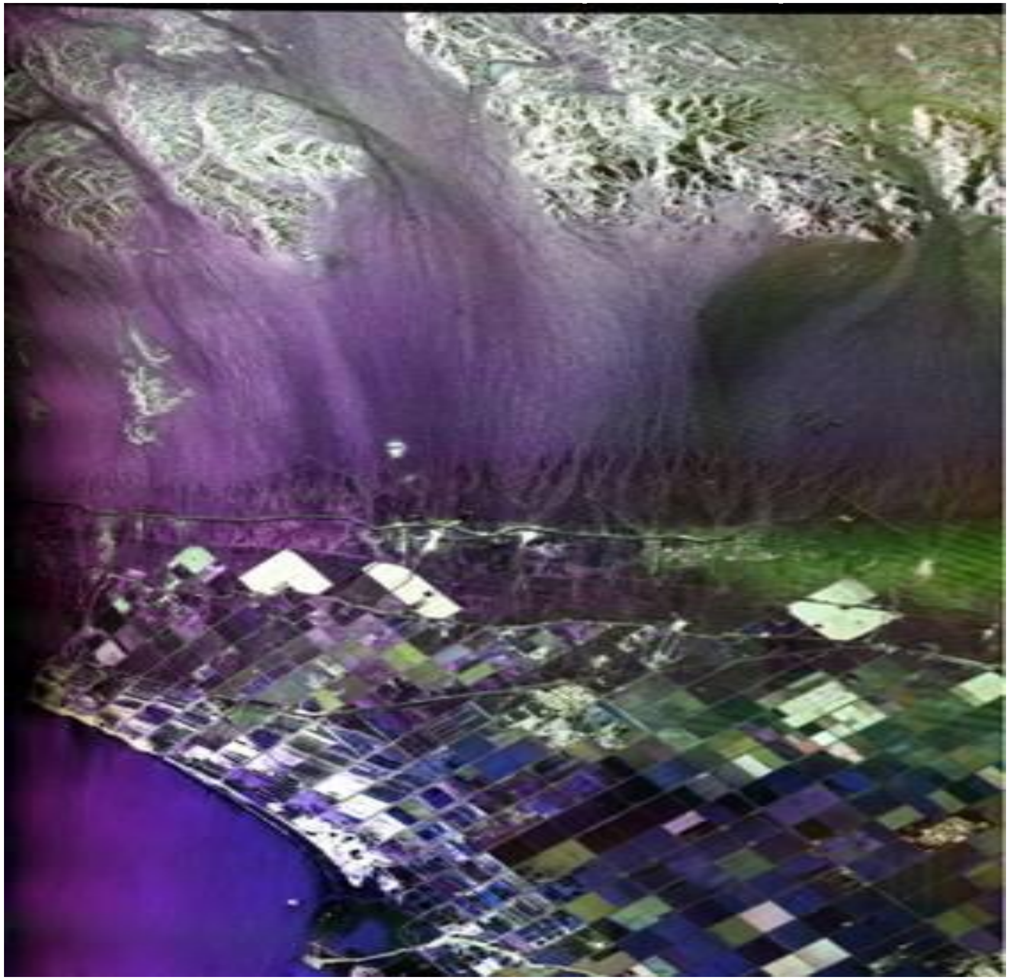

(HH-VV, HV, HH+VV)

UAVSAR Port To Global Hawk

- Measuring millimeter-scale surface deformation at both high temporal and spatial resolution (20 minutes to years at resolutions down to 10 m)
- Full polarimetric imagery enables reflectivity analysis of surface properties supporting
  - Soil moisture and sea surface salinity measurement
  - Biomass measurement and land surface classification
  - Archeological studies
- Global Hawk application with two UAVSAR pods would enable high precision topographic map generation and single pass fully polarimetric interferometry for vegetation structure measurements
- Global Hawk endurance of nearly a day would enable long loiter time over dynamic targets such as volcanoes and earthquake prone regions for pre-event signature studies or post-event scientific and hazard management activities
- Global Hawk range on the order of 8500 nm could enable data collection of distant areas of interest (e.g. Greenland, Aleutians) without complicated campaign deployments
- Global Hawk would be an ideal platform to performing mapping and regional science using the UAVSAR

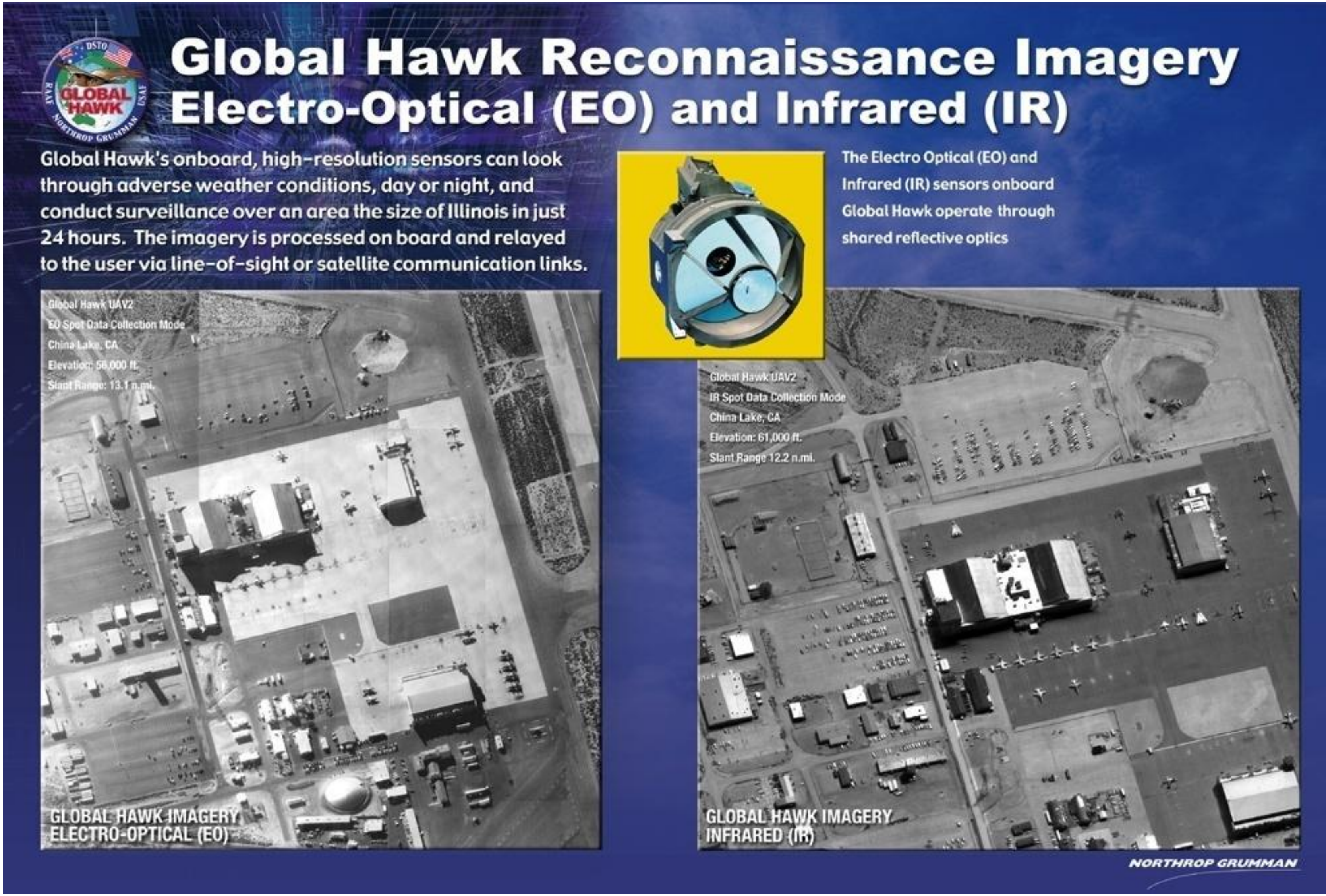
Global Hawk Reconnaissance Imagery
Electro-Optical (EO) and Infrared (IR)
Global Hawk's onboard, high-resolution sensors can look through adverse weather conditions, day or night, and conduct surveillance over an area the size of Illinois in just 24 hours. The imagery is processed on board and relayed to the user via line-of-sight or satellite communication links.
The Electro Optical (EO) and Infrared (IR) sensors onboard Global Hawk operate through shared reflective optics
Global Hawk UAV2
EO Spot Data Collection Mode
China Lake, CA
Elevation: 56,000 ft.
Slant Range: 13.1 n.mi.
GLOBAL HAWK IMAGERY
ELECTRO-OPTICAL (EO)
Global Hawk UAV2
IR Spot Data Collection Mode
China Lake, CA
Elevation: 61,000 ft.
Slant Range 12.2 n.mi.
GLOBAL HAWK IMAGERY
INFRARED (IR)
NORTHROP GRUMMAN

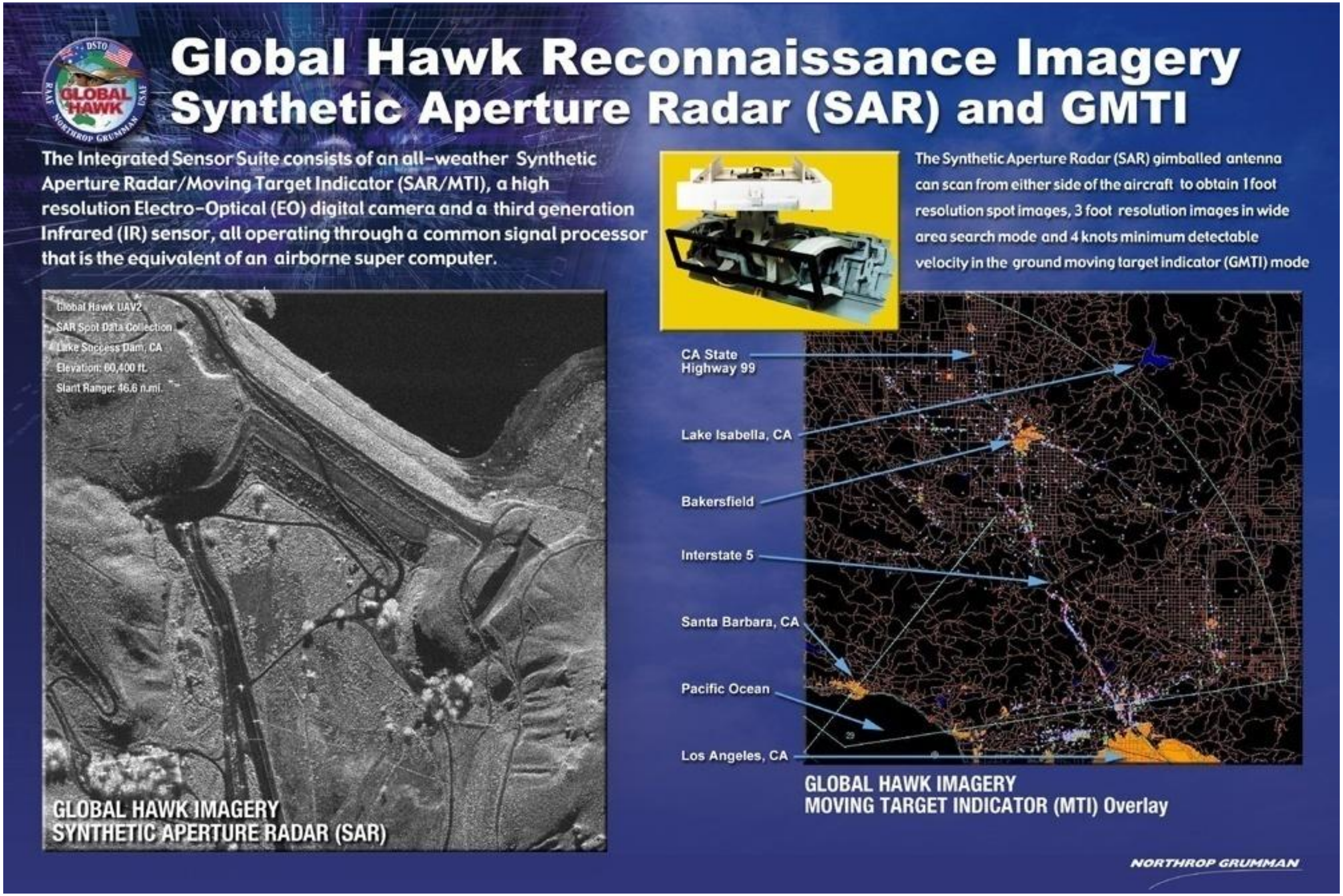
DSTO
GLOBAL HAWK
RAAF
USAF
NORTHROP GRUMMAN
Global Hawk Reconnaissance Imagery
Synthetic Aperture Radar (SAR) and GMTI
The Integrated Sensor Suite consists of an all-weather Synthetic Aperture Radar/Moving Target Indicator (SAR/MTI), a high resolution Electro-Optical (EO) digital camera and a third generation Infrared (IR) sensor, all operating through a common signal processor that is the equivalent of an airborne super computer.
The Synthetic Aperture Radar (SAR) gimballed antenna can scan from either side of the aircraft to obtain 1 foot resolution spot images, 3 foot resolution images in wide area search mode and 4 knots minimum detectable velocity in the ground moving target indicator (GMTI) mode
Global Hawk UAV2
SAR Spot Data Collection
Lake Success Dam, CA
Elevation: 60,400 ft.
Slant Range: 46.6 n.mi.
GLOBAL HAWK IMAGERY
SYNTHETIC APERTURE RADAR (SAR)
CA State Highway 99
Lake Isabella, CA
Bakersfield
Interstate 5
Santa Barbara, CA
Pacific Ocean
Los Angeles, CA
GLOBAL HAWK IMAGERY
MOVING TARGET INDICATOR (MTI) Overlay
NORTHROP GRUMMAN

GROB Super-High-Altitude UAV

Grob G520T Egret D-FSTN

THE UAVSAR INSTRUMENT: DESCRIPTION AND EXAMPLE DATA SETS

Dr Scott Hensley

PI and Chief Scientist

UAVSAR Overview

- UAVSAR developed under NASA ESTO funding beginning in 2004.
- UAVSAR is an L-band fully polarimetric SAR employing an electronically scanned antenna that has been designed to support a wide range of science investigations.
  - Science investigations supported by UAVSAR include solid earth, cryospheric studies, vegetation mapping and land use classification, archeological research, soil moisture mapping, geology and cold land processes.
  - To support science applications requiring repeat pass observations such as solid earth and vegetation applications the UAVSAR design incorporates:
    - A precision autopilot developed by NASA Dryden that allows the platform to fly repeat trajectories that are mostly within a 5 m tube.
    - Compensates for attitude angle changes during and between repeat tracks by electronically pointing the antenna based on attitude angle changes measured by the INU.
- UAVSAR is testing new experimental modes, e.g. the multi-squint mode whereby data is collected simultaneously at multiple squint angles to enable vector deformation measurements with a single repeat pass.

Initial Flight Testing of UAVSAR

San Andreas Fault Repeat-Pass Baseline
80 km Datatakes on February 12 and 20 of 2008.

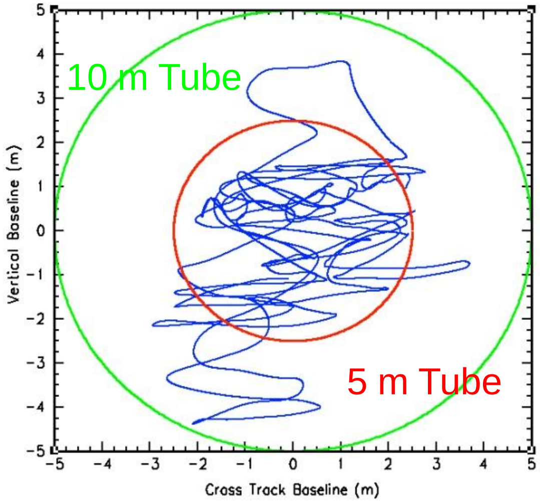

Mt. St Helens Repeot Poss Boseline
5 m Tube in Red – 10 m Tube in Grreen.

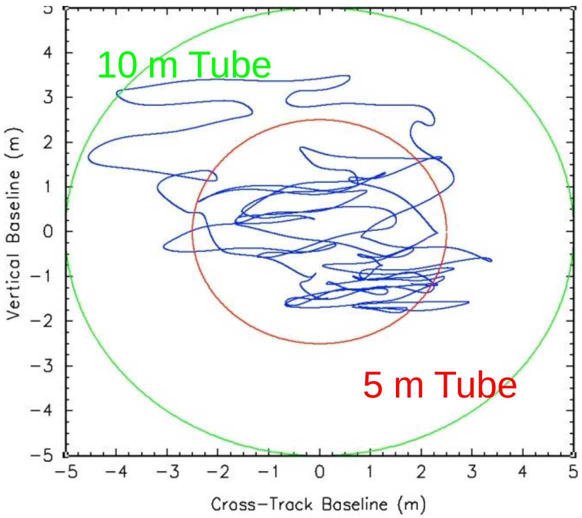

San Andreas Fault

(HH-Red, HV – Green, VV – Blue)

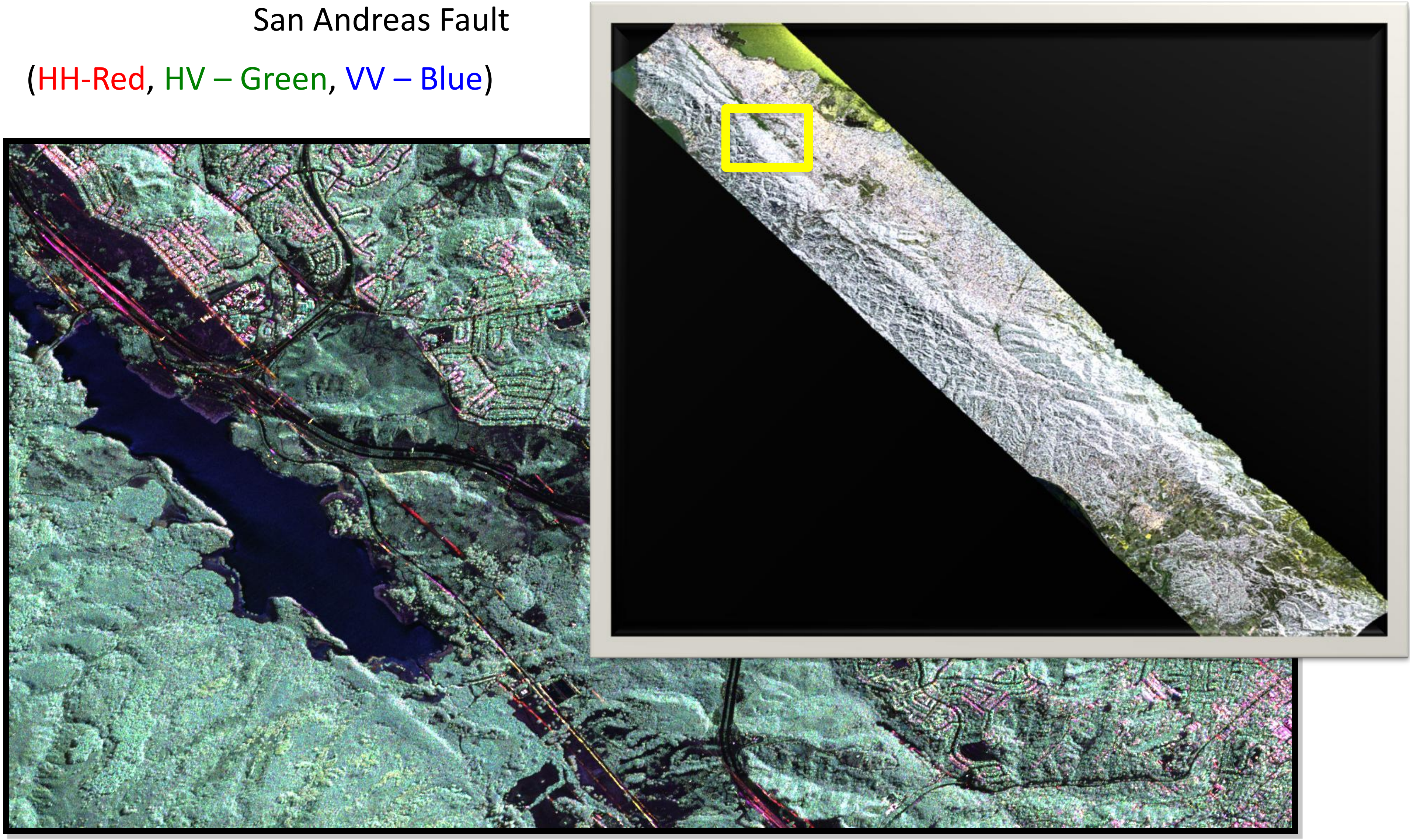

San Andreas Fault Imagery

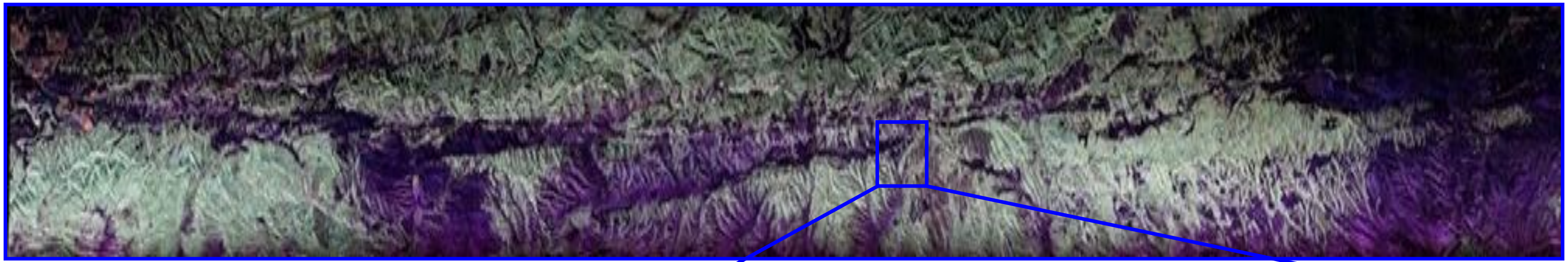

The same trees in Google Earth image can be seen in UAVSAR L-band image

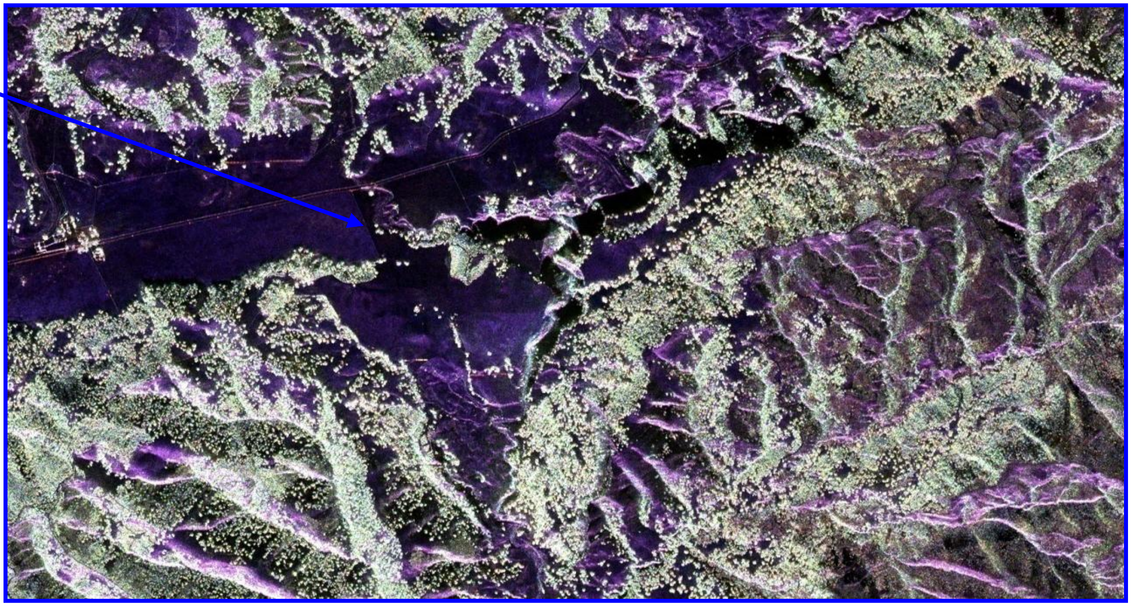

The different colors in the UAVSAR image generally correspond to different vegetation characteristics on the surface. Compensation for & projection to surface topography not applied.

1 km

LHH=red
LHV=green
LVV=blue

Data collected Feb 12, 2008

2x6 looks (3m resolution)

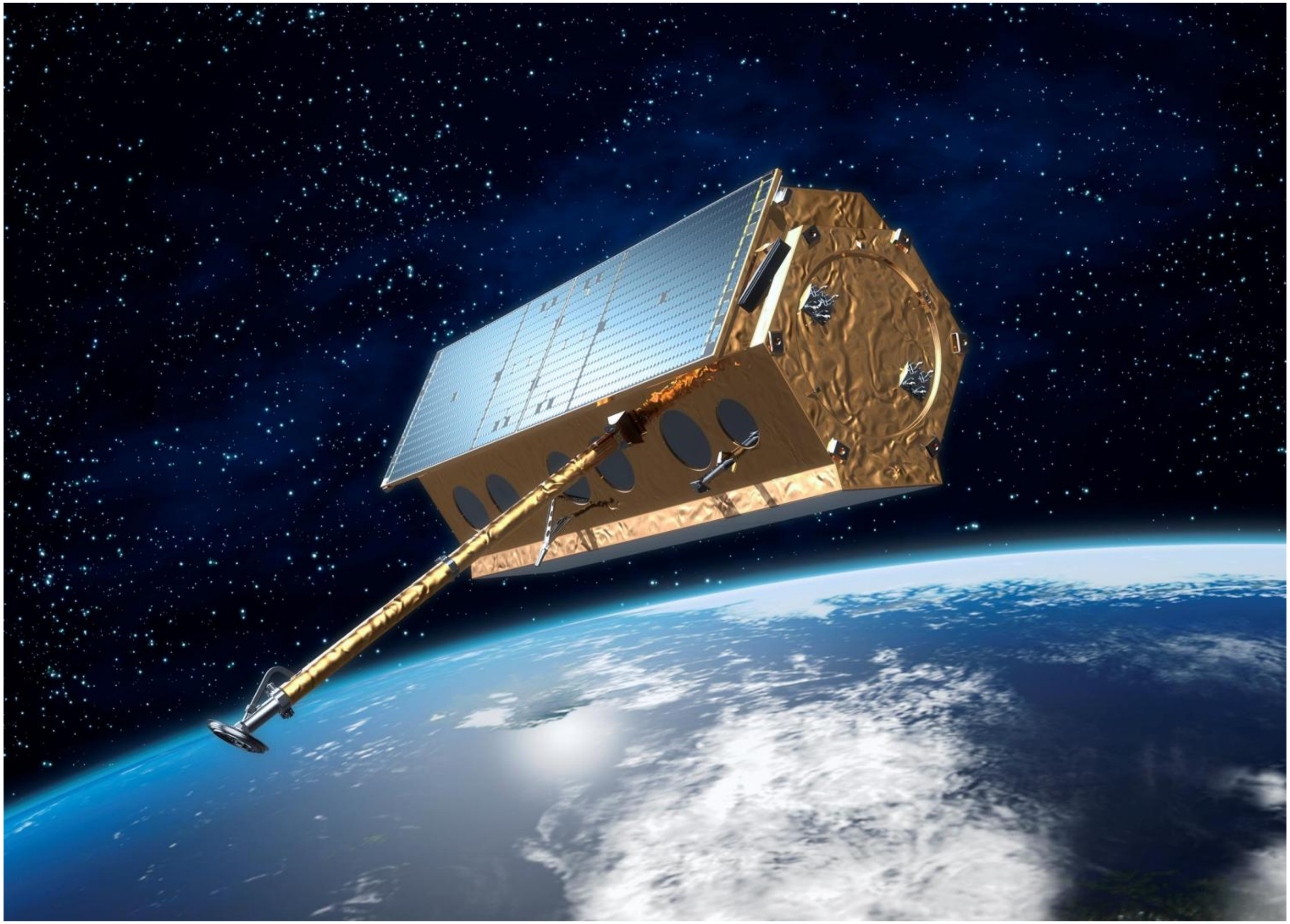

The TerraSAR-X Satellite

Overview of effects

Effects:

- delay
- **attenuation**
- noise
- scintillation

caused by:

- atmospheric gases
- **rain, precipitation**
- clouds, fog
- ionosphere

Transmission spectrum of the atmosphere / Attenuation

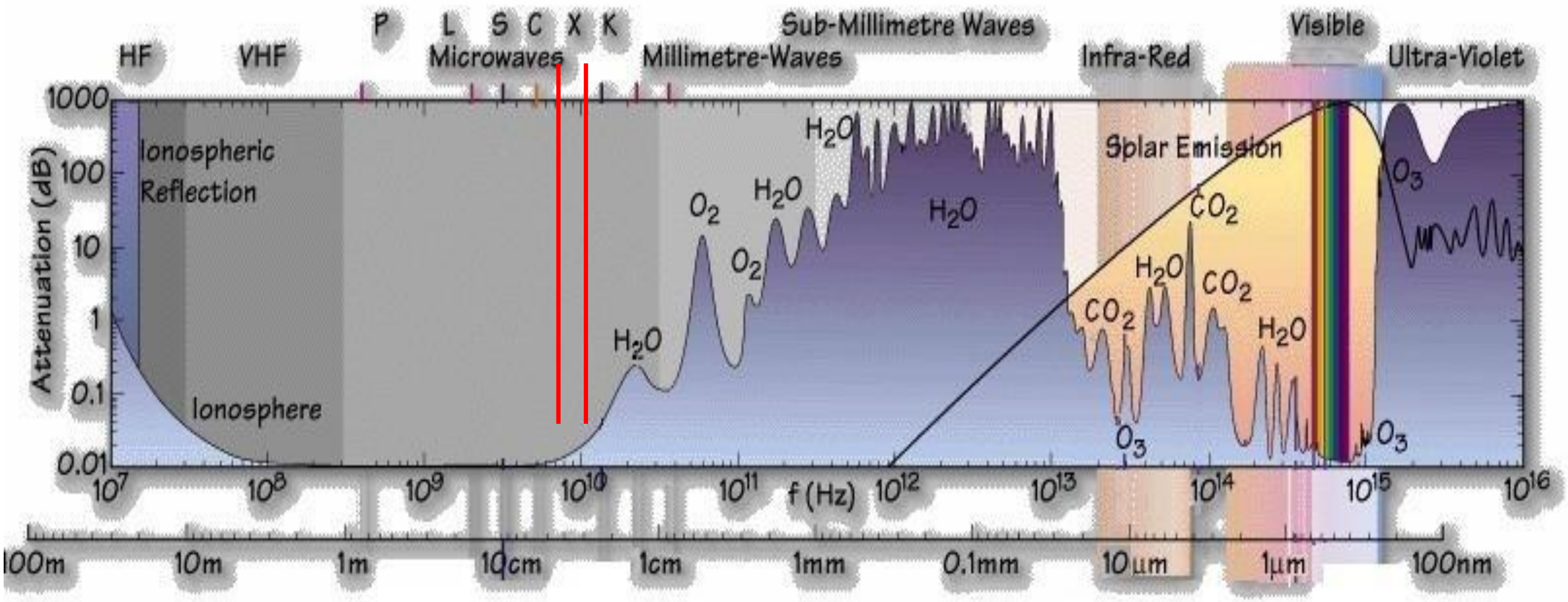

Gaseous attenuation negligible

→ focus on precipitation

→

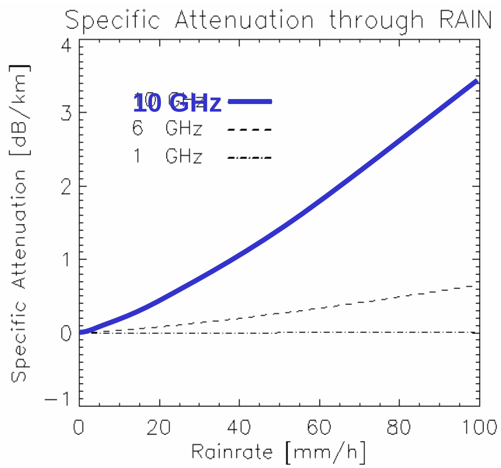

Most affected global precipitation regions

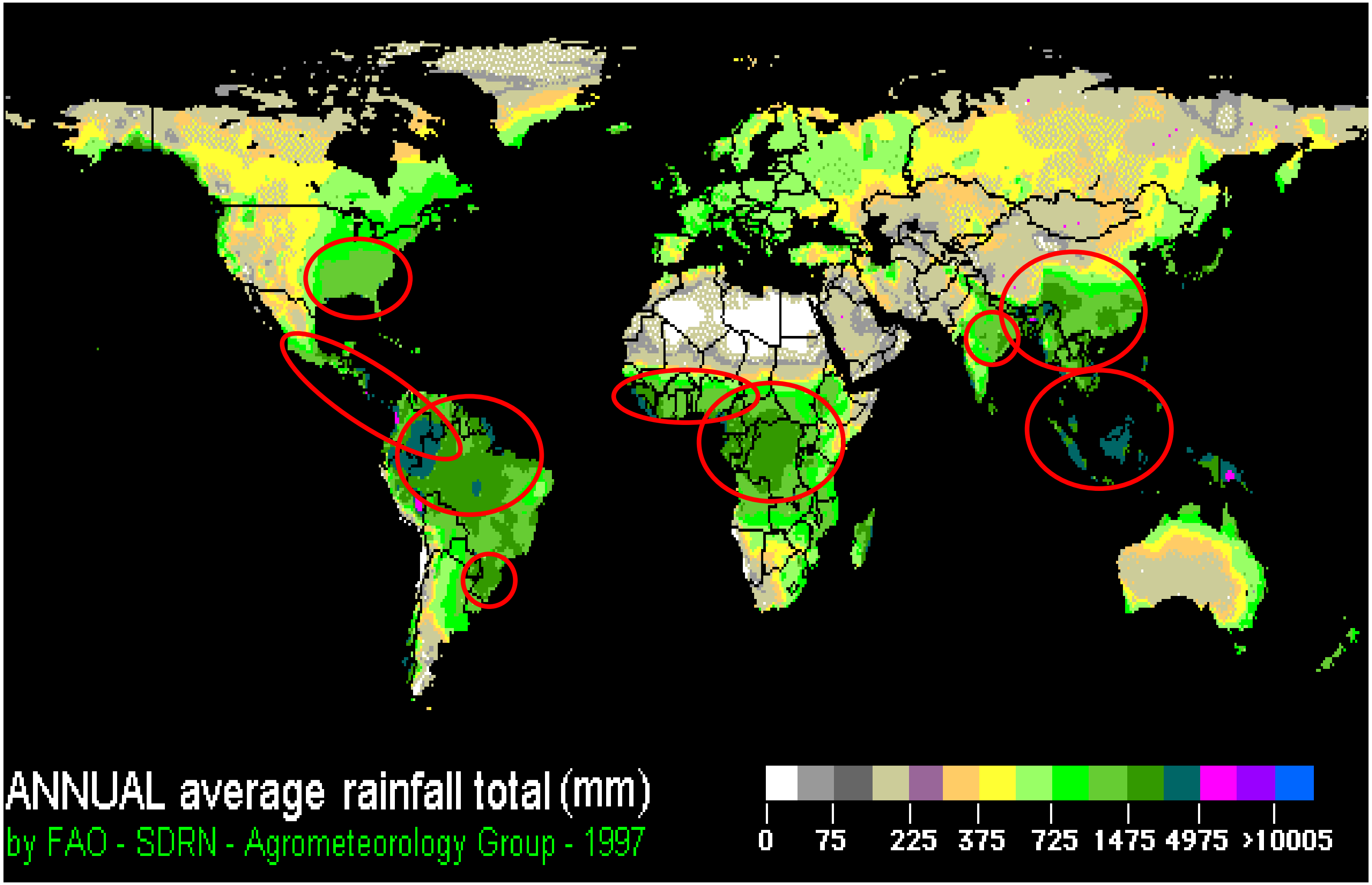

Physical interpretation of rain cell signatures

- Partial backscattering at hydrometeors (precipitation volume)
- Attenuation of incident wave

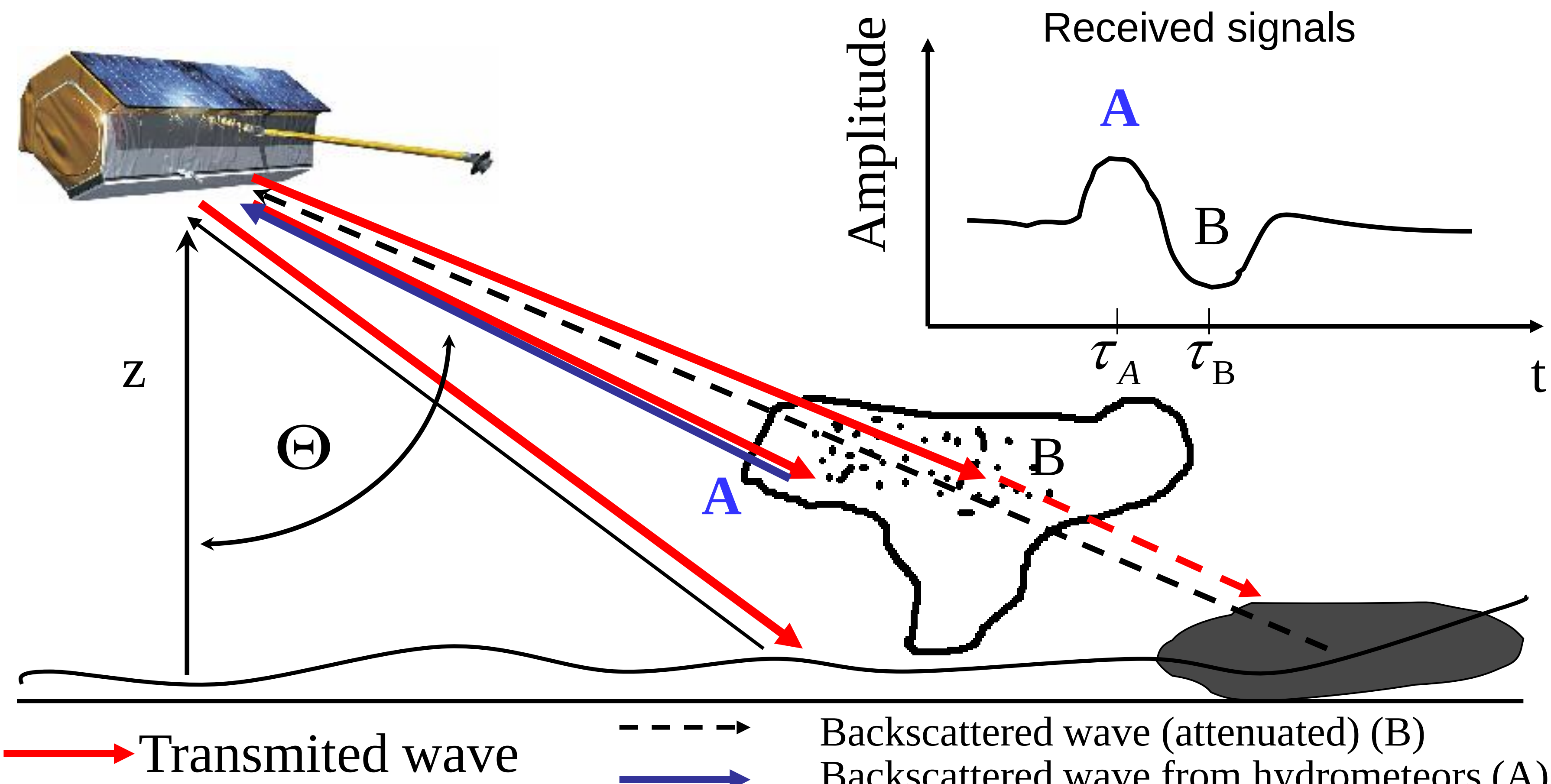

Taj Mahal – Agra, Uttar Pradesh, India

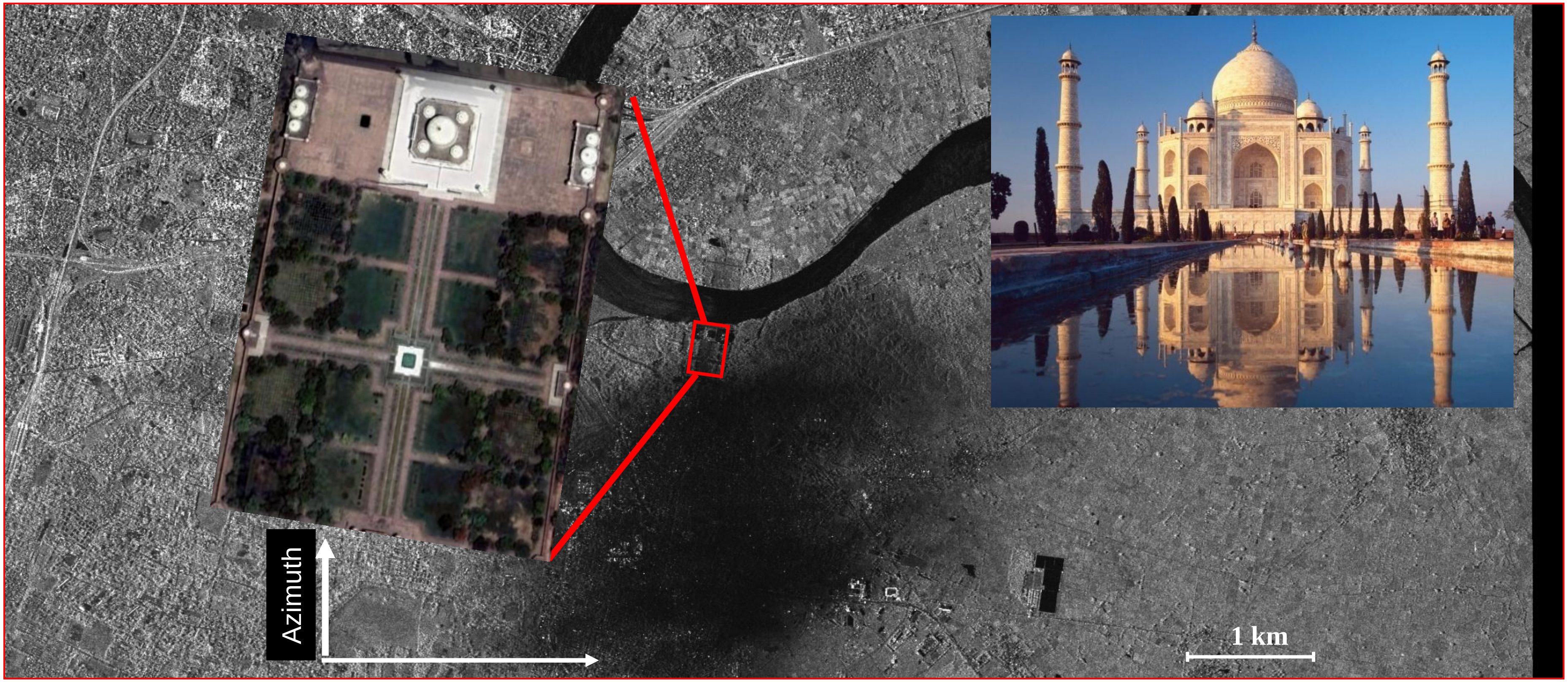

Raincell signatures at Davangere, Karnataka, India

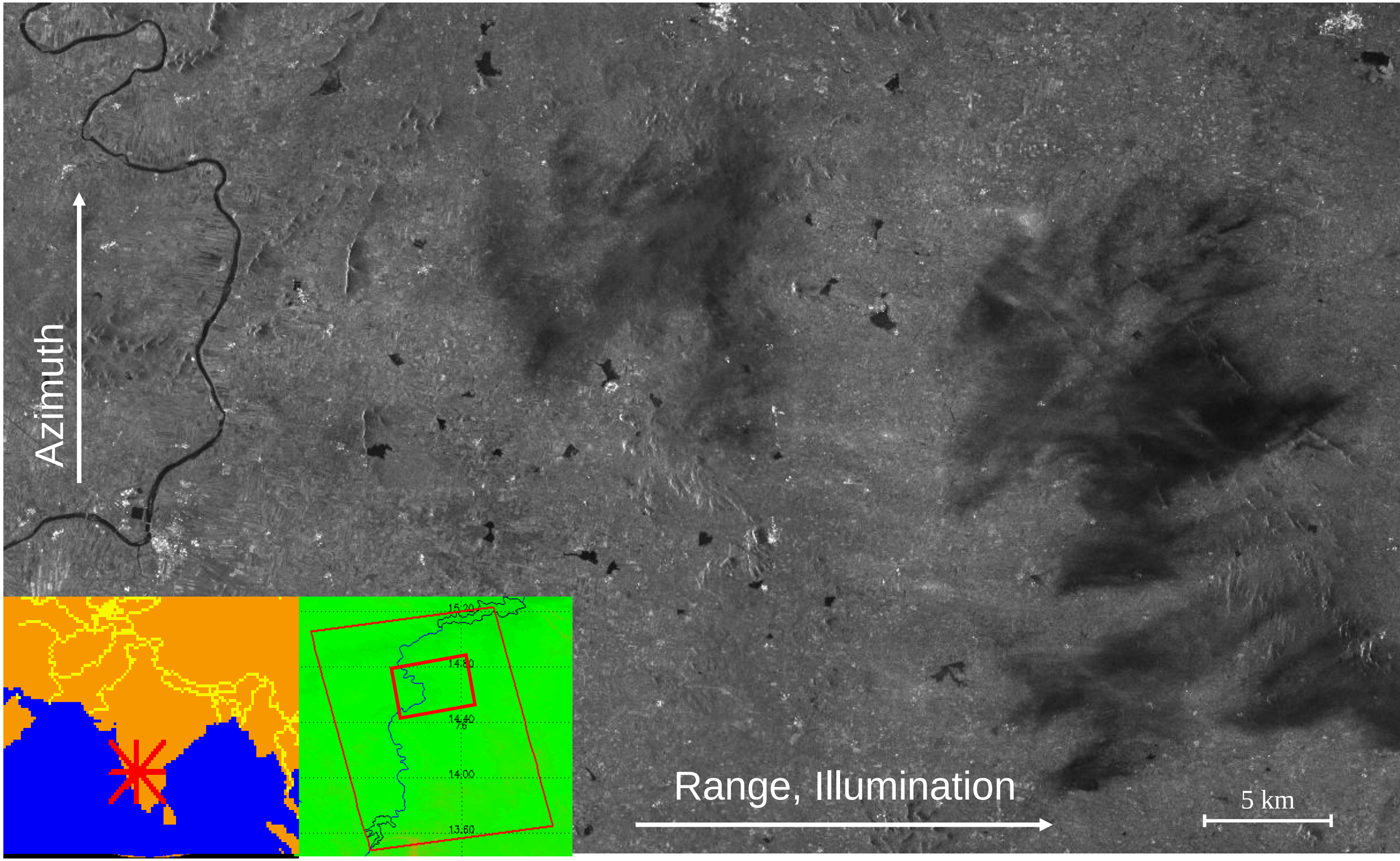

Clouds over Melaka Strait
TerraSAT-X X-Band

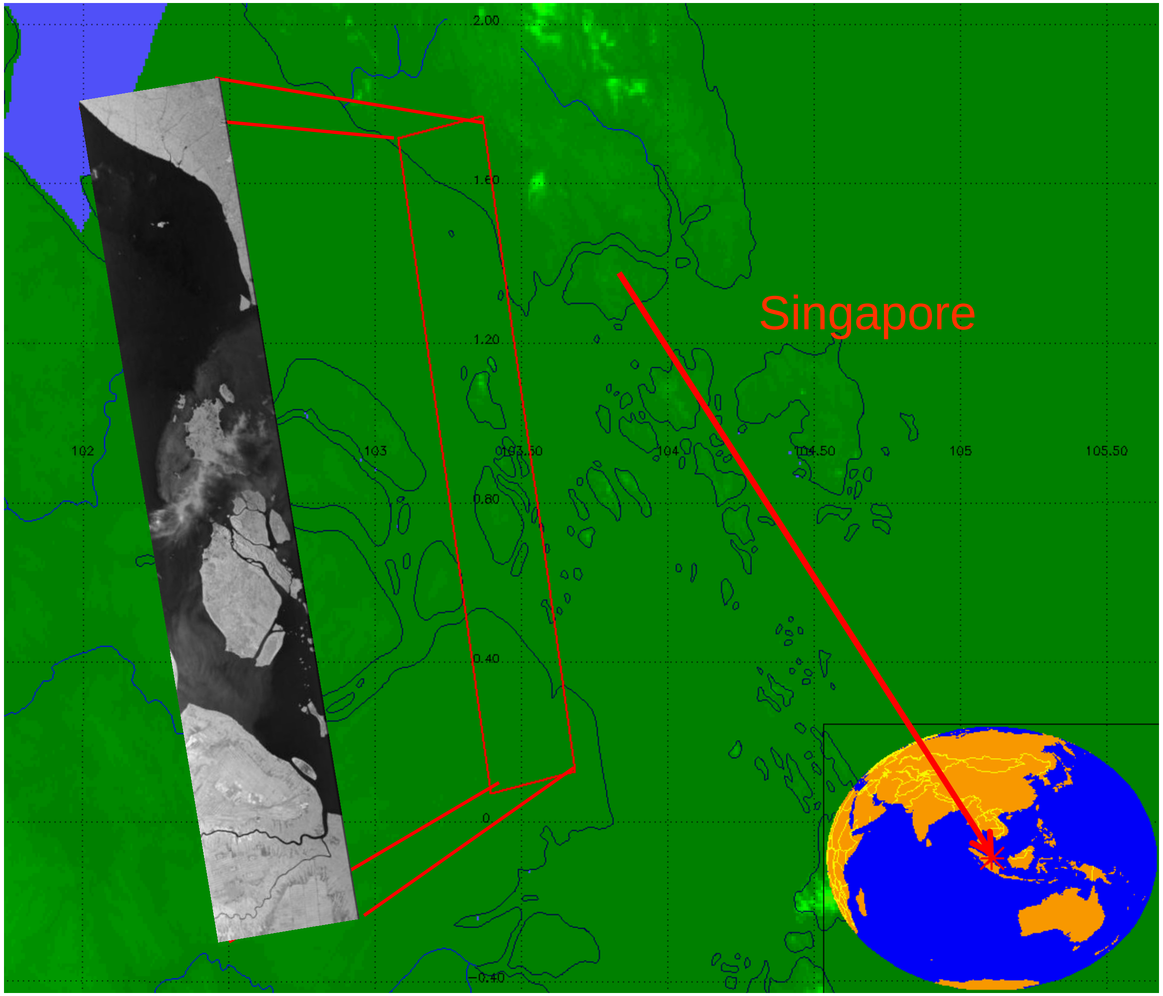

A. Danklmayer

Microwaves and Radar Institute

German Aerospace Center (DLR)

Outlook

- ✓ The **disadvantage of rain features** in SAR imagery **may turn out** to be a **useful source for assessing precipitation intensity** over SAR surveyed areas such as oceanic surfaces, a problem hitherto only poorly addressed.

- ✓ **TerraSAR-X** offers **new possibilities for investigation of propagation** effects. **New Experiments are scheduled** in order to use TerraSAR-X as a measurement device for precipitation, possibly in a Nadir looking geometry

- ✓ **Simultaneous measurements with weather radars and SAR are now available and will be implemented** for further in-depth study of attenuation effects and quantification.

Prediction of Future Megastorms: California & East Coast

Outlook & Future Needs

- New Sensors, space-borne: TandemSAR-X, TandemSAR-L (Destiny), . . .
-New Sensors, air-borne: F-SAR (P, L, S, C, X, K, V, W) , …
- New Sensors, ultrahigh air-borne: JPL-UAV (Global Hawks), ...

- Algorithm Developments: Fully Polarimetric RP-POLinSAR assessment

- Applications: Focused increase providing clear-cut successes

POLinSAR 2011 Single & Tandem Space-borne POL-SAR Sensors, Increase number of Text books & Training Workshops

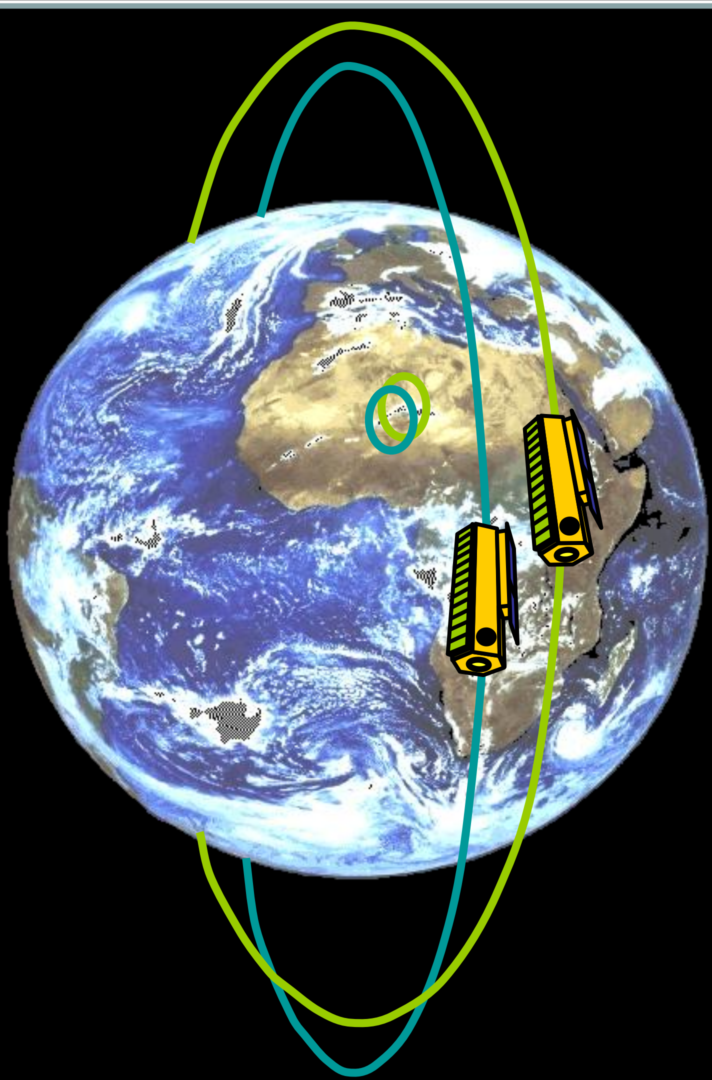

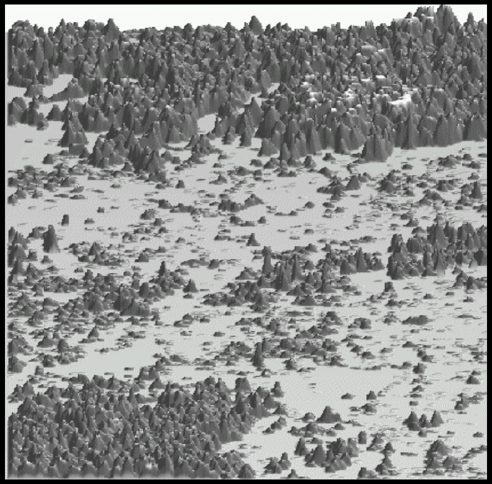

Global Monitoring of Bio-, Geo-, Cryo- and Hydrosphere processes with hith temporal and spatial resolution.
(Prof. A. Moreira – POLINSAR09)

Radar Interferometry

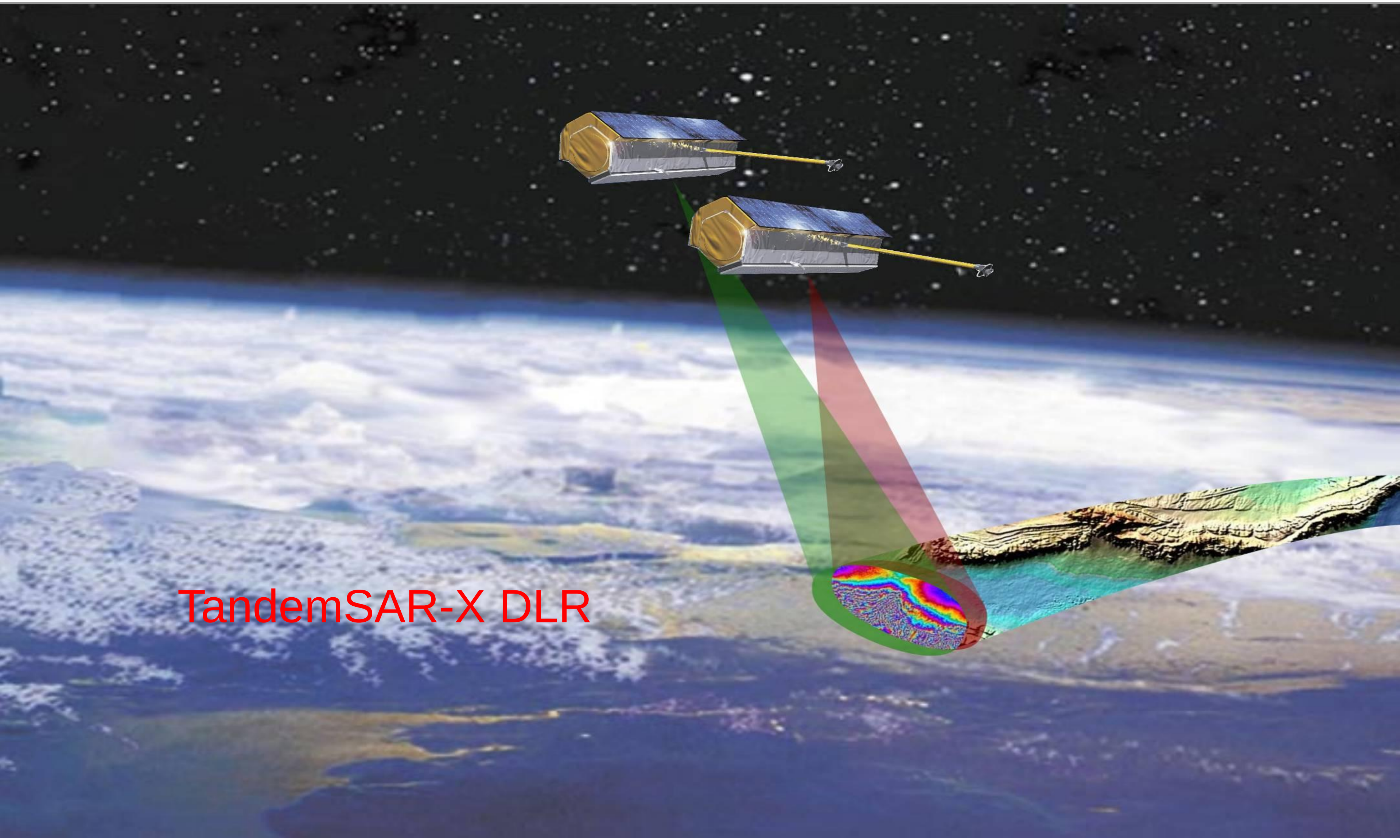
TandemSAR-X DLR

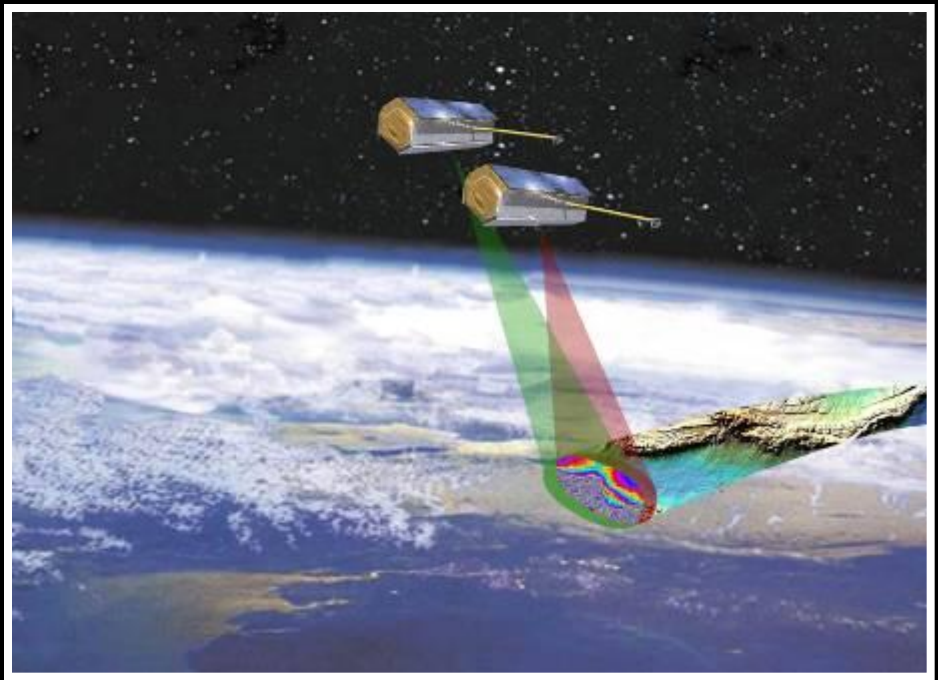

TerraSAR – X (1 & 2)
(2010)
Pol – InSAR Sensors
TanDEM-X

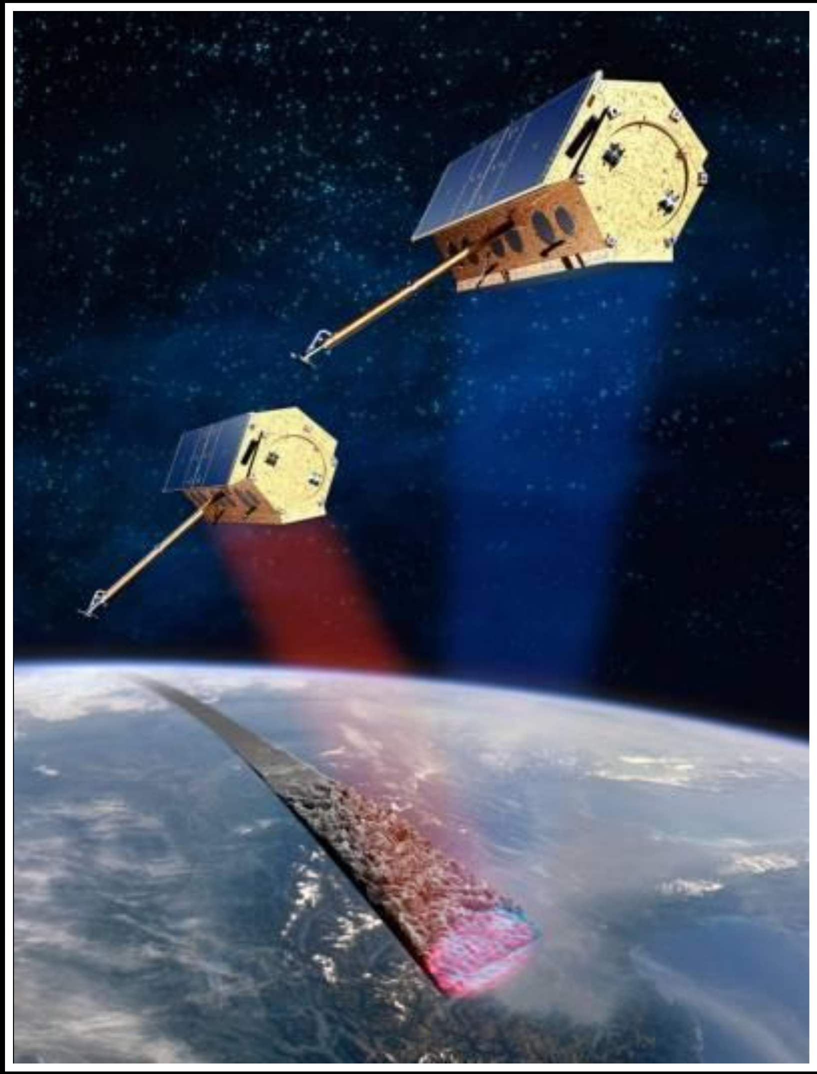

TandemSAR-L (Destiny): JPL & DLR

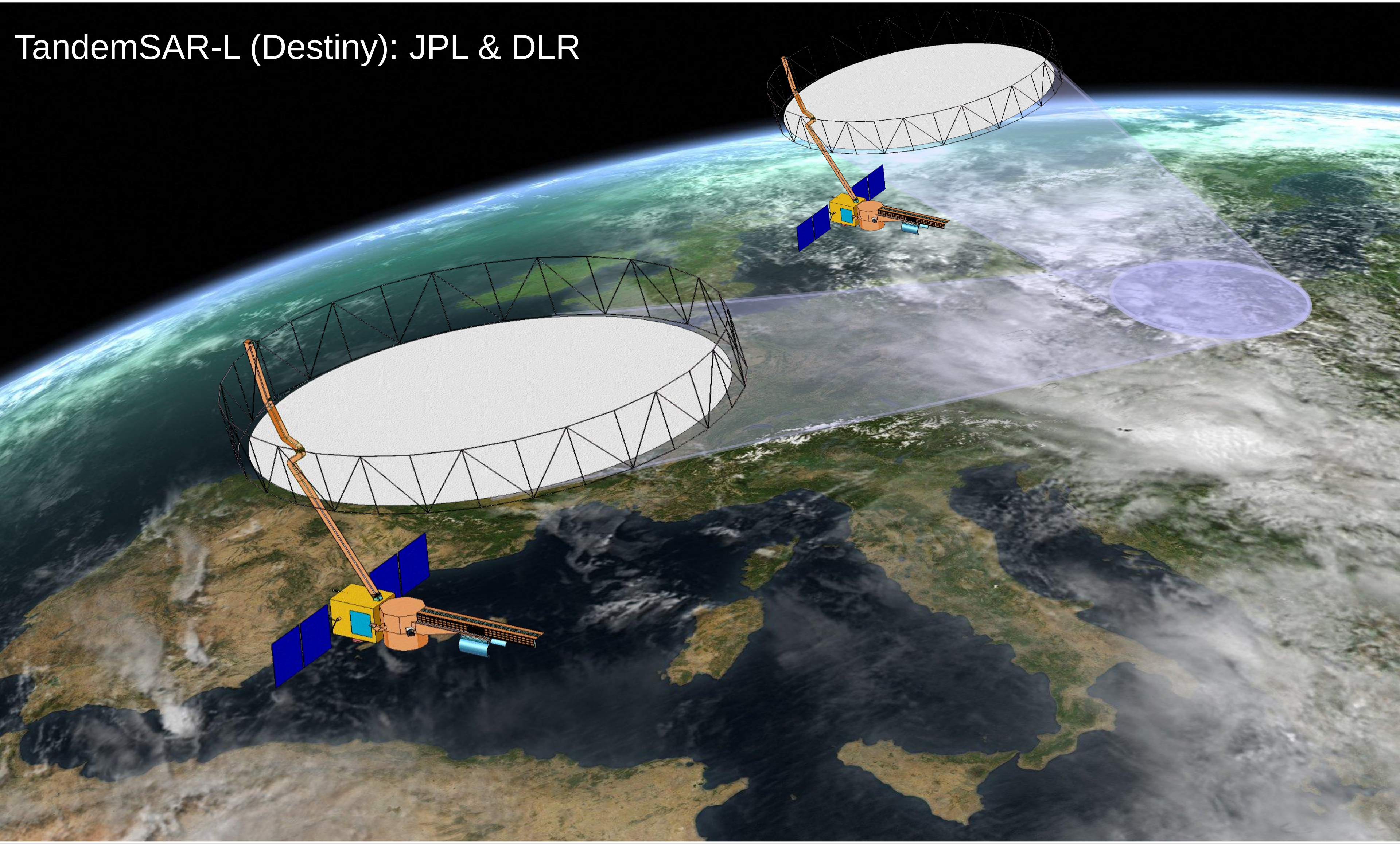

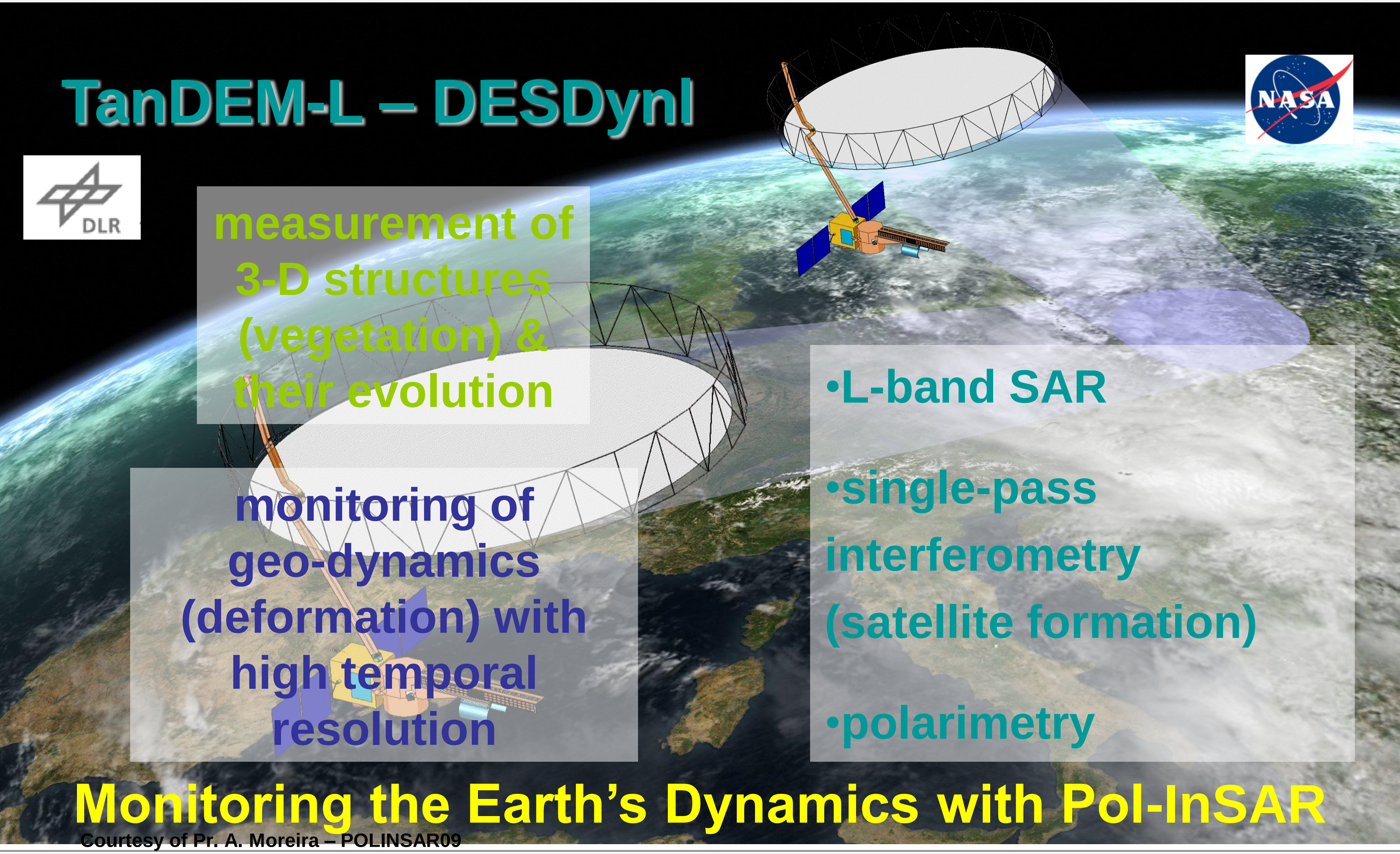
TanDEM-L – DESDynI
DLR
NASA
measurement of 3-D structures (vegetation) & their evolution
monitoring of geo-dynamics (deformation) with high temporal resolution
•L-band SAR
•single-pass interferometry (satellite formation)
•polarimetry
Monitoring the Earth's Dynamics with Pol-InSAR
Courtesy of Pr. A. Moreira – POLINSAR09

LAPAN-A2 ORBIT PROFILE
(14 pass per 24 hr / orbit time 100 minutes and stay above horizon at about 10 minutes)

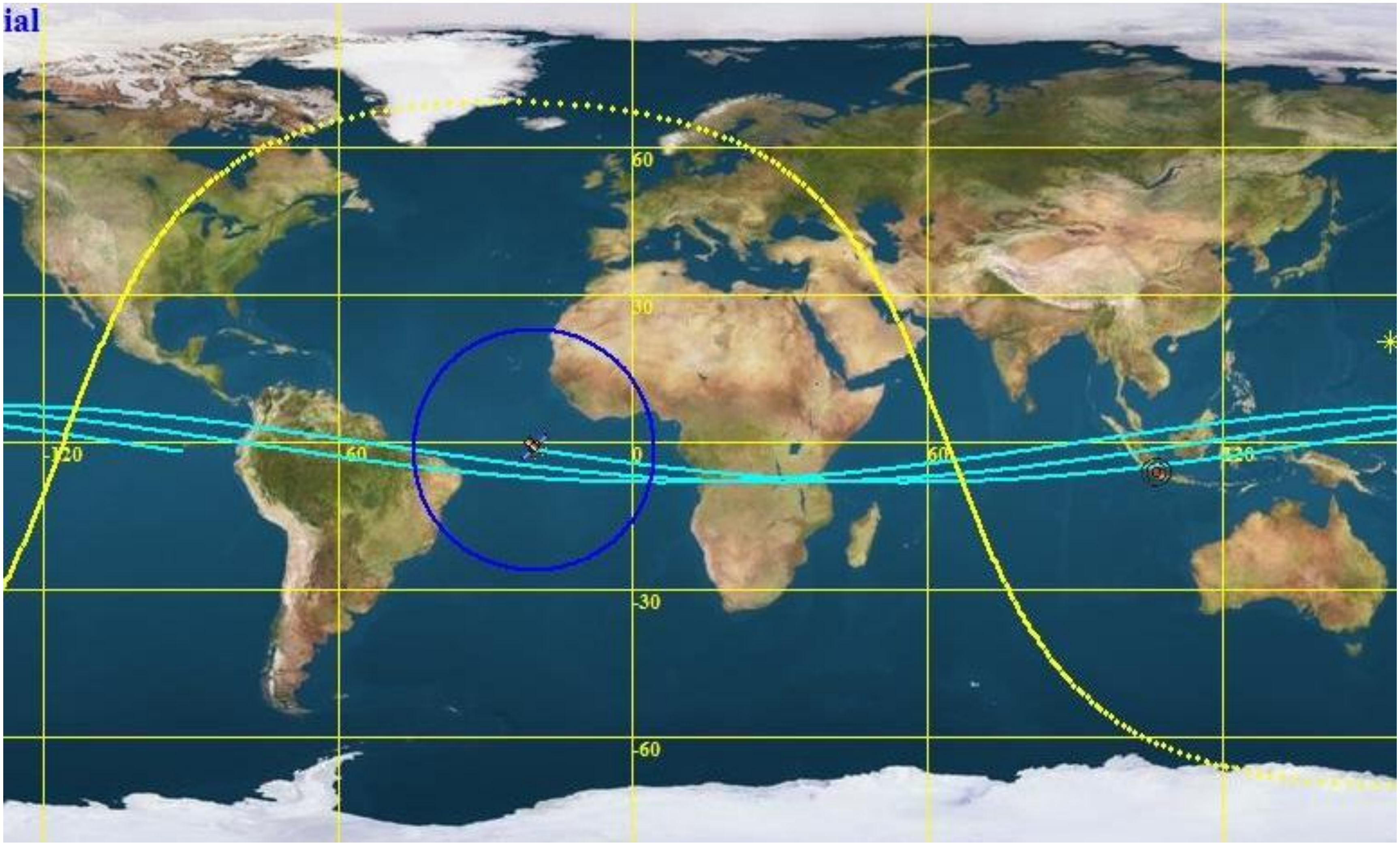

TUB-LAPAN-ORARI ORBIT PROFILE

(14 pass per 24 hr / orbit time 100 minutes and stay above horizon at about 10 minutes)

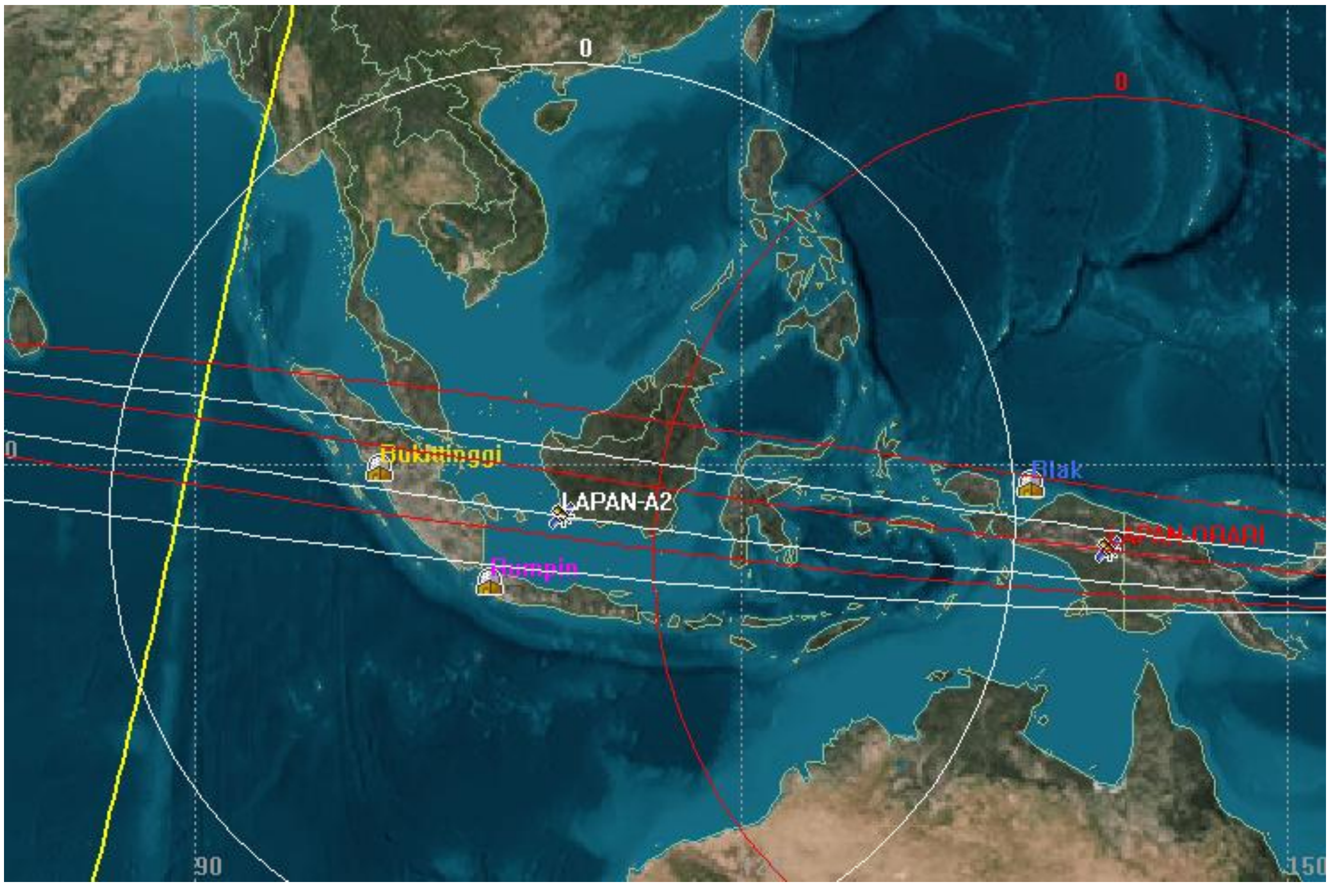

SATELLITES ORBIT PROFILES

(14 pass per 24 hr / orbit time 100 minutes and stay above horizon at about 10 minutes)

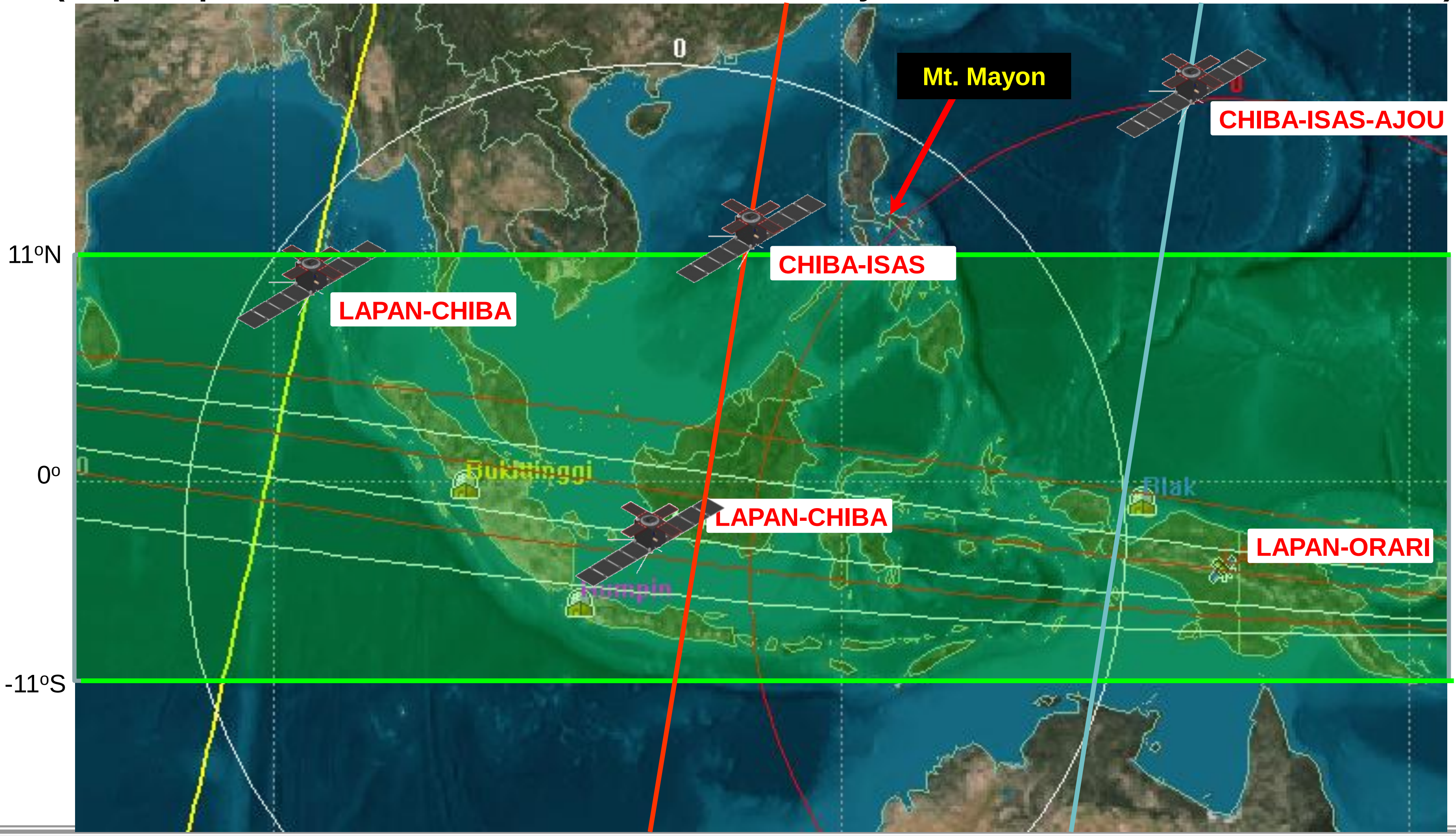

Recent Textbooks on Radar Polarimetry & Polarimetric Interferometry

Mott, Boerner, Yamaguchi, Souyris, Jin, Jin-Xu, Pottier-Lee, Cloude, Jian Yang,Cumming-Wong

Addendum: Boerner, Literature Assessment

Recent Books on Polarimetric Radar & SAR, Polarimetric Interferometry

Harold MOTT**, **Remote Sensing with Polarimetric Radar, Wiley-IEEE Press, 1st ed., January 2007, pp309 , ISBN: 978-0470074763 {also see previous books by late Harold Mott, 1986 & 1992}

Boerner, Wolfgang-Martin, *Introduction to Synthetic Aperture Radar (SAR) Polarimetry*, Wexford Press (reprinted *without permission* from W-M. Boerner (April 2007), Basics of SAR Polarimetry 1, *In Radar Polarimetry and Interferometry (pp. 3.1- 3-40)*, Educational Notes RTO-EN-SET-081bis, Paper 3, Neuilly-sur-Seine, France RTO, available from: http://www.rto.nato.int/abstracts.asp

Yamaguchi, Yoshio, *Radar Polarimetry from Basics to Applications: Radar Remote Sensing using Polarimetric Information (in Japanese),* IEICE Press, Dec. 2007, (soft cover), ISBN: 978-4-88552-227-7, http://www.ieicepress.com/

Masonnett Didier & Souyris Jean-Claude, *Imaging with Synthetic Aperture Radar*, EPFL/CRC-Press, Engineering Sciences/Electrical Engineering, Taylor & Francis Group, 2008, (hard-cover), ISBN 978-0-8493-8239-4; http://www.crcpress.com

Ya-Qiu JIN & Feng XU, *Theory and Approach for Polarimetric Scattering and Information Retrieval of SAR Remote Sensing (In Modern Chinese)*, Beijing: Science Press, 2008, (hard cover), ISBN978-7-03-022649-5; http://www.sciencep.com

Lee Jong-Sen & Pottier, Eric, *Polarimetric Radar Imaging – from basics to applications*, CRC Press – Taylor & Francis Group, January 2009, ISBN 978-1-4200-5497-2 (hard-cover), TK6580.L424.2009, 621.3848- -dc22; http://www.crcpress.com {Chinese version to be published by 2009 October}

Cloude, Shane Robert, *Polarisation: Applications in Remote Sensing,* Oxford University Press, UK & EU, August 2009, ISBN 978 -0-19-9569731-1 (352p, 260 line-ill: hard-copy), http://www.oup.com.contact/

vanZyl Jakob-Johannes & Kim Yun-Jin, Introduction *to SAR Polarimetry* – in progress and to be completed by 2009 December: To be published with the JPL Series, John Wiley.

Cumming, I. G. and F. W. Wong, "*Digital Processing of Synthetic Aperture Radar Data".* Artech House, 653-pages, January 2005. (Published in Chinese, October 2007).

ENGINEERING SCIENCES *Electrical Engineering*

IMAGING WITH SYNTHETIC APERTURE RADAR

Didier Massonnet & Jean-Claude Souyris

Synthetic Aperture Radar (SAR) is a field that has been transformed by the recent availability of data from a new generation of space and airborne systems, and the authors take full advantage of this data to offer a synthetic geometrical approach to the description of the SAR technique, one that addresses physicists, radar specialists, as well as experts in image processing.

The book begins with a "theoretical emergency kit" that provides the foundation necessary to understand the math and science behind the SAR technology. It then provides a comprehensive description of the technique itself, stressing the geometrical approach to radar processing, followed by a description of how these principles are applied by considering SAR design from a radiometric perspective. The authors then turn their attention to radar interferometry, explaining the practical aspects behind obtaining interferometric products from radar data, in the context of resolving ambiguity interpretation, the availability of space-borne systems, radar-data archives and software-processing resources. The book closes with a detailed description of radar polarimetry.

Richly illustrated with a careful mathematical development of the basic scientific concepts, the book is intended for both academic use (by professors and students), as well as by professionals working in industry or government laboratories.

DIDIER MASSONNET of the CNES is an IEEE fellow and an AGU member; he's the author of several patents, notably the interferometric cartwheel.

JEAN-CLAUDE SOUYRIS is head of the altimetry and radar department at the CNES. He is an IEEE member, and Associate Editor for Geoscience and Remote Sensing Letters.

EPFL Press
2008, 290 pages, Hardcover,
EPFL Press ISBN 2-940222-15-5
(CRC Press ISBN 978-0-8493-8239-4)
CRC Press Taylor & Francis Group

CONTENTS:

ORDER FORM

EPFL Press

You may order our books through your bookshop or:

If you are ordering from **Switzerland, France, Belgium, North Africa:**

• ✆ + 41 - 21 / 693 41 31 • Fax: + 41 - 21 / 693 40 27 • E-mail: ppur@epfl.ch • Internet: www.ppur.org
or return this form directly to PPUR, EPFL – CM, CP 119, CH-1015 Lausanne, Switzerland

I wish to order:	Switzerland (CHF incl. VAT)	France, Belgium (€ excl. VAT):
______copies « **Imaging with Synthetic Aperture Radar** »	135.–	85.00

(prices may be subject to modification)

Payment (Payment in advance = free delivery)

❑ By postal payment or bank transfert to p.c. account 80-2-2 (UBS SA Lausanne) indicating account No. F9-351 963.0

❑ By bank cheque (Please add CHF 5.– or 3.50 € for bank charges)

Other Payment (with postal charges)

❑ Visa / Eurocard-Mastercard

Card number: Expiration:

❑ On receipt of the invoice plus postal charges. Outside of Switzerland, this is reserved exclusively for schools, libraries and administrations together with an official order.

Company / Institute:

Name / First name:

Delivery address: E-mail:

Zip code: City: Land:

Date: Signature:

OTHER COUNTRIES:
You may order this book through www.crcpress.com


Jin.xpr 05-07-2005 16:56 Pagina 1
20 mm
FC
Theory and Approach of Information Retrievals from Electromagnetic Scattering and Remote Sensing
Ya-Qiu Jin
This book presents some new progress on the theoretical and numerical approaches for information retrieval of the remote sensing via electromagnetic scattering and emission. It covers the vector radiative transfer theory for inhomogeneous scatter media, polarimetric scattering theory for the synthetic aperture radar (SAR) imagery and some innovative applications, new approach and data validation for current space-borne remote sensing programs, fast computational method and numerical simulation for bistatic scattering of randomly rough surface with a target presence, especially at low grazing angle. Some inverse problems in radiative transfer and inverse scattering are also discussed. Novel electromagnetics of complex media are also presented.
This book is intended as a textbook for graduate students and a reference book for scientists to see the most recent progress in the author's research laboratory.
springeronline.com
ISBN 1-4020-4029-6
9 781402 040290
Theory and Approach of Information Retrievals from Electromagnetic Scattering and Remote Sensing
Ya-Qiu Jin
Theory and Approach of Information Retrievals from Electromagnetic Scattering and Remote Sensing
Ya-Qiu Jin
Springer


(P-1788.0101)
金亚秋　1970年毕业于北京大学，1978年中国科学院首批公派出国研究生，1982、1983、1985年先后获美国麻省理工学院(MIT)科学硕士、电气工程师、博士学位。曾任职于AER、纽约城市大学、英国York大学、美国NOAA/NESDIS、香港城市大学、日本东北大学。现为复旦大学信息科学与工程学院教授、波散射与遥感信息教育部重点实验室主任。他是国家级有突出贡献的中青年科技专家、上海市劳动模范、国家重点基础研究973项目首席科学家、IEEE Fellow、Electromagnetics Academy Fellow、IEEE Transactions on Geoscience and Remote Sensing副主编。他曾获国家自然科学奖等十多项科技奖励。他的研究领域为自然环境中电磁波散射辐射传输与传播、空间遥感与对地监测信息理论与技术、复杂系统中计算电磁学等。他在国内外发表了540多篇学术论文、11部学术专著与文集。
徐丰　2003年获东南大学工学士学位，2007年获复旦大学博士学位。现为美国NOAA/NESDIS博士后研究员。他曾获东南大学优秀研究生一等奖、复旦大学优秀研究生一等奖、中国电子学会优秀青年学者论文奖、复旦大学研究生创新基金、每年全世界遴选一名的美国SUMMA研究生奖学金、上海市高校科创杯奖等。他的研究领域为星载遥感建模与SAR成像技术等。他在国内外学术刊物上发表了40多篇学术论文。
定价：90.00元
极化散射与SAR遥感信息理论与方法
科学出版社
973
国家重点基础研究发展计划
极化散射与SAR遥感
信息理论与方法
Theory and Approach for Polarimetric Scattering and
Information Retrieval of SAR Remote Sensing
金亚秋　徐　丰　著
科学出版社
www.sciencep.com


NEW!
Use polarimetric imaging radar for remote sensing applications
Polarimetric Radar Imaging
From Basics to Applications
Offers the PolSARpro software available for download
Jong-Sen Lee
Life Fellow, IEEE, and US Naval Research Laboratory, Washington, DC, USA (retired)
Eric Pottier
IETR-UMR CNRS 6164, University of Rennes 1, France

POLSARPRO

The development of POLSARPRO Software is a direct result of recommendations made during the POLinSAR Workshops held at ESA-ESRIN in January 2003.

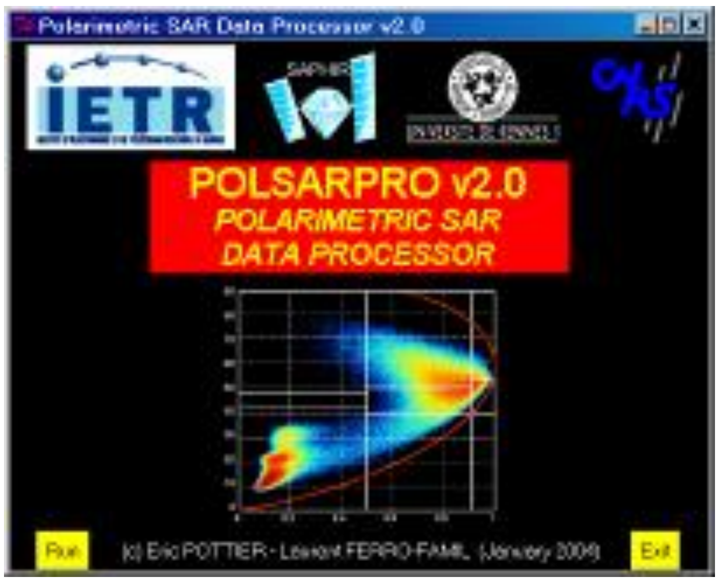

2003

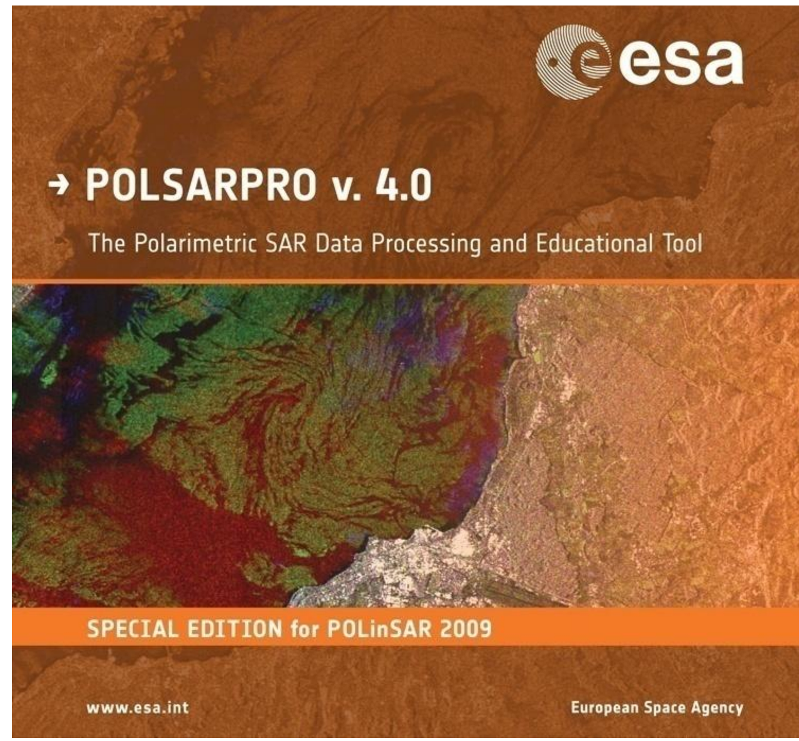

New version 4.0 released in occasion of POLinSAR 2009

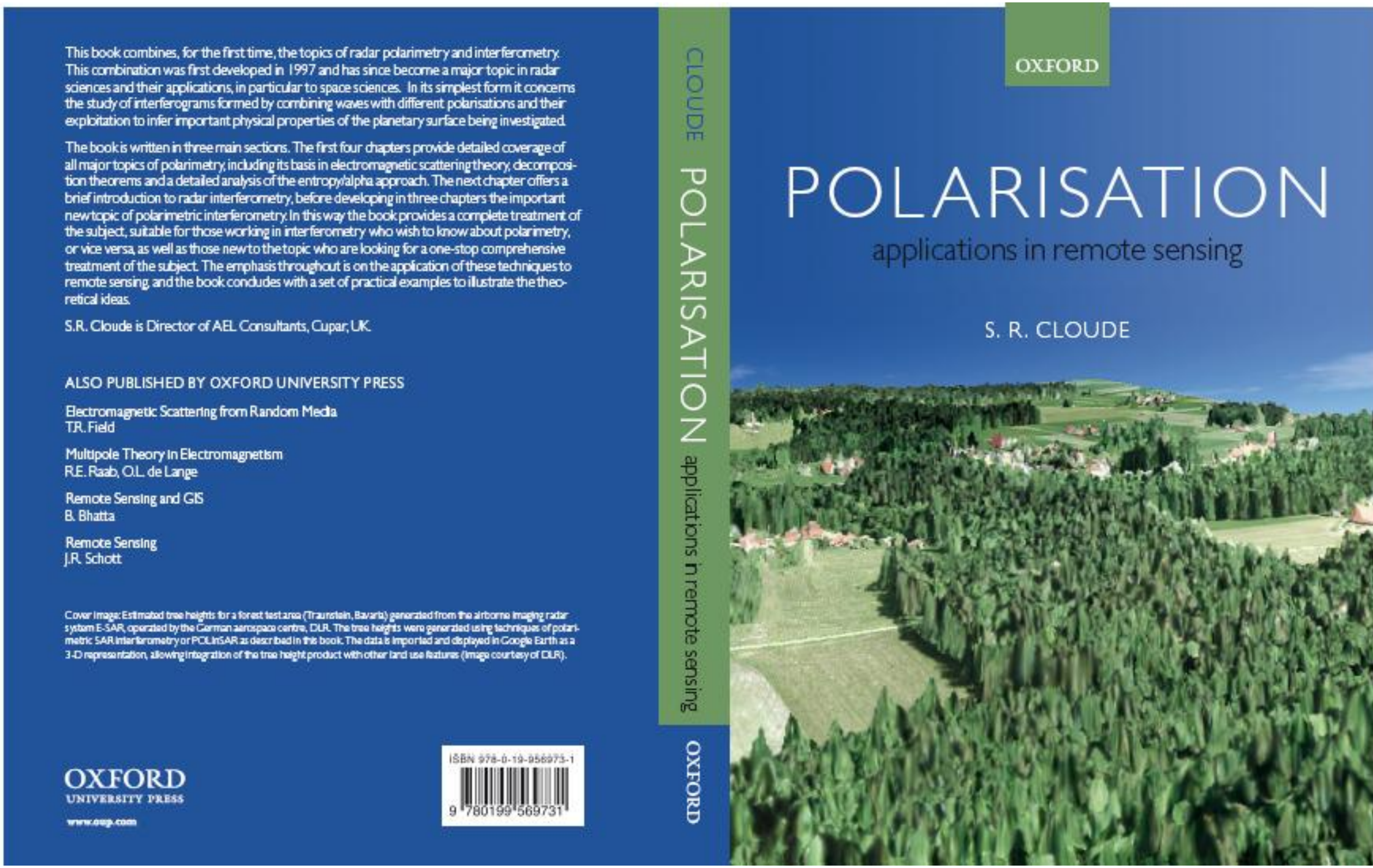
This book combines, for the first time, the topics of radar polarimetry and interferometry. This combination was first developed in 1997 and has since become a major topic in radar sciences and their applications, in particular to space sciences. In its simplest form it concerns the study of interferograms formed by combining waves with different polarisations and their exploitation to infer important physical properties of the planetary surface being investigated.
The book is written in three main sections. The first four chapters provide detailed coverage of all major topics of polarimetry, including its basis in electromagnetic scattering theory, decomposition theorems and a detailed analysis of the entropy/alpha approach. The next chapter offers a brief introduction to radar interferometry, before developing in three chapters the important new topic of polarimetric interferometry. In this way the book provides a complete treatment of the subject, suitable for those working in interferometry who wish to know about polarimetry, or vice versa, as well as those new to the topic who are looking for a one-stop comprehensive treatment of the subject. The emphasis throughout is on the application of these techniques to remote sensing, and the book concludes with a set of practical examples to illustrate the theoretical ideas.
S.R. Cloude is Director of AEL Consultants, Cupar, UK.
ALSO PUBLISHED BY OXFORD UNIVERSITY PRESS
Electromagnetic Scattering from Random Media
T.R. Field
Multipole Theory in Electromagnetism
R.E. Raab, O.L. de Lange
Remote Sensing and GIS
B. Bhatta
Remote Sensing
J.R. Schott
Cover image: Estimated tree heights for a forest test area (Traunstein, Bavaria) generated from the airborne imaging radar system E-SAR, operated by the German aerospace centre, DLR. The tree heights were generated using techniques of polarimetric SAR interferometry or POLInSAR as described in this book. The data is imported and displayed in Google Earth as a 3-D representation, allowing integration of the tree height product with other land use features (image courtesy of DLR).
OXFORD
UNIVERSITY PRESS
www.oup.com
ISBN 978-0-19-956973-1
9 780199 569731
CLOUDE POLARISATION applications in remote sensing OXFORD
OXFORD
POLARISATION
applications in remote sensing
S. R. CLOUDE

POLSARPRO

- Developed to be accessible to a wide range of users from novices to experts in the field of POLSAR and POL-InSAR
- Educational Software offering a tool for self-education in the field of **POLSAR** and **POL-InSAR** data processing and analysis
- Open Source Software Development

Supported Polarimetric SAR datasets

Airborne	Spaceborne
AIRSAR & TOPSAR	SIR-C
EMISAR	Envisat ASAR
E-SAR -> F-SAR	RADARSAT-2
Pi-SAR	ALOS PALSAR
SAR580-Convair	TerraSAR-X
RAMSES	TandemSAR-X

http://earth.esa.int/polsarpro

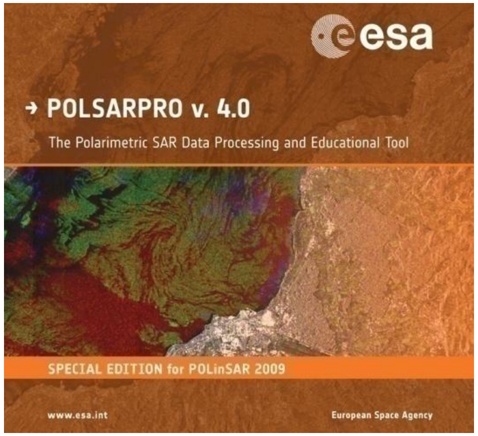

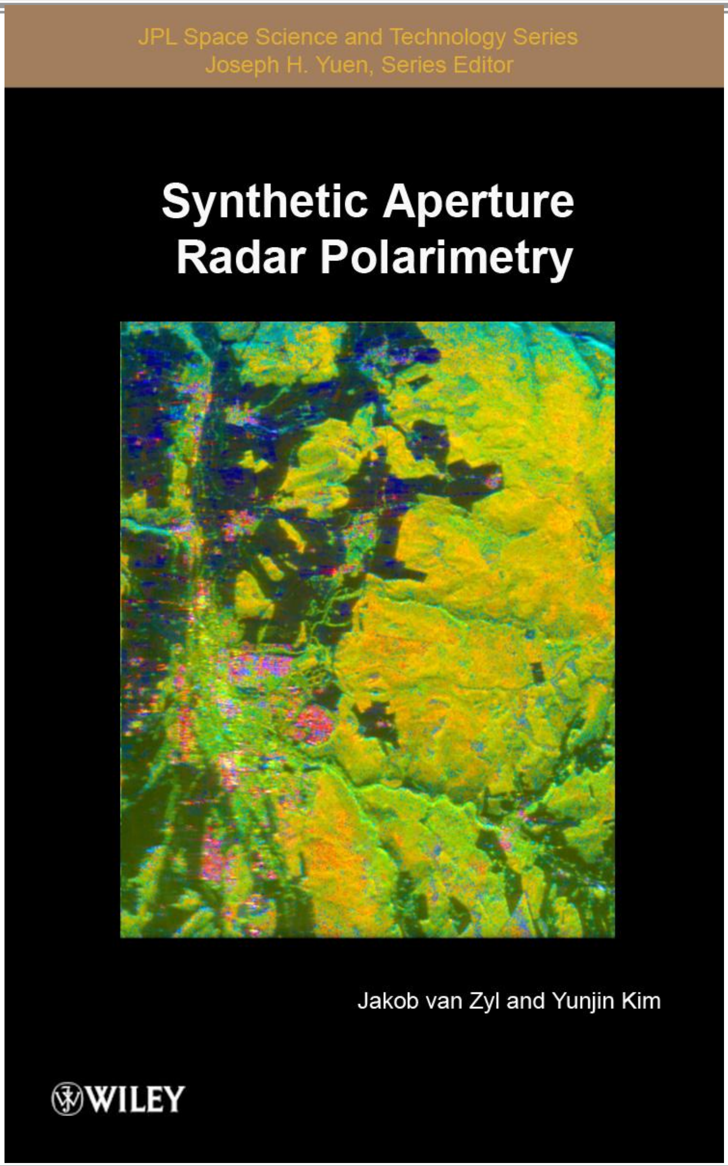

Contents List

To appear in 2010 July
John Wiley & Sons, Inc.
ISBN:

Major Paradigm for Remote Sensing from Air and Space of the Terrestrial Covers:

"Natural hazards are inevitable! Natural disasters are not & how can we reduce aftereffects?"

Accomplished with fully Polarimetric POLinSAR Sensors at all pertinent frequency bands:

ACQUISITION OF NEW BANDS FOR ROTHPASSIVE & ACTIVE SENSING

• Deep earth sounding	ULF - LF
• Ground penetrating radar	LF - VHF
• Mineral resource exploration	HF - UHF
• Biomass and vegetative cover estimation	HF – EHF (P/L/C-Band)
• Man made surface structure monitoring	HF – EHF (C/X/K-Band)
• Atmospheric passive remote sensing	cm – sub-mm

◊ **We need to put our act together as the global remote sensing community and request from ITU/WMO the protection of the "fundamental natural resource: the e-m spectrum", and for providing the spectral bands for us to fulfill our professional duties as**

"The Remote Sensing Pathologists and Radiologists of Earth and Planetary Covers"

THE IMMINENT COLLISION:

Passive vs Active Spectrum Users, e. g. radio-astronomy vs global telecommunications complex

- **CLEAN THE PROPAGATION SPACE FROM PROPAGATION LITTER:**
  - **users not requiring free propagation space must be relegated to the use of the global EO fiber transmission network**

- **PRESERVE THE GLOBAL NATURAL RESOURCE – THE E-M SPECTRUM FROM MISUSE:**
  - **misuse of spectral band acquisition by aggressive telecommunication complex must be put to an end**

- **ASSIST AERONOMISTS AND RADIO ASTRONOMERS IN ESTABLISHING THE BACKGROUND NATURAL NOISE SIGNATURES OF TERRESTRIAL, PLANETARY AND GALACTIC ORIGIN**
  - **establish natural background signatures in all spectral bands**

- **THERE DOES NOT EXIST A SINGLE SPECTRAL BAND IN WHICH THE TERRESTRIAL COVERS DO NOT POSSESS DISTINCT EIGEN-RESONANCES**
  - **the measurement and monitoring of natural eigen-resonances is essential for natural hazard prediction and mitigation – short term and long term**

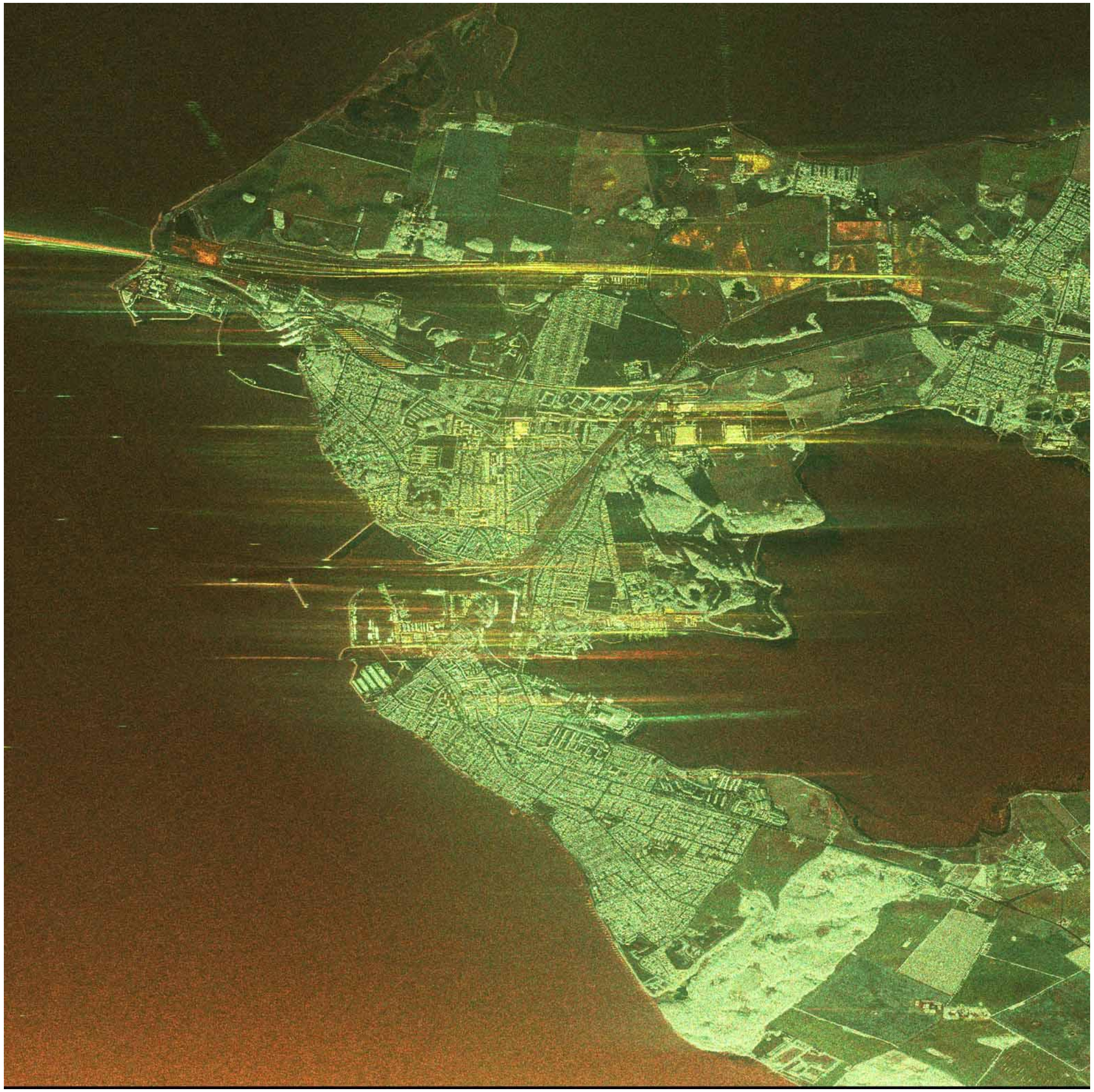

Interference Obstruction: EMI-SAR

RFI monitoring by JERS-1 SAR (1992-1998)

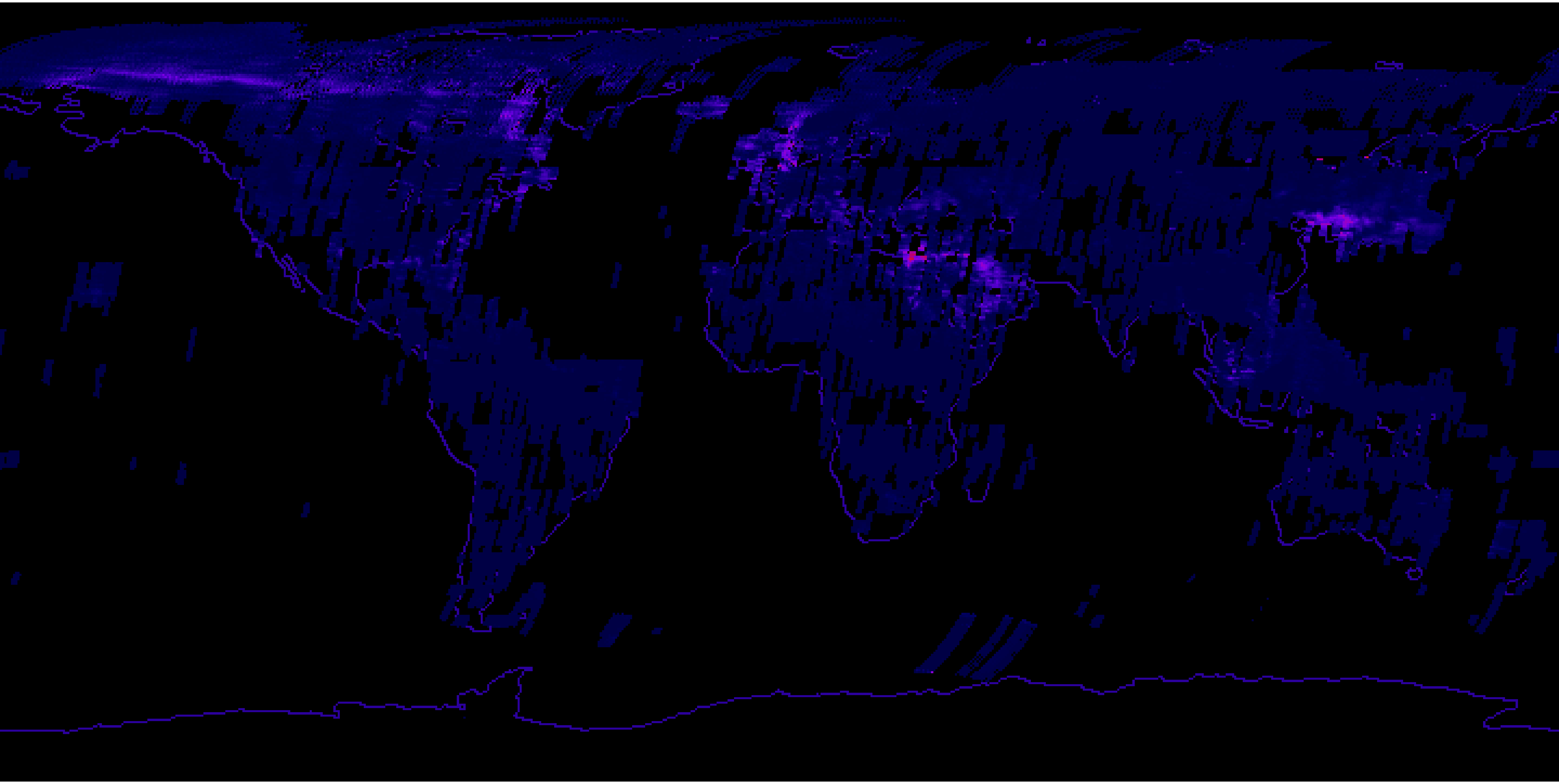

Normalized zero padded bandwidth (%)

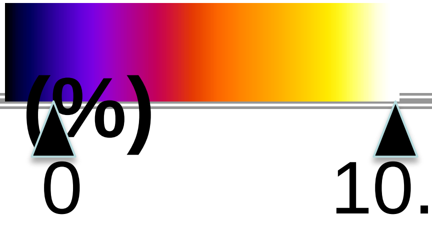

RFI monitoring by PALSAR (2010/4~2011/4)

Normalized zero padded bandwidth (%)

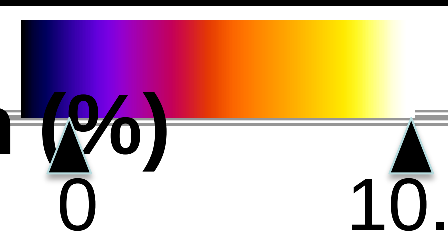

RFI Affected ALOS PALSAR Frames in the AADN Archive

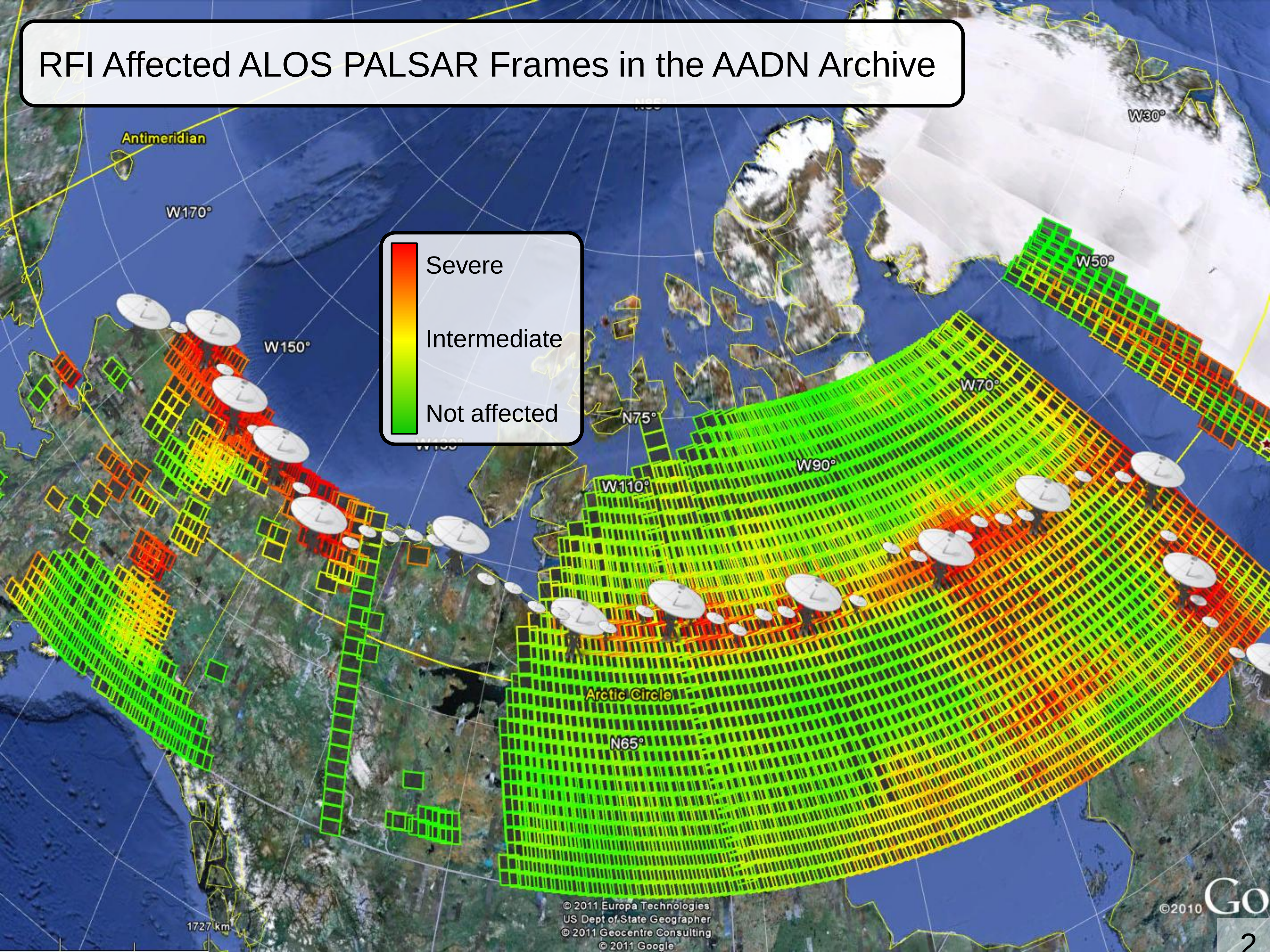

Pauli RGB Level 1.1

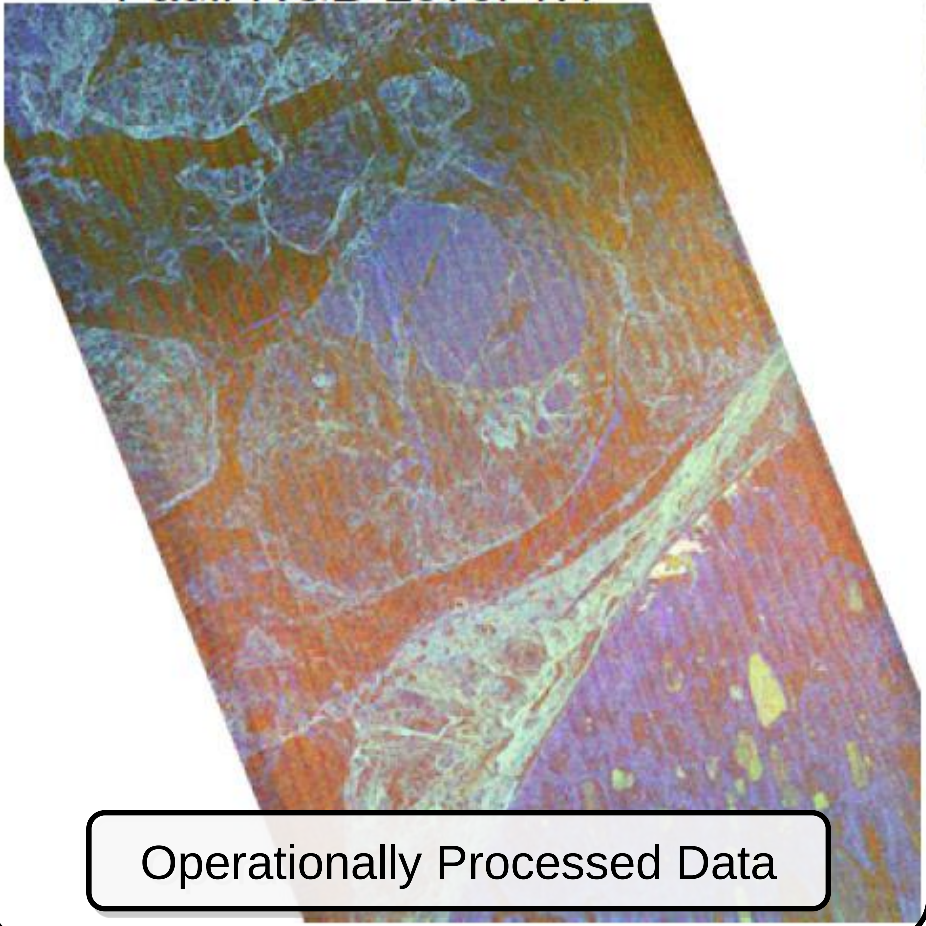

Operationally Processed Data

Pauli RGB Level 1.0

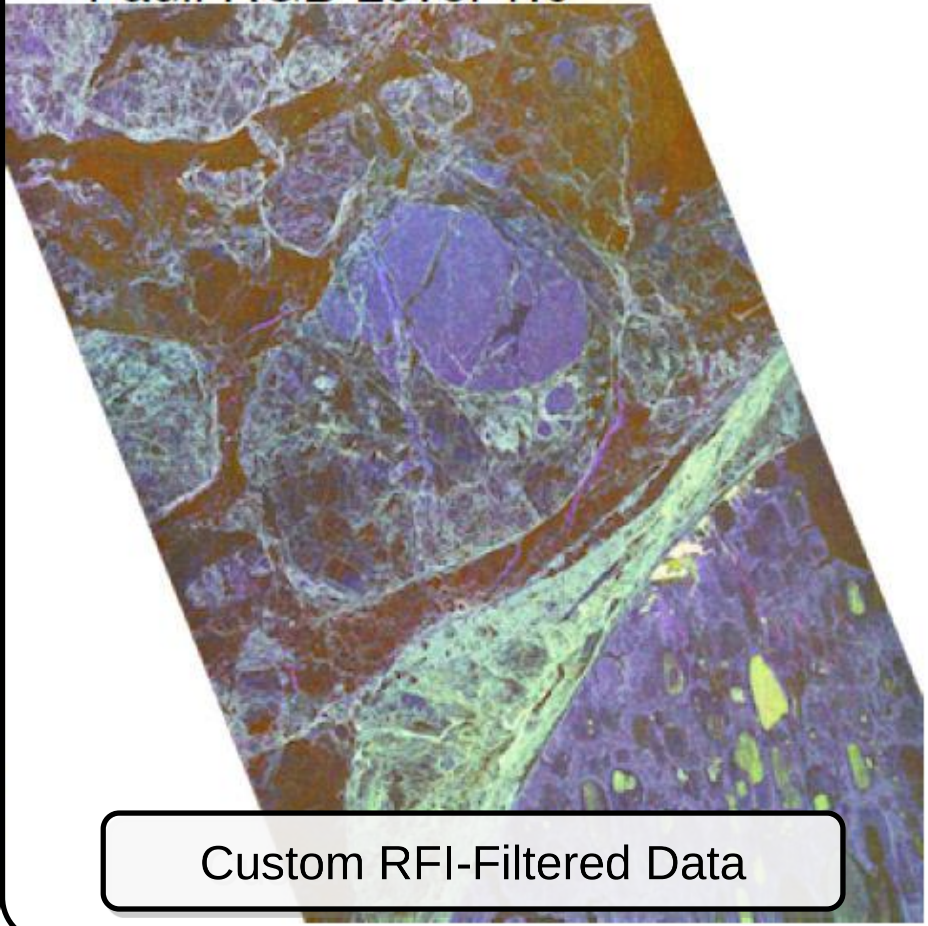

Custom RFI-Filtered Data

ESTABLISHMENT OF WORLD NATURAL HERITAGE ELECTROMAGNETIC QUIET SITES

Radio Astronomic Planetary and Galactic Background Signature Validation across the Entire Electromagnetic Spectrum

ULF – ELF: earthquake prediction

LF – HF: lithospheric sounding and solar terrestrial interactions

VHF – UHF: layer soil and vegetation cover remote sensing

UHF – EHF: vegetation canopy remote sensing and atmospheric monitoring

mm – sub-mm: atmospheric – mesospheric absorption bands monitoring

mm – sub-mm: transmission windows remote sensing

Recent Advances in Fully Polarimetric Space SAR Development and Its Applications

Conclusions:

The Vector Electromagnetic Spectrum:
A Natural Global Treasure

Terrestrial Remote Sensing with PolSAR **:**
The *Diagnostics of the Health of the Earth*
at all weather and volcanic conditions
and at day and night